

---

Electronic Thesis and Dissertation Repository

---

1-19-2012 12:00 AM

# Miniaturized Fractionation and Purification of Analytes of Interest in Complex Mixtures: Protein Enrichment and Purification with Capillary Electrophoresis and Identification of Pesticide Chemicals in Bio-oils

Christina J. Booker  
*The University of Western Ontario*

Supervisor  
Dr. Ken Yeung  
*The University of Western Ontario*

Graduate Program in Chemistry  
A thesis submitted in partial fulfillment of the requirements for the degree in Doctor of Philosophy  
© Christina J. Booker 2012

Follow this and additional works at: <https://ir.lib.uwo.ca/etd>

 Part of the [Analytical Chemistry Commons](#)

---

## Recommended Citation

Booker, Christina J., "Miniaturized Fractionation and Purification of Analytes of Interest in Complex Mixtures: Protein Enrichment and Purification with Capillary Electrophoresis and Identification of Pesticide Chemicals in Bio-oils" (2012). *Electronic Thesis and Dissertation Repository*. 373.  
<https://ir.lib.uwo.ca/etd/373>

This Dissertation/Thesis is brought to you for free and open access by Scholarship@Western. It has been accepted for inclusion in Electronic Thesis and Dissertation Repository by an authorized administrator of Scholarship@Western. For more information, please contact [wlsadmin@uwo.ca](mailto:wlsadmin@uwo.ca).

MINIATURIZED FRACTIONATION AND PURIFICATION OF ANALYTES OF  
INTEREST IN COMPLEX MIXTURES:

PROTEIN ENRICHMENT AND PURIFICATION WITH CAPILLARY  
ELECTROPHORESIS *AND*

IDENTIFICATION OF PESTICIDE CHEMICALS IN BIO-OILS

(Spine title: Miniaturized Purification from Complex Samples: Proteins and Bio-oils)

(Thesis format: Integrated Article)

by

Christina J. Booker

Graduate Program in Chemistry

A thesis submitted in partial fulfillment  
of the requirements for the degree of  
Doctor of Philosophy

The School of Graduate and Postdoctoral Studies  
The University of Western Ontario  
London, Ontario, Canada

© Christina J. Booker 2012

THE UNIVERSITY OF WESTERN ONTARIO  
School of Graduate and Postdoctoral Studies

**CERTIFICATE OF EXAMINATION**

Supervisor

Examiners

\_\_\_\_\_  
Dr. Ken Yeung

\_\_\_\_\_  
Dr. Clara J. Wren

Supervisory Committee

\_\_\_\_\_  
Dr. Viktor N. Staroverov

\_\_\_\_\_  
Dr. Mel C. Usselman

\_\_\_\_\_  
Dr. Daniel Figeys

\_\_\_\_\_  
Dr. Richard J. Puddephatt

\_\_\_\_\_  
Dr. Harvey Goldberg

The thesis by

**Christina Joanne Booker**

entitled:

**Miniaturized Fractionation and Purification of Analytes of Interest in  
Complex Mixtures:  
Protein Enrichment and Purification with Capillary Electrophoresis *and*  
Identification of Pesticide Chemicals in Bio-oils**

is accepted in partial fulfillment of the  
requirements for the degree of  
Doctor of Philosophy

\_\_\_\_\_  
Date

\_\_\_\_\_  
Chair of the Thesis Examination Board

# Abstract

The ability to isolate and detect an analyte of interest is vital for many different facets of life today, from disease detection to environmental safety. The goal of the method development discussed within this thesis is to isolate and identify unique analytes from complex matrices and to do so in a scaled down approach. Removal of an analyte from a diverse background of molecules is often required for successful detection and determination of analyte properties. As well, many samples are only available at low volumes and at trace levels so miniaturized techniques that only require small sample volumes are designed and discussed herein. Two unique classes of analytes are examined with one common theme of isolation for successful detection.

Proteins and peptides are enriched and purified from permanently charged and buffering ions, which are common biological contaminants, using discontinuous buffers with capillary electrophoresis. This method only uses sub-microliter quantities of sample and exploits the isoelectric point of the biological macromolecules in buffers of different pH. Successful removal of sodium chloride, TRIS, phosphate, and MES is demonstrated. Subsequent enhanced mass spectral detection and separation of a protein mixture exhibited the improved analyte detection by employing discontinuous buffers. Magnetic beads are used to isolate phosphorylated peptides at micro to nanoliter volumes by covalent derivatization of the post-translational modification and selective enrichment, further demonstrating the on-line CE sample preparation capabilities.

The second challenging sample examined is bio-oil, a complex mixture of thousands of chemicals. The novel pesticide properties of this sample are explored as the chemical complexity of pyrolysis bio-oil from tobacco leaves is reduced through isolation by solid phase extraction, liquid-liquid extraction, and heating. Mass spectrometry is used to identify the compounds after separation by gas chromatography. Three problematic microorganisms in Canada, *S. scabies*, *C. michiganensis*, and *P. ultimum*, are negatively affected by the bio-oil. It is determined that the most abundant phenolic species are not responsible for the observed pesticide activity from the bio-oil. A few minor components

are identified that could contribute to the observed antimicrobial activity, but no abundant, active chemicals could be identified with the current technology.

## **Keywords**

capillary electrophoresis, proteins, peptides, phosphorylation, enrichment, desalting, pH-junction, discontinuous buffers, sample clean-up, mass spectrometry, magnetic beads, derivatization, bio-oil, pesticide, bacteria, fungi, pyrolysis, phenol, gas chromatography mass spectrometry

# Statement of Co-Authorship

Chapters 1, 2, 3, 5, and 6 contain published content from the following articles:

1. C.J. Booker & K.K.C. Yeung. In-Capillary Protein Enrichment and Removal of Nonbuffering Salts Using Capillary Electrophoresis with Discontinuous Buffers, *Analytical Chemistry*, **2008**, *80*, 8598-8604. (Chapter 1 and 2).

Experiments were designed and performed by the author. The manuscript first draft was written and revisions performed by the author.

2. C.J. Booker, S. Sun, S. Woolsey, J.S. Mejia & K.K.-C. Yeung. Removal of sample background buffering ions and myoglobin enrichment via a pH junction created by discontinuous buffer in capillary electrophoresis, *Journal of Chromatography A*, **2011**, *1218*, 5705-5711. (Chapter 1 and 3).

Experiments were designed and performed by the author. Three undergraduate students (S. Sun, S. Woolsey, and J.S. Mejia) performed initial data collection under supervision of the author, but all data included in the manuscript was performed by the author. The first draft was written by the author, and revisions performed in collaboration with K. Yeung.

3. C.J. Booker, R. Bedmutha, I.M. Scott, K. Conn, F. Berruti, C. Briens & K.K.C. Yeung. Bioenergy II: Characterization of the Pesticide Properties of Tobacco Bio-Oil, *International Journal of Chemical Reactor Engineering*, **2010**, *8*. (Chapter 5 and 6).

All experiments were designed and performed by the author. Bio-oil was provided by R. Bedmutha. F. Berrutti and C. Briens were the Faculty of Engineering co-supervisors for the project, while I.M Scott and K. Conn were the collaborating scientists at Agriculture and Agri-Food Canada. K. Yeung was the author's supervisor. These five supervisors provided materials for experiments and feedback on the manuscript. The manuscript was written and revised by the author.

4. C.J. Booker, R. Bedmutha, T. Vogel, A. Gloor, R. Xu, L. Ferrante, K.K.C. Yeung, I.M. Scott, K.L. Conn, F. Berruti & C. Briens. Experimental Investigations into the Insecticidal, Fungicidal, and Bactericidal Properties of Pyrolysis Bio-oil from Tobacco Leaves Using a Fluidized Bed Pilot Plant, *Industrial & Engineering Chemistry Research*, **2010**, *49*, 10074-10079. (Chapter 5 and 6).

Data selected from this manuscript was designed and performed by the author. R. Bedmutha provided the bio-oil and pyrolysis data for the manuscript and was not included in this thesis. Undergraduate student T. Vogel worked with the author for some data collection (included in this thesis), while A. Gloor contributed some additional data (not included in this thesis). The initial draft was written by R. Bedmutha, but was later significantly rewritten and organized, including figure adjustments, making the author of this thesis first author for the manuscript. All revisions were also performed by the author.

5. R. Bedmutha, C.J. Booker, L. Ferrante, C. Briens, F. Berruti, K.K.-C. Yeung, I.M. Scott & K.L. Conn. Insecticidal and bactericidal characteristics of the bio-oil from the fast pyrolysis of coffee grounds, *Journal of Analytical and Applied Pyrolysis*, **2011**, *90*, 224-231. (Chapter 5 and 6).

Data collection was performed by both R. Bedmutha and the author. The same five supervisors were used for consultation. Post-doctoral fellow L. Ferrante worked with R. Bedmutha for bio-oil pyrolysis. Initial draft was written by R. Bedmutha, and substantial revisions performed by the author. The data from this manuscript enclosed in this thesis was collected by the author and only referred to for comparison to the tobacco bio-oil results.

# Acknowledgements

Four years of research and study could not have been successful without the support and guidance of many people.

My supervisor, Dr. Ken Yeung, was instrumental in the completion of my thesis. His valuable insight and thoughtful advice over the years has been significant. He was always available for questions, discussions on the latest data, feedback on my written work, and even frequent instrument repairs. Dr. Yeung challenged me to try new projects, network with other research groups, apply for scholarships, and submit my work for publication and conferences. His open office door, patience, and kindness were extremely valuable to me. I am sincerely grateful for his generosity and input during my graduate studies.

I would also like to thank my undergraduate thesis supervisor, Dr. Z. F. Ding for his encouragement and challenge to pursue a graduate degree. I had not considered a PhD in chemistry until after an inspiring summer research position in his electrochemistry laboratory. Dr. Ding also encouraged me to apply for graduate scholarships and wrote my support letters. I am continually grateful for this wise advice and support.

The Natural Sciences and Research Council of Canada (NSERC) has supported me for my entire four years of thesis work, including my four month maternity leave, and two undergraduate summer research positions. This financial support made it possible for me to continue my work at the university, focus on my research, and complete this thesis.

Collaborations with other scientists were highly valuable. My bio-oil project was a collaborative work with the Faculty of Engineering and Agriculture and Agri-Food Canada. A special thanks to Dr. Cedric Briens, Dr. Franco Berrutti, Dr. Ken Conn, Dr. Ian Scott, and Dr. Brian McGarvey for access to their unique instruments and materials, and for their specialized feedback in this research. Thanks is also expressed to Dr. Walter Siqueira for his contributions and advice with the phosphorylated peptide enrichment project with magnetic beads.



Thank-you to my committee members, Dr. Mel Usselman, Dr. Clara Wren, Dr. Viktor Staroverov, and Dr. Puddephatt for their guidance and interest in my research and progress. My appreciation is also expressed to my examiners, Dr. Clara Wren, Dr. Viktor Staroverov, Dr. Daniel Figeys, and Dr. Harvey Goldberg for their time and attention to my thesis and defence.

My parents, John and Cheryl Scorgie, have provided immeasurable help and love over the years. From raising me with a desire to learn and always do my best, to arranging the many swimming and music lessons I was grateful to receive, they have showered me with blessings. Their love and prayers for me every day has made the greatest impact on my life.

Finally, my husband of five years, Joel Booker, has supported and encouraged me every step of the way through my PhD work. We were married as undergraduate students and continued through graduate school together. Our one year old daughter, Bethany, is a joy and delight, and I appreciate all his hard work as a high school teacher and father. We have worked as a team, and I am grateful for his friendship and love as I have completed my graduate education.

# Dedication

To my husband and parents for their support and love.

# Table of Contents

Thesis Title Page.....	i
CERTIFICATE OF EXAMINATION.....	ii
Abstract.....	iii
Keywords.....	iv
Co-Authorship Statement.....	v
Acknowledgments.....	vii
Dedication.....	ix
Table of Contents.....	x
List of Tables.....	xv
List of Figures.....	xvi
List of Equations.....	xxi
List of Abbreviations.....	xxii
Preface.....	xxv
<b>Chapter 1: Introduction to Capillary Electrophoresis as a Sample Preparation Tool for Mass Spectrometry Analysis of Proteins and Peptides.....</b>	<b>1</b>
<b>1.1 Proteins and Peptides.....</b>	<b>2</b>
<b>1.2 Capillary Electrophoresis.....</b>	<b>6</b>
<b>1.3 Sample Preparation with Capillary Electrophoresis.....</b>	<b>11</b>
<b>1.4 Discontinuous Buffers – a Response to Enrichment Problems in CE.....</b>	<b>15</b>
<b>1.5 Magnetic Beads – a Response for Specific Isolation of Analytes in CE.....</b>	<b>18</b>
<b>1.6 References.....</b>	<b>20</b>
<b>Chapter 2: In-Capillary Protein Enrichment and Removal of Non-Buffering Salts using Capillary Electrophoresis with Discontinuous Buffers.....</b>	<b>24</b>
<b>2.1 Introduction.....</b>	<b>25</b>
<b>2.2 Materials and Methods.....</b>	<b>27</b>

2.2.1 Apparatus.....	27
2.2.2 Reagents.....	28
2.2.3 Enrichment and Desalting by Discontinuous Buffers.....	29
2.2.4 MALDI Mass Spectral Analyses.....	30
2.2.5 CZE of Enriched Protein Mixture.....	31
2.2.6 Computer Simulations.....	31
<b>2.3 Results and Discussion.....</b>	<b>33</b>
2.3.1 Effect of Non-buffering Salt on Protein Enrichment by Discontinuous Buffers.....	33
2.3.2 Non-Buffering Salt Removal Evaluated by Optical Detection.....	38
2.3.3 Computer Simulations and UV-absorbing Buffers: Investigations into the Ion Migration within Discontinuous Buffers.....	40
2.3.4 Protein Enrichment and Mass Spectral Analysis of Salt-Containing Proteins Samples.....	52
2.3.5 CZE of Enriched Protein Mixture.....	54
<b>2.4 Conclusions.....</b>	<b>57</b>
<b>2.5 References.....</b>	<b>58</b>
<b>Chapter 3: Removal of Sample Background Buffering Ions and Myoglobin Enrichment at a pH Junction Created by Discontinuous Buffers in Capillary Electrophoresis.....</b>	<b>61</b>
<b>3.1 Introduction.....</b>	<b>62</b>
<b>3.2 Materials and Methods.....</b>	<b>64</b>
3.2.1 Apparatus.....	64
3.2.2 Reagents.....	64
3.2.3 Enrichment of Proteins by a pH Junction.....	65
3.2.4 Computer Simulations.....	66
<b>3.3 Results and Discussion.....</b>	<b>66</b>
3.3.1 Protein Enrichment and Removal of TRIS.....	66
3.3.2 Protein Enrichment and Removal of MES.....	73

3.3.3 Migration of Phosphate at the pH Junction.....	76
3.3.4 Phosphate Removal during Protein Enrichment.....	80
<b>3.4 Conclusions.....</b>	<b>86</b>
<b>3.5 References.....</b>	<b>87</b>
<b>Chapter 4: Enrichment of Phosphorylated Peptides using Selective Retention with Magnetic Beads On-line in Capillary Electrophoresis.....</b>	<b>90</b>
<b>4.1 Introduction.....</b>	<b>91</b>
<b>4.2 Materials and Methods.....</b>	<b>96</b>
4.2.1 Apparatus.....	96
4.2.2 Reagents.....	97
4.2.3 MALDI MS Analysis.....	97
4.2.4 $\beta$ -Casein Digestion.....	97
4.2.5 Phosphorylated Sample Derivatization.....	98
4.2.6 Solid Phase Clean-up (C18 ZipTips™).....	98
4.2.7 Thiol-Activated Magnetic Bead Experiments.....	99
<b>4.3 Results and Discussion.....</b>	<b>100</b>
4.3.1 DTT-Derivatization of Phosphorylated Peptides (Steps I and II).....	101
4.3.2 Solid-Phase Removal of excess DTT (Step III).....	108
4.3.3 In-Vial Isolation of Phosphorylated Peptides by Disulfide-Thiol Interchange (Steps IV and V).....	109
4.3.4 Elution of the Covalently Bound Derivatized Peptides In-Vial (Step VI).....	113
4.3.5 Magnetic Bead Plug in Capillary.....	116
4.3.6 Isolation of Phosphorylated Peptides in Capillary.....	118
<b>4.4 Conclusions.....</b>	<b>122</b>
<b>4.5 References.....</b>	<b>125</b>
<b>Chapter 5: Introduction to Pyrolysis Bio-oils and Potential Application as a Pesticide.....</b>	<b>128</b>

<b>5.1 Biomass Sources for Pyrolysis</b> .....	129
<b>5.2 Pyrolysis Process</b> .....	131
<b>5.3 Chemical Composition of Bio-oil</b> .....	135
<b>5.4 Potential Value and Applications of Bio-oil</b> .....	137
<b>5.5 Bio-oil as a Pesticide</b> .....	138
<b>5.6 References</b> .....	140
<b>Chapter 6: Investigations into the Antimicrobial Activity of Bio-oil: From Biomass Sources to Chemical Composition</b> .....	144
<b>6.1 Introduction</b> .....	145
<b>6.2 Materials and Methods</b> .....	147
6.2.1 Chemicals and Bio-oil.....	147
6.2.2 Bio-oil Sample Preparation.....	148
6.2.2.1 Liquid-Liquid Fractionation.....	148
6.2.2.2 Solid Phase Extraction and Heating.....	149
6.2.2.3 Preparative Scale Liquid Chromatography/Flash Chromatography.....	150
6.2.2.4 Derivatization of Active Fraction.....	150
6.2.3 Gas Chromatography-Mass Spectrometry Sample Analysis.....	151
6.2.4 Bio-assays for Microorganisms.....	151
6.2.4.1 Disk Diffusion Assay.....	151
6.2.4.2 Microtiter Plate Bioassay.....	152
<b>6.3 Results and Discussion</b> .....	154
6.3.1 Antimicrobial Activity from Bio-oil from multiple Biomass Sources.....	154
6.3.2 Investigation into the Effect of Pyrolysis Temperature on Pesticide Activity for Tobacco and Coffee Bio-oil.....	156
6.3.3 Investigation into the Liquid-Liquid Extraction Fractions of Tobacco Bio-oil.....	158
6.3.4 Composition and Activity Analysis of the Active, Nicotine-Free	

Tobacco Bio-oil Fraction.....	161
6.3.4.1 Further Liquid-liquid Extraction.....	161
6.3.4.2 Identification of Standards.....	162
6.3.4.3 Bio-assays of the Standard Compounds in the Active, Nicotine-Free Fraction.....	165
6.3.4.4 Chemical Composition Comparison between Tobacco and Coffee Grounds Bio-oils.....	168
6.3.4.5 Activity from Other Chemicals.....	169
6.3.5 Reduction of the Chemical Complexity of the Active, Nicotine-Free Tobacco Bio-oil Fraction.....	170
6.3.5.1 Solid Phase Extraction.....	170
6.3.5.2 Low Temperature Heating.....	172
6.3.5.3 Preparative Scale Liquid Chromatography/ Separation by Flash Chromatography for GC-MS Analysis.....	174
6.3.6 Sample Derivatization for GC-MS Analysis.....	184
<b>6.4 Conclusions</b> .....	186
<b>6.5 References</b> .....	189
 <b>Chapter 7: Conclusions and Future Work</b> .....	192
 <b>7.1 Discussion of Conclusions and Future Work</b> .....	193
<b>7.2 References</b> .....	198
 <b>Appendix 1 – Copyright Permissions</b> .....	199
 <b>Curriculum Vitae</b> .....	213

# List of Tables

<b>Table</b>	<b>Description</b>	<b>Page</b>
<b>4.1</b>	A list of observed and corresponding theoretical monoisotopic mass values of a $\beta$ -casein trypsin digest.	<b>102</b>
<b>4.2</b>	Forms of the monophosphorylated peptide (FQpSEEQQQTEDELQDK) from a $\beta$ -casein trypsin digest.	<b>104</b>
<b>6.1</b>	List of bio-oil biomass sources and microorganism activity.	<b>155</b>
<b>6.2</b>	List of the largest peaks identified from the GC-MS chromatogram of Fraction M.	<b>164</b>
<b>6.3</b>	List of compounds found in Fraction 9, 10, and 11 and absent in Fraction 1, 2, and 3.	<b>180</b>
<b>6.4</b>	List of compounds found in Fraction 5, 6 and 7 and absent in Fraction 1, 2, 3, 10, 11, and 12.	<b>183</b>
<b>6.5</b>	List of common silyl derivatized compounds and their original analog found in derivatized Fractions 9, 10, and 11.	<b>185</b>



# List of Figures

<b>Table</b>	<b>Description</b>	<b>Page</b>
<b>1.1</b>	Simple schematic of CE set-up.	<b>7</b>
<b>1.2</b>	Schematics showing EOF formation (A) and EOF flow profile (B), as opposed to laminar flow profile (C).	<b>8</b>
<b>1.3</b>	Schematics showing analyte stacking based on a change in conductivity (A), a change in pH (B), and through the addition of solid phase (C).	<b>13</b>
<b>1.4</b>	Schematic of protein enrichment using discontinuous buffers.	<b>17</b>
<b>2.1</b>	Schematics and electropherograms of protein enrichment using discontinuous buffers without addition of salt.	<b>35</b>
<b>2.2</b>	Schematics and electropherograms of protein enrichment in the presence salt using discontinuous buffers.	<b>37</b>
<b>2.3</b>	The absorbance and the current recorded during the enrichment of myoglobin by discontinuous buffers containing sodium bromide (A), or benzyltrimethylammonium chloride (B).	<b>39</b>
<b>2.4</b>	Simul 5.0 computer simulation of the discontinuous buffers with a plug of myoglobin after 0 s (B), 60 s (C) and 600 s (D) of voltage.	<b>42</b>
<b>2.5</b>	A schematic (A) and simulation results of discontinuous buffers with a plug of sodium chloride after 0 s (B), 60 s (C), and 1200 s (D) of voltage.	<b>46</b>
<b>2.6</b>	UV-absorbing discontinuous buffers after 0 and 300 s of voltage (30 kV).	<b>49</b>
<b>2.7</b>	Experimental results from two sets of UV-absorbing discontinuous buffers with salt.	<b>51</b>
<b>2.8</b>	MALDI MS spectra of the enriched, desalted myoglobin fraction collected from capillary (A), and the untreated sample (B).	<b>53</b>

<b>2.9</b>	Diagram of procedure of protein enrichment by discontinuous buffers followed by CZE.	<b>55</b>
<b>2.10</b>	Absorbance at 200 nm recorded during CZE on enriched, desalted proteins.	<b>56</b>
<b>3.1</b>	Schematics representing the injection of myoglobin and TRIS and the subsequent ion migration upon voltage application.	<b>68</b>
<b>3.2</b>	Simul 5.0 computer simulation of the discontinuous buffers after 1000 s of voltage application in the absence (A) and presence (B) of TRIS.	<b>71</b>
<b>3.3</b>	Schematics representing the selective injection of myoglobin from TRIS and the corresponding UV-signal.	<b>73</b>
<b>3.4</b>	Schematics (A) and UV-absorption signal (B) representing the injection and ion migration of myoglobin.	<b>75</b>
<b>3.5</b>	Schematics of the experimental set-up and proposed migration behaviour of phenyl phosphate (A) with corresponding absorbance signals (B).	<b>78</b>
<b>3.6</b>	Simul 5.0 computer simulated results during voltage application with phosphate containing discontinuous buffers at 0 s (A) and 30 s (B).	<b>80</b>
<b>3.7</b>	A schematic (A) and UV-absorbance signals (B) showing the electrofocussing of a plug of myoglobin with sodium.	<b>82</b>
<b>3.8</b>	Simul 5.0 computer simulated results of pH, conductivity, phosphate concentration, and sodium concentration at 0 s (A), 30 s (B), 150 s (C), and 270 s (D).	<b>84</b>
<b>4.1</b>	Chemical reactions for the derivatization of phosphorylated peptides.	<b>94</b>
<b>4.2</b>	Reaction schematic for the DTT-derivatization and isolation of the monophosphorylated peptide from a $\beta$ -casein tryptic digest.	<b>103</b>

<b>4.3</b>	Mass spectra of the DTT-derivatization of the monophosphorylated peptide standard (A) with 5 mM (B), 20 mM (C), and 100 mM (D) DTT.	<b>106</b>
<b>4.4</b>	Graph comparing the mass spectral signal intensities of the DTT-derivatized peptide to the phosphorylated peptide under different derivatization reaction conditions.	<b>107</b>
<b>4.5</b>	Schematics of the isolation of the DTT-derivatized phosphopeptide from the non-derivatized/non-phosphorylated peptides using thiol activated magnetic beads in-capillary and in-vial.	<b>111</b>
<b>4.6</b>	MS signal intensities of the elution of DTT-derivatized peptides in-vial from thiol-activated magnetic beads under different conditions.	<b>113</b>
<b>4.7</b>	Mass spectra of the $\beta$ -casein digest (A), after DTT derivatization (B), after clean-up with ZipTips <sup>TM</sup> (C), and isolation of the derivatized peptide in vial with thiol-magnetic beads (D).	<b>115</b>
<b>4.8</b>	Migration of a neutral marker with pressure through a capillary with (A) and without (B) a magnetic bead plug and the corresponding photograph of the magnetic bead plug (C).	<b>117</b>
<b>4.9</b>	Schematic of the two sample introduction methods for in-capillary isolation of derivatized peptides.	<b>118</b>
<b>4.10</b>	MS signals of in-capillary experiments with a derivatized $\beta$ -casein digest, after DTT-removal via ZipTips <sup>TM</sup> .	<b>121</b>
<b>4.11</b>	Concluding schematic of optimized procedures for analyte derivatization and magnetic beads reactions.	<b>123</b>
<b>5.1</b>	Simple schematic of the pyrolysis process.	<b>132</b>
<b>5.2</b>	A schematic of the Western Fluidization Group's fluid bed pyrolysis pilot plant. Figure adapted from [15].	<b>134</b>
<b>6.1</b>	Fractionation scheme for tobacco bio-oil.	<b>149</b>
<b>6.2</b>	A graph of the effect of pyrolysis temperature on the diameter of growth inhibition for the three affected microorganism species and bio-oil yield.	<b>157</b>

<b>6.3</b>	A graph of the measured diameters of inhibition for three microorganisms by the six tobacco bio-oil fractions.	<b>159</b>
<b>6.4</b>	GC-MS chromatograms for the six tobacco bio-oil fractions tested on the microorganisms.	<b>160</b>
<b>6.5</b>	A graph of the diameters of inhibition for the initial fraction, Fraction Z and the active, terminal fraction, Fraction M.	<b>162</b>
<b>6.6</b>	GC-MS chromatogram of Fraction M.	<b>163</b>
<b>6.7</b>	A graph showing the diameters of inhibition for the bacteria <i>C. michiganensis</i> and <i>S. scabies</i> , and the level of inhibition for the fungus, <i>P. ultimum</i> from ten chemical standards.	<b>166</b>
<b>6.8</b>	A graph showing the diameters of inhibition for <i>C. michiganensis</i> , <i>S. scabies</i> , and <i>P. ultimum</i> from the standard chemical mixture.	<b>167</b>
<b>6.9</b>	Photographs of a packed C18 column for a solid phase extraction technique on tobacco Fraction M.	<b>171</b>
<b>6.10</b>	Chromatograms of Fraction M before (A) and after (B) solid phase extraction with methanol.	<b>172</b>
<b>6.11</b>	GC-MS chromatograms and corresponding microorganism growth on Fraction M after solid phase extraction and heating for 0 min (A), 50 min (B), and 90 min (C).	<b>173</b>
<b>6.12</b>	GC-MS chromatograms of flash chromatography samples generated from Fraction M.	<b>175</b>
<b>6.13</b>	A graph showing the activity of the sample containing the peak of interest, sample of remaining fractions, sample combining all fractions, and Fraction M before separation.	<b>176</b>

- 6.14** A graph showing the average percent growth over multiple microwell assays of Fraction M fractions after SPE, separation by flash chromatography, and heating at 65 °C. **177**
- 6.15** Histogram showing the number of compounds identified by AMDIS from various fractions with and without sample derivatization. **179**
- 6.16** Mass spectrum isolated from Fraction 10 at 38.68 min (A) and the mass spectrum of Duvatriene from the NIST 2005 library (B). **181**
- 6.17** Mass spectrum isolated from Fraction 10 at 14.62 min (A) and the mass spectrum of methenamine from the NIST 2005 library (B). **182**

# List of Equations

Equation	Description	Page
1.1	$P = V I$	6
1.2	$N = \frac{\mu_e E l}{2 D}$	6
1.3	$v = \mu_e E$	7
1.4	$F_E = E q$	7
1.5	$F_F = -6 \pi \eta r v$	7
1.6	$\mu_e = \frac{q}{6 \pi \eta r}$	7
1.7	$\mu_{EOF} = \frac{\varepsilon \zeta}{\eta}$	9
1.8	$V = I R$	11
1.9	$E = J \sigma^{-1}$	11
2.1	$\frac{m_+^{\alpha} c_+^{\alpha}}{\kappa^{\alpha}} - \frac{m_-^{\beta} c_-^{\beta}}{\kappa^{\beta}} = v^{\alpha\beta} (c_+^{\alpha} - c_-^{\beta})$	44

## List of Abbreviations

ACN	Acetonitrile
AMDIS	Automated Mass Spectral Deconvolution and Identification System
BGE	Background electrolyte
BOA	Benzoic acid
BTMA	Benzyltrimethylammonium
BYA	Benzylamine
C18	Octadecyl reversed phase
ca.	Circa, around
CAF-IEF	Carrier ampholyte free isoelectric focusing
CE	Capillary electrophoresis
CHES	2-(Cyclohexylamino)ethanesulfonic acid
CHCA	$\alpha$ -cyano-4-hydroxycinnamic acid
CPB	Colorado Potato Beetle
CTAB	Cetyltrimethyl/tetradecyltrimethyl ammonium bromide
CZE	Capillary zone electrophoresis
Da	Dalton (1 Da = 1 atomic mass standard)
DDAB	didodecyldimethylammonium bromide
DHB	2,5-dihydroxybenzoic acid
DLPC	1,2-dilauroyl- <i>sn</i> -glycero-3-phosphocholine
DTT	Dithiothreitol
DTG	Differential thermogravimetric analysis
E	Electric field
EOF	Electroosmotic flow
ESI	Electrospray ionization
FASS	Field amplified sample stacking
FESI/FASI	Field enhanced/amplified sample injection
FTIF	Fourier transform infrared spectroscopy
GC-MS	Gas chromatography mass spectrometry
HPLC	High performance liquid chromatography

I	Current
i.d.	Inner diameter
IMAC	Immobilized metal affinity chromatography
ITP	Isotachopheresis
J	Current density
LD <sub>50</sub>	Median lethal dose
LE	Leading electrolyte
LVSS	Large-volume sample stacking
MALDI	Matrix assisted laser desorption ionization
MeOH	Methanol
MES	2-( <i>N</i> -morpholino)ethanesulfonic acid
min	Minutes
MO	Mesityl oxide
MRB	Moving reaction boundary
MS	Mass spectrometry
m/z	Mass to charge ratio
NIST	National Institute of Standards and Technology
NRB	Neutralization reaction boundary
o.d.	Outer diameter
PBS	Phosphate Buffered Saline
pI	Isoelectric point
pKa	Acid ionization constant
PP	Phenyl phosphate
PTM	Posttranslational modification
R	Resistance
s	Seconds
SDS-PAGE	Sodium dodecyl sulphate polyacrylamide gel electrophoresis
SPE	Solid phase extraction
TBS	TRIS Buffered Saline
TE	Terminating electrolyte
TFA	Trifluoroacetic acid



TG	Thermogravimetric analysis
TMS	Trimethylsilyl
TOF	Time-of-flight
TRIS	Tris(hydroxymethyl)aminomethane
TSB	Tryptic soy broth
UV-vis	Ultra violet visible
V	Voltage
$\sigma$	Conductivity

# Preface

Two unique classes of compounds are analyzed in this thesis, but a unifying theme is woven throughout of miniaturized method development for the isolation and identification of analytes from complex samples. These two projects complement each other to demonstrate the broad field of analytical chemistry applications, but also the common goals fractionation from complex backgrounds for successful detection by mass spectrometry. Miniaturized techniques allow limited volume samples to be successfully analyzed as well as reduce the amount of waste materials. The goal of this thesis is to develop miniaturized sample preparation techniques for the identification of analytes of interest from complex backgrounds. The opening chapter provides the background information to biological sample analysis with capillary electrophoresis to prepare the reader for the following three data chapters which cover miniaturized method development with CE to prepare proteins and peptides for MS detection. Chapter 2 and 3 discuss the extensions of the discontinuous buffers enrichment technique for the removal of permanently charged ions and buffering ions, respectively. The final CE method development chapter, Chapter 4, incorporates magnetic beads into the capillary for specific isolation of phosphorylated peptides. Chapter 5 brings the transition to bio-oil as the complex matrix with pesticide chemicals as the analyte of interest. This chapter introduces the reader to the developing field of bio-oil generation, analysis, and applications. Chapter 6 explores bio-oil as a potential source for valuable chemicals through a series of analytical techniques using mass spectrometry for the detection of pesticide chemicals in bio-oil. Thus, the common theme of miniaturized method development for the fractionation of analytes of interest for successful detection is developed on two diverse sample groups.

# Chapter 1: Introduction to Capillary Electrophoresis as a Sample Preparation Tool for Mass Spectrometry Analysis of Proteins and Peptides

---

Reproduced in part with permission from **C.J. Booker**, S. Sun, S. Woolsey, J.S. Mejia & K.K.-C. Yeung. Removal of sample background buffering ions and myoglobin enrichment via a pH junction created by discontinuous buffer in capillary electrophoresis, *Journal of Chromatography A*, **2011**, 1218, 5705-5711. Copyright (2011) Elsevier.

Reproduced in part with permission from **C.J. Booker** & K.K.C. Yeung. In-Capillary Protein Enrichment and Removal of Nonbuffering Salts Using Capillary Electrophoresis with Discontinuous Buffers, *Analytical Chemistry*, **2008**, 80, 8598-8604. Copyright (2008) American Chemical Society.

## 1.1 Proteins and Peptides

Proteins are the tools that perform almost all of the functions inside living cells. Such vital functions include metabolism and defence mechanisms. Thus, the expression levels of certain proteins are an excellent method for early disease detection and many biomarkers are currently being identified. These large molecules are formed from long, meticulously folded sequences of amino acids. Peptides are simply short chains of amino acids, fragments of a protein. This primary structure of amino acids is dictated by the cell's DNA sequence, which is transcribed into RNA, processed into messenger RNA, and finally translated into the protein. Alas, the genome alone cannot determine the existence, abundance, or structure of all the proteins in living systems. Post translational modifications (PTMs) can activate or deactivate a protein and currently, this process cannot be predicted from the genome. The number of genes identified through the Human Genome Project was only 20 000 to 25 000 [1], but the number of unique proteins in the human body is far greater due to posttranslational modifications and alternate splicing. Many proteins have yet to be identified. The identification and characterization of the proteins in living creatures is an extremely complex field, including isolation and sequencing, protein-protein interactions, modifications, function, and protein localization [2]. This broad field is termed proteomics, and many analytical methods are being designed to advance the understanding in this field [3].

One challenge involving protein analysis is the wide dynamic range of protein expression in biological systems. Proteins range from 10 to 1,000,000 copies per cell. The ability to identify low abundance proteins will make a significant impact on our understanding of how biological systems function as well as the identification of significant biomarkers. Separation methods exist to remove the high abundance proteins, and many methods are being developed to enrich the low abundance proteins so that these molecules can be detected. The purpose of the following chapters is to develop miniaturized methods to enrich and isolate low abundance proteins and peptides from contaminating matrices for enhanced MS detection.

Key separation techniques rely on the isoelectric point of the protein. Most amino acid residues are neutral, in that they do not take on charge in acidic or basic solutions. However, some amino acid residues, as well as the C-terminal and N-terminal of each peptide, can lose a proton in alkaline solutions or gain a proton in acidic solutions. Each protein or peptide thus has its own isoelectric point (pI). The isoelectric point is the pH value of a solution where the protein has no overall charge. This does not mean that there are no charges on the protein, but that the positive and negative charges sum to zero. At pH values greater than the pI, a protein will carry a negative overall charge, while the opposite is true in solutions of lower pH values. This property can be exploited to separate proteins.

Two dimensional gel electrophoresis is the most common technique to separate many proteins in a complex biological sample as it has the ability to resolve thousands of proteins. Electrophoresis is based on the differential movement of solutes in an applied electric field. The first dimension is isoelectric focusing and is based upon separation of the proteins by their isoelectric point during voltage application. In the second dimension, SDS-PAGE (sodium dodecyl sulphate polyacrylamide gel electrophoresis) is often performed. Although electrophoresis separates analytes based on their charge-to-size ratio, the SDS adheres to the molecules at a constant ratio so that the protein's overall charge is proportional to its size. Hence, the gel acts as a size sieve while the electric field causes the proteins to move down through the gel according to their molecular weight. The gel can then be stained using Coomassie<sup>TM</sup> Blue or silver stain to visualize the spots and the spots can be removed and digested. In this way, two dimensional gel electrophoresis separates proteins based on both their isoelectric point and their size. Although this method is widely used, it suffers from poor reproducibility, overlapping protein bands, and sensitivity limitations. Even so, the resultant peptides can be analyzed using mass spectrometry (MS) and the peptide mass-to-charge ratios can be compared to a database to identify the original proteins. These peptides can also be analyzed using tandem mass spectrometry to determine the sequence of a novel protein of interest.

The development of mass spectrometry with soft ionization techniques has caused an explosion of discoveries in the proteomics field, allowing for the detection and

sequencing of proteins at lower concentrations and even detection of post translational modifications. Previously, mass spectrometry employed hard ionization techniques, such as electron impact ionization, that were extremely effective with small molecules but were not successful with large biological molecules. Electron impact MS is often performed in sequence with gas chromatography, and this type of mass spectrometry is used to analyze chemicals in bio-oil in Chapter 6. To ionize the analytes, the already volatile molecules are exposed to a beam of electrons which can remove an electron from the analyte. The excess energy from the electron removal leads to a set pattern of fragmentation to the molecule and the resultant fragments are measured according to their charge-to-size ratio. This “mass fingerprint” can be compared to established libraries of spectra to identify the analyte. This method does not work for larger molecules, however, as the analyte must already be volatile (in gaseous state), which is not feasible for proteins, and the fragmentation is too extensive for successful identification.

In contrast to electron impact ionization, Matrix Assisted Laser Desorption Ionization (MALDI) is a soft ionization technique which leads to little fragmentation, if any, and also vaporizes the intact sample into a gaseous state. MALDI was first introduced in 1988 [4] and has become a popular and robust technique for protein and peptide analysis [5,6]. A matrix molecule that can absorb the laser light (often 337 nm) is co-crystallized with the analyte. This dried sample spot on a target plate is then placed in a vacuum and irradiated with a short pulse of laser. The matrix molecules transfer the laser energy to the analyte molecules by ionizing the analyte (adding or removing a proton) and desorbing the sample into gaseous phase. This process leads to a charged, intact protein or peptide in gaseous state, and this is the method of choice for analysis of proteins and peptides in this thesis.

A second soft ionization technique is electrospray ionization (ESI) and this method allows for a continuous flow of liquid sample into the mass spectrometer at atmospheric pressure [7]. Highly charged droplets are generated by the application of voltage to the needle tip (or capillary tip) from which the analyte is sprayed. Through evaporation and fission, highly charged gas phase ions are generated. In this case, the analyte often collects multiple charges per molecule and a large distribution of peaks is observed for proteins and peptides, in contrast to MALDI where a singly charged molecular ion is

most common. ESI is also routinely used for protein and peptide analysis [8], and is easily interfaced on-line with liquid phase separation techniques, such as HPLC or CE [9,10].

For both ionization techniques, the analyte is detected by its mass to charge ratio through a mass analyzer. A few mass analyzers are currently used in the proteomics field, including the time-of-flight (TOF), and orbitrap. Ions can be selected for sequencing analysis from a mixture by having two mass analyzers in tandem, the first to select, the second to detect (MS/MS). An ion gate and a collision cell separate the two mass analyzers. Examples include a TOF-TOF and QTrap. The TOF analyzer was used for analysis in this thesis and can detect large proteins (6000 to >100 000 Da) in linear mode as well as smaller proteins and peptides (400 to 6000 Da) in reflectron mode. The increased flight length allows for greater time and distance to resolve the analytes. The direction reversal in the reflector by voltage compensates for the slightly different kinetic energies amongst ions of the same mass to charge. Reflectron mode thus leads to greater resolution for smaller analytes, with a typical resolution value of 20 000 and a mass accuracy of 2 to 50 ppm.

Mass spectrometry is a revolutionary tool for identifying large biological molecules. Even with this powerful technique however, suitable sample preparation is still required. The most abundant proteins must be removed (such as albumin), and the least abundant proteins must often be enriched for successful detection. Biological samples also contain other contaminating molecules, such as salts and buffering ions, which can suppress the mass spectral detection and therefore should also be removed during sample preparation. MS analysis only requires nano to microliter volume samples and so the development of sample preparation methods on this scale should improve the detection capabilities for analytes that only exist at low abundance. Chapter 2 and 3 examine the removal of contaminating ions using a miniaturized enrichment technique to enhance the detection of low abundance compounds. Chapter 4 examines a different miniaturized enrichment technique for the specific isolation of phosphorylated peptides to enhance the detection of these lower abundance, post-translationally modified peptides. These method developments are built on the miniaturized capabilities of capillary electrophoresis.

## 1.2 Capillary Electrophoresis

Capillary electrophoresis (CE) augments basic gel electrophoresis into a greater analytical separation tool through automation, high applied electric fields, shorter analysis times, and easier detection methods. This method is most commonly known for its separation capabilities, but is now also being investigated as a sample preparation technique for subsequent mass spectral analysis.

Capillaries are long, narrow tubes, usually made of silica, with inner diameters (i.d.) of 25 to 100  $\mu\text{m}$ . Lengths of these capillaries for typical experiments range from 25 to over 100 cm. Capillaries have extremely high surface area to volume ratios. This allows for excellent dissipation of heat. Heat generation is related to the power (P) in an electrical system, and power is based upon the applied voltage (V) and resultant current (I).

$$P = V I \quad (\text{Equation 1.1})$$

High voltages (5000 – 30,000 V) are thus commonly applied to capillaries without causing excessive heat formation. Experiments can also be performed in short time intervals (minutes) due to the application of higher electric fields (E, in  $\text{V cm}^{-1}$ ) as compared to slab gel electrophoresis where experiments take hours. The ability to apply such high voltages leads to exceptionally high plate numbers, as the plate number is directly related to the applied electric field,

$$N = \frac{\mu_e E l}{2 D} \quad (\text{Equation 1.2})$$

where  $\mu_e$  is the electrophoretic mobility of the ion,  $l$  is the effective length of the capillary (to the on-line detector), and  $D$  is the diffusion coefficient of the analyte. This diffusion coefficient is a property of the analyte and cannot be adjusted, but the extent of diffusion can be minimized by having fast separations through high applied voltages.

Usually, the capillary is filled with a buffer solution and a vial of buffer is placed at each end of the capillary. The sample is usually injected (hydro-dynamically or electro-



kinetically) as a small plug of ions at the inlet of the capillary. Detection for CE is simple, as this can be performed on-line, most commonly by a UV-visible absorbance detector. CE is reproducible and can be automated. A simple schematic of a CE set-up is shown in Figure 1.1.

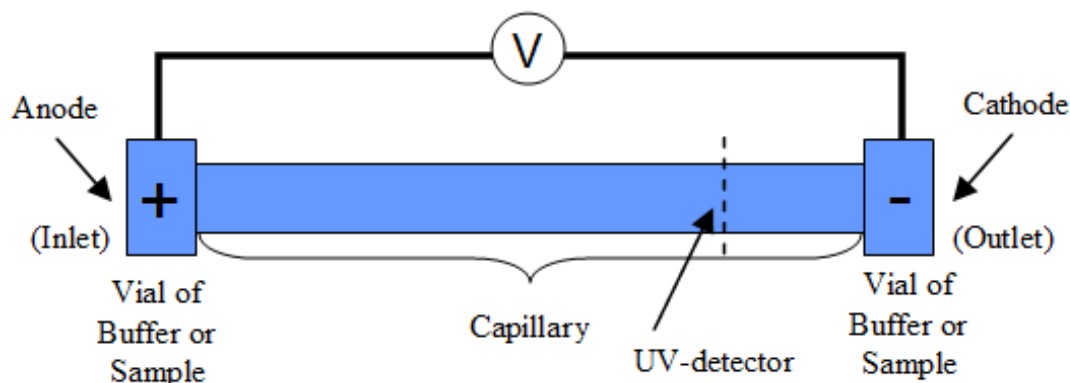


**Figure 1.1.** Simple schematic of CE set-up.

The velocity ( $v$ ) of the ions in CE is due to the electrophoretic mobility ( $\mu_e$ ) and applied electric field ( $E$ ).

$$v = \mu_e E \quad (\text{Equation 1.3})$$

The mobility of each ion in the capillary is determined by the electric force ( $F_E$ ) applied on the ion and the opposite friction force ( $F_F$ ) from the solution,

$$F_E = E q \quad (\text{Equation 1.4})$$

$$F_F = -6 \pi \eta r v \quad (\text{Equation 1.5})$$

where  $q$  is the ion charge,  $r$  is the ion radius, and  $\eta$  is the solution viscosity. These two force equations can be combined with Equation 1.3 to yield the final electrophoretic mobility equation.

$$\mu_e = \frac{q}{6 \pi \eta r} \quad (\text{Equation 1.6})$$

Accordingly, larger ions move slower through the capillary than smaller ions, while molecules with greater charge move faster than molecules with lower charge. Ions are separated by their charge to size ratio in conventional capillary zone electrophoresis (CZE).

The most unique component of CE is the creation of the electro-osmotic flow (EOF). The silanol groups forming the inner wall of the capillary are easily ionized from SiOH to SiO<sup>-</sup> at a pH greater than 3. This creates a stationary area of negative charge over the entire inner surface of the capillary. When the capillary is filled with a solution, positive ions from the solution gather around the negatively charged capillary wall to maintain charge balance (Figure 1.2 A). The inner Stern layer of positive charges remains stationary. However, upon voltage application, the build-up of hydrated, positive ions in the diffuse layer moves towards the cathode, dragging along the bulk solution. This creates a flat profile of flow (Figure 1.2 B), as opposed to the laminar flow observed in chromatography methods when pressure is used to drive the flow of the solution (Figure 1.2 C). A flat flow profile yields sharper peaks.

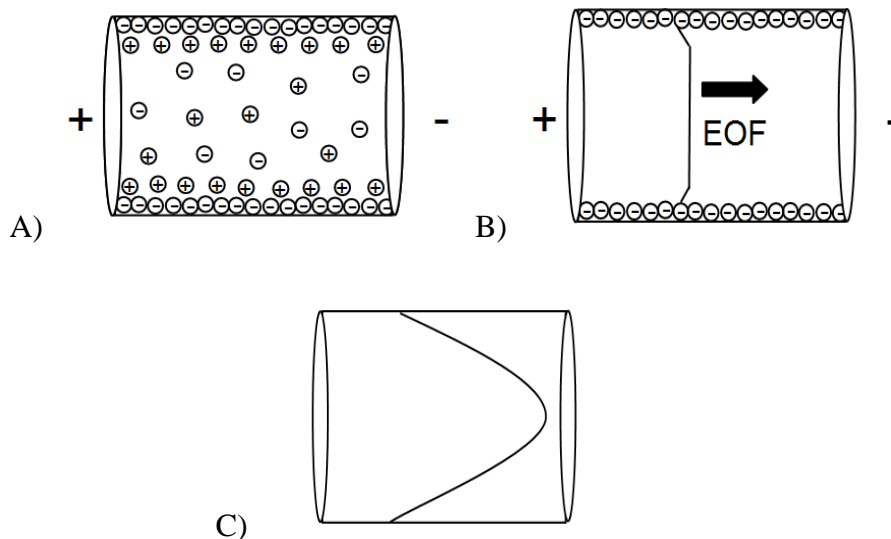


**Figure 1.2.** Schematics showing EOF formation (A) and EOF flow profile (B), as opposed to laminar flow profile (C).

The magnitude of the electroosmotic mobility can be explained theoretically through the following equation,

$$\mu_{\text{EOF}} = \frac{\varepsilon \zeta}{\eta} \quad (\text{Equation 1.7})$$

where  $\varepsilon$  is the dielectric constant and  $\zeta$  is the zeta potential. The zeta potential is a function of the charge on the inner capillary wall, which is related to the pH of the buffer solution (which determines the extent of silanol ionization on the inner capillary wall) and to the ionic strength of the buffer solution (which generates a shielding effect of the wall charge). As the buffer pH decreases, the extent of ionization decreases leading to a slower EOF. As the ionic strength of the buffer solution increases, the zeta potential decreases, also leading to a slower EOF.

Although this electroosmotic flow allows for incredibly sharp peaks during analysis compared to laminar flow, this bulk flow of solution can be too fast and cause the contents in the capillary to be carried out of the capillary in a matter of seconds. For analyses that require longer separation or reaction times, the inner capillary wall can be modified to suppress the EOF. Modifications to the inner capillary wall also solve a second, even more significant problem in CE, which is the adsorption of some samples to the capillary wall. The negative charge on the capillary wall can cause adsorption of proteins and peptides to the wall, which decreases the sample recovery and can also cause peak tailing. A variety of coatings have been proposed to overcome both issues. They include permanent, covalently bonded coatings based on polymers [11,12] and surfactant-based dynamic [13,14] and semi-permanent [15] coatings. Dynamic coatings are based upon a reversible adsorption of the additive to the capillary wall and require the additive to be present in the running buffer, while semi-permanent coatings are more stable and only require the additive molecule to be flushed through the capillary and the excess can be flushed away before each experiment. Permanent coatings are ideal in that the adsorption and EOF problems can be solved in one process before the analysis experiments begin. However, it is difficult to synthesize a reproducible, stable permanent coating with the preferred EOF properties. Many options exist for dynamic coatings, which allows for exact manipulation of the EOF for each experimental run. CTAB,

cetyltrimethyl (or tetradecyltrimethyl) ammonium bromide is one of the most common surfactants for a dynamic coating and consists of a polar head group and long hydrophilic tail that forms micelles in solution [16]. The drawback to this selection of coating modification, however, is that the modifying molecule must be present in the running buffer of each experiment. These surfactants can interfere with the mobility of the analyte and the subsequent mass spectral analysis. The final option currently available is the semi-permanent coating that can be flushed through the capillary before each experimental run, but does not need to be present in the running buffer.

Lucy and colleagues have developed a variety of coatings, most notably some semi-permanent coatings [15,17]. They have explained that the change that makes these semi-permanent coatings more stable than traditional dynamic coatings is the utilization of molecules that have a double chain hydrophobic tail, in contrast to the dynamic coatings that only have one tail [17]. This changes the shape of the molecule from cylindrical to cone-shaped, and thus the formation of a bilayer is preferred over the formation of micelles. A now common example is didodecyldimethylammonium bromide (DDAB) that has the same polar headgroup as CTAB, but is much more stable with its double-chained tail. A limitation to this coating is that DDAB can only generate a cationic surface for cationic protein separations [17]. The most popular article from Lucy's research team, currently referenced 118 times in the literature, is that of their phospholipid bilayer coating that has a double chained tail, 1,2-dilauroyl-*sn*-glycero-3-phosphocholine (DLPC). The novel feature of this semi-permanent coating is the zwitterionic headgroup, in contrast to a cationic headgroup (CTAB, DDAB), which allows for both anionic and cationic separations [15]. It is this phospholipid bilayer coating that was used to reduce protein adsorption and suppress the EOF for the experiments presented in this thesis. Semi-permanent coatings allow for subsequent MS analysis, although some minor bleeding of the surfactant can occur. Efforts to improve the stability of semi-permanent coatings include cross-linking the tails of a phospholipid bilayer coating, termed oligomerized bilayers [18], and optimizing the coating solution properties of buffer selection [19], ion additives, such as  $\text{Ca}^{2+}$  [15,20] and the concentration of the surfactant [20]. Although the literature demonstrates impressive EOF stability over multiple runs with semi-permanent coatings, typical experiments display

EOF variability from run to run, which can lead to challenges in experimental reproducibility. Further research continues into the ideal coating for CE.

## 1.3 Sample Preparation with Capillary Electrophoresis

Capillary electrophoresis has been established as an effective analytical separation tool for a wide variety of analytes, ranging from small inorganic ions to biological macromolecules [21-24]. In some cases, inorganic ions and DNA for instance, CE has become the industry's method of choice. However, developments in CE remain largely in the proof-of-principle stage in regard to protein analysis.

The wide dynamic range of protein expression leads to the fact that many proteins, especially ones with post-translational modifications, exist at such low abundance that they are difficult to detect. To add to this problem, the volume of a capillary is very small. For example, a capillary 48 cm long with an i.d. of 50  $\mu\text{m}$  has an internal volume of less than 1  $\mu\text{L}$ . In conventional CE, a sample plug is less than 1 cm long, making a typical injection volume less than 20 nL. In addition, although CE has convenient on-line detection by UV-visible absorbance, the short path length of the inner diameter of the capillary makes detection of low abundance components extremely difficult. Given these problems, an on-line enrichment step must be in place to allow for detection of all components.

Many clever enrichment techniques have been developed for the analysis of proteins with CE. The simplest and most common on-line enrichment technique is stacking [25,26]. Stacking is based on the following equations; Ohm's law, and the continuum of Ohm's law;

$$V = I R \quad (\text{Equation 1.8})$$

$$E = J \sigma^{-1} \quad (\text{Equation 1.9})$$

where voltage is  $V$ , current is  $I$ , resistance is  $R$ , current density is  $J$ , conductivity is  $\sigma$ , and electric field is  $E$ . The principle of stacking (Figure 1.3 A) is based on a reduction in the analyte mobility across the boundary between the sample plug (low  $\sigma$ , high  $E$ ) and the separation electrolyte (high  $\sigma$ , low  $E$ ). The ions move quickly through the sample zone (high  $E$ ) but slow down and stack at the interface (low  $E$  begins). This leads to a reduction in the length of the sample zone, which enriches the analyte molecules. This form of stacking is very widely used in CE and can be referred to as field amplified sample stacking (FASS) or large-volume sample stacking (LVSS) [27], depending upon the size of the sample plug [28,29]. In LVSS, the sample plug can be up to a full capillary in length, but this size is limited by the mobility of the analytes, as the analytes must reach the sample/buffer interface while this temporary boundary remains sharp. Typical injection lengths are one third of a capillary volume. Electrokinetic sample injection combined with the principles of FASS (field enhanced/amplified sample injection, FESI/FASI) has been successfully applied on proteins and peptides for enrichment prior to separation and MS detection [30,31]. However, these stacking techniques require the sample to be prepared in low conductivity, thus limiting their direct application on real samples of biological origin.

Stacking need not rely upon changes in conductivity. Stacking can also occur between solutions of different pH. The property of conductivity can be paralleled to the protein analyte charge based on the pH of the solution. The proteins may carry positive charge in one solution, but carry negative charge after passing the interface between the solutions. This interface is termed the pH junction. When the charge of an analyte changes, its direction reverses and the analyte moves towards the opposite electrode (Figure 1.3 B). These methods are generally referred to as pH-mediated sample stacking [29] and enrichment factors in the thousand-range have been reported for peptides and proteins [31,32]. Since these methods rely on pH changes rather than conductivity changes between solutions, these methods are more favourable towards samples that contain biological salts and will be discussed in the following chapters.

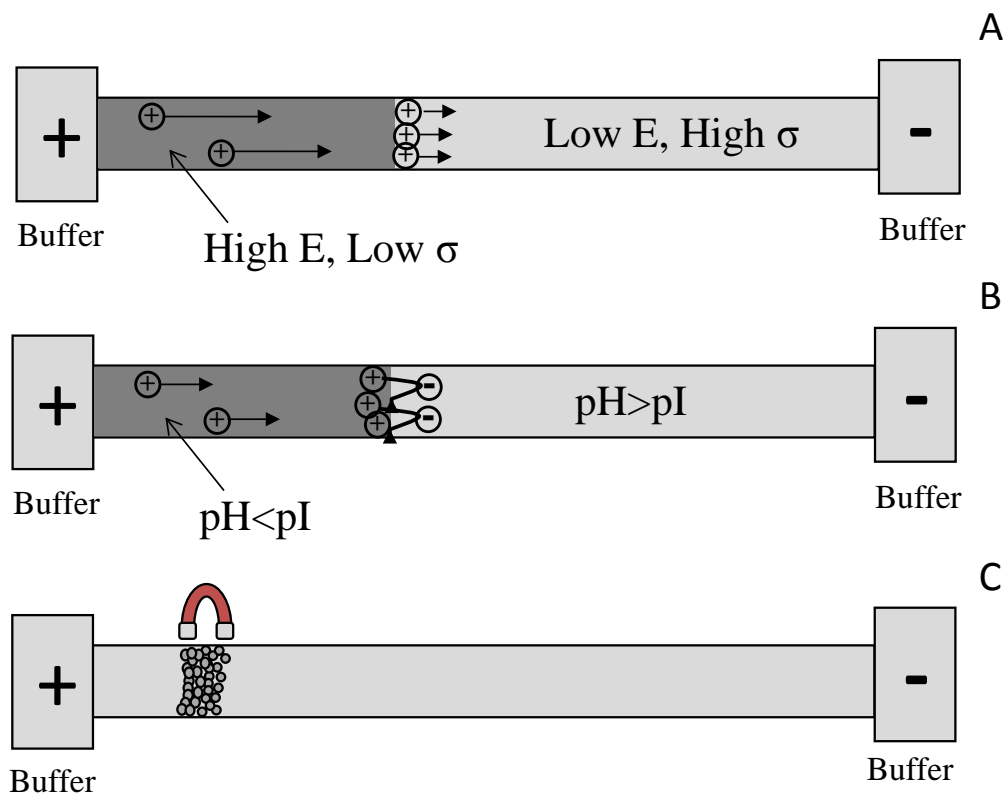


**Figure 1.3.** Schematics showing analyte stacking based on a change in conductivity (A), change in pH (B), and addition of solid phase (C).

Sample stacking can also occur with the addition of solid phase (Figure 1.3 C). A miniaturized packed column can be coupled to the capillary for salt removal and concurrent enrichment prior to separation with CE [33]. Using an on-line plug of magnetized solid phase collected in the capillary by an external magnet is a new, emerging field that also has many opportunities and is discussed in Section 1.5.

Finally, sample preconcentration can also be conducted in CE *via* transient isotachopheresis (ITP) [34] which falls between these stacking techniques based on conductivity and pH changes. With ITP, the sample molecules are compressed between a leading electrolyte containing ions of highest mobility and a terminating electrolyte containing ions of lowest mobility [35-37]. Samples containing salt can be successfully enriched, but judicious attention must be paid to the selection of electrolytes for each specific sample [38-40].

Enrichment is essential for effective CE analysis of protein samples, but a second issue has been noted and must also be addressed before CE can be used for successful protein experiments. Biological samples not only contain proteins, but also other ions, such as salt and buffering ions that increase the ionic strength of the sample. This complex matrix increases conductivity in regions of the capillary which can lead to Joule heating and band-broadening. Joule heating is caused by high levels of electrical current and voltage. Localized increases in heat cause changes in solvent viscosity and thus unequal changes in the mobilities of the ions. Band-broadening results. High heat can also cause gas bubble formation in the capillary, temporarily inhibiting the flow of current. Therefore, it is imperative that Joule heating be controlled. Band-broadening can also result from electrodispersion, essentially the differential movement of ions in changing conductivity zones and this is also due to the presence of salts. The background matrix ions can also lead to ionization suppression in subsequent mass spectral analysis [41]. Salt ions cause broader analyte peaks in MS analysis which reduces the intensity and thus the sensitivity of detection.

Enrichment and sample clean-up have been investigated to avoid these issues of Joule heating, band-broadening, and detection suppression. Methods that focus on manipulating the pH of buffer solutions (such as pH mediated sample stacking) are not as hindered with high ionic strength samples as compared to conductivity based techniques, as contaminating salt affects the conductivity of solutions more than their pH. For example, a dynamic pH junction was designed by Britz-McKibbin *et al.* where a short-lived pH junction was established between two buffers, one acidic, one basic. A sample of nucleic acids was enriched, even in the presence of salt [42]. Monton *et al.* then adapted this pH junction method for protein enrichment demonstrating a 124-fold amplified analyte signal [43]. This method however, as most other methods do, only allowed for a small injection of sample. This limits the sample capacity and enrichment capabilities.

A prolonged pH junction has been reported by our research group using discontinuous buffers that allows for an entire capillary of sample to be enriched [44]. A similar approach was also reported by Pospíchal and coworkers, named carrier ampholyte



free isoelectric focusing (CAF-IEF) [45,46], and was also later applied to the enrichment of proteins [47]. Despite the differences in configuration, both of these approaches were described and generalized as examples of sample stacking by moving neutralization reaction boundary (NRB) in a review by Cao *et al.* [48]. In both of these methods, a pH junction is established between two buffers and is maintained by a neutralization reaction. The amount of  $H^+$  and  $OH^-$  reacting to form water is miniscule compared to the water already in the aqueous buffering solutions. This pH junction can be maintained during an entire experiment.

## **1.4 Discontinuous Buffers - a Response to Enrichment Problems in CE**

Recently our research group designed a method to create a prolonged pH junction for the enrichment of submicroliter volume, intact proteins. Enrichment factors of over 1000-fold were reported [44]. The discontinuous buffer system used for protein enrichment consisted of two buffers, an acidic buffer and a basic buffer. The buffers were chosen to provide sufficiently constant concentrations of  $OH^-$  and  $H^+$  and little buffer capacity at neutral pH. The term “discontinuous buffers” was given due to the fact that each buffer had exclusive pH regions of buffering capacity and no buffering capacity existed at the interface between the buffers. Previous data demonstrated that the width of the enriched protein band was predominately controlled by the steepness of the pH gradient between the discontinuous buffers, which in turn was determined by the choice of buffers [49]. The buffers used for this method were not the traditional arrangement of buffers that consists of the buffer and a non-buffering counter ion; e.g., sodium acetate or ammonium chloride. In order to adjust the pH values of these buffers, and not introduce any new ions (with unique mobilities) to the system, the discontinuous buffers were prepared only with ammonium hydroxide and acetic acid, one as the buffering ion, the other as the counter ion. The “ammonium buffer” (with acetate as the counter ion) was prepared with 10 mM ammonium hydroxide (pKa 9.25), using acetate as the counter ion to adjust the pH to

9.75. The “acetate buffer” (with ammonium as counter ion) was prepared in a similar manner, with 10 mM acetic acid and ammonium as the counter ion to adjust the pH to 4.25. In the narrow capillary, the surface area of interaction between the discontinuous buffers was very small. Upon voltage application, this pH junction was sustained during the entire experiment by the  $\text{OH}^-$  and  $\text{H}^+$  fluxes respectively from the catholyte and anolyte, and this neutralization reaction has given this pH junction the name, Neutralization Reaction Boundary (NRB) [48].

Under normal CE conditions, the EOF would flush the contents out of the capillary in a matter of minutes if the buffer was acidic, or even in seconds if the buffer was basic. However, the inner-capillary wall for our discontinuous buffers system was modified with the semi-permanent, zwitterionic, phospholipid bilayer coating, DLPC, which suppressed the EOF allowing the pH junction to remain in the capillary for well over ten minutes. Since the coating was zwitterionic, neither cationic nor anionic analytes were retained on the wall. Under basic conditions with the zwitterionic coating, the EOF was cathodic (towards the cathode) but slow, while under acidic conditions, the EOF was reversed, but with an even slower mobility. A schematic of a typical experiment with discontinuous buffers is displayed in Figure 1.4 and began with an entire capillary filled with the basic buffer. A slow, forward EOF was observed. As the bulk solution moved towards the cathode, the acidic buffer was drawn into the capillary, leading to an even greater suppression of the forward EOF. The pH junction passed the detector before the slow forward effect under the basic conditions balanced the even slower, reversed effect of the acidic conditions. The net result was a suppressed EOF that allowed for prolonged enrichment and carried the pH junction past the detector.

When amphoteric molecules, such as proteins, with isoelectric points between the two buffer pH values (i.e.  $4.25 > \text{pI} > 9.75$ ) were introduced, they possessed opposite net charges on either side of the neutralization reaction boundary, and as a result were trapped and enriched at the pH junction. The experimental design is depicted in Figure 1.4 A using myoglobin as a model protein (pI 7). Myoglobin was prepared in the ammonium buffer and was injected to fill the entire capillary (internal volume of 0.95  $\mu\text{L}$ ). In contrast to a small sample plug of traditional CE enrichment techniques,

discontinuous buffers allows an entire capillary full of sample to be enriched. The sample loading is not even limited to one capillary volume, as it has been demonstrated that the sample can be prepared in both the ammonium and acetate buffers, (filling the capillary and in the reservoir vials) leading to 2000-fold enrichment [49]. When the acidic and basic buffers were placed at the anode and cathode, respectively, a sharp pH junction was formed at the interface between the acetate buffer reservoir and the myoglobin-ammonium buffer at the capillary inlet (Figure 1.4 A). Proteins stacked at this pH junction as zwitterions (Figure 1.4 B). A cathodic, suppressed EOF slowly pushed the entire capillary content forward towards the detector (Figure 1.4 C). Thus, an entire capillary full of sample was enriched into a sharp band which was mobilized by the EOF to the detector.

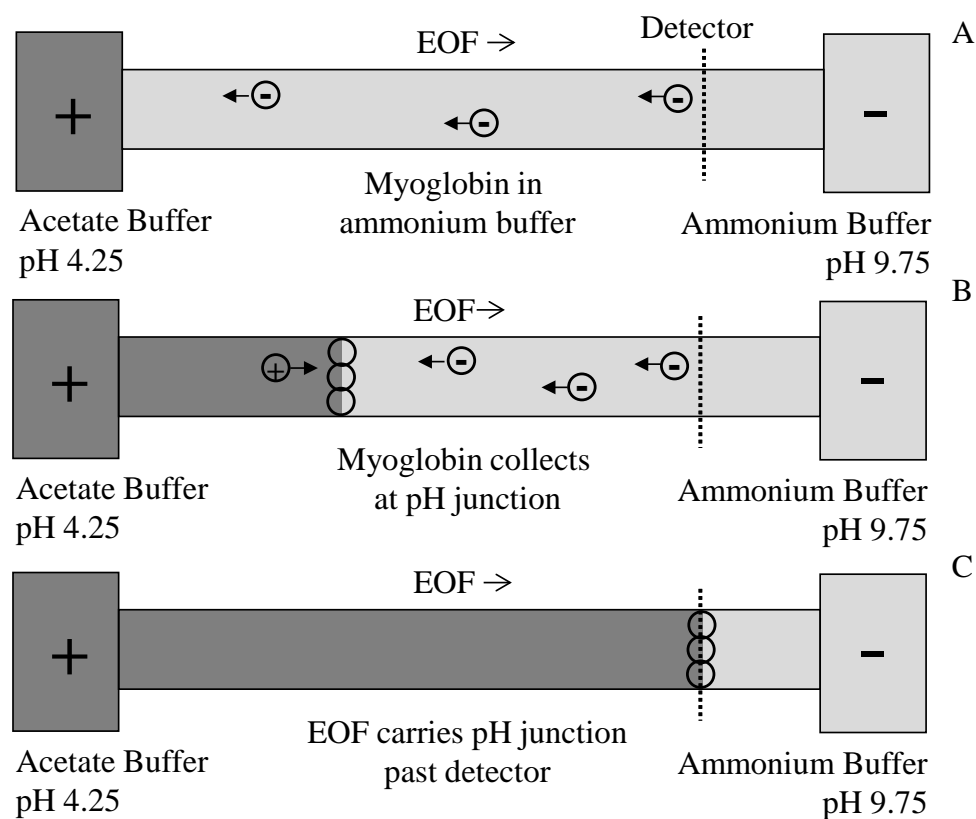


**Figure 1.4.** Schematic of protein enrichment using discontinuous buffers. A step-pH junction was created by acetate and ammonium under voltage application. The myoglobin molecules (circles) inside the capillary electromigrated either as cations (in acetate) or anions (in ammonium) toward the junction and were trapped at the junction.

Until this point, discontinuous buffer experiments were conducted with pre-purified protein standards, free of contaminating salts [44,49,50]. Thus, to prepare this discontinuous buffer method for real biological samples, the effect of the background matrix, such as ionic salts and buffering ions, must be investigated. The challenges and successful adaptation of discontinuous buffers to samples containing these contaminating ions are discussed in the following two chapters.

## **1.5 Magnetic Beads – a Response for Specific Isolation of Analytes in CE**

Although discontinuous buffers is an adaptable technique, this method does possess limitations that required the integration of new methodologies. The method of discontinuous buffers is based on the assumption that the analyte possesses an isoelectric point between the pH values of the acidic and basic buffer. The active pH range can be extended by using different buffers, but an inherent limitation exists in the stability of the DLPC coating (pH range 3-10 [15]) and the stability of the capillary (silica begins to dissolve above pH 10). In addition to the isoelectric point limitation, the end result of an enriched, purified protein band can only be in one or both of the discontinuous buffers. This limits the sample recovery options. An astute solution is to incorporate magnetic beads into the capillary, which allows for specific capture, enrichment, and clean-up for a wider range of peptides. Background information on the use of magnetic beads and the developments explored by the author are discussed in Chapter 4.

Capillary electrophoresis is an excellent tool for sample separation and is becoming an excellent tool for sample preparation. Proteomics is an expanding and challenging field that requires method development that can reach its unique demands. Enrichment of low abundance proteins, selective enrichment of modified peptides, and removal of contaminating ions for successful sample preparation, separation and mass spectral detection is required. The following chapters discuss the investigations into using

discontinuous buffers as a sample preparation technique as well as using magnetic beads within the capillary for selective sample enrichment and clean-up.

## 1.6 References

- [1] L.D. Stein. Human genome - End of the beginning, *Nature*, **2004**, *431*, 915-916.
- [2] P.R. Graves & T.A.J. Haystead. Molecular Biologist's Guide to Proteomics, *Microbiology and Molecular Biology Reviews*, **2002**, *66*, 39-63.
- [3] Z.B. Ning, H. Zhou, F.J. Wang, M. Abu-Farha & D. Figeys. Analytical Aspects of Proteomics: 2009-2010, *Analytical Chemistry*, **2011**, *83*, 4407-4426.
- [4] M. Karas & F. Hillenkamp. Laser desorption ionization of proteins with molecular masses exceeding 10000 daltons, *Analytical Chemistry*, **1988**, *60*, 2299-2301.
- [5] R. Haselberg, G.J. de Jong & G.W. Somsen. Capillary electrophoresis-mass spectrometry for the analysis of intact proteins 2007-2010, *Electrophoresis*, **2011**, *32*, 66-82.
- [6] A. Armirotti & G. Damonte. Achievements and perspectives of top-down proteomics, *Proteomics*, **2010**, *10*, 3566-3576.
- [7] J.B. Fenn, M. Mann, C.K. Meng, S.F. Wong & C.M. Whitehouse. Electrospray ionization for mass-spectrometry of large biomolecules, *Science*, **1989**, *246*, 64-71.
- [8] P. Liuni & D.J. Wilson. Understanding and optimizing electrospray ionization techniques for proteomic analysis, *Expert Review of Proteomics*, **2011**, *8*, 197-209.
- [9] C. Desiderio, D.V. Rossetti, F. Iavarone, I. Messina & M. Castagnola. Capillary electrophoresis-mass spectrometry: Recent trends in clinical proteomics, *Journal of Pharmaceutical and Biomedical Analysis*, **2010**, *53*, 1161-1169.
- [10] A.L. Capriotti, C. Cavaliere, P. Foglia, R. Samperi & A. Lagana. Intact protein separation by chromatographic and/or electrophoretic techniques for top-down proteomics, *Journal of Chromatography A*, **2011**, *1218*, 8760-8776.
- [11] H. Wan, M. Ohman & L.G. Blomberg. Bonded dimethylacrylamide as a permanent coating for capillary electrophoresis, *Journal of Chromatography A*, **2001**, *924*, 59-70.
- [12] S. Hjerten. High-Performance Electrophoresis - Elimination Of Electroendosmosis And Solute Adsorption, *Journal Of Chromatography*, **1985**, *347*, 191-198.

- [13] Q. Liu, Y.Q. Li, F. Tang, L. Ding & S.Z. Yao. Cationic gemini surfactant as dynamic coating in CE for the control of EOF and wall adsorption, *Electrophoresis*, **2007**, 28, 2275-2282.
- [14] N.E. Baryla & C.A. Lucy. Simultaneous separation of cationic and anionic proteins using zwitterionic surfactants in capillary electrophoresis, *Analytical Chemistry*, **2000**, 72, 2280-2284.
- [15] J.M. Cunliffe, N.E. Baryla & C.A. Lucy. Phospholipid bilayer coatings for the separation of proteins in capillary electrophoresis, *Analytical Chemistry*, **2002**, 74, 776-783.
- [16] N.E. Baryla, J.E. Melanson, M.T. McDermott & C.A. Lucy. Characterization of surfactant coatings in capillary electrophoresis by atomic force microscopy, *Analytical Chemistry*, **2001**, 73, 4558-4565.
- [17] J.E. Melanson, N.E. Baryla & C.A. Lucy. Double-chained surfactants for semipermanent wall coatings in capillary electrophoresis, *Analytical Chemistry*, **2000**, 72, 4110-4114.
- [18] C.Z. Wang & C.A. Lucy. Oligomerized phospholipid bilayers as semipermanent coatings in capillary electrophoresis, *Analytical Chemistry*, **2005**, 77, 2015-2021.
- [19] M.D. Gulcev & C.A. Lucy. Effect of coating electrolytes on two-tailed surfactant bilayer coatings in capillary electrophoresis, *Analytica Chimica Acta*, **2011**, 690, 116-121.
- [20] M.D. Gulcev & C.A. Lucy. Factors affecting the behavior and effectiveness of phospholipid bilayer coatings for capillary electrophoretic separations of basic proteins, *Analytical Chemistry*, **2008**, 80, 1806-1812.
- [21] F. Kvasnicka. Application of CE in hydrodynamically closed system for analysis of bioactive compounds in food, *Electrophoresis*, **2007**, 28, 3581-3589.
- [22] M. Sniehotta, E. Schiffer, P. Zurbig, J. Novak & H. Mischak. CE - a multifunctional application for clinical diagnosis, *Electrophoresis*, **2007**, 28, 1407-1417.
- [23] Y. Li, X.B. Yin & X.P. Yan. Recent advances in on-line coupling of capillary electrophoresis to atomic absorption and fluorescence spectrometry for speciation analysis and studies of metal-biomolecule interactions, *Analytica Chimica Acta*, **2008**, 615, 105-114.
- [24] V. Garcia-Canas & A. Cifuentes. Recent advances in the application of capillary electromigration methods for food analysis, *Electrophoresis*, **2008**, 29, 294-309.

- [25] Z.K. Shihabi & Z. Deyl. Preconcentration and sample enrichment techniques - Preface, *Journal of Chromatography A*, **2000**, 902, 1-1.
- [26] J.L. Beckers & P. Bocek. Sample stacking in capillary zone electrophoresis: Principles, advantages and limitations, *Electrophoresis*, **2000**, 21, 2747-2767.
- [27] M.S. Chun, D. Kang, Y. Kim & D. Chung. Protein analysis with large volume sample stacking with an electrosmotic flow pump: a potential approach for proteomics, *Microchemical Journal*, **2001**, 70, 247-253.
- [28] M.C. Breadmore. Recent advances in enhancing the sensitivity of electrophoresis and electrochromatography in capillaries and microchips, *Electrophoresis*, **2007**, 28, 254-281.
- [29] D.M. Osbourn, D.J. Weiss & C.E. Lunte. On-line preconcentration methods for capillary electrophoresis, *Electrophoresis*, **2000**, 21, 2768-2779.
- [30] Y.Z. Yang, R.I. Boysen & M.T.W. Hearn. Optimization of field-amplified sample injection for analysis of peptides by capillary electrophoresis-mass spectrometry, *Analytical Chemistry*, **2006**, 78, 4752-4758.
- [31] M.R.N. Monton & S. Terabe. Field-enhanced sample injection for high-sensitivity analysis of peptides and proteins in capillary electrophoresis-mass spectrometry, *Journal of Chromatography A*, **2004**, 1032, 203-211.
- [32] W.S. Law, J.H. Zhao & S.F.Y. Li. On-line sample enrichment for the determination of proteins by capillary zone electrophoresis with poly(vinyl alcohol)-coated bubble cell capillaries, *Electrophoresis*, **2005**, 26, 3486-3494.
- [33] F.W.A. Tempels, W.J.M. Underberg, G.W. Somsen & G.J. de Jong. Design and applications of coupled SPE-CE, *Electrophoresis*, **2008**, 29, 108-128.
- [34] P. Gebauer & P. Bocek. Recent progress in capillary isotachopheresis, *Electrophoresis*, **2000**, 21, 3898-3904.
- [35] P. Gebauer & P. Boček. Recent progress in capillary isotachopheresis, *Electrophoresis*, **2000**, 21, 3898-3904.
- [36] J. Petr, V. Maier, J. Horáková, J. Ševčík & Z. Stránský. Capillary isotachopheresis from the student point of view - images and the reality, *Journal of Separation Science*, **2006**, 29, 2705-2715.
- [37] B. Jung, R. Bharadwaj & J.G. Santiago. On-chip millionfold sample stacking using transient isotachopheresis, *Analytical Chemistry*, **2006**, 78, 2319-2327.
- [38] Z.K. Shihabi. Transient pseudo-isotachopheresis for sample concentration in capillary electrophoresis, *Electrophoresis*, **2002**, 23, 1612-1617.



- [39] C.A. Nesbitt, H.X. Zhang & K.K.C. Yeung. Recent applications of capillary electrophoresis-mass spectrometry (CE-MS): CE performing functions beyond separation, *Analytica Chimica Acta*, **2008**, 627, 3-24.
- [40] A.R. Timerbaev & T. Hirokawa. Recent advances of transient isotachopheresis-capillary electrophoresis in the analysis of small ions from high-conductivity matrices, *Electrophoresis*, **2006**, 27, 323-340.
- [41] T.M. Annesley. Ion Suppression in Mass Spectrometry, *Clinical Chemistry*, **2003**, 49, 1041-1044.
- [42] P. Britz-McKibbin, G.M. Bebault & D.D.Y. Chen. Velocity-difference induced focusing of nucleotides in capillary electrophoresis with a dynamic pH junction, *Analytical Chemistry*, **2000**, 72, 1729-1735.
- [43] M.R.N. Monton, K. Imami, M. Nakanishi, J.B. Kim & S. Terabe. Dynamic pH junction technique for on-line preconcentration of peptides in capillary electrophoresis, *Journal of Chromatography A*, **2005**, 1079, 266-273.
- [44] C.A. Nesbitt, J.T.M. Lo & K.K.C. Yeung. Over 1000-fold protein preconcentration for microliter-volume samples at a pH junction using capillary electrophoresis, *Journal of Chromatography A*, **2005**, 1073, 175-180.
- [45] J. Pospíchal & E. Glovinová. Analytical aspects of carrier ampholyte-free isoelectric focusing, *Journal of Chromatography A*, **2001**, 918, 195-203.
- [46] J. Pospíchal, J. Chmelík & M. Deml. Micropreparative Focusing of Proteins in Carrier-Ampholyte-Free Solution with Electrically Controlled Compositions of Electrolytes, *Journal of Microcolumn Separations*, **1995**, 7, 213-219.
- [47] J. Budilová, J. Pazourek, P. Krásenský & J. Pospíchal. Continuous mode of operation for large volume dosing in analytical carrier ampholyte-free isoelectric focusing of proteins applied to off-line detection of fractions, *Journal of Separation Science*, **2006**, 29, 1613-1621.
- [48] C.X. Cao, L.Y. Fan & W. Zhang. Review on the theory of moving reaction boundary, electromigration reaction methods and applications in isoelectric focusing and sample pre-concentration, *Analyst*, **2008**, 133, 1139-1157.
- [49] K. Jurcic, C.A. Nesbitt & K.K.C. Yeung. Characterization of discontinuous buffer junctions using pH indicators in capillary electrophoresis for protein preconcentration, *Journal of Chromatography A*, **2006**, 1134, 317-325.
- [50] C.A. Nesbitt, K. Jurcic & K.K.C. Yeung. Nanoliter-volume protein enrichment, tryptic digestion, and partial separation based on isoelectric points by CE for MALDI mass spectral analysis, *Electrophoresis*, **2008**, 29, 466-474.

## **Chapter 2: In-Capillary Protein Enrichment and Removal of Non-Buffering Salts using Capillary Electrophoresis with Discontinuous Buffers**

---

Reproduced in part with permission from **C.J. Booker** & K.K.C. Yeung. In-Capillary Protein Enrichment and Removal of Nonbuffering Salts Using Capillary Electrophoresis with Discontinuous Buffers, *Analytical Chemistry*, **2008**, *80*, 8598-8604. Copyright (2008) American Chemical Society.

## 2.1 Introduction

Remarkable efficiencies of over a million plates per meter have been reported using capillary electrophoresis (CE) for protein separations [1-4] but only with pre-purified protein standards prepared in solvents. At least two issues must be resolved before CE can be applied to separate proteins in real biological samples. The first challenge is the wide dynamic range of protein expression in biological systems. Given the small sample injection volume of CE, a comprehensive, on-line enrichment step must be in place to allow for sufficient injection of the low abundance components. The second challenge is the complex nature of the biological sample background. In an electrophoretic based separation, the presence of abundant ionic salts is detrimental by causing band-broadening from excessive Joule heating and/or electrodispersion. The presence of salt increases the current flow which leads to increased heat, Joule heating, and changes the conductivity in a region of the capillary which changes the analyte mobility between regions causing peak tailing or fronting, electrodispersion.

An approach to address the above two issues is the use of solid phase mini-beds coupled on-line to CE [5]. In essence, a very short chromatography column packed with reversed phase beads is connected to the CE capillary for subsequent separation. The enrichment and salt removal is based on selective retention of proteins on reversed phase materials while the salt passes through unhindered. Using UV-visible absorption detection, the limit of detection (LOD) has been lowered 100-fold to the low  $\text{ng mL}^{-1}$  level for a mixture of standard peptides [6]. On-line mass spectral detection displayed reduced matrix effects with a LOD in the  $\text{fmol mL}^{-1}$  range for a complex mixture of peptides from a protein digest [7]. The major drawbacks of this method include the need for custom fabrication of the solid phase mini-bed, the challenge being to achieve high bed-to-bed reproducibility at such small dimensions, and the requirement for alterations to the CE instrument and/or custom designed components for the coupling.

Alternative enrichment techniques free of any solid phases have also been reported for CE and were discussed in Chapter 1, namely field-amplified sample stacking, pH-

mediated sample stacking, and isotachopheresis. Background matrix removal, however, must also be addressed.

Several attempts have been reported on overcoming problems associated with high ionic strength samples. Shihabi [8] performed sample stacking in the presence of salt by using acetonitrile to reduce the conductivity of the sample zone. Acetonitrile and other small organic solvents can act as terminating ions in transient pseudo isotachopheresis, allowing the sample to be separated in the presence of salt [9]. Other methods focused on the pH manipulation of the buffer solutions to enrich samples. These pH-mediated methods were less affected by the presence of salt in samples as compared to methods that rely solely on the conductivity of different regions. An example of a pH-mediated sample stacking method was reported by Park and Lunte [10] in which they created a zone of low conductivity between the sample plug and the acidic running buffer by electrokinetically injecting a plug of strong acid after the sample plug. Titration caused the catecholamine analytes to stack, regardless of the sample salt content [10]. A seven-fold increase in peak intensity was observed with no deterioration in separation efficiency in subsequent CZE (190,000 plates) [10]. This method, however, was only performed on small molecules with high mobilities, as opposed to larger peptides or proteins that have slower mobilities. A temporary pH junction between an acidic and basic solution, as opposed to a titration zone by a strong acid injection as above, was formed in the dynamic pH junction method developed by Britz-McKibbin *et al.* [11]. An acidified sample of nucleotides containing salt was and injected onto a capillary filled with a basic buffer, creating a pH junction between the sample zone and running buffer. A 50-fold enrichment was recorded for a mixture of nucleotides from a cell extract (including the naturally occurring salt levels). This dynamic pH junction method was then applied by Monton *et al.* [12] to the enrichment and separation of peptides. A 124-fold improvement in detection was observed. It is noteworthy that such pH junctions typically dissipate early in the run, and hence the above pH-mediated methods only allow for a small injection of a sample.

In contrast, we reported the use of a discontinuous buffer in CE to create a pH junction that endured through the entire run, permitting the entire capillary to be filled

with the sample solution. The capillary in this case was coated with a zwitterionic phospholipid bilayer [4] in order to prevent protein adsorption and to suppress the electroosmotic flow (EOF). Pre-purified protein standards were used to develop the discontinuous buffers method [13-15], but the effect of ionic salts must be explored to apply this method to real biological samples. It was speculated that ions possessing permanent charges, such as sodium and chloride, should maintain their mobilities when crossing the pH junction and thus eventually migrate out of the capillary.

In this chapter, the capability of discontinuous buffers in withstanding and removing non-buffering ionic salts present in the samples is investigated. Sodium chloride and myoglobin are used as the model salt and model analyte, respectively. In addition to in-capillary experiments with UV-absorbing ions, computer simulations were explored to provide further understanding to the ion mobility at the pH junction. Identification of the enriched and desalted protein sample is performed by offline matrix-assisted laser desorption ionization mass spectrometry (MALDI MS).

Following the methodology characterization based on a single protein (myoglobin), application on a protein mixture is also performed. This work builds on the existing discontinuous buffers protein enrichment and desalting operation by incorporating a subsequent capillary zone electrophoresis (CZE) separation. This coupling requires a reconfiguration of the buffer set-up following the enrichment and desalting step. A concentrated acid is introduced to remove the pH junction, and thus allow for the CZE separation.

## 2.2 Materials and Methods

### 2.2.1 Apparatus

An Agilent <sup>3D</sup>Capillary Electrophoresis (Palo Alto, CA, USA) instrument with a direct UV-vis absorbance detector was used for all experiments. Data acquisition was handled by the Agilent <sup>3D</sup>CE ChemStation software. The dimension of all capillaries used was 50

$\mu\text{m}$  i.d. and  $364 \mu\text{m}$  o.d., with a total length of 48.5 cm and a length-to-detector of 40.0 cm. The capillary was thermostated to  $25^{\circ}\text{C}$  at all times. Uncoated fused silica capillaries were purchased from Polymicro Technologies (Phoenix, AZ, USA). A semi-permanent coating of 1,2-dilauroyl-*sn*-glycero-3-phosphocholine (DLPC) was used to modify the capillary inner wall, in order to suppress the electroosmotic flow and prevent protein adsorption [4].

Mass spectral analyses were performed on a Bruker Reflex IV MALDI time-of-flight mass spectrometer (Bremen/Leipzig, Germany) equipped with a 337 nm nitrogen laser. Video monitoring was used to direct the laser to select “hot-spots” for optimal MS signals.

### 2.2.2 Reagents

Deionized water ( $18.2 \text{ M}\Omega\cdot\text{cm}$ ) from a Millipore water purification system (Bedford, MA, USA) was used to prepare all solutions. Glacial acetic acid and ammonium hydroxide were purchased from EM Science (Gibbstown, NJ, USA) and used to make the buffer solutions. The DLPC solution was prepared by dissolving the reagent (Avanti Polar Lipids, Alabaster, AL, USA) at a concentration of 0.1 mM, in a 20 mM tris(hydroxymethyl)aminomethane (TRIS; Aldrich, St. Louis, MO, USA) and 20 mM calcium chloride (Caledon Laboratories, Georgetown, ON, Canada) aqueous solution. The pH of the TRIS buffer was adjusted to 7.2 by hydrochloric acid (EM Science Gibbstown, NJ, USA). Myoglobin from horse heart, bovine serum albumin, and  $\beta$ -lactoglobulin from bovine milk (Sigma, St. Louis, MO, USA) were used as received. Sodium chloride (EM Science) was used as the model non-buffering ions, and sodium phosphate (EM Science) was used as a model buffering ion. They were added directly to the protein solution prepared in ammonium buffer. Benzyltrimethylammonium chloride (Sigma) and sodium bromide (EM Science) were used as the UV-absorbing salts, while benzylamine (Aldrich) and benzoic acid (EM Science) were used as the UV-absorbing buffering ions.  $\alpha$ -Cyano-4-hydroxy-cinnamic acid, CHCA, was purchased from Sigma and then purified in ethanol according to the recrystallization procedure provided by

Sigma/Aldrich. Trifluoroacetic acid (TFA, Fisher Scientific), HPLC grade acetone (Fisher Scientific, Nepean, ON, Canada) and HPLC grade methanol from Caledon Laboratories were used in the CHCA matrix preparation.

### **2.2.3 Enrichment and Desalting by Discontinuous Buffers.**

Each new capillary was washed by flushing, at 1 bar, with 0.1 M NaOH for 10 min, followed by water for 10 min. The DLPC coating formation was performed by flushing (1 bar) with the DLPC solution for 20 min [4]. In between runs, the capillary was recoated by flushing (1 bar) with the DLPC solution for 10 min. For storage, the capillaries were rinsed (1 bar) with water for 10 min.

The discontinuous buffer system used for protein enrichment consisted of two buffers, an acidic acetate buffer (pH 4.25) and a basic ammonium buffer (pH 9.75). As discussed in Chapter 1, these buffers were not the traditional design of buffers with a buffering ion and simple counter ion. The acetate buffer was prepared by adding a small amount of ammonium hydroxide as the counter ion to 10 mM acetic acid until pH 4.25 was reached. This solution was thus an acetate buffer with an ammonium counter ion, and for short, was called “acetate buffer.” Likewise the ammonium buffer was prepared by adding acetic acid as counter ion to 10 mM ammonium hydroxide. This buffer was an ammonium buffer with an acetate counter ion, and referred to as the “ammonium buffer.” Proteins, at concentrations from 1 to 100 ng  $\mu\text{L}^{-1}$ , were prepared in the 10 mM ammonium buffer unless stated otherwise. Various amounts of salts were also added to this protein solution to study the effect of non-buffering salts on the enrichment process.

The discontinuous buffers protein enrichment was conducted as follows. First, the capillary was filled with the protein sample solution in ammonium buffer by rinsing at 1 bar for 1 min. Then voltage was applied with the acidic buffer placed at the anode and the basic buffer at the cathode. Depending of the amount of sodium chloride present in the sample, the voltage was adjusted to avoid Joule heating due to the excess current flowing

through the capillary. Generally, the voltage was limited to 30 kV and the current was limited to 40  $\mu$ A. The current was monitored and recorded during voltage application.

Unless otherwise stated, the capillary end with the absorbance detection window was placed at the cathode and the absorbance was monitored to determine the arrival of the pH junction and the enriched proteins. The presence of salt in the sample was later found to reduce the magnitude of the electroosmotic flow in the DLPC-modified capillary to near-zero. Hence, application of low pressure (20 mbar) was used when necessary to mobilize the pH junction toward the detection window. At this point, the proteins at the pH junction were ready for either deposition on the MALDI MS sample target plate or reconfiguration that facilitates subsequent CZE separation.

#### **2.2.4 MALDI Mass Spectral Analyses**

To fraction collect the enriched protein band on the MALDI MS target plate, all voltage and pressure applications were suspended for approximately 1 min after the pH junction passed the detection point. This extra minute allowed further mobilization of the protein band to the capillary end. The cathodic end of the capillary was repositioned to outside of the instrument, as described previously [13]. Pressure (50 mbar) was applied at the anodic end to push the capillary content out for deposition on the MALDI MS target plate. The deposition frequency was 20 s, which resulted in a volume of approximately 40 nL. Typically 10 sample spots were collected to ensure capture of the protein band.

Four layers of CHCA matrix were pre-deposited on the target plate, prior to deposition from the capillary as the final layer. The first CHCA layer was 0.350  $\mu$ L of 5 mg mL<sup>-1</sup> CHCA in acetone and methanol (4:1), followed by the three layers of 0.200  $\mu$ L saturated CHCA solution in water/methanol (3:2, v/v) and 0.1% TFA. The multiple layers of CHCA and TFA were required to neutralize sample fractions that contain basic buffer, and in turn improve the MS signals.

All MS spectra were acquired in positive ion, linear mode. The voltage settings were left at the preset instrument default settings. Each MS spectrum shown is a sum of



100 laser shots, collected by multiples of two. Igor Pro software (WaveMetrics, Lake Oswego, OR, USA) was used to process the data for presentation.

### **2.2.5 CZE of Enriched Protein Mixture**

In this experiment, detection windows were created at both ends of the capillary, both at 8.5 cm from the ends. The enriched protein band was first detected after traveling 40 cm in length toward the cathode (outlet) under constant voltage application (30 kV). Then the voltage was suspended and pressure (30 mbar) was applied for 135s to push the protein band close to the end of the capillary (outlet). Next, the capillary was reversed in direction, such that the protein band was at the inlet end. Both buffer solutions were replaced with 100 mM acetic acid (measured pH 2.7). The voltage was resumed (30 kV) and the proteins were separated by CZE as they electromigrated towards the second detection window at 40-cm from the inlet.

### **2.2.6 Computer Simulations**

The pH junction formation during discontinuous buffers was investigated using Simul 5.0, a free, on-line simulation program developed by Gas and colleagues, found at <http://web.natur.cuni.cz/~gas/Simul50.exe> [16]. Computer simulations were employed to provide further insight into the ion mobility at the pH junction. This computer simulation software was specifically designed for CE applications and has been incorporated into studies on isotachopheresis [17], isoelectric trapping [18], transient isotachopheresis with a dynamic pH junction to predict the separation of analytes [19], and has been discussed in a review by Thormann *et al.* [20]. A variety of pH junction techniques have also been investigated with this simulation tool, including a dynamic pH junction by Britz-McKibbin *et al.* [21,22] and a neutralization reaction boundary by Vitcova *et al.* [23]. In Simul 5.0, a series of partial differential equations in time and one-dimensional space account for the electromigration (including analyte charge and mobility), diffusion, and bulk flow of each species in solution. These equations also incorporate the principles of

electroneutrality and equilibria for the dissociation-association of weak electrolytes and ampholytes to predict the concentration of each species in the capillary at each time point [16].

To visualize our discontinuous buffers process with Simul 5.0, the pH junction was established in the middle of the capillary with the ammonium and acetate buffers input as the leading and terminating electrolytes, respectively. The capillary length was reduced 10 fold (48.5 cm to 48.5 mm) to allow for faster simulations. To maintain the effective electric field strength so that the ion movement for one experimental centimetre correlated to one simulated, the actual field strength was also reduced by a factor of ten (i.e., the voltage was adjusted from 30 kV to 300 V). The leading electrolyte (LE) was input as 10 mM ammonium adjusted with 2.33 mM acetate to a final pH value of 4.25. Similarly, the terminating electrolyte (TE) was 10 mM acetate adjusted with 2.33 mM ammonium to a final pH value of 9.75. Myoglobin analyte was added to the simulation program by inputting the number and  $pK_a$  values of the basic and acidic amino acids in myoglobin. The  $pK_a$  values used for myoglobin were 3.5 (C-terminal), 3.9 (aspartic acid), 4.1 (histidine), 8.0 (N-terminal), 10.5 (tyrosine and lysine) and 12.5 (arginine). Simulations involving the UV-absorbing buffer benzylamine had the leading electrolyte as 5 mM benzylamine (2 mM acetate, pH 9.50) and 5 mM acetate (1.75 mM benzylamine, pH 4.50). Salt plugs were input as analyte ions, with a sample plug length and location as indicated in the figures. Peak edge was input as 0.1 mm, the capillary diameter as 50  $\mu\text{m}$ , and the temperature as 25  $^{\circ}\text{C}$ . All other parameters were left at the default values.

## 2.3 Results and Discussion

In conventional CZE separation, it is advantageous to prepare samples at ionic strengths lower than that of the separation background electrolyte (BGE). This causes a higher electrical field to be established within the sample zone compared to the rest of the capillary. The analyte molecules therefore experience a reduction in mobility as they leave the sample zone, resulting in stacking as discussed in Section 1.3. By the same mechanism, the opposite of stacking will occur to induce band broadening when the ionic strength of the sample is higher than that of the BGE.

The effect of salt is less predictable in a discontinuous buffer system. In this case, the electromigration and isoelectric trapping of proteins is primarily controlled by the pH changes across the buffer junction. Previous data demonstrated that the width of the enriched protein band was predominately controlled by the steepness of the pH gradient, which in turn was determined by the choice of discontinuous buffers [15]. Non-buffering ions are therefore not expected to play a major role in defining the width of the enriched protein band. Nevertheless, the presence of ionic salts should result in a higher current and additional Joule heating. In the following study, experiments were performed to determine how the higher ionic strength would affect the formation of the pH junction, and to monitor the migration of non-buffering salt ions in the capillary as the run progressed.

### 2.3.1 Effect of Non-buffering Salt on Protein Enrichment by Discontinuous Buffers

The discontinuous buffer combination of pH 4.25 acetate and pH 9.75 ammonium, both at 10 mM, was previously determined to be very effective in the isoelectric trapping enrichment of a model protein, myoglobin (pI 7.2) [14,15]. The experiment was set up as depicted in Figure 2.1 A. Myoglobin was prepared in the ammonium buffer, which was injected to fill the entire capillary (internal volume of 0.95  $\mu\text{L}$ ) at the beginning of the run. The application of constant voltage (30 kV) commenced with the acetate and ammonium buffers positioned respectively at the anodic and cathodic ends of the

capillary. Formation of the pH junction began at the interface between the acetate buffer reservoir and the myoglobin-ammonium buffer at the capillary inlet.

At the early stage of enrichment, the DLPC-coated capillary was primarily occupied by the pH 9.75 ammonium (Figure 2.1 A). The EOF independently measured in this buffer was ca.  $+1 \times 10^{-4} \text{ cm}^2 \text{ V}^{-1}\text{s}^{-1}$ . This cathodic, suppressed EOF slowly pushed the entire capillary content forward, drawing the pH 4.25 acetate buffer into the capillary from the inlet reservoir. However, the EOF independently measured in pH 4.25 acetate was reversed in direction (anodic), though with a much lower mobility of  $< 1 \times 10^{-5} \text{ cm}^2 \text{ V}^{-1}\text{s}^{-1}$ . As a result, the cathodic suppressed EOF gradually reduced in magnitude as the experiment progressed (Figure 2.1 B). In this case, the EOF alone was still sufficient to carry the pH junction with the enriched protein past the on-capillary detection window in approximately 27 min. The UV-absorbance signal recorded at 200 nm is presented as Figure 2.1 C. In addition, the current was recorded to reveal conductivity changes inside the capillary during the enrichment (Figure 2.1 D). A gradual, asymptotic current drop, from 7 to 4  $\mu\text{A}$ , was observed. These two numbers respectively corresponded to the current recorded when the capillary was filled entirely with pH 9.75 ammonium buffer and with pH 4.25 acetate buffer.

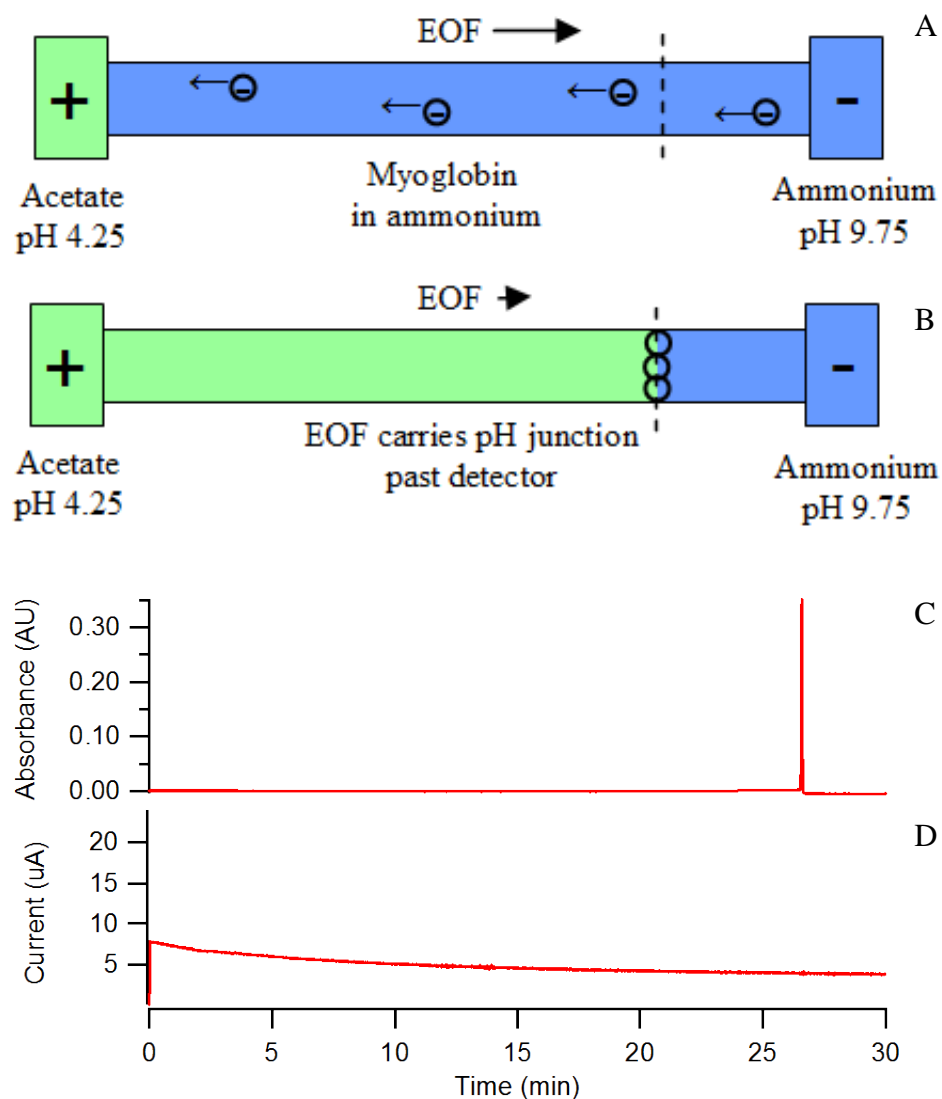


**Figure 2.1.** Schematics and electropherograms of protein enrichment using discontinuous buffers without addition of salt. Myoglobin,  $10 \text{ ng } \mu\text{L}^{-1}$ , was prepared in  $10 \text{ mM}$  ammonium buffer and filled the capillary (A). The pH junction formed and the proteins were enriched (B). The enriched protein band was detected at  $200 \text{ nm}$  (C). Current recorded during the run (D). Conditions:  $10 \text{ mM}$  discontinuous buffers at reservoirs, pH  $9.75$  ammonium (cathode) and pH  $4.25$  acetate (anode); Voltage  $30 \text{ kV}$ .

To determine the effect of non-buffering salt, the experiment was repeated with a myoglobin sample prepared in 10 mM pH 9.75 ammonium buffer, with 10 mM of NaCl (Figure 2.2 A). In this case, the enriched myoglobin peak was not observed after 40 min of voltage application (Figure 2.2 C). Hence, a small pressure (20 mbar) was used to assist the mobilization. A small amount of voltage was kept (5 kV) to maintain the pH junction formation and thus minimize the band-broadening due to laminar flow [14,15]. The low voltage was selected to avoid the creation of a significant reversed EOF during pressure mobilization, in what was now a mostly acetate buffer-containing capillary.

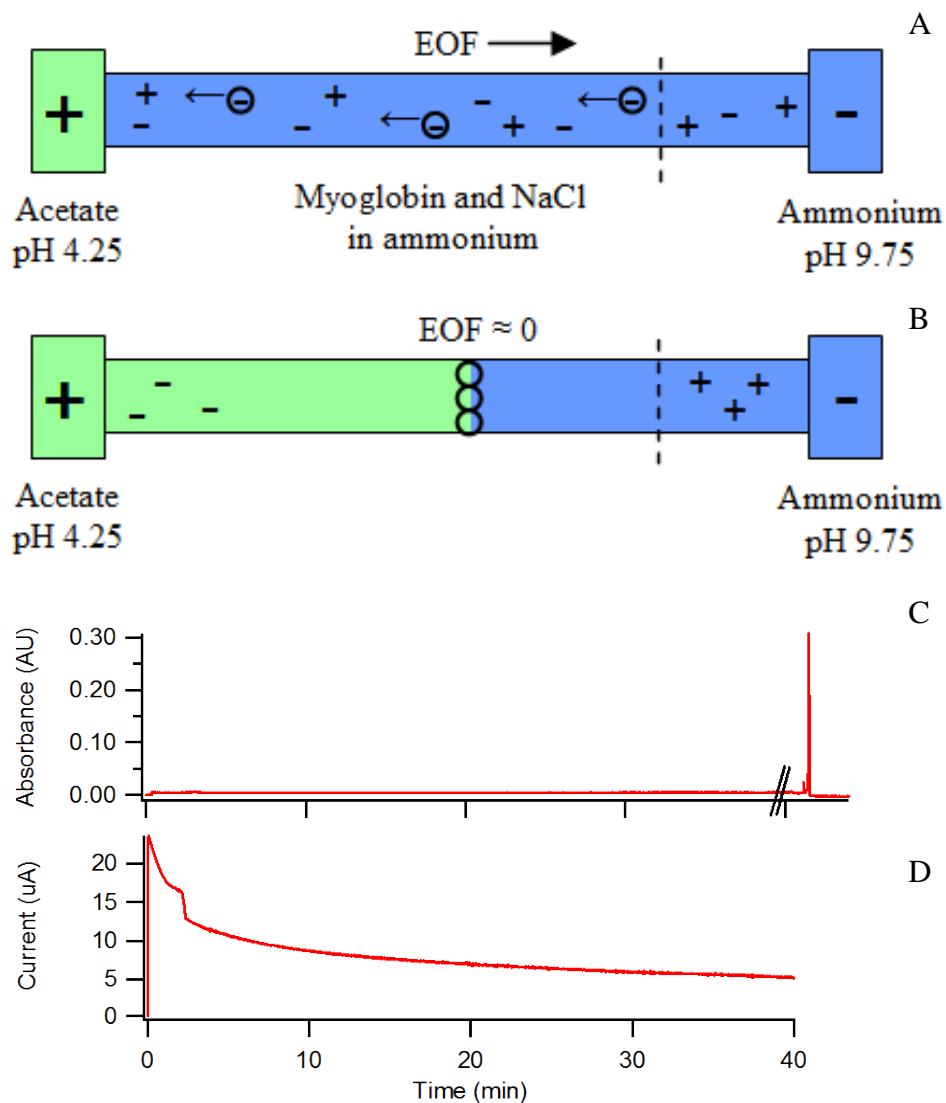


**Figure 2.2.** Schematics and electropherograms of protein enrichment of  $10 \text{ ng } \mu\text{L}^{-1}$  myoglobin in the presence  $10 \text{ mM}$  salt using discontinuous buffers. Sample was prepared in  $10 \text{ mM}$  ammonium buffer and filled the capillary (A). Proteins enriched at the pH junction while the permanent ions moved towards the oppositely charged electrodes (B). Absorbance at  $200 \text{ nm}$  (C) and current (D) recorded during run. Constant voltage ( $30 \text{ kV}$ ) was applied during the first  $40 \text{ min}$ . After  $40 \text{ min}$ , voltage was reduced to  $5 \text{ kV}$  and pressure ( $20 \text{ mbar}$ ) was applied simultaneously. Conditions otherwise the same as Figure 2.1.

The delayed detection of the enriched protein peak in Figure 2.2 C was caused by a reduction in EOF due to the presence of NaCl. EOF reduction resulting from an increased ionic strength is well documented in the literature, for both bare silica [24-26] and dynamically coated [27] capillaries. In this case, the already weak cathodic EOF was further suppressed by NaCl. Since the mobilization of the pH junction by the EOF occurred mostly in the initial stage of the run, when the capillary was primarily filled with the ammonium buffer, pressure was required to push the enriched proteins past the detector positioned near the capillary outlet.

The current profile was also recorded during protein enrichment in the presence of NaCl (Figure 2.2 D). As expected, a higher initial current (23  $\mu\text{A}$ ) was observed due to the increased ionic strength in the capillary. Importantly, the current decreased as the run progressed, and the current recorded near the end of the experiment, (5  $\mu\text{A}$ ) was similar to that from a sample that did not contain any NaCl (4  $\mu\text{A}$ , Figure 2.1 D). This suggested that most of the  $\text{Na}^+$  and  $\text{Cl}^-$  ions, responsible for the high initial current, were removed from the capillary by the discontinuous buffer during enrichment. Similar decreases in current during voltage application had been reported in the desalting step of capillary isoelectric focusing [28-30].

### **2.3.2 Non-Buffering Salt Removal Evaluated by Optical Detection**

An additional noteworthy remark on Figure 2.2 D is the small sudden current drop, or a deviation from the gradual asymptotic current curve, observed at approximately 2 min. This abrupt drop in the current curve became more pronounced as we increased the NaCl concentration in the sample (data not shown). Hence, it was speculated to be related to the removal of  $\text{Na}^+$  and  $\text{Cl}^-$  ions out of the capillary. To test this hypothesis, the on-capillary UV-absorption detection was used to study the migration of salt ions during protein enrichment by discontinuous buffer.

In the first experiment (Figure 2.3 A), enrichment was performed on a myoglobin sample containing NaBr. UV-absorption at 200 nm was used to detect the presence of  $\text{Br}^-$



ions in the capillary. The anodic end was repositioned closer to the detector, as opposed to the regular inlet location, to detect the  $\text{Br}^-$  ions immediately before they exited the capillary. The capillary was initially filled with  $\text{Br}^-$ -containing sample, and thus a strong UV absorbance was recorded in the beginning of the run. Upon voltage application, the  $\text{Br}^-$  ions within the capillary electromigrated toward the anode. The back end of the  $\text{Br}^-$  plug subsequently passed the detection point positioned near the anode at approximately 2 min, resulting in a sharp drop in UV-absorbance. This roughly coincided with the drops observed in the current curves of both NaBr- and NaCl-containing samples (Figures 2.3 A and 2.2 D, respectively).

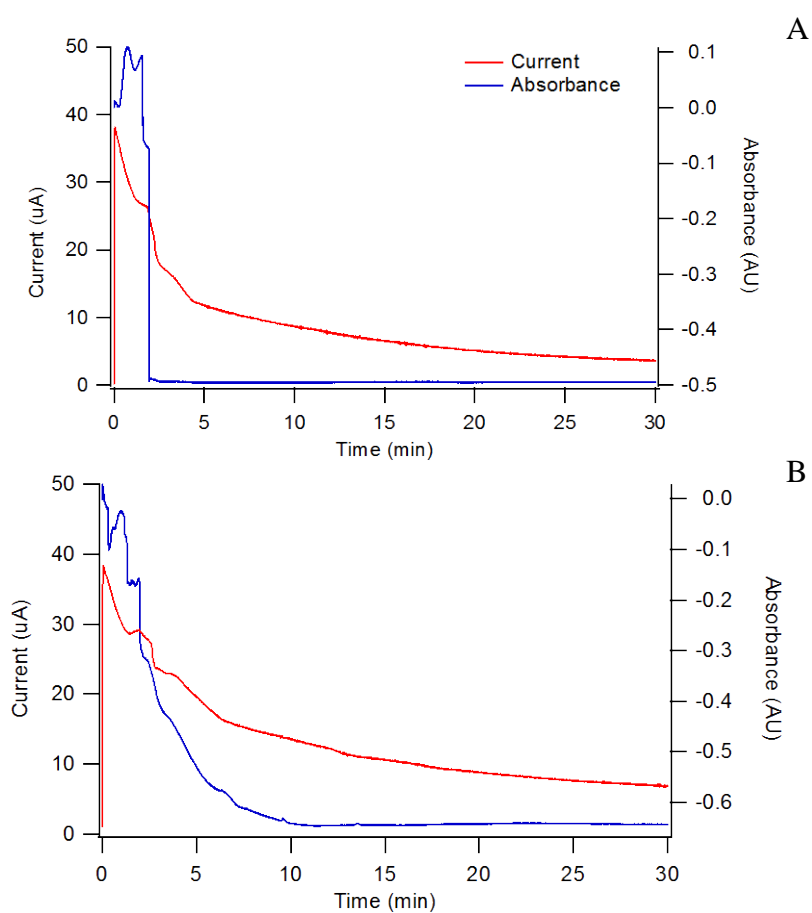


**Figure 2.3.** The absorbance (blue) and the current (red) recorded during the enrichment of myoglobin by discontinuous buffers containing 20 mM NaBr (A), or 20 mM benzyltrimethylammonium chloride (B).

Likewise, an experiment was conducted on a sample containing benzyltrimethylammonium (BTMA) chloride. The cathodic end of the capillary was relocated by the detector. In general, similar behaviour was observed, namely the majority of the UV-absorbing  $\text{BTMA}^+$  migrated past the detection window in approximately 2-3 min (Figure 2.3 B). The UV-signal drop, however, occurred more gradually in comparison to that of  $\text{Br}^-$  (Figure 2.3 A).

This tailing behaviour was attributed to electrodispersion. The conductivity of  $\text{BTMA}^+$  ( $34.6 \times 10^{-4} \text{ m}^2\text{Smol}^{-1}$ ) [31] was significantly lower than that of  $\text{NH}_4^+$  ( $73.5 \times 10^{-4} \text{ m}^2\text{Smol}^{-1}$ ) [31], the co-ion in the discontinuous buffer. As a result, electro-dispersion took place at the back end of the  $\text{BTMA}^+$  plug, causing the tailing observed in Figure 2.3 B. In contrast, the mobility of the  $\text{Br}^-$  ions ( $78.1 \times 10^{-4} \text{ m}^2\text{Smol}^{-1}$ ) [31] was faster than that of the acetate ions ( $40.9 \times 10^{-4} \text{ m}^2\text{Smol}^{-1}$ ) [31], the opposite (sharpening) occurred, and a step boundary was observed. In addition to the conductivity differences between these light-absorbing ions, the size difference caused the large,  $\text{BTMA}^+$  ions to move through the capillary at a slower rate than the smaller  $\text{Br}^-$  ions. Thus, the current for the BTMACl experiment decreased at a slower rate than the NaBr ion experiment.

Aside from these differences, the results from both experiments in Figure 2.3 indicated that effective removal of non-buffering salt ions took place within the first few minutes of protein enrichment with discontinuous buffers.

### **2.3.3 Computer Simulations and UV-absorbing Buffers: Investigations into the Ion Migration within Discontinuous Buffers**

The discontinuous buffers method has thus been shown to successfully enrich proteins even in the presence of salt, and these contaminating salt ions were removed from the capillary. Even so, it was important to determine what exactly occurred at the pH junction during the ion removal and protein enrichment. To do so, a computer simulation program with correlating experiments was employed. The following investigations were performed after the publication of the work that comprises the majority of this chapter.

This simulation program was brought to our attention by an insightful reviewer of the article [32] that comprises the next chapter, Chapter 3.

The first simulation experiments were performed to validate the method by which the pH junction was sustained during voltage application. To visualize this process, the ammonium and acetate buffers were input as the leading and terminating electrolytes, respectively. A diagram of the initial set-up of the computer simulated capillary set-up is shown in Figure 2.4 A. The ammonium ion and acetate counter ion in the leading electrolyte (ammonium LE, acetate LE) are shown as separate traces from the acetate ion and ammonium counter ion in the terminating electrolyte (acetate TE, ammonium TE) in order to explain the unique mobilities of the ions (Figure 2.4 B-D). A sharp pH junction can be visualized at 20 mm. A 10 mm plug of myoglobin was set in the ammonium buffer to the cathodic side of the pH junction (Figure 2.7 B). As was explained in Chapter 1, the isoelectric point of myoglobin is 7, resulting in an overall negative charge on the protein when prepared in the pH 9.75 buffer. The EOF was not a contributing factor in the simulation and the EOF was input as zero.

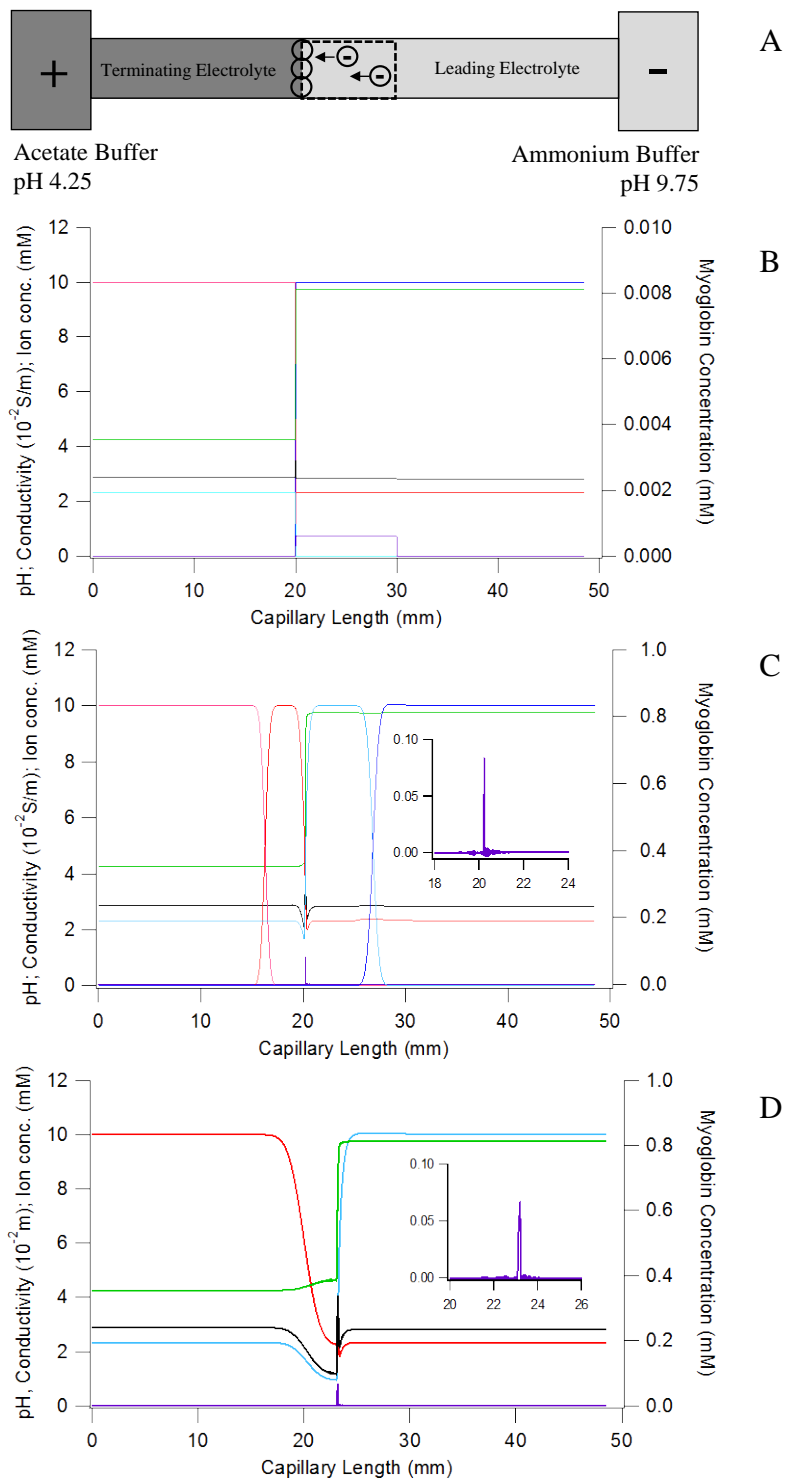


**Figure 2.4.** Simul 5.0 computer simulation of the discontinuous buffers with a plug of myoglobin ( $6 \mu\text{M}$ ) located on the basic side of the pH junction after 0 s (B), 60 s (C) and 600 s (D) of voltage: pH (—), conductivity (—), acetate terminating (—), acetate leading (—), ammonium terminating (—), ammonium leading (—) and myoglobin (—). Inset — myoglobin traces expanded. Experimental conditions can be found in Section 2.2.6.

Upon voltage application, the computer simulation showed the acetate counter ions in the leading electrolyte (red) crossing the junction towards the anode, while the acetate in the terminating electrolyte (pink) simply moved away from the pH junction towards the anode. As the acetate crossed the junction, it collected at a 10 mM concentration (Figure 2.4 B). The ammonium also moved towards its respective electrode, with the counter ions in the terminating electrolyte (light blue) crossing the junction. The mobility of ammonium ions was faster than acetate ions, which was reflected by the larger plug of ammonium TE (light blue) on the cathodic side of the pH junction compared to the plug of acetate LE (red) on the anodic side of the junction. A slight dip in the conductivity (black) was observed at the junction at 60 s, but the pH junction remained sharp and relatively stationary after one minute (inset). The plug of myoglobin was observed as a sharp peak at the pH junction, which was exactly what was observed during discontinuous buffer experiments on a full capillary of myoglobin (Figure 2.1).

After 600 s of voltage application, some surprising results were found. The most important fact remained true, that the myoglobin molecules remained tightly collected at the sharp pH junction. However, the pH junction electromigrated slightly towards the cathode, even with a zero EOF. A surface analysis could postulate that this occurred because the ammonium electromigrated towards the cathode faster than the acetate to the anode, and thus pulled the pH junction in that direction. However, this explanation is incorrect. A simulation where the acetate and ammonium mobilities were input as exactly the same still had the junction move in the cathodic direction. The correct reason for this migration was due to the balance in the flux of the  $H^+$  and  $OH^-$  ions. Protons move much faster than hydroxide ions (equivalent ionic conductivities of  $350$  and  $198 \times 10^{-4} \text{ m}^2 \text{ S mol}^{-1}$ , respectively). Since the pH values of the discontinuous buffers are equidistant from neutral, the concentration of  $H^+$  in the acetate buffer was equivalent to the concentration of  $OH^-$  in the ammonium buffer. Thus, although the concentration of ions was equal on either side of the junction, the protons had a greater mobility, and therefore, the flux of protons was greater and titrated the pH junction in the direction of the cathode.

This phenomenon has been called the moving reaction boundary (MRB) or neutralization reaction boundary (NRB) by Cao and colleagues [33]. An equation that demonstrates the pH junction movement reliance on the mobility and concentration of the buffering ions on either side of the junction was published by the above group and is shown below, where  $\alpha$  indicates the first phase (the solution on one side of the junction),  $\beta$  the second phase (opposite side of the junction),  $m$  is the constituent mobility ( $\text{m}^2 \text{V}^{-1} \text{s}^{-1}$ ),  $c$  is the constituent concentration (including all subspecies, equivalents  $\text{m}^{-3}$ ),  $\kappa$  is the specific conductivity of the solution ( $\text{S m}^{-1}$ ), and  $v$  is the displacement ( $\text{m}^3 \text{C}^{-1}$ ).

$$\frac{m_+^\alpha c_+^\alpha}{\kappa^\alpha} - \frac{m_-^\beta c_-^\beta}{\kappa^\beta} = v^{\alpha\beta} (c_+^\alpha - c_-^\beta) \quad \text{Equation 2.1}$$

A MRB was observed and the pH junction remained stable throughout this mild titration, albeit the lower pH value of the pH junction was noticeably increased. This titration was also responsible for the drop in conductivity, and hence the decreased concentration of acetate and ammonium, between the original junction (20 mm) and the new junction location at 600 s (22.7 mm). A lower conductivity translated to a higher local field strength, so the acetate ions crossing the junction electromigrated faster through that region, and thus did not collect to their full 10 mM concentration until they passed the original junction location (20 mm). Therefore, the mobility of the pH junction past the detector during the discontinuous buffers method is not solely due to the EOF, as was originally understood, but is also a factor of the MRB. The implications of this MRB are currently being explored and will be discussed later in this thesis.

After analyzing the computer simulations for typical discontinuous buffer experiments, the next step was to determine how the presence of high concentration ionic salt may affect the migration behaviour of ammonium and acetate ions. Experimental results demonstrated that ionic salts were successfully removed from the protein sample with discontinuous buffers during enrichment, as was discussed in sections 2.3.1 and 2.3.2. Removal was confirmed through the UV signals of bromide and benzyltrimethylammonium salts (Figure 2.3). The model protein enriched at the junction and the MS signals were enhanced after using discontinuous buffers (Figure 2.4).

However, when Simul 5.0 was used to simulate this process, it was found that the removal of salts was not as simple as previously understood.

Simulations suggested that as the ionic salts were removed, the buffering ions accumulated near the pH junction in their place. A time sequence computer simulation of this process with a plug of a 50 mM sodium chloride next to the junction is shown in Figure 2.5 A and B. After one minute of voltage, the sodium (purple) began to move towards the cathode and chloride (orange) to the anode. However, the ammonium (blue) and acetate (red) began to collect on either side of the salt plug as they entered the salt zone (Figure 2.5 C). This collection was due to the higher ionic strength and hence the lower electric field in this zone. By 10 min of voltage, the sodium and chloride ions exited the capillary (data not shown), but the increased ammonium and acetate concentrations remained. After 1200 s, the concentration of the buffering ions somewhat decreased, but significant amounts still remained on either side of the junction (Figure 2.5 D). Even so, the pH junction was maintained (Figure 2.5 insets in B and D).

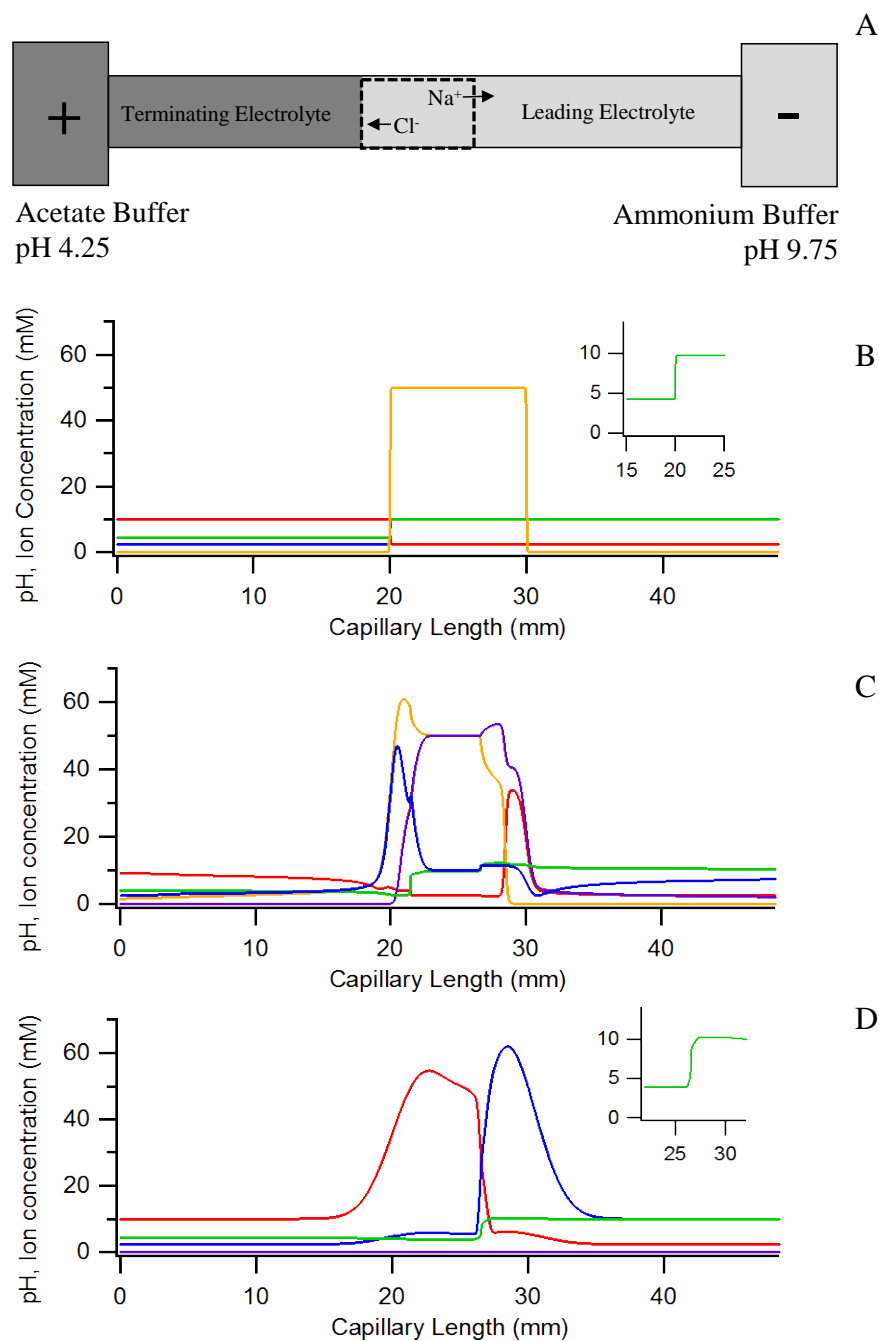


**Figure 2.5.** Simulation results of discontinuous buffers with a plug of 50 mM sodium chloride prepared in the basic buffer set next to the pH junction (A). Results for pH (—), acetate (—, leading and terminating traces combined), ammonium (—, leading and terminating traces combined), chloride (—) and sodium (—) after 0 s (B), 60 s (C), and 1200 s (D) of voltage. Insets display a clear view of the pH junction at 0 and 1200 s of voltage application. Simulations correspond to the discontinuous buffers experimental conditions used throughout this thesis: 10 mM ammonium (2.33 mM acetate, pH 9.75), 10 mM acetate (2.33 mM ammonium, 4.25).



Simul 5.0 successfully simulated the enrichment of myoglobin using the discontinuous buffers set-up and demonstrated a stable pH junction, which supported the previous experimental results and deemed this simulation program to be valuable. However, it was important to validate the simulated movement of the buffering ions through experimentation, especially in light of the suggested buffering ion collection at the pH junction as ionic salts were removed. For this purpose, two light absorbing buffering ions, benzylamine (pKa 9.33,  $\mu$   $34.7 \times 10^{-4} \text{ m}^2\text{S mol}^{-1}$ ) and benzoic acid (4.20,  $33.6 \times 10^{-4} \text{ m}^2\text{S mol}^{-1}$ ), were chosen to model the movements of ammonium (9.25,  $76.2 \times 10^{-4} \text{ m}^2\text{S mol}^{-1}$ ) and acetate (4.75,  $42.4 \times 10^{-4} \text{ m}^2\text{S mol}^{-1}$ ). It is important to note that these UV absorbing ions cannot exactly model the ammonium acetate buffers as their pKa values and mobilities are different than the ions they are modeling. The experimental pH values of the UV-absorbing buffers were adjusted from 9.75 and 4.25 (for ammonium and acetate buffers) to 9.50 and 4.50 in order to have the pH values more equidistant to their pKa values. The concentration of the model ions was also reduced from 10 mM to 5 mM to stay within the linear range of the absorbance detector and moderate the EOF. Since these UV-absorbing ions both absorbed light at 200 nm, separate experiments were performed to analyze the movement of the basic and acidic buffering ions. Computer simulations were re-run with the new sets of UV-absorbing discontinuous buffers and the results were very similar those with ammonium and acetate (Figure 2.4, new buffer simulations not shown). The simulation results for the UV-absorbing buffers were not altered significantly by the reduction in concentration nor at the slight pH changes in the discontinuous buffers. A sharp pH junction was still observed (data not shown). The mobility differences between the discontinuous buffers involving benzoic acid resulted in the pH junction mobility towards the anode. Even so, these experiments supported the use of the model ions benzylamine and benzoic acid as indicators of the buffering ion movement at the pH junction, as well as the use of Simul 5.0 as a modeling program for discontinuous buffers.

The experiments executed with benzylamine discontinuous buffers closely matched the results predicted by the simulation program, while some experiments with the benzoic acid discontinuous buffers revealed slightly more complicated results. These diversions from the simulations were likely due to interactions between benzoic acid and

the capillary wall. Thus, for simplicity and brevity, the key results are discussed using benzylamine as a model for ammonium and the applications extended to acetate.

In order to monitor the experimental movement of the discontinuous buffers around the pH junction with no salt, a pH junction was established with 5 mM benzylamine (acetate as counter ion) and 5 mM acetate (benzylamine as counter ion). Voltage was applied for a time (from 0 to 10 min) and the capillary content was pushed past the detector with pressure (30 mbar). The results after 0 and 300 s are shown in Figure 2.8. After 300 s, the concentration of the benzylamine on both sides of the pH junction was maintained, with a sharp transition at the pH junction. The model buffering ions crossed the junction and collected on the opposite side at the expected concentration. This crossing of the pH junction was confirmed by an additional set of experiments using benzylamine only as the counter ion (in 5 mM acetate) with 5 mM ammonium (acetate as counter ion) on the opposite side (data not shown). The absorbance traces with increasing voltage time demonstrated the counter ion crossed the junction and collected on the opposite side at a higher concentration.

A significantly higher concentration of benzylamine was observed on the cathodic side of the pH junction, compared to the anodic side, demonstrating a step-change in absorbance at 6.8 min (Figure 2.6). A small amount of myoglobin was then included in the system to mark the location of the pH junction. This increase in benzylamine concentration at 6.8 min was confirmed as the location for the pH junction by the collection of zwitterionic myoglobin at the same position.

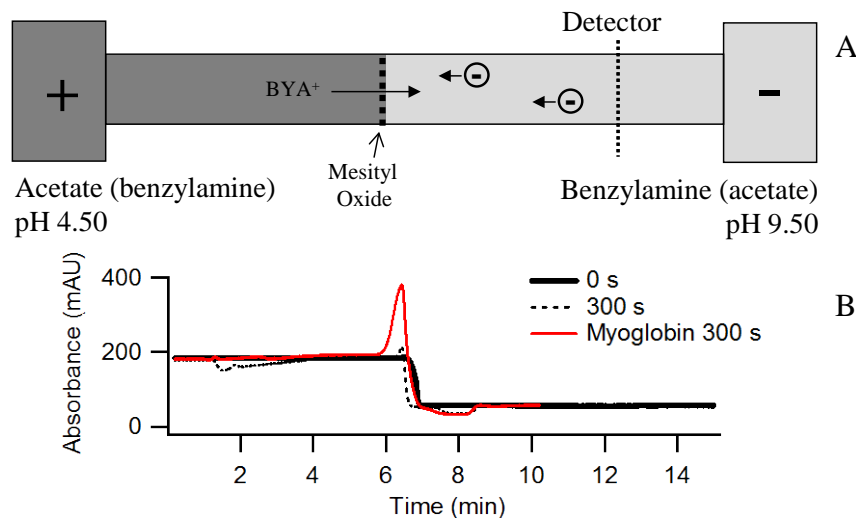


**Figure 2.6.** UV-absorbing discontinuous buffers (5 mM benzylamine, counter ion acetate, pH 9.50 and 5 mM acetic acid, counter ion benzylamine, pH 4.50) after 0 and 300 s of voltage (30 kV). Overlay (red) was same experimental design but with  $0.1 \text{ mg mL}^{-1}$  myoglobin prepared in the basic buffer and enriched at the pH junction for 300 s. After voltage application, pressure (30 mbar) mobilized the contents past the detector. Traces were aligned to a mesityl oxide internal standard that marked the initial pH junction point.

After confirming the validity of these new UV-absorbing buffers as models of ammonium and acetate, the experiments were repeated in the presence of 50 mM salt, prepared in the basic buffer. The enrichment of the buffering ions in place of the ionic salt was clearly confirmed (Figure 2.7). An increased concentration of benzylamine was observed on the side of the junction with the salt plug as the  $\text{BYA}^+$  ions crossed the junction and were stacked in the lower electric field region (Figure 2.7 B). (Note that the content in the schematics is in a reversed order to the electropherograms. The content on the right hand side in the schematic, closest to the detector, passes the detector first and elutes at an earlier time, on the left hand side of the electropherogram.) The benzoic acid also stacked in the salt plug, but its stacking occurred as the  $\text{BOA}^-$  entered the capillary towards the pH junction. The  $\text{BOA}^-$  in the acid electromigrated towards the anode and a depletion zone was observed as these ions left the region. These ions were not replaced at the same rate as they left due to the stacking effect on the other side of the salt plug.

It is hypothesized that this depletion of ions on the opposite side of the junction from the salt plug is the limiting factor for the application of discontinuous buffers to highly concentrated salty samples. Experiments with very high salt concentrations ( $\geq 100$  mM NaCl) resulted in a sudden drop of current in the capillary within a few minutes of applying voltage. The use of UV-absorbing buffering ions to monitor the movements of the discontinuous buffers in conjunction with computer simulations has provided greater insight into the formation, stability, and limitations of the pH junction. The results have supported the successful removal of ionic salts, but also the stacking of the discontinuous buffering ions at the junction. The enrichment of the buffering ions in place of the ionic salts is being addressed in on-going research. Notably, the pH junction mobility can be manipulated by adjusting the proton flux (the pH values of the discontinuous buffers) of the moving reaction boundary, and this process can titrate the pH junction out of the salt plug/collection of buffering ions. This collaborative work is in preparation for publication and discussed further in the future work section of Chapter 7.

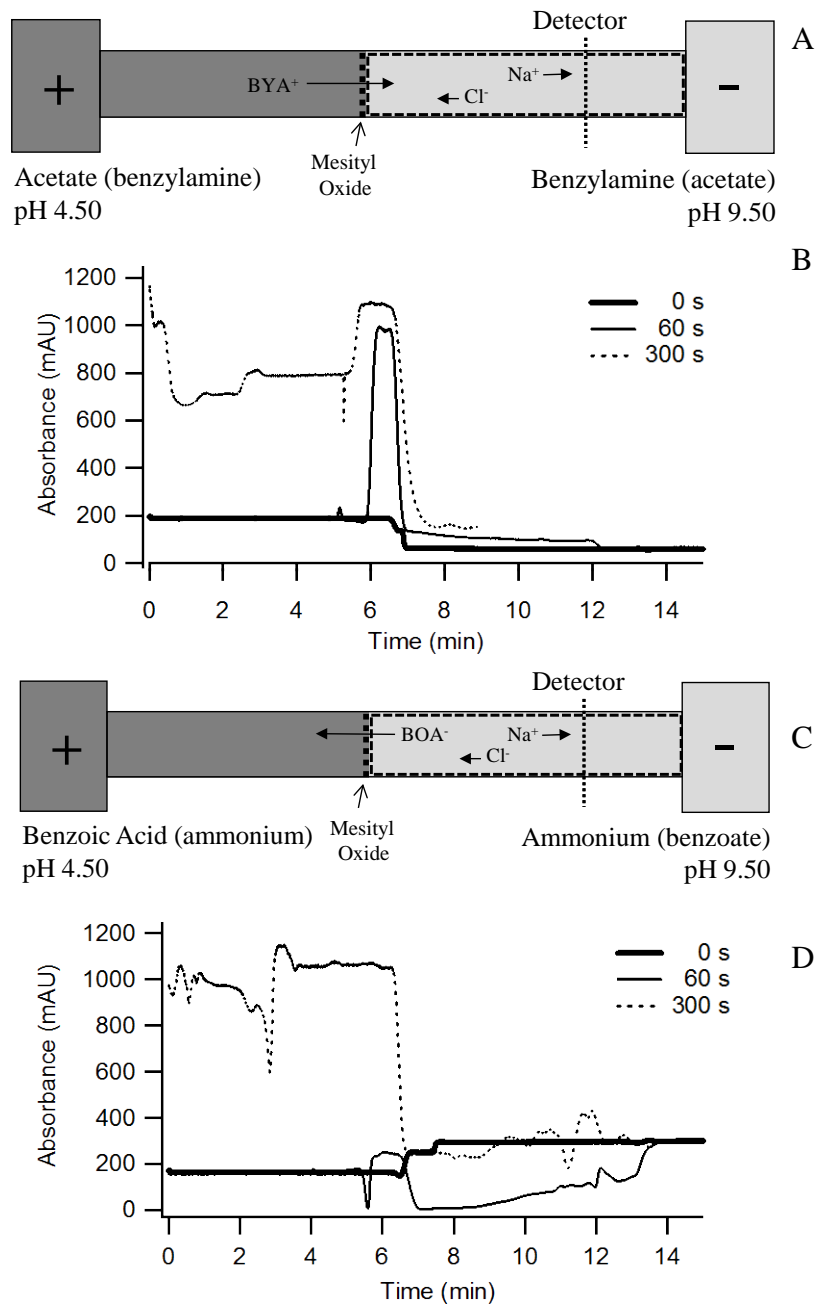


**Figure 2.7.** Experimental results from two sets of discontinuous buffers with salt. The basic UV-absorbing buffering ion (benzylamine A, B) and acidic UV-absorbing buffering ion (benzoic acid C, D) were monitored at 200 nm. A: UV-absorbing buffer set-up with 5 mM benzylamine (counter ion acetate, pH 9.50) and 5 mM acetate (counter ion benzylamine, pH 4.50) and the corresponding electropherogram (B). C: UV-absorbing discontinuous buffers set-up with 5 mM benzoic acid (counter ion ammonium, pH 4.50) and 5 mM ammonium (counter ion benzoic acid) and the corresponding electropherogram (D). The capillary was filled with the basic buffer and 50 mM salt, the acidic buffer was injected half way to the detector, voltage was applied for 0, 60, or 300 s, and the capillary content was pushed out of capillary (30 mbar). The time scale between traces was adjusted to a mesityl oxide internal standard, aligning the initial pH junction locations.

### 2.3.4 Protein Enrichment and Mass Spectral Analysis of Salt-Containing Protein Samples

Even with the stacking of buffering ions at the pH junction, it was of interest to determine if the enrichment and salt removal enhanced the mass spectrometry detection of the sample. MALDI mass spectral analysis was previously performed on sub- $\mu\text{L}$  myoglobin samples enriched by our discontinuous buffer system [13]. MALDI was selected as the choice of MS ionization, as it facilitated the convenient direct deposition of ultrasmall (nL-level) sample volume from the capillary without any specialized interfaces. In addition, the pure aqueous (organic solvent free) environment of our discontinuous buffer system was less suitable for electrospray ionization.

In this experiment, enrichment was performed on a  $10 \text{ ng } \mu\text{L}^{-1}$  myoglobin sample containing 50 mM NaCl. The high sample ionic strength resulted in very high current at the beginning of the run. Therefore, the experiment was performed in constant current mode (40  $\mu\text{A}$ ), with a maximum voltage of 30 kV. As the run began, the current was constant at 40  $\mu\text{A}$  while the voltage increased up to 30 kV. Upon reaching 30 kV, the current began to drop. This gradual decrease in conductance throughout the run suggested a removal of NaCl. A sharp peak was later observed in the UV-absorption signal (not shown). The peak height and sharpness resembled that obtained from the NaCl-free myoglobin sample of identical concentration in terms of peak shape and height.

The enriched myoglobin sample was spotted as  $\sim 40 \text{ nL}$  droplets on a sample target plate pre-deposited with MALDI matrix. Figures 2.8 A and 2.8 B displayed the mass spectra, respectively, from a sample enriched and desalted by discontinuous buffers and the untreated original sample. The mass spectra confirmed the identity of the analyte band to be myoglobin, and the presence of NaCl did not appear to hinder the enrichment. Significant improvement in both signal-to-noise ratio and peak resolution was clearly demonstrated.

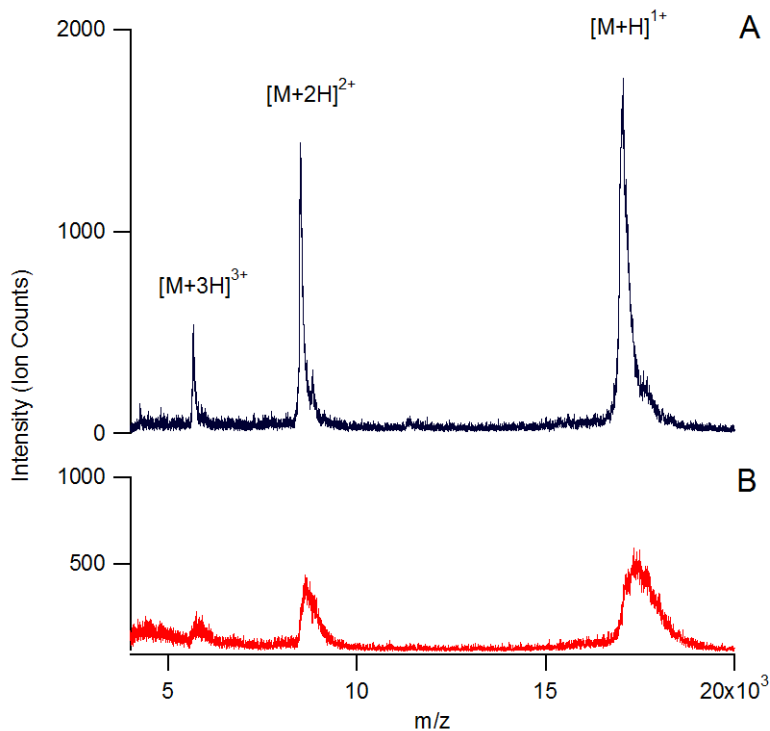


**Figure 2.8.** MALDI MS spectra of the enriched, desalted myoglobin fraction collected from capillary (A), and the untreated 10 ng  $\mu\text{L}^{-1}$  myoglobin in 50 mM NaCl (B).

Interestingly, the mass spectral signal from the original salt-containing sample (Figure 2.8 B) was only slightly weaker than that of the salt-free sample (Figure 2 B in ref. [13]). The presence of 50 mM NaCl only marginally reduced the ionization efficiency of myoglobin in this MALDI MS analysis. Nevertheless, MALDI MS signals, particularly those with intensities near the noise level, should not be considered as a reliable quantitative measurement. Suffice it to conclude that the enrichment of the minuscule-volume myoglobin sample was successful and was not affected in any way by the presence of NaCl.

The mass spectral traces in Figure 2.8 demonstrated that the removal of salt and enrichment of protein were more significant for the sample detection than the increased concentration of the ammonium and acetate buffers. Sodium is known to have detrimental effects on mass spectral analysis, while ammonium and acetate are volatile, more compatible mass spectral molecules.

### 2.3.5 CZE of Enriched Protein Mixture

In this section, we investigated the possibility to perform a subsequent CZE separation of a protein mixture (myoglobin, BSA and  $\beta$ -lactoglobulin), immediately following enrichment via discontinuous buffers.

Examples of peptide and protein enrichment by dynamic pH junctions followed by CZE have been reported in the literature [12,34]. However, they were based on the injection of a short plug of solution with pH different than the BGE around the analyte zone. This created the dynamic, short-lived, pH junction for analyte enrichment. Regular CZE generally took place after dissipation of the pH junction. In contrast, it should be recognized that the discontinuous buffer described in this work is unique in that it creates a prolonged pH junction during the entire enrichment process (20+ min). Such a long enrichment time is necessary for slow migrating proteins to reach the pH junction. Hence the discontinuous buffers enrichment, until this point, was performed as a stand-alone operation without subsequent CZE separations [13-15].

Since an entire capillary of both the acidic (acetate) and basic (ammonium) buffers were used to create the pH junction, it was difficult to undo the pH junction solely by titration. Instead, after the enriched proteins were detected by UV absorption (Figure 2.9 A), the voltage (30 kV) was suspended. A predetermined amount of pressure (30 mbar for 135 s) was used to push the protein band close to the capillary exit, in order to remove most of the pH 9.25 ammonium buffer from the capillary. At this point, the voltage polarity was reversed (-30 kV) and a strongly acidic solution (100 mM acetic acid) was placed at both electrodes (Figure 2.9 B). The acetic acid at the anode was expected to titrate all ions in the sample zone, mobilizing all proteins as cationic molecules toward the second detection window near the cathode (Figure 2.9 C).



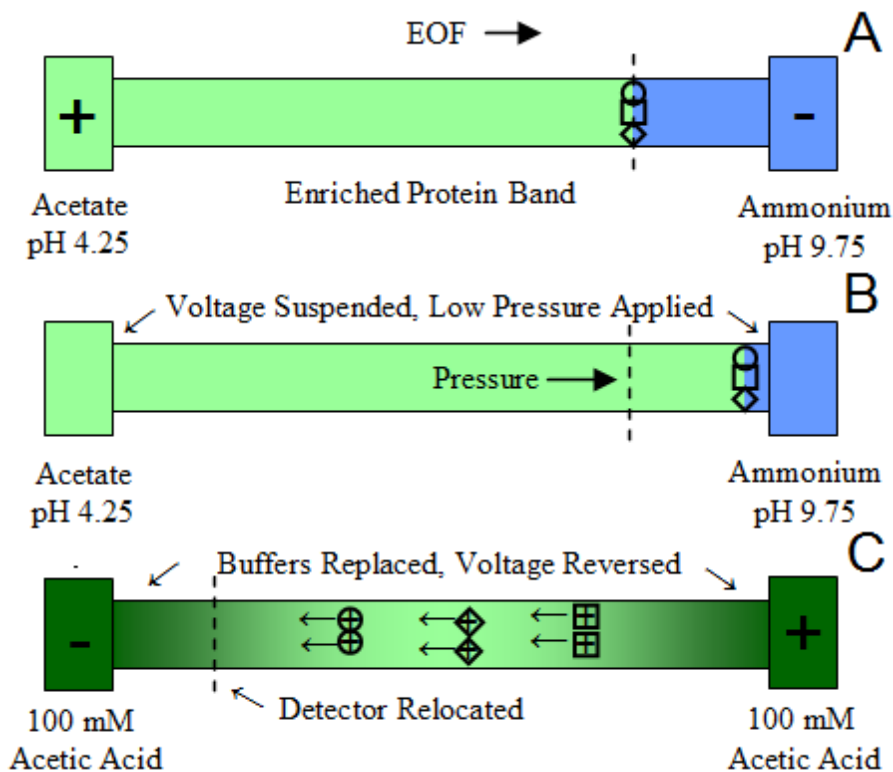


**Figure 2.9.** Diagram of procedure of protein enrichment by discontinuous buffers followed by CZE: detection of enriched and desalted proteins (A); pressure application to move the pH junction near the exit (B); replacement of discontinuous buffer with 100 mM acetic acid and voltage application to facilitate CZE (C). Circles, squares and diamonds represent three different proteins.

In this experiment, CZE was performed following discontinuous buffers of a protein mixture containing myoglobin ( $10 \text{ ng } \mu\text{L}^{-1}$ ), BSA ( $20 \text{ ng } \mu\text{L}^{-1}$ ) and  $\beta$ -lactoglobulin ( $10 \text{ ng } \mu\text{L}^{-1}$ ) in the presence of 25 mM NaCl and 10 mM ammonium buffer (pH 9.75). The electropherogram from the CZE step is shown in Figure 2.10. As expected, the proteins were co-enriched at the junction despite the presence of NaCl, and were eventually resolved in the subsequent CZE separation. A CZE separation of the original sample mixture, without the enrichment step, was also performed, and the result was shown as the figure inset. A significant improvement in the signal intensities was clearly demonstrated, with an estimated enrichment factor of 70. The peak efficiencies ranged from 1000 to 7000 plates  $\text{m}^{-1}$ . The enrichment factor and peak efficiencies were not suppressed due to the presence of salt in the original sample. When the same method was

applied to the same protein sample, with the exception that no NaCl was present, the absorbance trace of the CZE protein separation was nearly identical to the one shown in Fig. 2.10. It is acknowledged that higher peak efficiencies ( $10^5$  plates  $m^{-1}$ ) have been reported on the CZE of cationic and anionic proteins in capillaries similarly modified with DLPC [4]. However, to achieve such high efficiencies, the separation had to be performed in high ionic strength buffers (20 mM Tris-HCl and 20 mM CHES) that were not compatible with subsequent MS analysis.

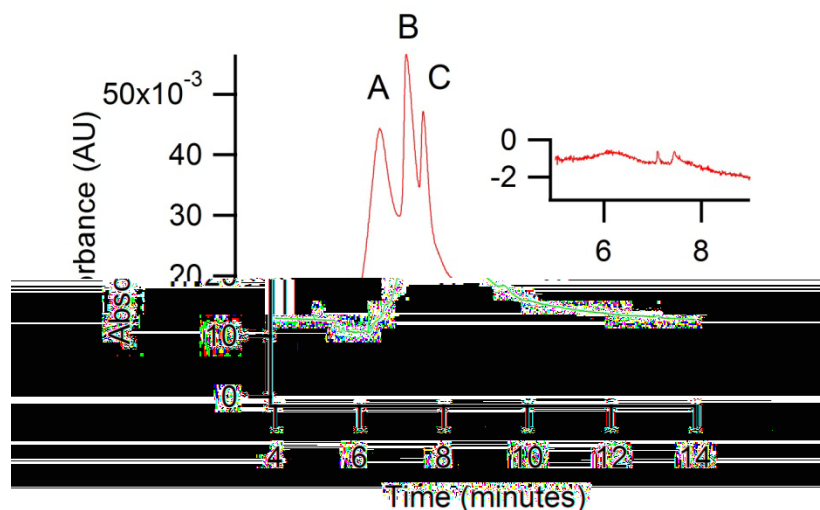


**Figure 2.10.** Absorbance at 200 nm recorded during CZE on enriched, desalted proteins. Sample: 25 mM NaCl, 20 ng  $\mu L^{-1}$  bovine serum albumin (A), 10 ng  $\mu L^{-1}$  myoglobin (B), and 10 ng  $\mu L^{-1}$   $\beta$ -lactoglobulin (C), in 10 mM ammonium buffer. Conditions: Voltage, 30 kV; Procedure as shown in Figure 2.8. Figure inset: Absorbance from CZE of the original sample without enrichment. Conditions: Injection volume, 6 nL; BGE, 100 mM acetic acid.

Finally, the extremely low pH of 100 mM acetic acid was suspected to impose band-broadening, by reducing the ability of DLPC to prevent protein adsorption and by creating a moderately fast reversed EOF. The phosphate headgroup of DLPC was estimated to have a  $pK_a \sim 1$ , and thus the authors strongly advised readers to work at  $pH > 3$  for the DLPC molecules to remain as true zwitterions [4]. In other words, the ability of DLPC in preventing protein adsorption may be limited at pH 2.7. Furthermore, a moderately fast reversed EOF ( $2.3 \times 10^{-4} \text{ cm}^2 \text{ V}^{-1} \text{ s}^{-1}$ ) was recorded at pH 2.7. This

magnitude was significantly higher than that of the 10 mM pH 4.25 acetate ( $< 1 \times 10^{-5} \text{ cm}^2\text{V}^{-1}\text{s}^{-1}$ ). Such a mismatched EOF, now in the absence of a self-sharpening pH junction, most likely contributed to the observed reduced efficiencies. Future work will focus on the use of alternative coatings that exhibit near-zero EOF at highly acidic pH conditions. Despite the current limitation, CZE of proteins was successfully performed, for the first time, following the enrichment and desalting by discontinuous buffers. Even though only partial resolution was achieved, such separation was in most cases sufficient to significantly improve the quality of the subsequent MS analysis.

## 2.4 Conclusions

CE is gradually becoming more amicable to sample preparation and analysis of biological samples. The presence of salt, problematic to traditional CE methods and overly abundant in biological samples, did not appear to disrupt our protein enrichment with discontinuous buffer. Not only were proteins from high ionic strength solutions enriched, the salt ions were actually removed from the capillary during enrichment. Computer simulations and investigations with UV-absorbing buffering ions uncovered the concurrent collection of the buffering ions while the ionic salts were removed. The MALDI-MS data confirmed the identity of the enriched protein band and the signal-to-noise enhancement resulted from protein enrichment with discontinuous buffers.

For the first time, our novel discontinuous buffers protein enrichment was coupled with subsequent CZE, which partially resolved a mixture of three standard proteins containing non-buffering salt. Although this chapter has examined the impact of permanently charged ions in the protein sample, other factors must be examined, such as the effect of buffering ions and high abundance proteins, before this method can be applied to real samples. Even so, this work represents a major step toward developing this pH junction technique into a miniaturized comprehensive sample preparation platform for biological samples.

## 2.5 References

- [1] M.M. Yassine & C.A. Lucy. Enhanced stability self-assembled coatings for protein separations by capillary zone electrophoresis through the use of long-chained surfactants, *Analytical Chemistry*, **2005**, *77*, 620-625.
- [2] A.M. MacDonald & C.A. Lucy. Highly efficient protein separations in capillary electrophoresis using a supported bilayer/diblock copolymer coating, *Journal of Chromatography A*, **2006**, *1130*, 265-271.
- [3] E. Cordova, J.M. Gao & G.M. Whitesides. Noncovalent polycationic coatings for capillaries in capillary electrophoresis of proteins, *Analytical Chemistry*, **1997**, *69*, 1370-1379.
- [4] J.M. Cunliffe, N.E. Baryla & C.A. Lucy. Phospholipid bilayer coatings for the separation of proteins in capillary electrophoresis, *Analytical Chemistry*, **2002**, *74*, 776-783.
- [5] F.W.A. Tempels, W.J.M. Underberg, G.W. Somsen & G.J. de Jong. Design and applications of coupled SPE-CE, *Electrophoresis*, **2008**, *29*, 108-128.
- [6] M.A. Strausbauch, B.J. Madden, P.J. Wettstein & J.P. Landers. Sensitivity Enhancement And 2nd-Dimensional Information From Solid-Phase Extraction-Capillary Electrophoresis Of Entire High-Performance Liquid-Chromatography Fractions, *Electrophoresis*, **1995**, *16*, 541-548.
- [7] D. Figeys, A. Ducret & R. Aebersold. Identification of proteins by capillary electrophoresis tandem mass spectrometry - Evaluation of an on-line solid-phase extraction device, *Journal of Chromatography A*, **1997**, *763*, 295-306.
- [8] Z.K. Shihabi. Sample stacking by acetonitrile-salt mixtures, *Journal of Capillary Electrophoresis*, **1995**, *2*, 267-271.
- [9] Z.K. Shihabi. Transient pseudo-isotachopheresis for sample concentration in capillary electrophoresis, *Electrophoresis*, **2002**, *23*, 1612-1617.
- [10] S. Park & C.E. Lunte. On-column sample concentration of high-ionic-strength samples in capillary electrophoresis, *Journal of Microcolumn Separations*, **1998**, *10*, 511-517.
- [11] P. Britz-McKibbin, G.M. Bebault & D.D.Y. Chen. Velocity-difference induced focusing of nucleotides in capillary electrophoresis with a dynamic pH junction, *Analytical Chemistry*, **2000**, *72*, 1729-1735.

- [12] M.R.N. Monton, K. Imami, M. Nakanishi, J.B. Kim & S. Terabe. Dynamic pH junction technique for on-line preconcentration of peptides in capillary electrophoresis, *Journal of Chromatography A*, **2005**, *1079*, 266-273.
- [13] C.A. Nesbitt, K. Jurcic & K.K.C. Yeung. Nanoliter-volume protein enrichment, tryptic digestion, and partial separation based on isoelectric points by CE for MALDI mass spectral analysis, *Electrophoresis*, **2008**, *29*, 466-474.
- [14] C.A. Nesbitt, J.T.M. Lo & K.K.C. Yeung. Over 1000-fold protein preconcentration for microliter-volume samples at a pH junction using capillary electrophoresis, *Journal of Chromatography A*, **2005**, *1073*, 175-180.
- [15] K. Jurcic, C.A. Nesbitt & K.K.C. Yeung. Characterization of discontinuous buffer junctions using pH indicators in capillary electrophoresis for protein preconcentration, *Journal of Chromatography A*, **2006**, *1134*, 317-325.
- [16] V. Hruška, M. Jaroš & B. Gaš. Simul 5 - Free dynamic simulator of electrophoresis, *Electrophoresis*, **2006**, *27*, 984-991.
- [17] P. Gebauer, Z. Mala & P. Bocek. Recent progress in analytical capillary ITP, *Electrophoresis*, **2009**, *30*, 29-35.
- [18] V. Hruska, B. Gas & G. Vigh. Simulation of desalting that occurs during isoelectric trapping separations, *Electrophoresis*, **2009**, *30*, 433-443.
- [19] R. Lee, A.S. Ptolemy, L. Niewczas & P. Britz-McKibbin. Integrative metabolomics for characterizing unknown low-abundance metabolites by capillary electrophoresis-mass spectrometry with computer simulations, *Analytical Chemistry*, **2007**, *79*, 403-415.
- [20] W. Thormann, M.C. Breadmore, J. Caslavská & R.A. Mosher. Dynamic computer simulations of electrophoresis: A versatile research and teaching tool, *Electrophoresis*, **2010**, *31*, 726-754.
- [21] J.B. Kim, P. Britz-McKibbin, T. Hirokawa & S. Terabe. Mechanistic study on analyte focusing by dynamic pH junction in capillary electrophoresis using computer simulation, *Analytical Chemistry*, **2003**, *75*, 3986-3993.
- [22] R. Lee, A.S. Ptolemy, L. Niewczas & P. Britz-McKibbin. Integrative metabolomics for characterizing unknown low-abundance metabolites by capillary electrophoresis-mass spectrometry with computer simulations, *Analytical Chemistry*, **2007**, *79*, 403-415.
- [23] K. Vitkova, J. Petr, V. Maier, J. Znaleziona & J. Sevcik. Study of electromigration effects on a pH boundary during the on-line electrokinetic preconcentration by capillary electrophoresis, *Electrophoresis*, **2010**, *31*, 2771-2777.

- [24] W. Thormann, C.X. Zhang, J. Caslavská, P. Gebauer & R.A. Mosher. Modeling of the impact of ionic strength on the electroosmotic flow in capillary electrophoresis with uniform and discontinuous buffer systems, *Analytical Chemistry*, **1998**, *70*, 549-562.
- [25] K. Salomon, D.S. Burgi & J.C. Helmer. Evaluation Of Fundamental Properties Of A Silica Capillary Used For Capillary Electrophoresis, *Journal of Chromatography*, **1991**, *559*, 69-80.
- [26] T. Tsuda, K. Nomura & G. Nakagawa. Open-Tubular Microcapillary Liquid-Chromatography With Electroosmosis Flow Using A Uv Detector, *Journal of Chromatography*, **1982**, *248*, 241-247.
- [27] J.E. Melanson, N.E. Baryla & C.A. Lucy. Dynamic capillary coatings for electroosmotic flow control in capillary electrophoresis, *Trac-Trends In Analytical Chemistry*, **2001**, *20*, 365-374.
- [28] J.L. Liao & R. Zhang. Simple approach to eliminating disturbance in isoelectric-focusing caused by the presence of salts, *Journal of Chromatography A*, **1994**, *684*, 143-148.
- [29] N.J. Clarke, A.J. Tomlinson, G. Schomburg & S. Naylor. Capillary isoelectric focusing of physiologically derived proteins with on-line desalting of isotonic salt concentrations, *Analytical Chemistry*, **1997**, *69*, 2786-2792.
- [30] N.J. Clarke, A.J. Tomlinson & S. Naylor. On-line desalting of physiologically derived fluids in conjunction with capillary isoelectric focusing-mass spectrometry, *Journal Of The American Society For Mass Spectrometry*, **1997**, *8*, 743-748.
- [31] Handbook of Chemistry and Physics. CRC Press, Cleveland, Ohio, **2007-2008**.
- [32] C.J. Booker, S. Sun, S. Woolsey, J.S. Mejia & K.K.C. Yeung. Removal of sample background buffering ions and myoglobin enrichment via a pH junction created by discontinuous buffers in capillary electrophoresis, *Journal of Chromatography A*, **2011**, *1218*, 5705-5711.
- [33] C.X. Cao, L.Y. Fan & W. Zhang. Review on the theory of moving reaction boundary, electromigration reaction methods and applications in isoelectric focusing and sample pre-concentration, *Analyst*, **2008**, *133*, 1139-1157.
- [34] S.J. Wang, W.L. Tseng, Y.W. Lin & H.T. Chang. On-line concentration of trace proteins by pH junctions in capillary electrophoresis with UV absorption detection, *Journal of Chromatography A*, **2002**, *979*, 261-270.

## **Chapter 3: Removal of Sample Background Buffering Ions and Myoglobin Enrichment at a pH Junction Created by Discontinuous Buffers in Capillary Electrophoresis**

---

Reproduced in part with permission from **C.J. Booker**, S. Sun, S. Woolsey, J.S. Mejia & K.K.-C. Yeung. Removal of sample background buffering ions and myoglobin enrichment via a pH junction created by discontinuous buffer in capillary electrophoresis, *Journal of Chromatography A*, **2011**, 1218, 5705-5711. Copyright (2011) Elsevier.

The discontinuous buffers technique not only enriches proteins on-line, but can also remove contaminating permanently charged ionic species, as was discussed in Chapter 2. In the following chapter, the removal of contaminating buffering ions from protein samples during enrichment is discussed.

## 3.1 Introduction

Capillary electrophoresis (CE) is best known for its superior separation efficiency and ability to handle miniscule, nanoliter sample volumes. While separation is the primary purpose for CE, additional sample preparation steps, such as sample clean-up (removal of unwanted background) and enrichment can also be performed using CE at these small sample volumes [1-4]. Enrichment and sample clean-up are vital for the success of CE separations and subsequent mass spectral analysis, especially for protein samples [5-7]. The short path length in the capillary for absorbance detection requires that the analyte is present at enriched concentrations. As discussed in the previous chapter, background ions in the sample matrix can cause increased conductivity in the capillary leading to Joule heating [8]. These unwanted ions can also cause analyte ionization suppression in mass spectral (MS) analysis and reduce sensitivity [9].

Stacking that relies on conductivity changes between the sample zone and electrolyte become challenging to impossible when the sample contains high levels of salt. Rather than relying on conductivity differences in zones, one can achieve stacking of ionizable analytes, such as proteins and peptides, by manipulating their mobilities with a pH change between the sample zone and electrolyte [10]. This pH manipulation approach is generally referred to as pH-mediated sample stacking [11]. In the literature, it has been described as stacking by dynamic pH junction [12-14], and transient pH boundary or transient moving chemical reaction boundary [15,16]. Because the analyte mobilities are primarily controlled by pH and not field strength, stacking has been successfully demonstrated and modeled with high salt concentrations in the sample zone [15,17,18]. However, a limitation of pH-mediated stacking is the need to customize the electrolyte



pH to the  $pK_a$  of the analytes, making it difficult to simultaneously enrich analytes with a wide range of  $pK_a$  values. To address this issue, our group has reported the use of a prolonged step-pH transition for protein enrichment, the discontinuous buffers technique [19].

An advantage to using discontinuous buffers is the large sample injection of a full-capillary volume or more, by preparing the sample in the anolyte and/or catholyte [20]. Enrichment factors of up to 2000 were reported. Following enrichment, the stacked protein or protein mixture can be subsequently separated using capillary zone electrophoresis (CZE) or spotted onto a MALDI target for MS analysis, as was discussed in Chapter 2. Alternatively, the enriched protein band can be digested into peptides with trypsin prior to MS analysis [21,22], which has been performed in our research group.

To assess the ability of our discontinuous buffers in concentrating proteins from biological samples, the effect of ionic salts was explored in Chapter 2. The salt appeared to have little effect on the stability of the pH junction, and successful enrichment was demonstrated in the presence of up to 50 millimolar ionic salts in the protein sample. In addition to salt, extraction and/or solubilization protocols of proteins from biological samples typically require the use of buffers, such as Phosphate Buffered Saline (PBS), TRIS Buffered Saline (tris(hydroxymethyl)aminomethane, TBS), or the morpholine ring-containing buffers such as MES (2-(N-morpholino)ethanesulfonic acid), at high millimolar concentrations. Unlike the non-buffering, permanently charged salt, the presence of background buffering ions in the sample could potentially titrate the discontinuous buffers or alter the buffering capacity near the pH junction. Buffer ions present in the samples can significantly alter the local pH of the discontinuous buffers and thus potentially disrupt protein enrichment. In addition, the buffering ions can experience a change in their degree of ionization when crossing the pH junction. This could potentially lead to a mobility reduction and in turn, their stacking or accumulation near the pH junction. In this chapter, the effects of TRIS, MES, and phosphate buffers on the enrichment of myoglobin are investigated. The migration behaviour of TRIS and phosphate ions (with the UV absorbing phenyl phosphate) at the pH junction is

monitored. The results presented herein demonstrate the capability of the pH junction in tolerating and removing the background ions during protein enrichment.

## 3.2 Materials and Methods

### 3.2.1 Apparatus

All protein enrichment experiments were performed on an Agilent <sup>3D</sup>Capillary Electrophoresis instrument (Palo Alto, CA, USA) with a direct UV-visible absorbance detector. The Agilent <sup>3D</sup>CE ChemStation software was used for data collection. Unmodified fused silica capillaries of 50  $\mu\text{m}$  i.d. and 364  $\mu\text{m}$  o.d., were purchased from Polymicro Technologies (Phoenix, AZ, USA) and cut to a total length of 48.5 cm with an effective length of 40 cm. The capillary was thermostated to 25  $^{\circ}\text{C}$  during experiments. In order to suppress the electroosmotic flow (EOF) and prevent protein adsorption onto the capillary wall, a semi-permanent coating (1,2-dilauroyl-*sn*-glycero-3-phosphocholine, DLPC) was applied to the inner capillary wall [23].

### 3.2.2 Reagents

All solutions were prepared with deionized water (18.2 M $\Omega$ ) from a Millipore water purification system (Bedford, MA, USA). Glacial acetic acid and ammonium hydroxide were purchased from EM Science (Gibbstown, NJ, USA) and used to make the buffer solutions. Sodium hydroxide (EM Science) was used to wash the new capillaries. Buffering ions examined included sodium phenyl phosphate dibasic dihydrate (Sigma, St. Louis, MO, USA), sodium phosphate dibasic, anhydrous (EM Science), sodium phosphate monobasic, monohydrate (Caledon), 2-(*N*-morpholino)ethanesulfonic acid (MES, Sigma), and tris(hydroxymethyl)aminomethane (TRIS, Sigma). Mesityl oxide (Aldrich) solutions were prepared in water at 20 mM and used to mark the EOF. Myoglobin from horse heart (Sigma) was used as a model protein. The semi-permanent coating of phospholipid DLPC (Avanti Polar Lipids, Alabaster, AL, USA) was prepared as reported previously [23]. Briefly, DLPC (0.1 mM) was prepared in an aqueous solution

of 20 mM TRIS buffer and 20 mM calcium chloride (Caledon Laboratories, Georgetown, ON, Canada) and adjusted to pH 7.2 by hydrochloric acid (EM Science). Solubilization of the DLPC required several 10-minute, alternating cycles of sonication and magnetic bar stirring. Coating formation was performed by rinsing the capillary with this solution.

### 3.2.3 Enrichment of Proteins by a pH Junction

Washing and coating of new silica capillaries was performed by pressure application (1 bar) at the capillary inlet with sodium hydroxide (0.1 M) for 10 min, followed by water for 10 min and DLPC solution for 20 min. To prepare the two discontinuous buffers, 10 mM ammonium hydroxide was adjusted to pH 9.75 with acetic acid, and 10 mM acetic acid was adjusted to pH 4.25 with ammonium hydroxide. The enrichment experiments were performed as previously shown in Figure. 5C of Ref. [19] unless otherwise stated. Briefly, the capillary was filled with the sample solution of myoglobin ( $10 \text{ ng } \mu\text{L}^{-1}$ ) prepared in the 10 mM pH 9.75 ammonium buffer. The pH 4.25 acetate buffer was placed at the inlet (anode) and the pH 9.75 ammonium buffer was placed at outlet (cathode, near the detector). Voltage application was programmed to a constant voltage of 30 kV; however a maximum current limit of 100  $\mu\text{A}$  was in place to prevent excessive Joule heating when salt-containing samples were used. With the DLPC capillary coating, the suppressed, forward EOF and the moving NRB slowly carried the enriched proteins towards the detector. Absorption detection was performed at both 200 nm (absorption by peptide bond) and 408 nm (absorption by heme). The capillary coating was regenerated in between runs by rinsing (1 bar) with the DLPC solution for 5 to 10 min.

Sample solutions of myoglobin were prepared at the specified concentration in either the acetate or ammonium buffer. To prepare samples containing background buffer ions (TRIS, MES or phosphate), monobasic phosphate and MES were added to the acetate buffer, whereas dibasic phosphate and TRIS were added to the ammonium buffer. The final pH was maintained at 4.25 or 9.75 accordingly, and the final concentration of ammonium or acetate in the sample was kept at 10 mM. The presence of TRIS was

detected by UV-absorption at 200 nm. To study the migration of phosphate near the pH junction, a UV-absorbing analogue (also at 200 nm), phenyl phosphate, was used.

### **3.2.4 Computer Simulations**

Simul 5.0 developed by Bohuslav Gaš and coworkers was obtained online from <http://web.natur.cuni.cz/~gas/Simul50.exe> [24], and was used to computer simulate the formation of a pH junction and the movement of various ions during the enrichment of protein using discontinuous buffers. In the example provided with the software for isoelectric focusing (IEF\_1.sna) [24], the anolyte and catholyte were entered as the terminating electrolyte (TE) and leading electrolyte (LE). Hence, for the simulation of our discontinuous buffer system, the anolyte, pH 4.25, 10 mM acetate buffer (pH adjusted with ammonium hydroxide) was input as 10 mM acetate with 2.33 mM ammonium, while the pH 9.75, 10 mM ammonium buffer (pH adjusted by acetic acid) catholyte was input as 10 mM ammonium with 2.33 mM acetate. For both acetate and ammonium, the simulated ion concentration profiles (csv files) from the TE and LE were combined into one continuous trace. For simulations in the presence of TRIS, MES and phosphate, these ions were entered as analytes present in either the LE or TE. The capillary length was reduced by a factor of 10 to speed up the simulation process. Therefore the electric field strength was also reduced by 10 times to result in similar ion movements relative to the total capillary length; that is, a 2-mm movement in the simulation results corresponds to a 2-cm distance in an actual capillary.

## **3.3 Results and Discussion**

### **3.3.1 Protein Enrichment and Removal of TRIS**

TRIS is one of the most commonly used buffers for protein extraction and/or solubilization. It is considered a MS-compatible buffer, since the degree of MS ionization suppression from TRIS is much less than that from ionic salt such as sodium. Nevertheless, significant TRIS-protein adduct formation was reported with conventional

ESI from as low as 0.5 mM TRIS [25]. Herein, isolation of proteins from TRIS at sub-microliter sample volumes by discontinuous buffers is performed. Myoglobin was selected as the model protein for this chapter due to its unique UV absorption at 408 nm for identification. The enrichment of other proteins (carbonic anhydrase I, bovine serum albumin, lentil lectin, and  $\beta$ -casein) and peptides (tryptic digests of myoglobin, lentil lectin and  $\beta$ -casein, and endoproteinase Asp-N digest of myoglobin) with the same discontinuous buffer system has been demonstrated in the previous chapter and in other reports [19,21,22].

The acid dissociation constant of TRIS ( $pK_a$ ) is 8.1. It therefore exists as a cation in pH 4.25, or predominately as a neutral molecule in pH 9.75 (only 2 % in the protonated form). To facilitate the removal of TRIS from the protein, the sample was prepared in the ammonium buffer (pH 9.75), and was injected to fill the entire capillary as illustrated in Figure 3.1A. This setup allowed the protein (myoglobin,  $pI$  7.2) and TRIS to be differentiated by net charges, as anionic and near-neutral molecules, respectively. The experiment was performed with two TRIS concentrations, 10 and 100 mM, along with a blank (0 mM TRIS), and the results are shown in Figure 3.1B. In the absence of TRIS (lower trace of Figure 3.1B), myoglobin was enriched by the discontinuous buffers as expected and was carried by a slow EOF generated in the DLPC-modified capillary. This EOF, however, was not constant throughout the run. A cathodic EOF of roughly  $1 \times 10^{-4} \text{ cm}^2\text{V}^{-1}\text{s}^{-1}$  was measured in the pH 9.75 ammonium buffer and a slower anodic EOF of  $< 1 \times 10^{-5} \text{ cm}^2\text{V}^{-1}\text{s}^{-1}$  was observed in pH 4.25 acetate. As a result, the EOF varied between these two values during the experiment depending on the ratio of ammonium to acetate buffers inside the capillary. Most importantly, it mobilized the capillary content, including the pH junction and the enriched proteins, towards the detector near the cathode in approximately 22 min (Figure 3.1).



In the presence of TRIS, similarly sharp peaks at approximately the same time as in the blank were observed. The identity of these peaks was confirmed by the heme absorption at 408 nm (data not shown). As expected, these 408 nm peaks were not observed in the control experiments (no myoglobin) with 0 and 100 mM TRIS (data not shown). The TRIS molecules remained relatively stationary and were detected as plateaus while the protein molecules collected on the edge of the TRIS plateau. The runs in Figure 3.1 display a separation between the TRIS plateau and myoglobin peak, although this separation did not always occur in the replicate experiments. Four to six replicate experiments for 0, 10, and 100 mM TRIS with myoglobin were performed and resulted in a sharp protein peak for each run. The myoglobin peak was separated from the TRIS plug (10 and 100 mM) in about half of the replicates, with an average separation of 1 min (SD 1 min). The variance in migration time and enrichment factor was moderate due to the variability in EOF. The migration time of the protein peak varied between experiments, regardless of the TRIS concentration. Migration times ranged from 13-31 min over all replicates, with mean migration times (and standard deviations) of 18 (3), 16 (4), and 19 (7) min for 0, 10 and 100 mM TRIS respectively. Enrichment factors of myoglobin in 0, 10, and 100 mM TRIS samples were similar, ranging from 90-340 with mean (and standard deviation) values of 230 (70), 210 (100) and 180 (100) respectively.

Computer simulations of the discontinuous buffers method was performed for 1000 s in the presence and absence of TRIS (Figure 3.2). Two similar step-pH junctions were obtained in both cases, supporting the successful myoglobin enrichment, as the step junction location was confirmed as the place of protein enrichment in Chapter 2 (Figure 2.7). The simulated TRIS concentration profile (Figure 3.2B) confirmed that TRIS was immobile and stayed on the cathodic side of the pH junction. However, the gaps between the myoglobin peak and the end of the TRIS plug observed in Figure 3.1 B (10 and 100 mM TRIS) were not observed in the simulation. The edge of the simulated TRIS profile only appeared skewed away from the pH junction. Our experimental separations between the TRIS and myoglobin can be attributed to slight changes in the buffer ratios at the pH junction, and replicate experiments demonstrated separations of 0 to 2 min, as stated above. As discussed in Chapter 2, a moving reaction boundary exists at the pH junction. Slight fluctuations in the buffer compositions from run to run can lead to the slight

migration of the pH junction, which is most likely responsible for the separation between the TRIS plug and enriched myoglobin peak. Another noteworthy observation was the change in concentration profiles of ammonium and acetate between the two conditions. Namely, the addition of TRIS resulted in much higher concentrations of ammonium and acetate after voltage application and in turn a higher conductivity, near the pH junction. Similar accumulation of buffering ions was also observed in Chapter 2 simulations and experiments with the UV-absorbing buffering ions at the removal of sodium chloride. Finally, the enrichment factors calculated from the peak heights (Figure 3.1 B) were 174, 270, and 340 respectively for 0, 10, and 100 mM TRIS. Based upon the standard deviation values of the replicates, these enrichment values can be considered equivalent.



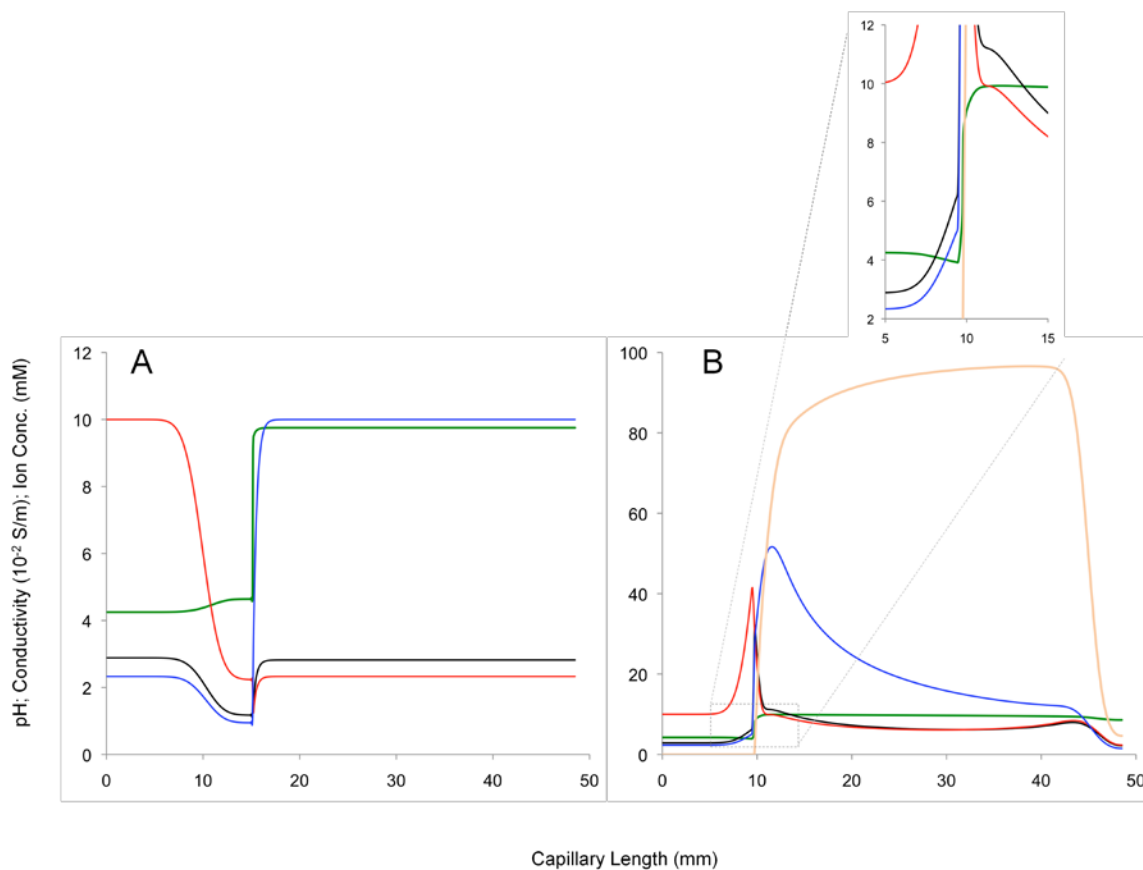


**Figure 3.2.** Simul 5.0 computer simulation of the discontinuous buffers after 1000 s of voltage application in the absence of TRIS (A) and with 100 mM TRIS (B): pH (—), conductivity (—), acetate concentration (—) and ammonium concentration (—) and TRIS concentration. (—). Simulation conditions: TE, 10 mM acetate and 2.33 mM ammonium; LE, 2.33 mM acetate and 10 mM ammonium; sample, 100 mM TRIS prepared in LE; initial pH boundary position, 10 mm; peak width, 0.1 mm for (A) and 35 mm for (B); peak edge, 0.1 mm; EOF, 0; capillary diameter, 50  $\mu$ m; capillary length, 48.5 mm; voltage, 300 V; and temperature, 25  $^{\circ}$ C. Other parameters were left at default values.

The setup in Figure 3.1 A corresponded to an injection of 1 capillary volume (0.95  $\mu\text{L}$ ). Injections of smaller sample volumes could easily be accommodated by partially filling the capillary with sample. Likewise the injection of sample volumes over 1  $\mu\text{L}$  could also be achieved, but required an alteration of the experimental setup in which the sample was placed in a vial at the cathode (Figure 3.3A). Under this condition, the anionic myoglobin molecules were introduced into the capillary during voltage application. They continued to migrate inside the capillary towards the anode until reaching the pH junction where they became trapped. The residual EOF eventually carried the pH junction with the enriched myoglobin to the detector, which was detected at 27 min with an enrichment factor of 470 (Figure 3.3B). TRIS (100 mM), present mainly as neutral molecules at pH 9.75, was not drawn into the capillary by the voltage application. Based on the peak heights, the protein enrichment factors for triplicate selective injection experiments at 0, 10 and 100 mM TRIS were 210 (70), 240 (130), and 260 (190) respectively and ranged from 130-470. The heme peak at 408 nm was observed in all cases. Control experiments with 0 and 100 mM TRIS resulted in no heme peak. The focussed myoglobin peaks were observed between 19 and 31 min due to the varying EOF. Although the average migration times increased with higher TRIS concentration (23, 24, 26 min), the ranges overlapped such that no real difference could be noted. Even greater sample loading could be achieved by introducing a counter balancing flow to keep the protein band from exiting the capillary, as previously demonstrated [20]. In practice, this was limited by electrolysis, which can significantly alter the pH of the discontinuous buffers. The volume of the buffered sample and the concentration of the buffer determine the maximum time for protein enrichment with selective injection. In the experiments performed in Figure 3.3, 50-100  $\mu\text{L}$  of sample solutions were placed at the cathode, and significant pH changes due to electrolysis were not evident in the presented experiments.

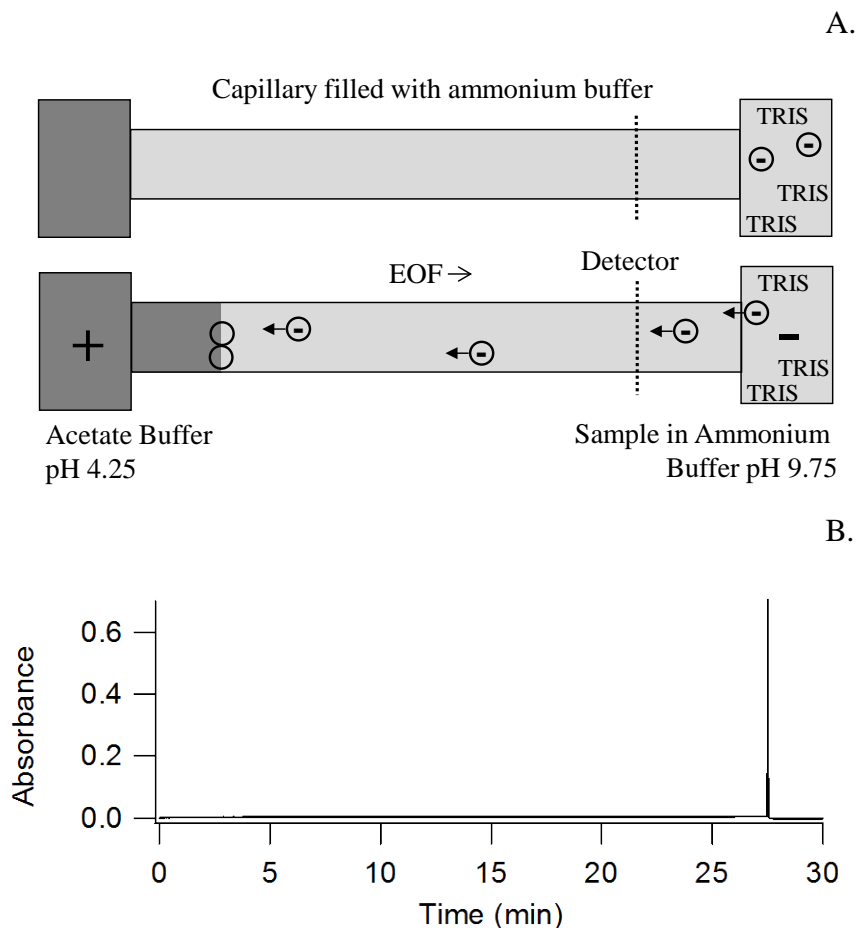


**Figure 3.3.** Schematics representing the selective injection of  $10 \text{ ng } \mu\text{L}^{-1}$  myoglobin from  $100 \text{ mM}$  TRIS prepared in  $\text{pH } 9.75$  ammonium buffer at the cathode and the sequential enrichment upon voltage application (A). The UV-signal recorded during voltage application (B).

### 3.3.2 Protein Enrichment and Removal of MES

Similar to TRIS, MES is a monoprotic weak base ( $\text{pK}_a$  around 6), but MES also has a strongly acidic sulfonate group. As a result, MES is net anionic when fully deprotonated (at  $\text{pH } 9.75$ ), and zwitterionic when fully protonated (at  $\text{pH } 4.25$ ). In a similar fashion performed for TRIS, the removal of MES as neutral, or zwitterionic in this case, molecules from myoglobin is presented. The capillary was filled with the protein-MES sample prepared in  $\text{pH } 4.25$  acetate (Figure 3.4 A). Upon voltage application, a  $\text{pH}$

junction was formed at the cathodic end of the capillary, the end closer to the detection point. The myoglobin molecules migrated as cations toward pH junction, while the zwitterionic MES molecules remained relatively stationary. At the beginning of the run, the capillary was filled with pH 4.25 acetate, resulting in a very small anodic (reversed) EOF. However, the anodic EOF was soon balanced by the cathodic EOF as the pH 9.75 ammonium buffer was drawn in from the cathode. A combination of voltage and pressure was therefore applied during the entire run to carry the myoglobin peak past the detection window. To compensate for EOF variation in replicate runs, the pressure at the anode was adjusted between -1 and -10 mbar, in order to bring the enriched proteins past the detector in approximately 5 min. Figure 3.4 B was produced with a pressure of - 5 mbar. The enrichment factors from 3 replicates ranged from 150 to 220. A control experiment was performed under the same conditions as in Figure 3.4 B with MES absent from the sample. We observed a nearly identical peak with an absorbance of 0.24 (160-fold enrichment), which allowed us to conclude that the protein enrichment was not affected by MES.

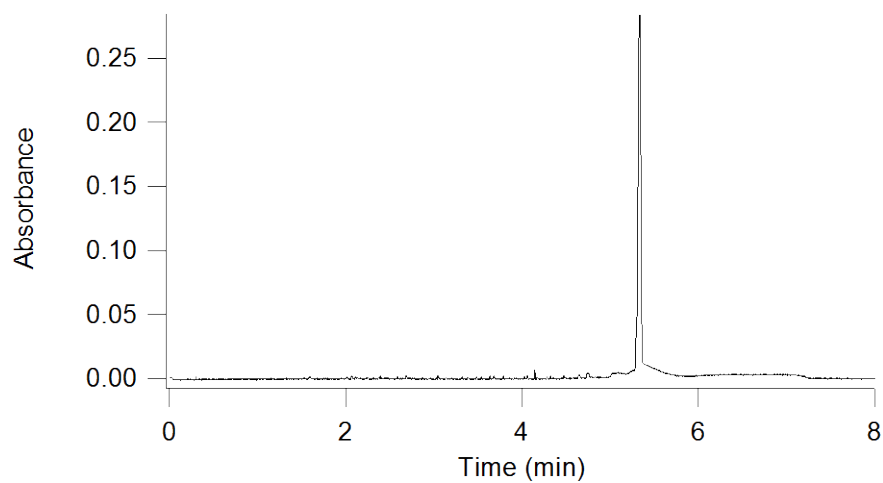
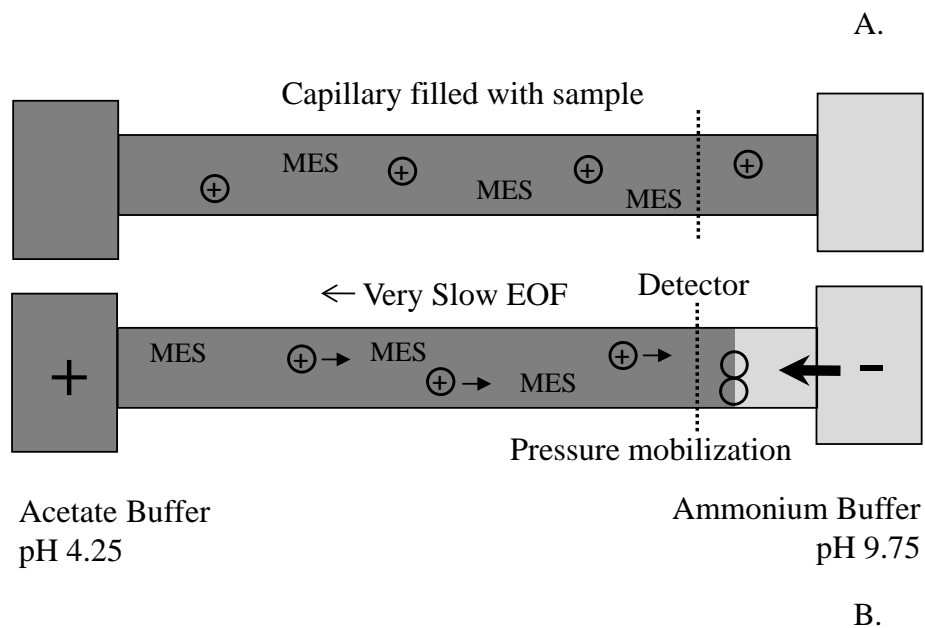


**Figure 3.4.** Schematics representing the injection of  $10 \text{ ng } \mu\text{L}^{-1}$  myoglobin with  $50 \text{ mM}$  MES (prepared in  $\text{pH } 4.25$  acetate) to fill the capillary and the subsequent ion migration (A). UV-absorption signal recorded when  $30 \text{ kV}$  and  $-5 \text{ mbar}$  pressure at the anode was applied simultaneously during the entire run (B).

While the peak heights observed in this experiment were lower than those in Figures 3.1 and 3.3, the differences can be attributed to the different enrichment time elapsed at the detection point. In theory, this could be improved by reducing the applied pressure to below -1 mbar. In practice, our instrument was not capable of delivering reproducible pressure at such a low level.

### 3.3.3 Migration of Phosphate at the pH Junction

The removal of phosphate in the discontinuous buffers is less straight forward compared to TRIS and MES. Phosphate's approximate  $pK_a$  values are 2, 7, and 12 (the actual values depend on the ionic strength). Unlike TRIS and MES, the neutral form of phosphate ( $H_3PO_4$ ) exists outside the operating pH of our discontinuous buffers, and thus it cannot be removed from the proteins as neutral molecules. Phosphate exists as the singly charged  $H_2PO_4^-$  in pH 4.25, and as the doubly charged  $HPO_4^{2-}$  in pH 9.75. In other words, it remains anionic on either side of the pH junction, and does not experience charge reversal like proteins at the pH junction. It was thus hypothesized that the removal of phosphate would occur by its continuous, anodic electromigration across the pH junction, similar to the electromigration of non-buffering anions such as chloride observed in Chapter 2.

To experimentally confirm the migration behaviour of phosphate crossing the pH junction, the UV-absorbing analogue of phosphate, sodium phenyl phosphate (PP), was selected. PP has  $pK_a$  values (2.3 and 5.9) similar to those of phosphate [26], and thus also exists as 1- and 2- ions in the discontinuous buffers used in this work. The experiment began with placing a plug of phenyl phosphate solution prepared in the ammonium buffer next to the discontinuous buffer junction, marked by a mesityl oxide plug (Figure 3.5 A, top). The UV absorbance signals confirmed that the PP was on the cathodic side of the pH junction (pH 9.75), with the mesityl oxide peak marking the end of 1-capillary volume (0 s, Figure 3.5 B). Variable periods of voltage were applied to induce electromigration to various extents, followed by pressure mobilization of the capillary content past the detector. After 120 s of voltage application, the signal revealed that PP ions indeed crossed the pH junction. The absorbance observed was lower on the anodic side of the pH

junction. The absorptivities of phenyl phosphate in pH 9.75 and 4.25 buffers were independently measured and verified to be essentially equal. Thus, the lower absorbance indicated a decrease in PP concentration after crossing the pH boundary.

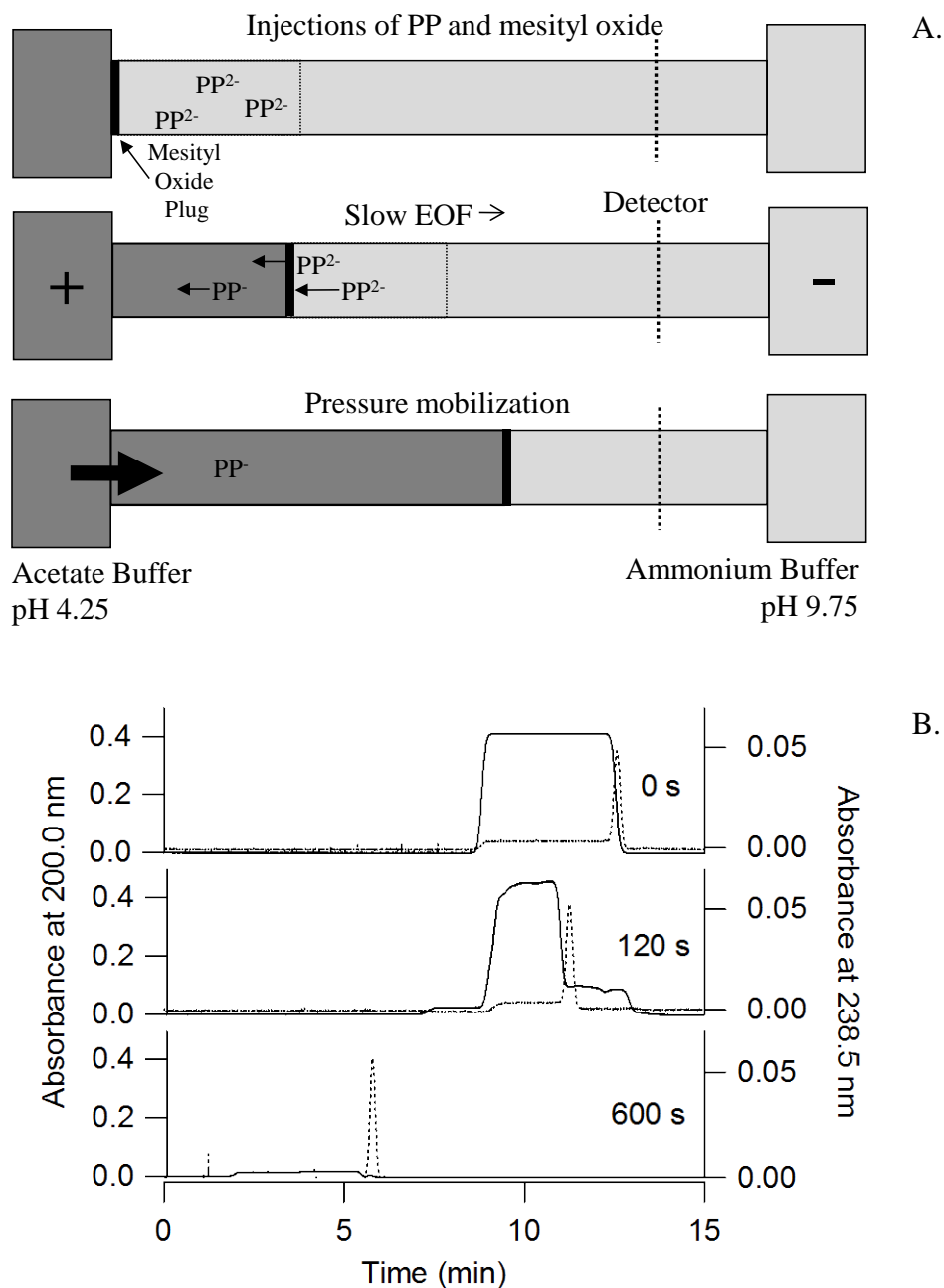


**Figure 3.5.** Schematics of experimental setup and proposed migration behavior of phenyl phosphate (PP) (A). Absorbance signals recorded during pressure mobilization of the capillary content after voltage application for the indicated time (B). Experimental conditions: sodium phenyl phosphate concentration, 10 mM prepared in 10 mM ammonium buffer; mesityl oxide concentration, 20 mM; voltage, 30 kV; mobilization pressure, 30 mbar; and detection, 200 nm for PP (solid line) and 238.5 nm for mesityl oxide (dashed line).



The concentration decrease was hypothesized to be a result of electrodispersion due to the difference in conductivity between the two sides of the pH junction. The ionic strength at the cathodic side of the pH boundary was higher due to the 10 mM PP. When the PP ions crossed the junction, they experienced a reduction in ionic strength (an increase in electrical field), and thus acquired a higher mobility in spite of their charge reduction. The higher mobility of the PP due to the ionic strength reduction was independently confirmed by mobility measurement in conventional capillary zone electrophoresis (data not shown). In addition, computer simulation by Simul 5.0 was used to predict the migration behaviour of phosphate when crossing the pH junction. The simulated phosphate signal (Figure 3.6) closely resembled the experimental phenyl phosphate signal observed in Figure 3.5 B, namely a decrease in phosphate (or phenyl phosphate) concentration was observed when the ions migrated from the basic (cathodic) side to the acidic (anodic) side of the pH junction. In addition, the simulated phosphate concentration drop coincided with the simulated conductivity drop, supporting the hypothesis on electrodispersion. Finally after 600 s of voltage application, the PP completely migrated out of the capillary and was not detected. The results importantly demonstrated that the phenyl phosphate ions crossed the pH junction and continued to electromigrate towards the anode, away from the enriched proteins at the pH junction. The experiment was repeated in triplicate with 10 mM PP for 0, 60, 120, and 600s. The plug shapes for each time matched those shown in Figure 3.5. The phenyl phosphate passed across the pH junction by 600 s in all cases.

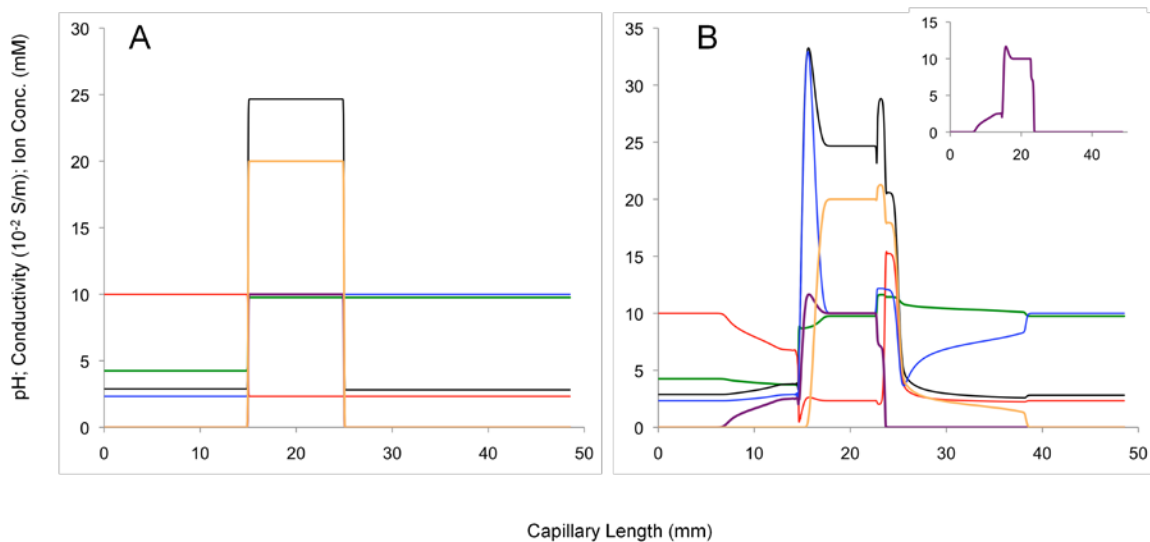


**Figure 3.6.** Simul 5.0 computer simulated results of pH (—), conductivity (—), acetate concentration (—), ammonium concentration (—), phosphate concentration (—) and sodium concentration (—) during voltage application with phosphate containing discontinuous buffers at two time points: (A) 0 s and (B) 30 s. Figure inset is the simplified version of panel B showing only the concentration profile of phosphate. Simulation conditions: TE, 10 mM acetate and 2.33 mM ammonium; LE, 2.33 mM acetate and 10 mM ammonium; sample, 10 mM phosphate and 20 mM sodium prepared in LE; Injection site, 20 mm; peak width, 10 mm; peak edge width 0.1 mm; EOF, 0; capillary diameter, 50  $\mu\text{m}$ ; capillary length, 48.5 mm; voltage, 300 V; and temperature, 25  $^{\circ}\text{C}$ . Other parameters were left at default values.

### 3.3.4 Phosphate Removal during Protein Enrichment

In this section, the enrichment of myoglobin in the presence of sodium phosphate was performed. To monitor the migration of myoglobin near the pH junction, a plug of myoglobin was positioned next to the pH junction, and an increasing duration of voltage was applied followed by pressure mobilization for detection. One had a choice of preparing the myoglobin-phosphate sample in pH 9.75 with ammonium and placing the plug at the cathodic side of the junction, or by bringing the pH to 4.25 with acetate and placing it at the anodic side of the junction. Having phosphate on the anodic side, as

illustrated in Figure 3.7 A, allowed its migration out of the capillary without having to cross the junction. This minimized the effect of phosphate on the pH junction, and therefore was the chosen setup for this experiment. Voltage application was allowed to proceed for 0, 1, 5, or 10 min, followed by pressure mobilization of the capillary content past the detector. The results are shown in Figure 3.7 B. A control experiment, using a sample without sodium phosphate, was also performed under the same conditions (Figure inset).

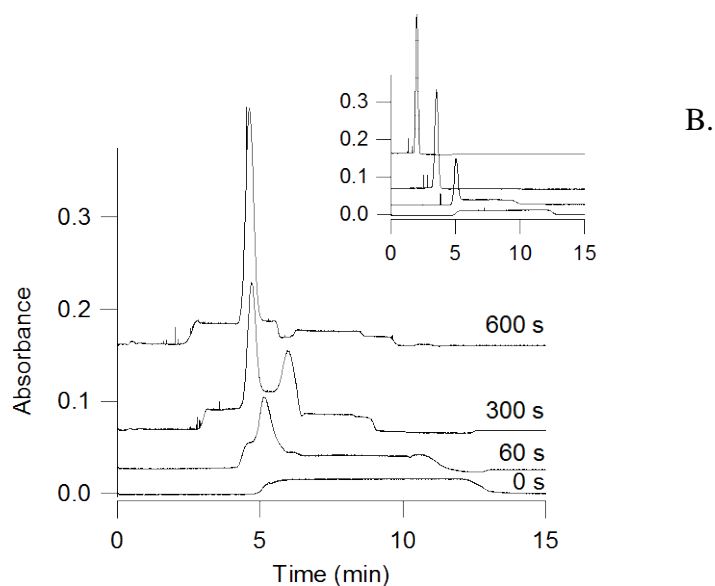
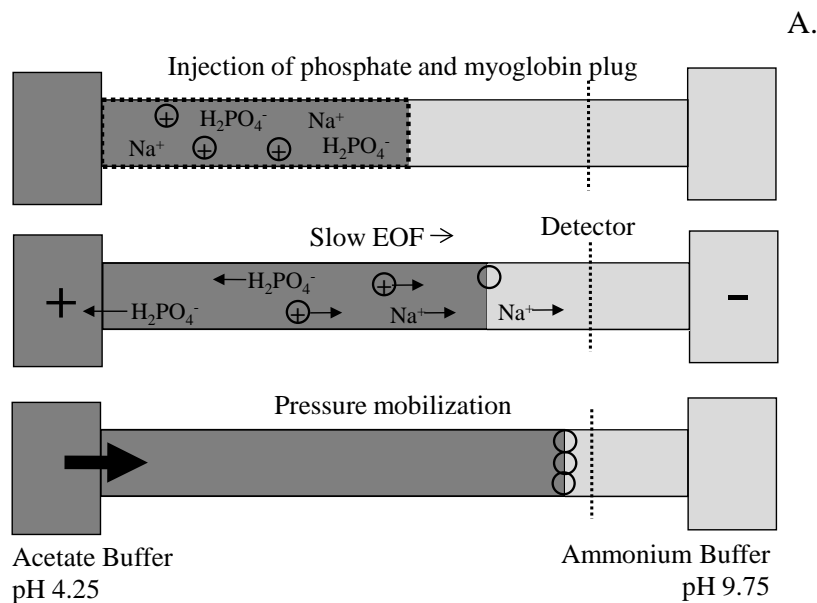


**Figure 3.7.** A schematic showing the electrofocussing of a plug of myoglobin ( $100 \text{ ng } \mu\text{L}^{-1}$ ) and sodium phosphate ( $30 \text{ mM}$ ) prepared in  $10 \text{ mM}$  pH 4.25 acetate buffer (A). The UV-absorbance signals recorded during pressure mobilization ( $30 \text{ mbar}$ ) of capillary content containing the myoglobin-phosphate sample after various periods of voltage application: 0, 1, 5 and 10 min (B). (Inset showing the results of control experiments obtaining from myoglobin without phosphate. Voltage application time was 0, 1, 5 and 10 min from bottom to top).

In the absence of phosphate, the enrichment was completed in five min of voltage application. The accumulation of myoglobin occurred as expected at the left side of the plug (inset of Figure 3.7 B); i.e., at the junction of the sample plug (prepared in acetate) and the ammonium buffer. The residual cathodic EOF slowly moved the capillary content towards the detector and resulted in the peak shift towards the y-axis. When sodium phosphate (30 mM) was added to myoglobin, the enrichment process also proceeded with accumulation of myoglobin at the left side of the sample plug (Figure 3.7B); however a second peak also appeared after 5 min of protein enrichment. The entire set of experiments was also repeated with 10 mM of sodium phosphate. Nearly identical protein enrichment behaviour was observed, although it occurred at a faster rate for the lower phosphate concentration. For example, the 300 s trace from 10 mM phosphate resembled that of the 600 s trace from 30 mM phosphate (data not shown).

To address the double peak observed during enrichment, Simul 5.0 computer simulation was applied to model the system (Figure 3.8). In the initial phase (Panel B), the phosphate and sodium zones electromigrated in opposite directions away from the sample zone. Upon their exit, they were replaced with acetate and ammonium ions. Most importantly, the zone passing between acetate and ammonium resulted in a substantial change in conductivity, and as a result, a two-step pH gradient was observed. This pH gradient profile was most likely responsible for the double-peak myoglobin signal observed in Figure 3.7B (at 300 s). Finally after a longer period, nearly all sodium and phosphate ions exited the capillary. The acetate and ammonium ion distribution also evolved to the point where a single-step pH transition was observed. This likely was responsible for the single myoglobin peak observed in Figure 3.7B (at 600 s). The absorbance of this peak was 0.23, (15-fold enrichment) which was lower than the absorbance of 0.25 and 0.38 (17- and 25- fold) from the control experiments respectively at 5 and 10 min. Nevertheless, the absorbance was recorded during pressure mobilization, and therefore the peak height was dependent on the position of the peak in reference to the detection point because of laminar flow band-broadening. Taking this into account, we can conclude that comparable peak height values were observed in the enrichment of myoglobin with and without sodium phosphate.

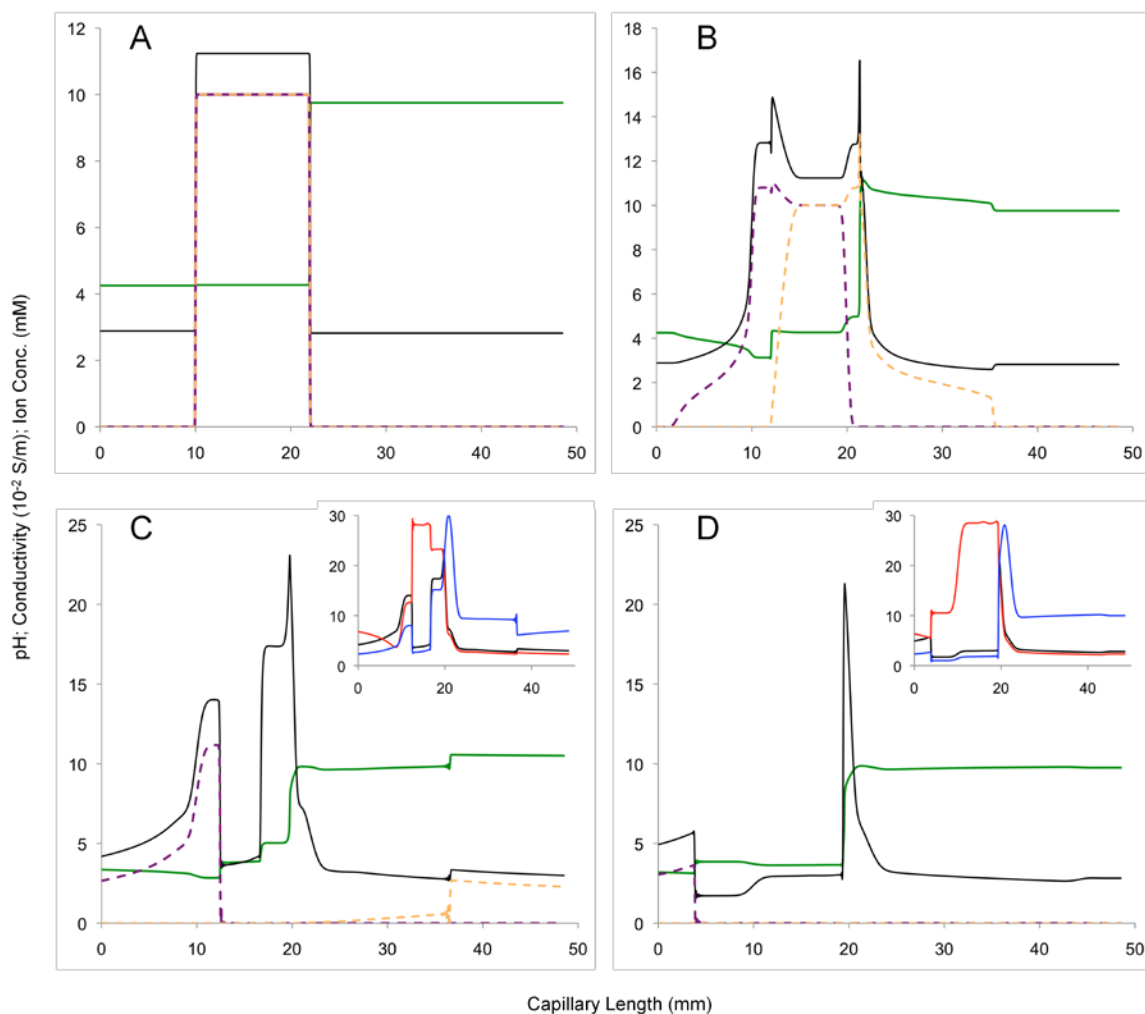


**Figure 3.8.** Simul 5.0 computer simulated results of pH (—), conductivity (—), phosphate concentration (- - -) and sodium concentration (- - -) at various time points: (A) 0 s, (B) 30 s, (C) 150 s and (D) 270 s. Figure insets display the concentration profiles of acetate (—) and ammonium (—) in order to illustrate their effects on the conductivity. Simulation conditions: TE, 10 mM acetate and 2.33 mM ammonium; LE, 2.33 mM acetate and 10 mM ammonium; sample, 10 mM phosphate and 10 mM sodium prepared in TE; Injection site, 16 mm; peak width, 12 mm; peak edge width 0.1 mm; EOF, 0; capillary diameter, 50  $\mu$ m; capillary length, 48.5 mm; voltage, 300 V; and temperature, 25  $^{\circ}$ C. Other parameters were left at default values.

To better compare the enrichment factors of myoglobin in the presence and absence of phosphate, experiments were repeated with the entire capillary filled with  $100 \text{ ng } \mu\text{L}^{-1}$  myoglobin prepared in pH 4.25 acetate. Voltage was applied during enrichment (30 min) followed by pressure mobilization for detection (conditions otherwise same as Figure 3.7). When 30 mM of phosphate was present in the sample, the enriched myoglobin band was found to locate at the anodic side of the detection window after 30 min of voltage application. It was detected as a sharp peak with an absorbance of 0.77 (51-fold enrichment) after 5 min of pressure mobilization at 30 mbar in the cathodic direction (data not shown). In the control experiment performed without phosphate, the myoglobin band stopped at the cathodic side of the detection point after voltage application, due to a different residual EOF obtained in the absence of phosphate. Pressure mobilization in the anodic direction at 30 mbar was used, and a peak with an absorbance of 0.63 was observed in approximately 3 min (42-fold enrichment, data not shown). Due to the use of pressure, the time and absorbance of the peaks were variable from run-to-run, and thus the enrichment factors could not be taken as precise values for comparison. Nevertheless, it was suffice to conclude that equally successful enrichment of myoglobin was obtained despite of the presence of phosphate.

## 3.4 Conclusions

Based on the results obtained with the model protein myoglobin, the use of discontinuous buffers to create a step-pH junction for protein enrichment is not only an effective method to enrich extremely small volumes of proteins, but can also remove unwanted buffering ions. The flexibility of the experimental setup accommodates the removal of different types of buffering ions. Namely, the protein samples can be prepared in either the ammonium buffer or the acetate buffer to facilitate the removal of different buffering ions. For TRIS, sample preparation in ammonium buffer allowed the negatively charged myoglobin to be removed from the predominately neutral TRIS. The removal of MES as zwitterions, on the other hand, required sample preparation in the acetate buffer. Phosphate does not exist as neutral molecules within the pH range of the discontinuous buffers, and therefore required a different removal mechanism. In that case, a sample containing phosphate was prepared in the acetate buffer. During voltage application, the phosphate ions migrated as anions away from the pH junction, while myoglobin migrated as cations toward the junction.

Despite the successes reported in this chapter, the developed method may not be readily applicable to any real samples, as compatibility with other commonly used additives or solubilization reagents in sample preparation such as urea and surfactants remains to be studied. The enrichment of proteins is also, in theory, limited to those with  $pI$  values between the two pH values of the discontinuous buffers. Nevertheless, the compatibility of our discontinuous buffers with buffering and non-buffering ions obviously represents an important step towards the handling of any samples from biological origins.



### 3.5 References

- [1] L.L. Sun, J.F. Ma, X.Q. Qiao, Y. Liang, G.J. Zhu, Y.C. Shan, Z. Liang, L.H. Zhang & Y.K. Zhang. Integrated Device for Online Sample Buffer Exchange, Protein Enrichment, and Digestion, *Analytical Chemistry*, **2010**, 82, 2574-2579.
- [2] L.A. Kartsova & E.A. Bessonova. Preconcentration techniques in capillary electrophoresis, *Journal of Analytical Chemistry, Chem.*, **2009**, 64, 326-337.
- [3] Z. Malá, A. Šlampová, P. Gebauer & P. Boček. Contemporary sample stacking in CE, *Electrophoresis*, **2009**, 30, 215-229.
- [4] S.L. Simpson, J.P. Quirino & S. Terabe. On-line sample preconcentration in capillary electrophoresis Fundamentals and applications, *Journal of Chromatography A*, **2008**, 1184, 504-541.
- [5] D.C. Simpson & R.D. Smith. Combining capillary electrophoresis with mass spectrometry for applications in proteomics, *Electrophoresis*, **2005**, 26, 1291-1305.
- [6] C.A. Nesbitt, H.X. Zhang & K.K.C. Yeung. Recent applications of capillary electrophoresis-mass spectrometry (CE-MS): CE performing functions beyond separation, *Analytica Chimica Acta*, **2008**, 627, 3-24.
- [7] M.R.N. Monton & S. Terabe. Sample enrichment techniques in capillary electrophoresis: Focus on peptides and proteins, *Journal of Chromatography B*, **2006**, 841, 88-95.
- [8] A.S. Rathore. Joule heating and determination of temperature in capillary electrophoresis and capillary electrochromatography columns, *Journal of Chromatography A*, **2004**, 1037, 431-443.
- [9] T.M. Annesley. Ion Suppression in Mass Spectrometry, *Clinical Chemistry*, **2003**, 49, 1041-1044.
- [10] M.C. Breadmore, M. Dawod & J.P. Quirino. Recent advances in enhancing the sensitivity of electrophoresis and electrochromatography in capillaries and microchips (2008-2010), *Electrophoresis*, **2011**, 32, 127-148.
- [11] Y.P. Zhao & C.E. Lunte. pH mediated field amplification on-column preconcentration of anions in physiological samples for capillary electrophoresis, *Analytical Chemistry*, **1999**, 71, 3985-3991.

- [12] A.S. Ptolemy & P. Britz-McKibbin. New advances in on-line sample preconcentration by capillary electrophoresis using dynamic pH junction, *Analyst*, **2008**, *133*, 1643-1648.
- [13] K. Imami, M.R.N. Monton, Y. Ishihama & S. Terabe. Simple on-line sample preconcentration technique for peptides based on dynamic pH junction in capillary electrophoresis-mass spectrometry, *Journal of Chromatography A*, **2007**, *1148*, 250-255.
- [14] M.N. Hasan, S.H. Park, E. Oh, E.J. Song, E. Ban & Y.S. Yoo. Sensitivity enhancement of CE and CE-MS for the analysis of peptides by a dynamic pH junction, *Journal of Separation Science*, **33**, 3701-3709.
- [15] C.-X. Cao, Y.-Z. He, M. Li, Y.-T. Qian, M.-F. Gao, L.-H. Ge, S.-L. Zhou, L. Yang & Q.-S. Qu. Stacking Ionizable Analytes in a Sample Matrix with High Salt by a Transient Moving Chemical Reaction Boundary Method in Capillary Zone Electrophoresis, *Analytical Chemistry*, **2002**, *74*, 4167-4174.
- [16] C.X. Cao, L.Y. Fan & W. Zhang. Review on the theory of moving reaction boundary, electromigration reaction methods and applications in isoelectric focusing and sample pre-concentration, *Analyst*, **2008**, *133*, 1139-1157.
- [17] M.C. Breadmore, R.A. Mosher & W. Thormann. High-resolution computer simulations of stacking of weak bases using a transient pH boundary in capillary electrophoresis. 1. Concept and impact of sample ionic strength, *Analytical Chemistry*, **2006**, *78*, 538-546.
- [18] W. Zhu, W. Zhang, L.-Y. Fan, J. Shao, S. Li, J.-L. Chen & C.-X. Cao. Study on mechanism of stacking of zwitterion in highly saline biologic sample by transient moving reaction boundary created by formic buffer and conjugate base in capillary electrophoresis, *Talanta*, **2009**, *78*, 1194-1200.
- [19] C.A. Nesbitt, J.T.M. Lo & K.K.C. Yeung. Over 1000-fold protein preconcentration for microliter-volume samples at a pH junction using capillary electrophoresis, *Journal of Chromatography A*, **2005**, *1073*, 175-180.
- [20] K. Jurcic, C.A. Nesbitt & K.K.C. Yeung. Characterization of discontinuous buffer junctions using pH indicators in capillary electrophoresis for protein preconcentration, *Journal of Chromatography A*, **2006**, *1134*, 317-325.
- [21] C.A. Nesbitt, K. Jurcic & K.K.C. Yeung. Nanoliter-volume protein enrichment, tryptic digestion, and partial separation based on isoelectric points by CE for MALDI mass spectral analysis, *Electrophoresis*, **2008**, *29*, 466-474.
- [22] C.A. Nesbitt & K.K.C. Yeung. In-capillary enrichment, proteolysis and separation using capillary electrophoresis with discontinuous buffers: application on proteins with moderately acidic and basic isoelectric points, *Analyst*, **2009**, *134*, 65-71.

- [23] J.M. Cunliffe, N.E. Baryla & C.A. Lucy. Phospholipid bilayer coatings for the separation of proteins in capillary electrophoresis, *Analytical Chemistry*, **2002**, *74*, 776-783.
- [24] V. Hruška, M. Jaroš & B. Gaš. Simul 5 - Free dynamic simulator of electrophoresis, *Electrophoresis*, **2006**, *27*, 984-991.
- [25] I.F. Shieh, C.Y. Lee & J. Shiea. Eliminating the interferences from TRIS buffer and SDS in protein analysis by fused-droplet electrospray ionization mass spectrometry, *J. Proteome Res.*, **2005**, *4*, 606-612.
- [26] H. Fretz. O-(carboxydifluoromethyl)-L-tyrosine: Design and synthesis of a novel non phosphorous-containing phosphotyrosine isostere, *Tetrahedron*, **1998**, *54*, 4849-4858.

**Chapter 4: Enrichment of Phosphorylated Peptides using Selective Retention with Magnetic Beads On-Line in Capillary Electrophoresis**

Enrichment of proteins and peptides is paramount for successful identification and sequencing, and the past two chapters have discussed how CE can be used as an on-line tool for both enrichment and sample clean-up. Discontinuous buffers can enrich proteins in the presence of permanently charged ionic and buffering ions. A limitation exists, however, in that the analyte must have an isoelectric point that falls between the pH values of the discontinuous buffers. A second limitation is in the sample recovery options, where the final sample must be in one or both of the buffers. Another novel option is to incorporate magnetic beads in the capillary for selective sample enrichment, purification, and unique sample recovery. An investigation into the preparation for using magnetic beads on-line is presented herein.

## 4.1 Introduction

The phosphoproteome is a subsection in the broad proteomics field, but one that is of extreme importance for biological regulatory pathways, including cell signalling, gene expression, and apoptosis. Proteins are activated or deactivated by posttranslational modifications (PTM) and this can be the difference between a healthy, functioning cell, and one that is in danger. Phosphorylation is only one of many types of PTM, but is one of greatest import for disease biomarkers and pharmaceutical targets. The presence or absence of a phosphorylation modification at a serine, threonine, or tyrosine residue is catalized by kinases which add a phosphate or by phosphatases which remove a phosphate [1]. Kinases are currently targets for potential cancer drugs [2]. The identification of phosphorylation sites is important for understanding diseases, early diagnosis, and drug targeting.

Phosphorylation is a dynamic process. Only a small ratio of an existing protein may be phosphorylated at any one time, and those phosphorylated may only be in that state for a limited time. Even the intact phosphate can become dissociated from the peptide during mass spectral analysis making it undetectable. An additional challenge is the inherent acidic nature of phosphorylated peptides. A phosphorylated peptide incurs additional

negative charges from its phosphate group which leads to a lower pKa value than its non-phosphorylated analog. Thus, more positive charges are required to ionize the sample. MALDI mass spectrometry is not a true quantitative technique, and easily ionized components compete with components that are difficult to ionize and the end result is that the signal from the phosphorylated peptides is suppressed. The low abundance, low pKa value, and labile group properties are the issues that must be resolved for successful phosphoproteome analysis.

To address the low abundance issue of phosphorylated peptides, enrichment can be performed to improve the detection sensitivity. Selective enrichment of only the phosphorylated peptides is an even better option as this can also reduce the ionization competition between analytes. Metal affinity or metal oxide affinity techniques are common phosphopeptides enrichment techniques. Immobilized metal affinity chromatography (IMAC) involves a ligand, such as tetradentate nitrilotriacetate, bound to a resin that binds a metal, such as Fe(III) [3]. This metal selectively interacts with acidic residues and has a great affinity for the negatively charged phosphate modification. This method was first proposed by Porath *et al.* [4] and modifications to the ligand [5], metal [6], binding and rinsing buffers have improved this technique for phosphopeptide analysis. By applying this type of interaction to a capillary column, Figeys and colleagues have demonstrated nanoliter-volume phosphopeptide enrichment integrated with protein digestion and LC-MS analysis for the identification of hundreds of phosphoproteins [7]. Drawbacks to IMAC include the nonspecific binding of acidic residues (aspartic acid and glutamic acid) and complete elution challenges. Metal oxide affinity designs are a more recent development than IMAC, are simpler to perform in that no mediating ligand is required, and are more stable over temperature and pH [3]. The most common metal oxide technique uses titanium dioxide directly bound to a resin. Titania has specific binding properties with the acidic phosphate group, more so than with other acidic residues. Experimental progress in the selection of binding and elution buffers has allowed this method to produce very high recoveries of phosphopeptides. An example of a methodological advance is to add the traditional MALDI matrix ion 2,5-dihydroxybenzoic acid (DHB) to the binding and rinsing buffers which leads to more selective adherence of the desired peptides [8]. These metal/oxide affinity binding

techniques have been investigated on different platforms, the most common being a column, but have also been applied to packed pipette tips [9], the high surface to volume ratio nanoparticles [10,11], magnetic beads [12,13], and even directly to the MALDI target plate [3].

An alternative category of enrichment techniques replaces or modifies the phosphate moiety prior to enrichment with a covalently bound tag (Figure 4.1, phosphate replacement with a tag). Reversible covalent binding techniques allow the enrichment step to be even more selective than methods that rely solely on affinity. The tag covalently binds with the resin while the non-modified peptides pass through unretained. Drawbacks to this technique include the additional steps required for derivatization which could lead to longer sample preparation times and potential sample loss. Even so, for covalent techniques that replace the phosphate group, the second and even more important element is that the location of the phosphate modification is securely labelled. The tag is not labile during MS analysis like the phosphate group and this makes the determination of the PTM location much easier to determine. Such a design was proposed by Oda, Nagasu and Chait for the study of phosphoserine and phosphothreonine where a dithiol molecule, subsequently modified with a biotin moiety, replaced the phosphate group and enrichment was performed through the well established biotin/streptavidin interaction [14]. The biotin group was added to the peptide after a  $\beta$ -elimination reaction and Michael addition with ethanedithiol. A simpler process was then developed by Rusconi and colleagues that did not require the biotin modification, but stopped after the Michael addition of a dithiol group, this time propanedithiol [15]. This thiol tag covalently bound to the resin (modified with dithiopyridine) and the peptides of interest were eluted by the preferred reaction with dithiothreitol (DTT). A notable application of this dithiol covalent chromatography technique was published by Salih *et al.* to investigate the human whole saliva phosphoproteome [16]. Many previously unknown phosphoproteins were identified through this reversible covalent binding technique. The work in this chapter was built upon the foundation of this covalent enrichment technique application. Other reversible covalent binding techniques have been developed, as discussed in this review [3], but further work must continue to improve the peptide recovery and limit the number of labour intensive steps.

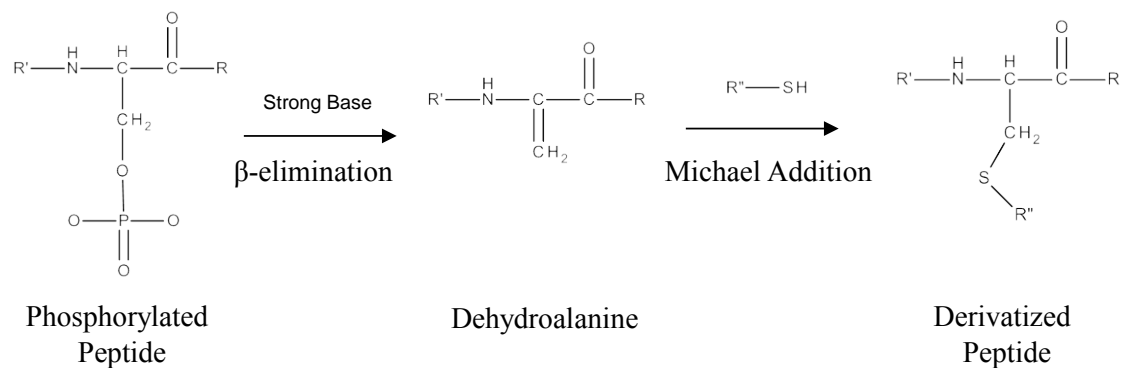


**Figure 4.1.** Chemical reactions for the derivatization of phosphorylated peptides.

Although chromatography is the most common platform for phosphopeptide enrichment and isolation techniques, miniaturized formats such as magnetic beads are being investigated. Magnetic beads are a unique platform that allows for more diversity in the enrichment and separation strategies. The experiment can be performed in-vial or even in a capillary and does not require the high pressures, packed columns, or instrumentation of high performance liquid chromatography (HPLC). These beads can be nano- to micro-size in diameter and be modified to selectively interact with the sample of interest, whereupon an external magnet can isolate the beads and desired analyte from a complex mixture. Analytes can range from whole cells, to DNA, to proteins [17]. The selective interaction between the analyte and modified magnetic beads can be based on metal/oxide-phosphate affinity, such as titania coated magnetic beads with phosphorylated samples [12], based on immunoaffinity, such as a phosphotyrosine antibody/Protein G for the isolation of phosphotyrosine peptides [18], based on other specific affinities, such as biotin/avidin interactions with modified analytes [19], or based on reversible covalent interactions, such as a thiol reaction in this work. In addition to analyte extraction, magnetic beads can be used for immobilization of specific compounds, such as enzymes like trypsin, for faster and more reproducible reactions in micro-sized channels [20]. The potential applications for magnetic beads are vast.

Magnetic beads in combination with capillary electrophoresis is an exciting and developing field. Magnetic beads are easily used for in-vial techniques by applying a magnet to the bottom of the vial to isolate the bound analyte. However, groups have also



investigated the potential of incorporating a plug of magnetic beads in a capillary or microfluidic device for miniaturized and automated selective isolation and enrichment of a variety of samples. An excellent review on the development and application of magnetic beads for microfluidic devices can be found in reference [17]. An example of a magnetic bead plug in a capillary used streptavidin-coated magnetic beads modified with a specific biotinylated RNA to isolate specific rRNA sequences through affinity capillary electrophoresis [19]. The modified magnetic particles were collected in the capillary by an adjacent magnet, the sample was injected, and only the analytes that interacted with the specific RNA sequence were retained while the others were washed from the capillary. The benefits of this method over traditional in-vial procedures was the short analysis time, automation, and quantitative detection (and separation) of various probes. Capillary electrophoresis is best known for its analyte separation capabilities, but as has been discussed in the previous chapters, CE can also be used as a new tool for automated and miniaturized sample preparation method, especially with the development of on-line magnetic bead procedures.

The enrichment of phosphorylated peptides by a covalent modification has been demonstrated by many research groups [3,16,21], and the DTT-derivatization of phosphorylated peptides has been published by other groups as well [16,22]. However, this enrichment has not yet been demonstrated, to our knowledge, using magnetic beads as the solid support, nor has this process been explored for applications in a capillary. The goal for this chapter was to merge the sample preparation abilities of CE with the versatility and specificity of magnetic beads to miniaturize a reversible covalent binding technique for phosphorylated peptides. In collaboration with one of the authors, Dr. Walter L. Siqueira, the phosphorylated peptide enrichment methodologies in [16] were miniaturized from large scale gels, columns, and millilitre sample volumes to magnetic beads, capillaries, and micro to nanoliter sample volumes. In contrast to the large scale saliva applications of [16], the work discussed in this chapter was designed for the ultra-low volume human acquired enamel pellicle, an uncharted but important protein rich film around the enamel surface of teeth [23,24]. The method developments for low volume samples discussed in this chapter could be applied to any such sample with low abundance proteins or samples of limited volume.

The small sample volumes used in CE and low abundance samples like the enamel pellicle phosphoproteome require the most efficient use of the available analyte for successful sample detection. Thus, the sample derivatization conditions and magnetic bead reaction conditions were analyzed in-vial to optimize the procedure to allow for the greatest sample recovery for applications in CE. These optimized conditions were then applied to preliminary in-capillary trials. The method developments for this low-volume sample enrichment technique have great potential for the exploration low abundance, uncharted phosphoproteomes.

## 4.2 Materials and Methods

### 4.2.1 Apparatus

In-vial experiments were performed in Maxymum Recovery microtubes. All in-capillary experiments were performed in a 50  $\mu\text{m}$  inner diameter (364  $\mu\text{m}$  o.d.) capillary, cut to 48.5 cm with a 40.25 cm effective length. These fused silica capillaries were purchased from Polymicro Technologies (Phoenix, AZ) and used in an Agilent <sup>3D</sup>Capillary Electrophoresis instrument (Palo Alto, CA) at 25 °C. An on-line UV-visible absorbance detector was used to monitor the experiment progress. The Agilent <sup>3D</sup>CE ChemStation software controlled the instrument and data acquisition. A ProMag neodymium (NdFeB) circular magnet (6.3 or 12.7 mm diameter, Magnum Magnetics Corp, Ohio) was reversibly adhered to the capillary cassette, 10.2 cm from the inlet.

An Applied Biosystems 4700 MALDI TOF mass spectrometer (Foster City, CA) equipped with a 355 nm ND:YAG laser (200 Hz) was used to analyze the protein and peptide samples. Data acquisition was performed using a 4000 Series Explorer (Applied Biosystems) while data processing was executed with the Data Explorer (Applied Biosystems) and Igor Pro software (WaveMetrics, Lake Oswego, OR). Each mass spectrum was a sum of 1000 shots. Linear and reflecton modes were used, with calibration for reflectron mode at 50 ppm.

#### 4.2.2 Reagents

Thiol-activated (2-pyridyl disulfide) long arm linker magnetic beads (1  $\mu\text{m}$  uniform diameter) were purchased from Bioclone Inc. (California, US). The beads were suspended in 20% ethanol (Commercial Alcohols, Canada). Buffer solutions were prepared from ammonium bicarbonate (Sigma), calcium chloride (Caledon Laboratories, Georgetown, ON), and ethylenediaminetetraacetic acid (EDTA, BioShop Canada Inc., Burlington, ON). Other solutions included trifluoroacetic acid (TFA, Fisher Scientific), acetonitrile (Caledon), and ammonium phosphate (Sigma).  $\alpha$ -cyano-4-hydroxycinnamic acid (CHCA, Sigma) was used as the MALDI matrix. DL-dithiothreitol (DTT, Sigma) was used as the “tag” for the phosphorylated peptides as well as the elution chemical. Samples for analysis included a monophosphorylated peptide from bovine  $\beta$ -casein (Sigma), and  $\beta$ -casein from bovine milk (Sigma Aldrich) digested with sequencing grade modified trypsin (Promega, Madison, WI).

#### 4.2.3 MALDI MS Analysis

For in-vial experiments, samples were premixed and spotted at a 1:1 ratio (v/v, total volume 0.73  $\mu\text{L}$ ) with CHCA matrix (5.5  $\text{mg mL}^{-1}$ ) in 6 mM ammonium phosphate monobasic, 50% acetonitrile and 0.1% trifluoroacetic acid. For sample spotting from the capillary, the outlet end of the capillary (by the detector) was removed from the instrument while the inlet end remained inside the instrument and approximate 200 nL spots (50 mbar for 120 s) were deposited directly onto the MALDI plate. A 200 nL drop of matrix (above 5.5  $\text{mg mL}^{-1}$  solution) was immediately added to this spot so that mixing occurred between the sample and matrix before drying.

#### 4.2.4 $\beta$ -Casein Digestion

In order to prepare a mixture of peptides containing some phosphorylated modifications, a trypsin digestion was performed on  $\beta$ -casein. Trypsin cleaves the protein at arginine (R)

and lysine (K) residues. A one milliliter reaction with  $\beta$ -casein from bovine milk (1 mg) and sequencing grade modified trypsin (20  $\mu$ g) to an overall ratio of 1:50 (w/w) trypsin to protein prepared in 50 mM ammonium bicarbonate (pH 8) and 2 mM calcium chloride was set at 37 °C overnight. The reaction solution was then lyophilized to dryness, resolvated in water at a 2 mg mL<sup>-1</sup> concentration, and stored in the freezer (-20 °C).

#### 4.2.5 Phosphorylated Sample Derivatization

Phosphorylated peptides were derivatized with a covalently bound DTT modification. Various reaction conditions were explored with purified monophosphorylated peptide and  $\beta$ -casein trypsin digest and the exact conditions are specified throughout this chapter. The peptides/protein (0.1 to 1 mg mL<sup>-1</sup>) were prepared in 300 mM NaOH and 5-100 mM DTT and gently mixed for 5 min to 8 hours at 50 °C. The reaction was quenched by the addition of trifluoroacetic acid and then stored in the freezer (-20 °C).

#### 4.2.6 Solid Phase Clean-up (C18 ZipTips™)

Once the samples were derivatized with the DTT tag, it was necessary to remove the excess DTT and NaOH from the reaction solution to allow the derivatized peptides to react with the thiol-activated magnetic beads. In order to perform this clean-up, solid phase C-18 in a pipet tip (ZipTips™, standard bed, Millipore Corporation) were used to bind the peptides and wash away the contaminants.

Enrichment and clean-up with ZipTips™ was performed according to the provided protocol with some minor variations. The tips were wetted with 50% ACN and prepared by aspirating with 0.1% TFA. The sample was then aspirated and adsorbed onto the tip (5-10  $\mu$ L, 0.05 to 4  $\mu$ g sample). The adsorbed peptides were then washed with 0.1% TFA. The sample was eluted with 5  $\mu$ L of 80% acetonitrile into a low retention microtube where it was air evaporated at room temperature to dryness. The sample was then resolvated in an appropriate buffer for the next experiment.

#### 4.2.7 Thiol-Activated Magnetic Bead Experiments

The thiol-activated magnetic beads were prepared as suggested in the protocol, with some minor adjustments. Initial magnetic bead solutions were prepared at a  $30 \text{ mg mL}^{-1}$  concentration in 20% ethanol and stored in the fridge ( $4 \text{ }^{\circ}\text{C}$ ). Prior to experimentation, the beads were rinsed with the buffer solution (50 mM ammonium bicarbonate, 5 mM EDTA) and prepared to the desired concentration ( $30 \text{ mg mL}^{-1}$ ).

In-vial reactions were performed as follows. Each rinsing step was executed by adding the solution to the beads with a pipette, mixing with the pipette tip (aspirating) or vortexing for 1-2 s, setting the microtube close to a magnet and waiting approximately one minute for the magnetic beads to settle to the bottom of the vial. The supernatant was removed by a pipette and the next solution was added immediately. Derivatized samples prepared in the buffer solution were added to the beads ( $0.1$  to  $0.2 \text{ mg mL}^{-1}$  sample) to a total volume of 5 or 10  $\mu\text{L}$ . The binding reaction times examined varied from 5 min to 8 h. The rinsing step to remove the unbound peptides was performed by adding 50:50 buffer:ACN to the vial, vortexing 1-2 s, setting the vial on the magnet, and removing the supernatant. Typical rinsing for a 10  $\mu\text{L}$  experiment involved three, 50  $\mu\text{L}$  washes. Elution was then performed with DTT prepared in water (5 mM to 100 mM) and the supernatant was collected after gentle rotation for 5 to 30 min.

In-capillary experiments were performed with similar reaction steps, but the apparatus set-up was unique. An external, cylindrical magnet was taped to the cassette that held the capillary such that the capillary crossed the magnet at 10.2 cm from the inlet end. The CE work in previous chapters required a coating on the inner capillary wall to suppress the electroosmotic flow and reduce analyte adsorption to the capillary. The experiments in this chapter did not employ a capillary coating as the analytes were peptides rather than proteins, which adsorb much less significantly than the large proteins.

Two sample injection techniques were tested. The first allowed the analyte and magnetic beads to be premixed in-vial before injection into the capillary. The second method allowed the magnetic bead plug to form in-capillary, followed by the sample injection and in-capillary mixing. The magnetic bead solution ( $30 \text{ mg mL}^{-1}$ ), or premixed

analyte and magnetic bead solution, was placed at the inlet and pressure (30 mbar) was applied for 60 s (3.1 cm plug, ~61 nL). As the magnetic bead dispersion was injected into the capillary, the beads collected at the magnet generating a small plug in the capillary. The length of the plug was directly dependent upon the concentration of the magnetic bead solution and the injection conditions of time and pressure. The plug could be detected through the polyimide coating by a sharp eye, and was photographed under a microscope (5x optical). Once the magnetic beads were injected, buffer was added (50 mbar, 300 s) to ensure all injected magnetic beads reached the detector. For the second sample injection technique, the sample was then injected into the capillary as a small plug (50 mbar, 48 s, equivalent to ~61 nL). Mixing was performed by mobilizing the sample to the magnetic beads plug (50 mbar) and then moving the sample across the magnetic beads plug for 10 min (+50, -50 mbar). The following steps were the same for both sample introduction techniques. The capillary was then rinsed (50 mbar) for 10 min with 50:50 buffer:ACN to remove the non-covalently bound sample from the magnetic bead band to the outlet. A plug of 100 mM DTT (~61 nL) was then injected into the capillary, and mixed in the same way as the sample (+50, -50 mbar) for 5 min. Finally, pressure (50 mbar) was used to mobilize the free peptides to the detector and spotted onto the MALDI target plate for MS analysis.

### **4.3 Results and Discussion**

Before it is possible to apply a magnetic bead phosphopeptide isolation method to the analysis of an unknown phosphoproteome, such as the low volume enamel pellicle, it is important to develop and optimize the method using standard peptide solutions. The steps to prepare this technique for on-line CE applications are discussed herein.

### 4.3.1 DTT-Derivatization of Phosphorylated Peptides (Steps I and II)

A simple, monophosphorylated peptide from a trypsin digest of  $\beta$ -casein was used as a standard to examine the potential for the derivatization and isolation of phosphorylated peptides via magnetic beads. A pure sample standard of this peptide was purchased, and a trypsin digest of a  $\beta$ -casein protein standard was prepared to obtain this peptide in a mixture of non-phosphorylated peptides. The sequence of the 209 amino acid phosphorylated protein was as follows (P02666 [16-224], Beta-casein, Bos Taurus, UniProtKB, 2011):

<u>RE</u> LEELNVPG	EIV <u>E</u> pSLpSpSpSE	ESIT <u>R</u> IN <u>K</u> KI	E <u>K</u> FQpSEEQQQ
TEDELQD <u>K</u> IH	PFAQTQSLVY	PFP <u>G</u> PIPN <u>S</u> L	PQNIPPLTQT
PVVVPPFLQP	EVMGV <u>S</u> <u>K</u> V <u>K</u> E	AMAP <u>K</u> <u>H</u> <u>K</u> EMP	FP <u>K</u> YPVEPFT
ES( <i>R</i> )QSLTLTDV	ENLHLPLPLL	QSWMHQPHQP	LPPTVMFPPQ
SVLSLSQ <u>S</u> <u>K</u> V	LPVPQ <u>K</u> AVPY	PQR <u>D</u> MPIQAF	LLYQEPVLGP
<u>VR</u> GPFP <u>I</u> <u>I</u> <u>V</u>			

This protein contained five phosphorylation sites, and digestion by trypsin generated two phosphorylated peptides, a monophosphorylated peptide that was examined in this thesis (FQpSEEQQQTEDELQDK, **1**), and a tetraphosphorylated peptide (RELEELNVPGEIVEpSLpSpSpSE ESITR) that was not examined. The list of observed peptides upon MALDI MS analysis of the digestion and the corresponding theoretical masses are listed in Table 4.1. The monophosphorylated peptide (**1**) was clearly observed, while the tetraphosphorylated peptide was not detected. A natural variant at residue 137 (S to R) resulted in an additional peptide in the digestion mixture (1137.58 m/z). The mass spectrum of the digestion mixture can be observed in Figure 4.7 A.

**Table 4.1.** A list of observed and corresponding theoretical monoisotopic mass values of a  $\beta$ -casein trypsin digest.

Observed Monoisotopic Mass [M+H] <sup>+1</sup>	Theoretical Monoisotopic Mass [M+H] <sup>+1</sup>	Sequence	Calculated pI
742.46	742.45	GPFPIIV	5.75
748.38	748.37	EMPFPK	6.22
780.50	780.50	VLPVPQK	10.01
830.47	830.45	AVPYPQR	9.00
1137.58	1137.56	YPVEPFTER	4.48
<b>2,061.85</b>	<b>2,061.83</b>	<b>FQpSEEQQTDELQDK</b>	<b>3.29</b>
2,186.18	2,186.17	DMPIQAFLLYQEPVLPVR	4.32

This monophosphorylated peptide was examined as the model peptide for the derivatization procedure. In contrast to affinity based enrichment techniques, this reversible covalent binding technique required a covalently bound tag in place of the phosphate modification. A covalent tag allows for more specific selection of the modified peptides from a mixture as well as a diagnostic peak shift in MSMS to later determine the exact location of the phosphorylation site. Although a phosphorylated serine residue was examined, this method is also applicable to phosphorylated threonine residues [15,16]. The phosphate group on **1** was removed through a  $\beta$ -elimination reaction in the presence of strong base (Figure 4.2, **I**). The resulting dehydroalanine (**2**) was converted into the DTT-tagged molecule (**3**) through a Michael addition with DTT (Figure 4.2, **II**). This type of derivatization has been demonstrated with phosphorylated serine and threonine residues, but is not effective on the rare phosphorylated tyrosine residues [14]. Phosphorylated modifications (serine:threonine:tyrosine) are estimated to occur at a ratio of 1800:200:1 [25], and so the majority of phosphorylated residues can be modified by this procedure. A question that must be proposed when applying this derivatization method to other peptides is what happens to the cysteine residues that also contain an SH group. According to Salih and colleagues,  $\beta$ -elimination did not occur to the cysteine residues, and thus these residues were not derivatized by the DTT tag [16]. Thus, no protection of the cysteine residues was necessary. If cysteine-containing peptides were retained on the thiol-activated magnetic beads, subsequent MSMS would distinguish



between peptides that did and did not have the DTT tag by the diagnostic mass loss of the DTT in the sequencing step [16]. The various forms of the monophosphorylated peptide from  $\beta$ -casein before and after derivatization, with corresponding mass to charge ratios, are displayed in Table 4.2. The addition of the DTT-tag resulted in a mass change of +56 Da from the phosphorylated form, while the dehydroalanine that did not receive the tag had a mass loss of 98 Da. The corresponding peptide with no post translational modification would have a mass 80 Da lower than that of the phosphorylated peptide.

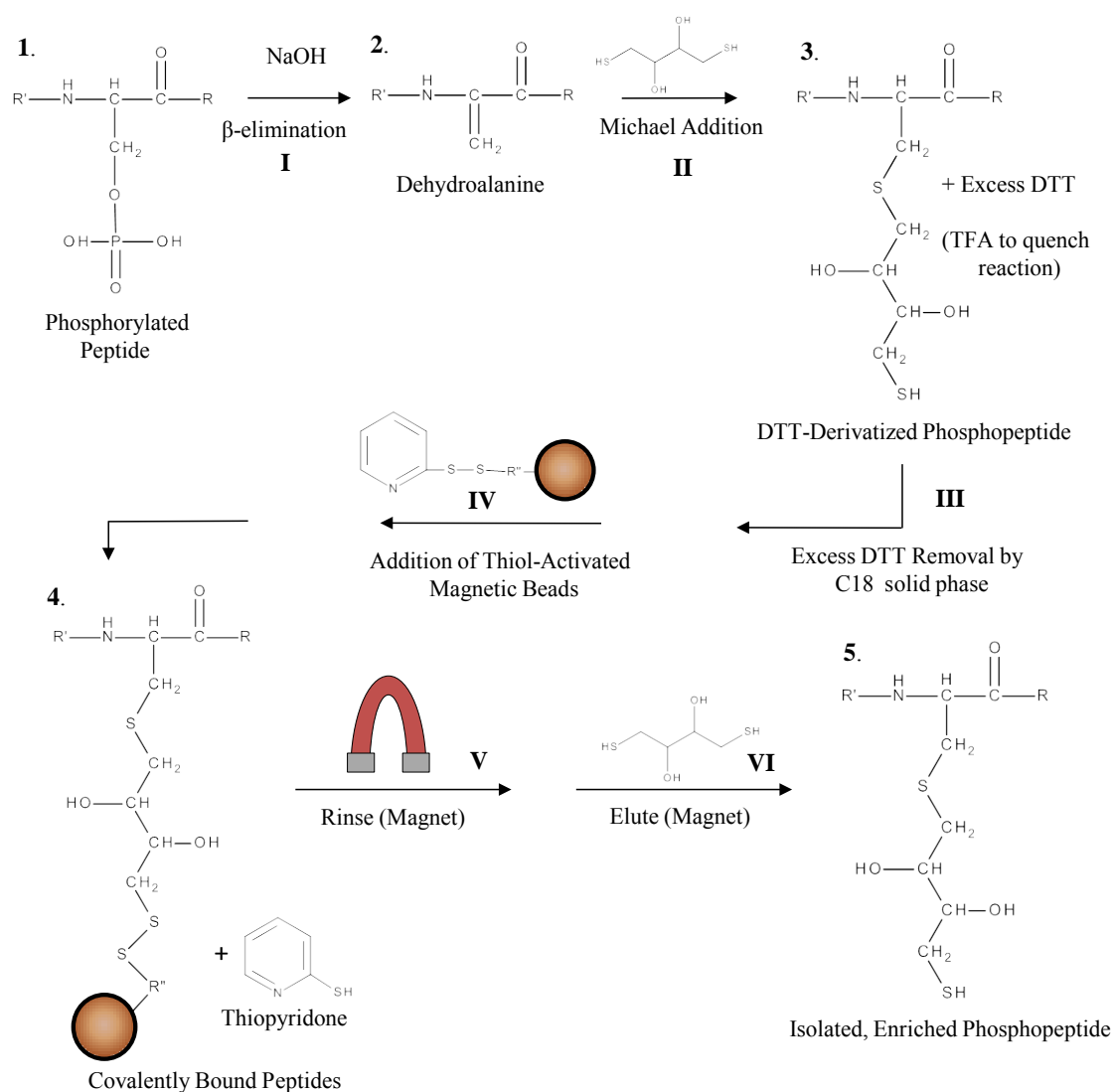


**Figure 4.2.** Reaction schematic for the DTT-derivatization and isolation of the monophosphorylated peptide from a  $\beta$ -casein tryptic digest.

**Table 4.2.** Forms of the monophosphorylated peptide (FQpSEEQQQTEDELQDK) from a  $\beta$ -casein trypsin digest, theoretical monoisotopic masses, structure numbers for reference, and the mass changes from the phosphorylated peptide.

Forms	Peptide	Phosphorylated Peptide	Dehydroalanine	DTT-Derivatized Peptide
$[M+H]^+$	1981.86	2061.83	1963.85	2117.86
Structure	<p><b>0</b></p>	<p><b>1</b></p>	<p><b>2</b></p>	<p><b>3 &amp; 5</b></p>
Mass Change from Phosphorylated Peptide				
	-80.0	0	-98.0	+ 56.0

The derivatization conditions including reaction time, ligand concentration, and peptide concentration, were optimized to produce the greatest amount of DTT-derivatization of **1**. Previous research performed the derivatization in a peptide mixture (approximately 1 mg mL<sup>-1</sup>) in 300 mM NaOH with 10 mM DTT for 1 h at 50 °C [16]. The first parameter examined in this chapter was the concentration of DTT in the reaction solution to confirm that these conditions produced the greatest amount of product. DTT concentrations of 5, 10, 20, 50 and 100 mM DTT were tested with 0.1 mg mL<sup>-1</sup> (48.5  $\mu$ M **1**), with the mass spectra of the lowest, middle and highest DTT concentration reaction solutions displayed in Figure 4.3. Each reaction solution was diluted 40% from 48.5  $\mu$ M to 19  $\mu$ M in water for MS analysis. This dilution lowered the Na<sup>+</sup> and DTT concentrations in the samples resulting in better MS signals.

The mass spectrum of the monophosphorylated peptide standard in water (Figure 4.3 A) revealed both the phosphorylated form (**1**) and dehydroalanine form (**2**). After a

one hour reaction time, 5 mM DTT converted some of the peptide to the DTT-derivatized form (**3**) while a substantial amount of peptide was not successfully tagged and simply lost its phosphate group to become **2** (Figure 4.3 B). Although the molar ratio of DTT to peptide under these conditions was one hundred to one (5000  $\mu\text{M}$  to 50  $\mu\text{M}$ ), the Michael addition reaction did not go to completion. Although this reaction volume was small (only 10  $\mu\text{L}$ ), these reactants may not have come into sufficient contact during the one hour reaction to go to completion. By increasing the concentration to 20 mM DTT, only minimal **2** was observed, with the major product being the desired DTT-derivatized peptide (**3**, Figure 4.3 C). The results with 10 mM DTT exactly matched those observed with 20 mM DTT, where the ratio of the MS signal for the **3** to **1** was approximately 14. As the concentration increased to 50 and 100 mM DTT, the amount of remaining **1** surprisingly increased. At 100 mM, the ratio of the MS signals of **3** to **1** was approximately 2. This result suggested that the  $\beta$ -elimination step had not gone to completion, and that such a high concentration of DTT could not function in only 300 mM NaOH.

Mass spectrometry is not necessarily a quantitative technique, and the background ions in the sample, the type of analyte, matrix concentration, and different areas of crystal clusters (hot spots) can easily change the signal intensity. Even multiple spectra (sum of 1000 laser shots) of the same sample spot result in signal intensity fluctuations. Thus, only large differences in signal intensity under similar conditions can imply changes in concentrations, and even this must be done carefully. That said, the comparison of the ratios of peaks within a spectrum, as was done in Figure 4.3, can provide a clear picture of the overall effect. Figure 4.3 D has a low intensity of all three peptide forms, **1**, **2**, and **3**, likely due to the greater amount of DTT in the sample that could suppress the MS signal (100 mM DTT, diluted to 40 mM for MS). Even so, the ratio of **3** to **1** still indicated poor derivatization of the sample. A concentration of 20 mM DTT was selected as the ideal concentration for the derivatization step. The optimal DTT concentration may vary depending on the sample analyzed, especially when real and complex mixtures are involved. However, this study has demonstrated that a large dehydroalanine concentration indicates too little DTT, or not enough mixing, while an incomplete  $\beta$ -elimination step may indicate too much DTT.

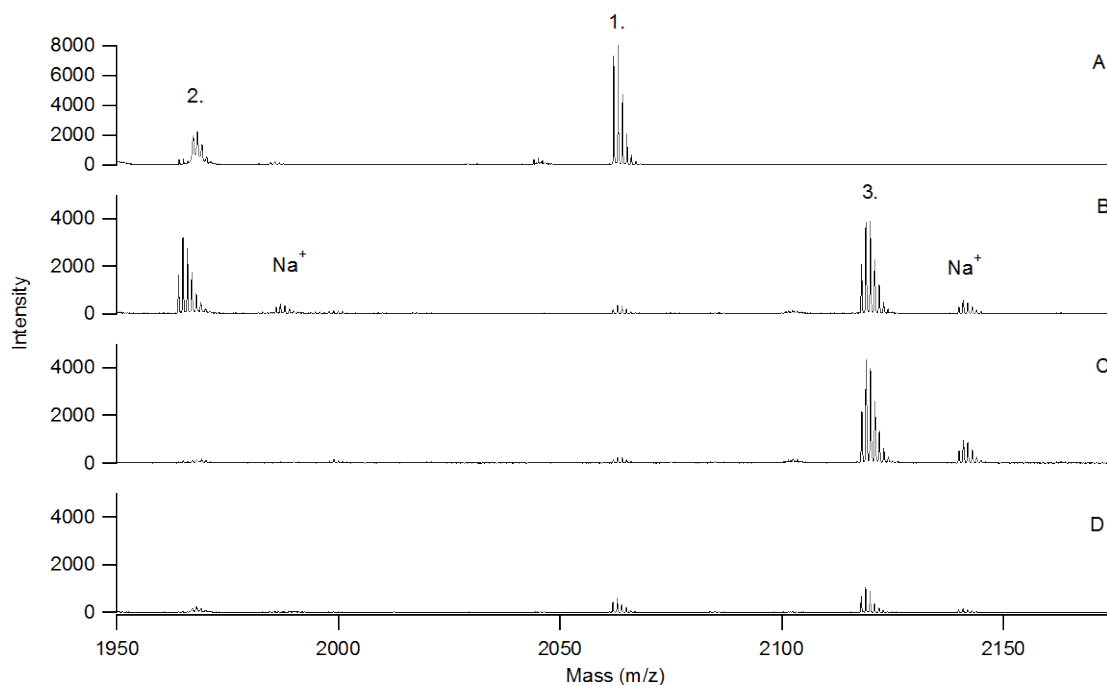


**Figure 4.3.** Mass spectra of the DTT-derivatization ( $\beta$ -elimination, **I**, and Michael addition, **II**) of the monophosphorylated peptide standard (A) with 5 mM (B), 20 mM (C), and 100 mM (D) DTT. The presence of the phosphorylated peptide (**1**), dehydroalanine (**2**), and DTT-derivatized peptide (**3**) and some salt adduct analogs were detected. Reaction conditions:  $0.1 \text{ mg mL}^{-1}$  **1** in 300 mM NaOH at  $50 \text{ }^\circ\text{C}$  for 1 h. All samples were diluted in water to  $0.04 \text{ mg mL}^{-1}$  ( $19 \text{ }\mu\text{M}$ ) for MALDI MS analysis.

The second factor considered for the derivatization reaction was the analyte concentration in the reaction solution. The following study examined the derivatization on a  $\beta$ -casein digest as it was important to determine the success of the derivatization with other peptides present. Even with this slightly more complex sample and reduced concentration of the phosphorylated peptide, the conversion of **1** to **3** was successful with 20 mM DTT. Four sample concentrations ( $0.1$  to  $1.0 \text{ mg mL}^{-1}$  digested peptides,  $4.2$  to  $42 \text{ }\mu\text{M}$  **1**) with 300 mM NaOH and 20 mM DTT were gently mixed for 15, 30, 60, and 120 min. The average MS signal ratio for **3** to **1** are recorded (Figure 4.4, six replicates,  $\pm$  one standard deviation). All of the reaction solutions were diluted to a common concentration of  $0.05 \text{ mg mL}^{-1}$  ( $2.1 \text{ }\mu\text{M}$  **1**) for MS analysis. Minimal, if any, differences were found between the selected sample concentrations in the success of the conversion from **1** to **3**.

The reaction solution with the highest protein digest concentration ( $1.0 \text{ mg mL}^{-1}$ ,  $42 \text{ }\mu\text{M}$  **1**) was similar in concentration to the monophosphorylated peptide reaction solution in Figure 4.4 ( $0.1 \text{ mg mL}^{-1}$ ,  $48 \text{ }\mu\text{M}$  **1**). However, this  $\beta$ -casein digest contained the tetraphosphorylated peptide, which increased the number of phosphorylated sites that could react with DTT. This may account for the small preference for the  $0.5 \text{ mg mL}^{-1}$  reaction concentration over the  $1.0 \text{ mg mL}^{-1}$  reaction concentration when  $20 \text{ mM}$  DTT was available. Although all of the tested concentrations produced the desired product (**3**), further DTT-derivatization experiments were carried out with  $0.5 \text{ mg mL}^{-1}$  digests.

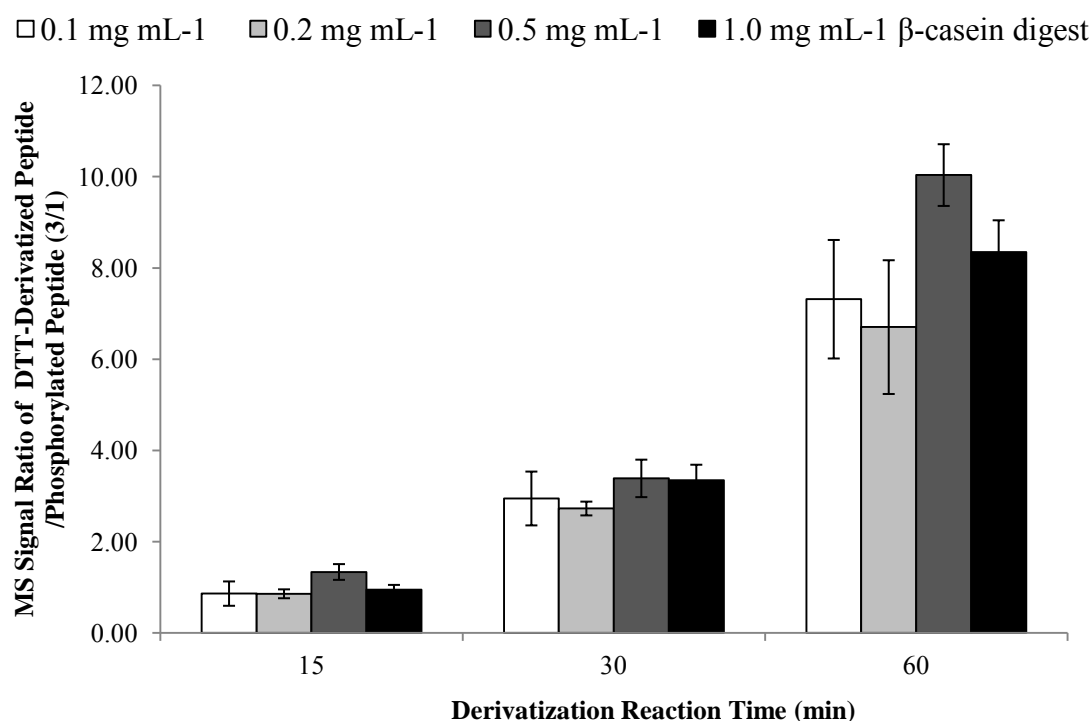


**Figure 4.4.** Graph comparing the mass spectral signal intensities of the DTT-derivatized peptide (**3**) to the phosphorylated peptide (**1**) under different derivatization reaction conditions (**I** and **II**). All  $\beta$ -casein digest reaction solutions ( $0.1 \text{ mg mL}^{-1}$  to  $1 \text{ mg mL}^{-1}$ ) were diluted in water to  $0.05 \text{ mg mL}^{-1}$  for MS analysis ( $2.1 \text{ }\mu\text{M}$  **1**). Ratios were averaged from six replicate spectra,  $\pm$  one standard deviation. Reaction conditions with  $\beta$ -casein digest:  $300 \text{ mM}$  NaOH,  $20 \text{ mM}$  DTT,  $50 \text{ }^\circ\text{C}$ .

The reaction time parameter had a much greater effect than the sample concentration on the conversion of **1** to **3**. Very clear distinctions were found as the time increased to one hour, with the greatest proportion of **3** obtained after one hour (Figure 4.4). After two hours, no signals were detected for **1** and **3**. The sample most likely adsorbed to the low retention microtube wall while heating, and since such low volume reaction solutions were used, minimal adsorption to the wall had a significant effect on the sample recovery after 2 h. A one hour reaction time was deemed optimal as the signal intensity for the remaining **1** was very small after one hour, and longer reaction times seemed unnecessary.

#### **4.3.2 Solid-Phase Removal of excess DTT (Step III)**

The excess DTT in the derivatization reaction solution could not be present when the thiol-activated magnetic beads were mixed with the analyte, as the DTT would competitively bind to the thiol beads in place of the derivatized peptides. As shown in the grand reaction scheme in Figure 4.2, the next step in the process after chemical derivatization was the removal of the excess DTT (and NaOH) from the derivatized peptide solution. Solid phase extraction (SPE) was performed for this step. Previously, this process employed reversed phase HPLC, with the DTT eluting in the first few minutes with 0.1% formic acid, while the tryptic peptides eluted over 20 min later with 80% ACN and 0.1% formic acid [16]. However, for such small sample volumes, this technique was not ideal for our CE application. Ideally, this step would be performed on-line in CE with reversed phase magnetic beads. Such beads were purchased from two different companies (C18 modified beads from MagnaMedics and Bioclone Inc.), but preliminary results showed incomplete retention of peptides (data not shown). It was suspected that this was caused by incomplete coverage of the iron oxide magnetic core by the silica and C18, which led to some degree of hydrophilic character on the surface of the beads and caused poor retention of the peptides. This step required further development, and so reversed phase pipette tips were used as an interim resolution. The standard sized C18 ZipTips<sup>TM</sup> were selected as they were most similar to the proven reversed phase used previously in HPLC [16]. SPE with ZipTips<sup>TM</sup> did not require the

expensive instrumentation of HPLC, could be performed on microliter volume samples, and eluted submicroliter volume, salt-free samples.

The sample loading capacity of the ZipTips<sup>TM</sup> was explored to ensure minimal sample loss. The manufacturer stated that the binding capacity of standard bed ZipTips<sup>TM</sup> was  $\geq 1 \mu\text{g}$ , and typically up to  $5 \mu\text{g}$ . Derivatization reaction solutions of 0.5, 1, or  $2 \mu\text{g}$  of peptide were examined (data not shown). Significant analyte was detected in the original solution after the adsorption step with  $2 \mu\text{g}$  of sample which demonstrated incomplete binding at this higher concentration. At lower digest amounts (0.5 and  $1 \mu\text{g}$ ), the remaining analyte was significantly reduced. The washes indicated no sample loss from the solid phase during rinsing. Thus, the binding capacity for our application was determined to be approximately  $1 \mu\text{g}$ . Section 4.3.4 integrates the results from the ZipTip<sup>TM</sup> clean-up with the optimized results from the following sections. In that section, Figure 4.7 demonstrates the signal enhancement from the  $\beta$ -casein reaction solution (B) after removing the salts and DTT with ZipTips<sup>TM</sup> (C). This figure provides an overview of the success of the covalent enrichment technique with magnetic beads.

### **4.3.3 In-Vial Isolation of Phosphorylated Peptides by Disulfide-Thiol Interchange (Steps IV and V)**

Once the derivatized peptides were free of the excess DTT, the isolation step with the magnetic beads could be performed (IV). The reaction conditions were optimized in-vial for application to the capillary. The uniform  $1 \mu\text{m}$ -diameter beads had a superparamagnetic iron oxide core ( $\text{Fe}_2\text{O}_3$ ) core, were coated in a high purity silica shell, and were modified with thiol functional groups (2-pyridyl disulfide). At  $30 \text{ mg mL}^{-1}$  (manufacturer's recommended concentration) the solution was a deep orange colour. The beads were easily dispersed in aqueous and organic solvents, but settled within 10 min, resulting in a clear supernatant and deep orange solid at the bottom of the vial. An external magnet collected the beads to the bottom of the vial in less than one minute.

The in-vial procedure is depicted on the right hand side of Figure 4.5 in comparison with the in-capillary procedure (left). After equilibrating the beads with the buffer solution, the beads were dispersed in buffer (50 mM  $\text{NH}_4\text{HCO}_3$ , 5 mM EDTA, Figure 4.5 A), followed by the addition of the sample (Figure 4.5 B). The inclusion of 5 mM EDTA was required to reduce the nonspecific adsorption of the peptides to the beads. One experiment with 0, 1, and 5 mM EDTA in the binding buffer resulted in increasingly enhanced recovery of the peptide from the beads, with the MS signal of the recovered DTT-derivatized peptide (**5**) almost three fold greater with 5 mM EDTA compared to no EDTA.



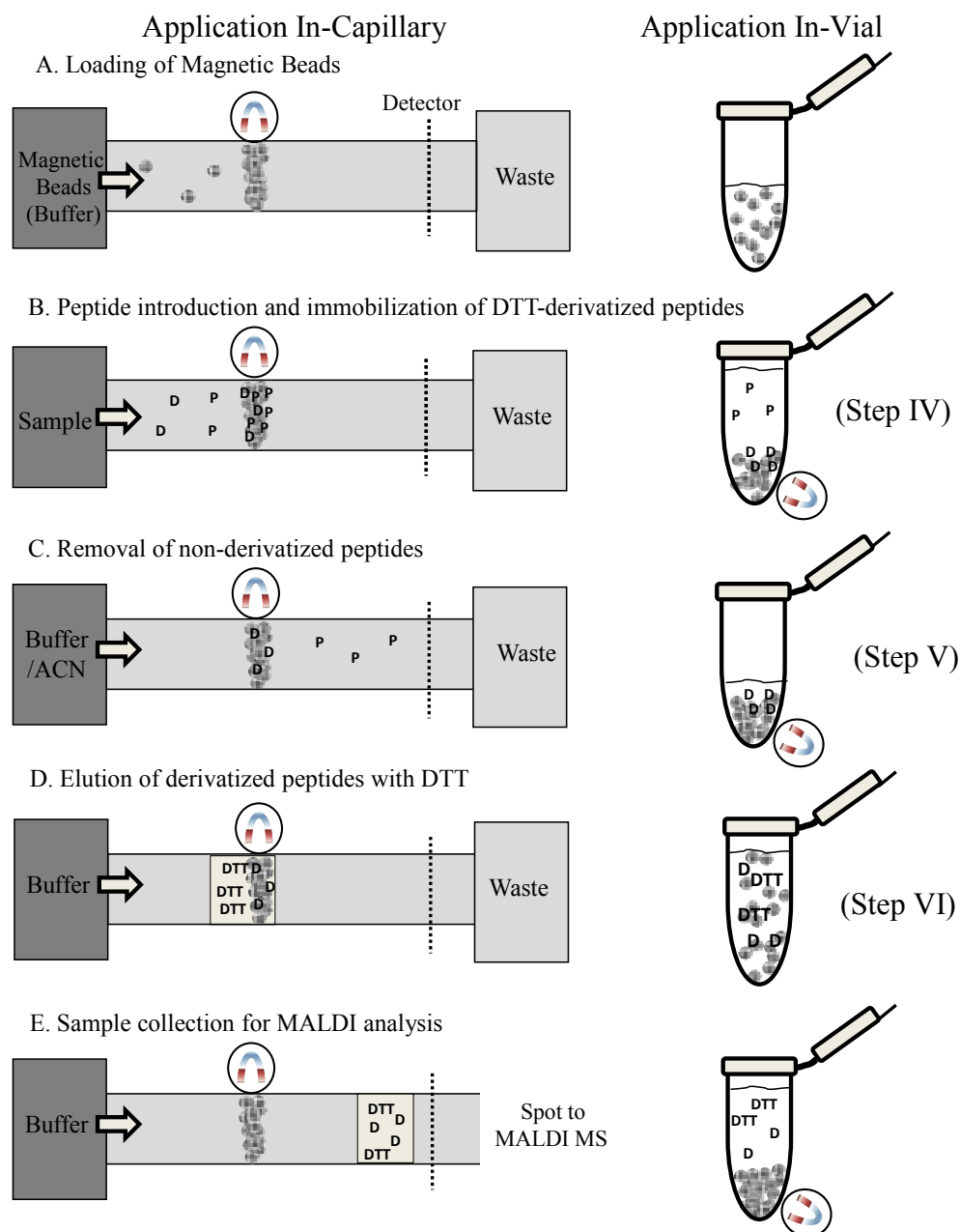


**Figure 4.5.** Schematics of the isolation of the DTT-derivatized phosphopeptide (**3, D**) from the non-derivatized/non-phosphorylated peptides (**P**) using thiol activated magnetic beads in-capillary (left) and in-vial (right). Capillary: Magnetic beads are flushed into the capillary (50 mbar, 60 s, 30 mg mL<sup>-1</sup>, in 50 mM ammonium bicarbonate, 5 mM EDTA) and collect at the location of the external magnet (A). A sample plug is injected past the plug (B) and the derivatized peptides covalently bind to the thiol beads while the non-derivatized peptides are washed through the capillary (C). A small plug of DTT is injected past the plug (D), and pressure is used to remove the released derivatized peptides (E) for MS analysis. Vial: The beads are added to the vial (A) with the sample (B), and the derivatized peptides bind to the magnetic beads. The beads are washed with the buffer/ACN, leaving the covalently bound, derivatized peptides (C). The addition of DTT (D) releases the derivatized peptides, and the supernatant is collected (E).

The binding reaction occurred fairly quickly between the magnetic particles and derivatized peptides generating the covalently bound peptides (**4**, step **IV**). The manufacturers recommended one hour or more for the binding to occur. This was in contrast to the 16 h reaction time for a similar disulfide-thiol linkage to occur previously in gel [16]. For real sample applications, especially with CE, short reaction times are ideal. Thus, it was important to determine the time required for complete binding, and to this end, binding times from 5 min to 8 h were compared. Using the derivatized  $\beta$ -casein digest, (cleaned up by ZipTips<sup>TM</sup>,  $0.2 \mu\text{g } \mu\text{L}^{-1}$ ,  $8 \mu\text{M } \mathbf{3}$ ), the sample was prepared in the buffer and added to the magnetic particles ( $30 \mu\text{g } \mu\text{L}^{-1}$ ). After the binding time allotted, the sample was rinsed and eluted with DTT. The average MS signal intensities of the DTT-derivatized peptides recovered from the magnetic beads between 5 and 60 min were all within  $\pm$  one standard deviation of error (4-6 replicate spectra). Thus, no significant difference could be deciphered after a 5 min reaction. However, as the time increased from one to eight hours, the average signal intensity actually decreased. Based on these results, a reaction time of 15 min was employed to ensure optimal binding. A simpler method to test the binding time would have been to examine the supernatant after the specified binding time. However, this solution contained the released thiopyridone and thus these samples did not dry on the MALDI plate. Further work could employ larger sample volumes and use UV-visible absorbance to monitor the release of this chemical to determine the amount of binding.

Although this isolation technique was based on a reversible covalent reaction, the non-derivatized peptides in the sample were also retained on the magnetic beads after the binding step. A rinsing step was required to remove the peptides that were nonspecifically bound (**V**). Preliminary experiments demonstrated that a 50:50 buffer:ACN rinse was very effective at removing the extra peptides. A cysteine rinse ( $8 \text{ mg mL}^{-1}$ , 30 min reaction) was proposed by the manufacturers to reduce the non-specific binding and block the excess active groups, but this step was found to be unnecessary and time consuming. Two parallel experiments with a small Histatin protein demonstrated similar rinsing abilities of the 50:50 buffer:ACN and cysteine rinse, but the buffer/ACN rinse could be performed in less than one minute, while the cysteine rinse reaction required an additional half hour. The removal of the nonspecifically bound peptides from the  $\beta$ -casein digest

was accomplished and can be observed in Figure 4.7 by comparing the sample solution before (C) and after (D) the rinsing (and elution) step.

#### 4.3.4 Elution of the Covalently Bound Derivatized Peptides In-Vial (Step VI)

Finally, the derivatized peptides were isolated from their nonphosphorylated counterparts. An elution reaction was required to remove the covalently bound analyte from the magnetic beads for successful MS analysis. It was determined that covalently bound peptides could not be detected in MS, but non-covalently bound peptides, even with magnetic beads in the solution, could be clearly detected by MALDI MS. In order to elute the covalently bound peptides from the magnetic beads, DTT was added and bound to the magnetic beads, releasing the derivatized peptides. The optimal concentration of DTT and elution time was explored.

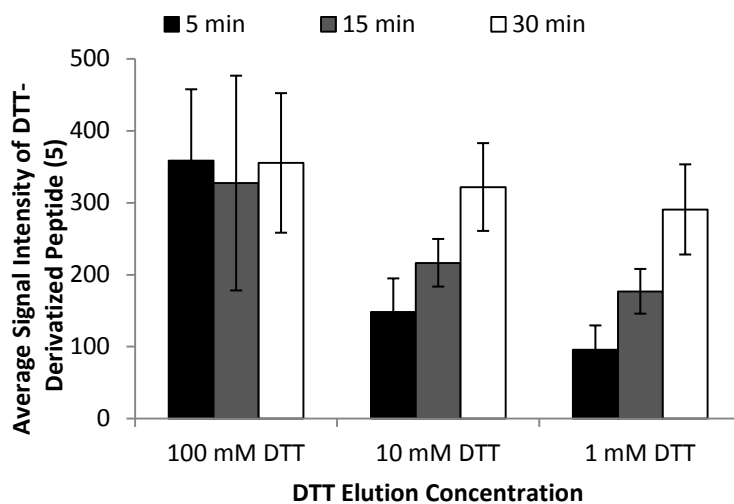


**Figure 4.6.** Elution of DTT-derivatized peptides (**5**) from thiol-activated magnetic beads, in-vial under different conditions (**VI**). The average MS signal intensities ( $\pm$  one standard deviation, 6 replicate spectra) of the DTT-derivatized peaks after elution with 100, 10, and 1 mM DTT for 5, 15, and 30 min. Experiment conditions: 30 mg mL<sup>-1</sup> thiol-activated beads in buffer (50 mM ammonium bicarbonate, 5 mM EDTA) mixed for 15 min with 0.15 mg mL<sup>-1</sup>  $\beta$ -casein digest, washed with 50:50 ACN:buffer. The elution supernatants were diluted ten-fold to 15  $\mu$ g mL<sup>-1</sup> (equivalent to 0.6  $\mu$ M **1**).

The elution time and DTT concentration required to break the disulfide bonds binding the peptides to the magnetic beads was determined through three time sequence experiments using 1, 10, and 100 mM DTT. A derivatized  $\beta$ -casein digest ( $0.15 \text{ mg mL}^{-1}$ ,  $6.3 \text{ }\mu\text{M}$  of **1**) was mixed with  $30 \text{ mg mL}^{-1}$  magnetic beads for 15 min, followed by elution with DTT for 5, 15, or 30 min (Figure 4.6). As was mentioned above, MALDI MS is not a reliable instrument to determine a sample concentration. However, trends were observed from replicate spectra with time and DTT concentration and these trends provided important insight to optimize this elution step. At 100 mM DTT elution concentration, no difference in analyte signal (**5**) could be detected between the three time lengths (Figure 4.6). However, at lower DTT concentrations, a longer time was required to generate the same signal intensities as were observed with 100 mM DTT. Thus, to have the shortest reaction times, the high 100 mM DTT elution concentration was selected as the best concentration. These conditions matched the manufacturers' suggested protocol (30 min, 100 mM DTT).

Each of the optimized conditions discussed over the past few pages was applied to one complete experiment, from analyte derivatization to elution of the sample from the magnetic beads in vial. These results are shown in Figure 4.7. The initial  $\beta$ -casein trypsin digest resulting in the peptides listed in Table 4.1 is displayed in Figure 4.7 A. After derivatization with DTT, the mass spectrum of the digest was recorded again, but this spectrum was recorded in the reaction solution in the presence of NaOH and DTT resulting in suppressed signal intensities (Figure 4.7 B). ZipTips<sup>TM</sup> successfully removed the contaminating ions and enhanced signal was again observed (Figure 4.7 C). Finally, the magnetic beads reaction was performed in vial on the sample in Figure 4.7 C which gave the isolated derivatized peptide peak (Figure 4.7 D). Again, this spectrum was recorded in the reaction solution with high concentrations of DTT which suppressed the signal intensity. ZipTips<sup>TM</sup> could be used to remove the DTT and enhance the signal, but this step was not performed for this experiment as the presence of **5** was still clearly observed.

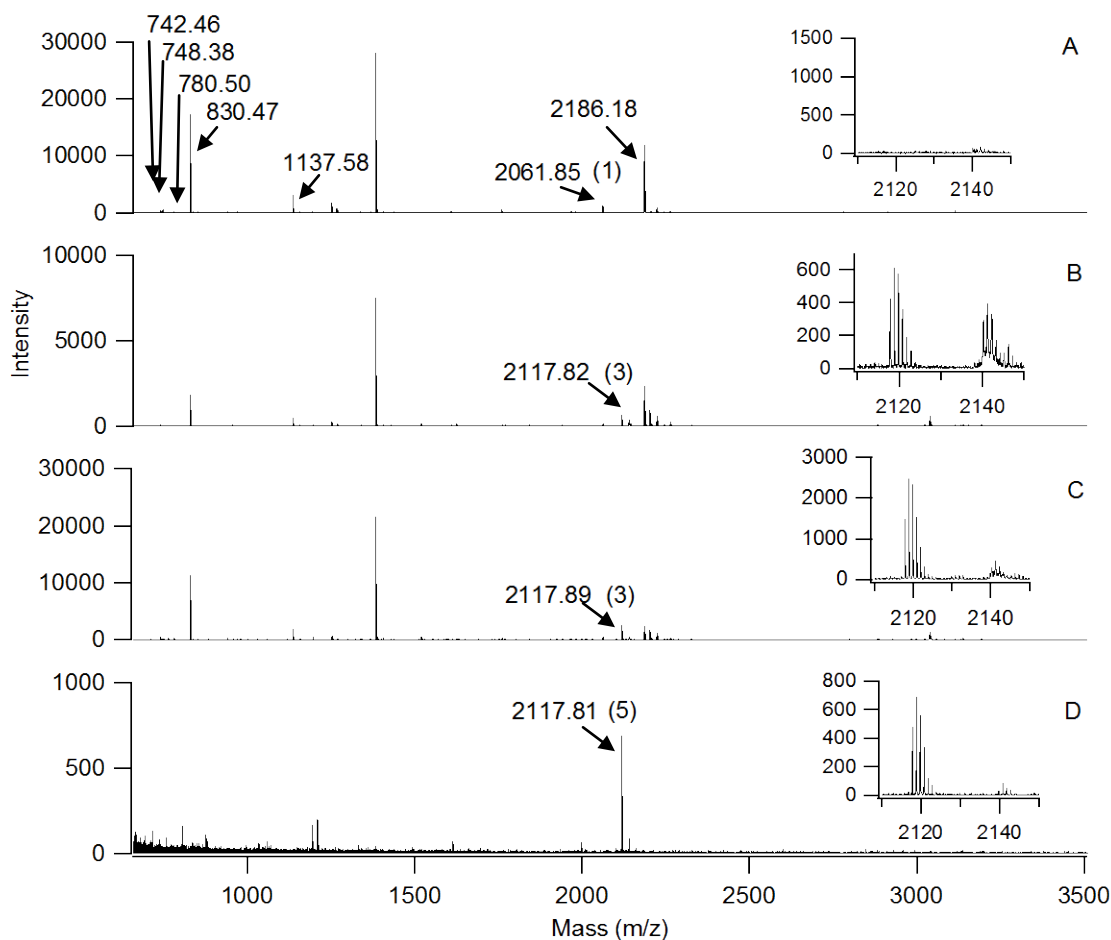


**Figure 4.7.** Mass spectra of the  $\beta$ -casein digest (A), after DTT derivatization (I and II) (B), after clean-up with ZipTips<sup>TM</sup> (IV) (C), and isolation of the derivatized peptide in vial with thiol-magnetic beads (V, and VI) (D). Conditions for DTT-derivatization: 0.2 mg mL<sup>-1</sup>  $\beta$ -casein digest, 20 mM DTT, 300 mM NaOH, 1 h at 50 °C. Conditions for ZipTip<sup>TM</sup> clean-up: 1  $\mu$ g digest in 0.1% TFA, wash with 0.1% TFA, eluted with 5  $\mu$ L of 80% ACN. Conditions for magnetic bead enrichment: 0.2 mg mL<sup>-1</sup>, 30 mg mL<sup>-1</sup> thiol activated beads, 15 min binding in buffer (50 mM ammonium bicarbonate, 5 mM EDTA), wash with 50:50 buffer:ACN, elution with 100 mM DTT for 30 min. Samples diluted to 0.05 mg mL<sup>-1</sup> (2.1  $\mu$ M 1) for MS analysis. Insets provide clear view of DTT-derivatized peptide region.

#### 4.3.5 Magnetic Bead Plug in Capillary

Magnetic beads are not limited to in-vial procedures. Already this novel reaction platform is being incorporated on-line for CE applications [19,26], and the purpose of the entire work in this chapter was to prepare the conditions for the magnetic beads to be used on-line in a capillary. The capillary becomes the reaction vial. To collect the magnetic beads at a specific location in the capillary, an external magnet can be placed next to the desired location on the capillary. Chen and colleagues investigated a one-magnet and two-magnet configuration to collect the magnetic particles in the capillary [27]. No difference was found by using multiple magnets. However, Girault's group employed a ring magnet surrounding the capillary which generated a greater magnetic field allowing higher pressures to be applied in the capillary [28]. For our method, a single round magnet was used as it provided a sufficient magnetic field to withstand with the pressure capabilities of our CE instrument. This magnet was reversibly adhered to the capillary cassette and the beads collected at the front end of the magnet upon injection into the capillary at moderate pressure. This magnet could easily be removed from the cassette between experiments to flush the magnetic particles from the capillary.

The volume of the magnetic bead plug in the capillary was limited by the diameter of the capillary, the magnitude of pressure available to run the experiment, and the time to inject the magnetic bead solution. In order to inject and rinse the sample through the magnetic beads plug in the capillary, the plug size could not exceed the pressure capabilities of the instrument. Our CE instrument was only capable of delivering monitored and controlled pressure levels between -50 to 50 mbar, and this was the limiting factor for the size of our magnetic bead plug. Various plug sizes were examined for their length and compatibility with the pressure application in the CE instrument. The largest plug size examined was obtained by injecting the magnetic bead solution (30 mg mL<sup>-1</sup>) at 30 mbar for 600 s. Through a light microscope, it was possible to see the magnetic bead plug through the polyimide coating of the capillary. The plug length was  $2.5 \pm 0.4$  mm in length (mean  $\pm$  standard deviation; n=3), fifty times the diameter of the capillary. The mass of magnetic beads in this plug could be estimated at 18  $\mu$ g (a 10 min injection is equivalent to a 31 cm length plug, equivalent to 610 nL, and from a 30 mg

$\text{mL}^{-1}$  dispersion, this equals  $18 \mu\text{g}$ ). However, upon injecting a mesityl oxide plug and applying the maximum pressure the instrument could deliver (50 mbar), no peak passed the detector in over 35 min. Thus, this plug length was too long for the pressure capabilities of our instrument. Injection of this same neutral marker in a capillary with no magnetic beads plug was detected by  $7.90 \pm 0.02$  min ( $n=3$ ) (Figure 4.8 A). It was necessary to reduce the injection time from 600 s to 60 s to have the neutral marker move through the capillary with the magnetic bead plug in a reproducible and timely manner. A 60 s injection of  $30 \text{ mg mL}^{-1}$  solution resulted in the neutral marker passing the detector in  $10.3 \pm 0.4$  min ( $n=3$ ) (Figure 4.8 B). At these injection conditions, the magnetic beads plug was  $1.6 \pm 0.2$  mm in length ( $n=3$ ), containing a calculated  $1.8 \mu\text{g}$  of magnetic beads (Figure 4.8 C). The neutral marker retained its symmetrical shape even after passing through the magnetic bead plug, displaying the compatibility of this magnetic beads plug with further CE applications.

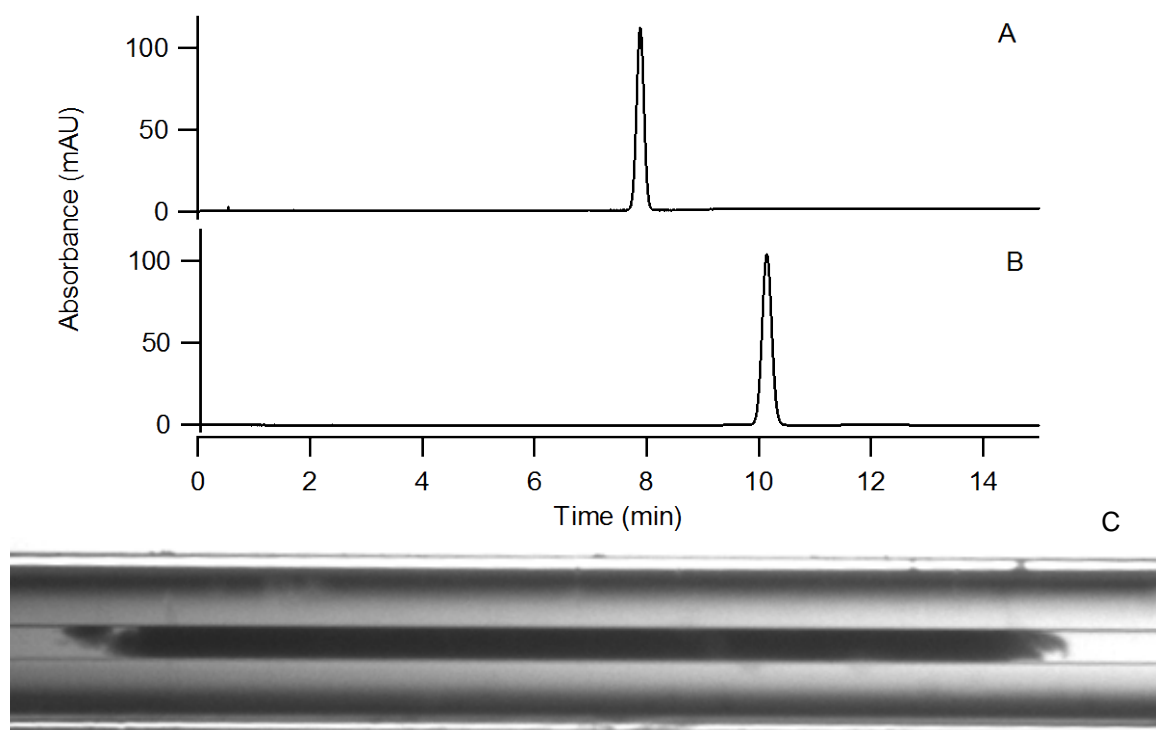


**Figure 4.8.** Migration of a neutral marker with pressure (50 mbar) through a capillary of buffer (A) and through a capillary with a 1.6 mm length magnetic bead plug in buffer (B). A photograph of the magnetic bead plug in the capillary taken under a light microscope ( $30 \text{ mg mL}^{-1}$  magnetic beads injected at 30 mbar for 60 s).

#### 4.3.6. Isolation of Phosphorylated Peptides in Capillary

The in-capillary magnetic beads experiments presented in this section represent our first attempt to demonstrate the potential for the use of magnetic beads and CE for minimized sample preparation and derivatization. The sample was introduced into the capillary in two ways. The first involved mixing the magnetic beads with the sample prior to injection in the capillary (Figure 4.9 A). This method is valuable as it allows a low abundance analyte to be recovered from a larger volume of complex sample. By premixing, a small amount of magnetic beads can specifically extract a very small amount of analyte after thorough mixing with a raw sample. The second method of introducing sample involves capturing the analyte already inside the capillary on the beads for enrichment and purification (Figure 4.9 B).

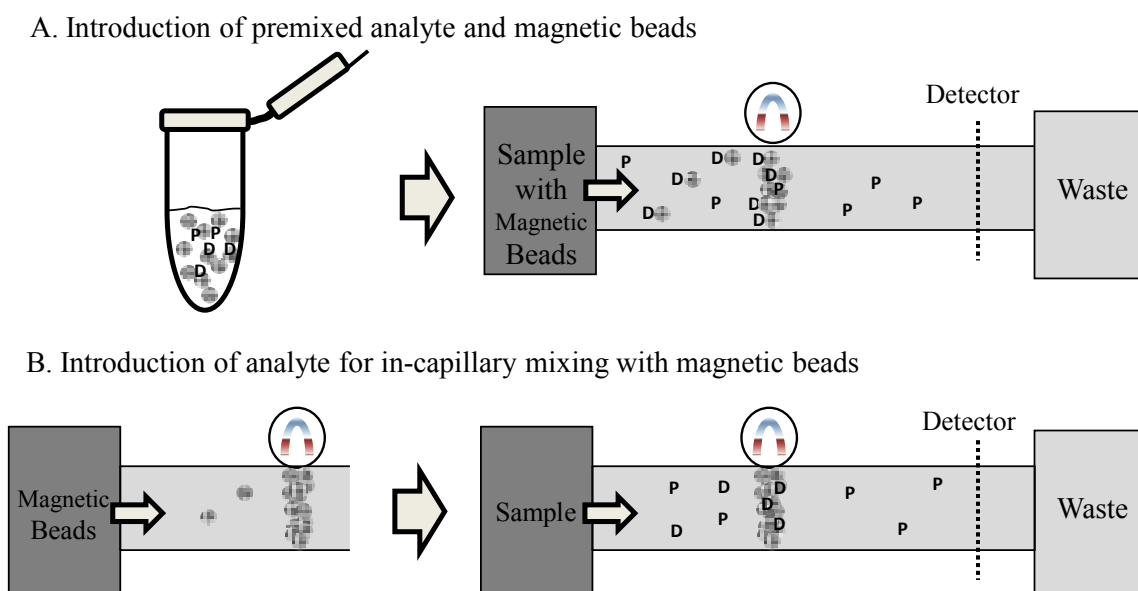


**Figure 4.9.** Schematic of the two sample introduction methods for in-capillary isolation of derivatized peptides.



Initial in-capillary experiments involved the first sample introduction method, with the derivatized peptides already covalently bound to the magnetic beads (4, Figure 4.9 A). The experimental conditions that were used for the optimized in-vial procedure (Figure 4.7 D) were applied to the in-capillary experiments, and the procedure steps are illustrated in Figure 4.5 (A and B combined, C-E as shown). The sample ( $0.2 \text{ mg mL}^{-1}$   $\beta$ -casein digest) was premixed with the magnetic beads for 15 min and then injected into the capillary (61 nL). The magnetic beads (with the covalently bound sample) collected at the external magnet and packed into a plug. The same rinsing solution used in-vial was also used to rinse the magnetic bead plug, only in this case, a continuous flow of rinsing buffer removed the excess peptides while the covalently bound peptides stayed at the magnetic beads plug. No repetitive steps of adding buffer, setting the vial on a magnet, removing the buffer were required. After 10 min of rinsing, a DTT plug the same size as the injected sample plug (61 nL) was injected and mixed at the magnetic bead plug. Forward and reverse pressure (50 mbar, 1 min each way) was used for mixing. Pressure was then applied to mobilize the eluted peptides in DTT away from the magnetic beads plug and spot the solution in 200 nL aliquots for MALDI MS analysis (Figure 4.10 B). It is possible to spot volumes that are only 20 nL, but the presence of DTT suppresses the MALDI MS signal, and by spotting such large volumes, the DTT plug was diluted about three fold.

The maximum signal that could be obtained is displayed in Figure 4.10 A as a control experiment, where a 61 nL sample of the  $\beta$ -casein digest (after ZipTip<sup>TM</sup> clean-up), prepared in buffer, was injected into a capillary with no magnetic beads and spotted directly onto the MALDI plate. The signal from the premixed analyte and magnetic beads (Figure 4.10 B) is significantly smaller than what it could be under optimal conditions. The presence of DTT in Figure 4.10 B certainly suppressed the analyte signal. For comparison, the ZipTip<sup>TM</sup> removal of DTT and NaOH from the derivatization reaction solution caused a four-fold increase in analyte intensity, although the removal of NaOH also contributed to the enhanced signal (Figure 4.7, B and C insets). Future method development will include an on-line clean-up, perhaps with C18 magnetic particles, to remove this excess DTT for enhanced MS detection. In addition, the mixing parameters for the DTT and magnetic bead sample plug need to be optimized to improve the sample

signal. Although the sample signal was lower than expected for the premixing analyte introduction, the derivatized peptide (**5**) was still clearly detected while the other peptides were successfully removed from the mixture.

The second sample introduction technique (Figure 4.9 B) was also performed with the results shown in Figure 4.10 C. This procedure followed the steps demonstrated in Figure 4.5 (A-E), where the magnetic beads were injected, followed by the sample addition (**IV**), mixing, rinsing (**V**), and elution with DTT (**VI**). The obtained mass spectrum just detected the derivatized peptide out of the baseline, but this signal was very poor (Figure 4.10 C). It is clear that the on-line mixing procedures must be improved to allow for better sample binding and elution. Such improvements may include lower pressure for slower mixing (5 mbar rather than 50 mbar), only forward pressure to move the reactants by each other, or longer mixing times.

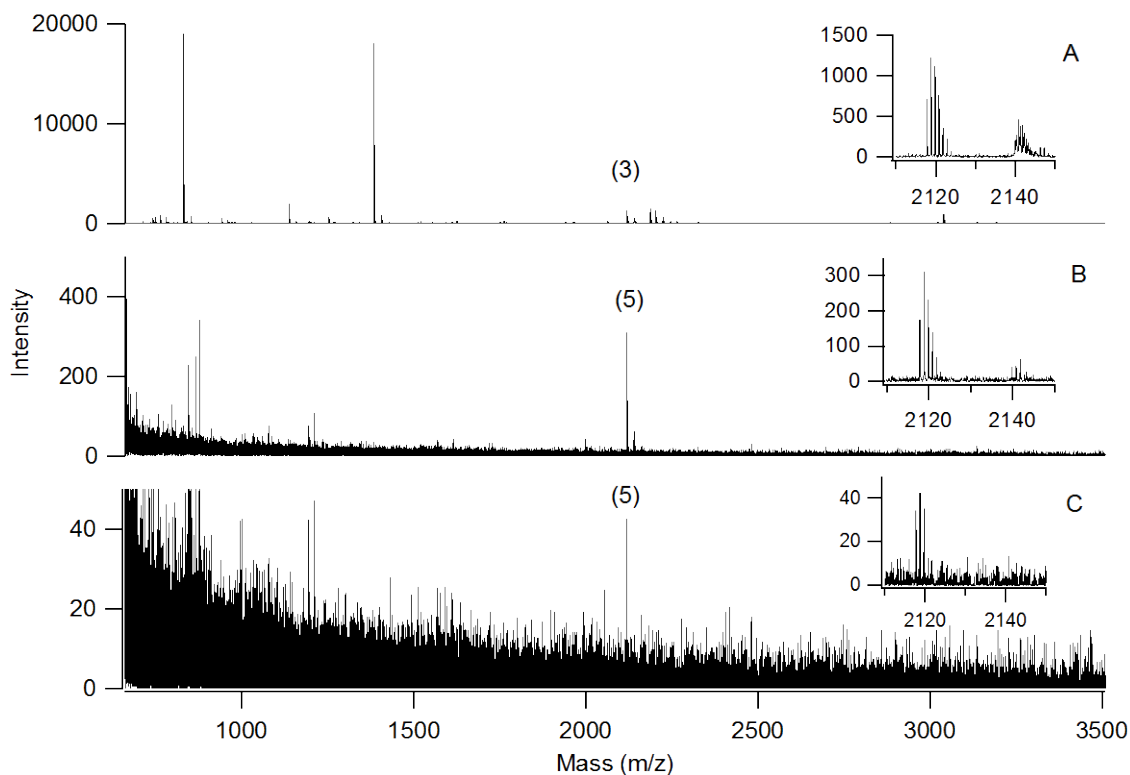


**Figure 4.10.** In-capillary experiments with a derivatized  $\beta$ -casein digest, after DTT-removal via ZipTips<sup>TM</sup> ( $0.2 \text{ mg mL}^{-1}$ ,  $8.4 \text{ }\mu\text{M}$ ). A: Control experiment with a sample plug injected into the capillary and spotted onto the MALDI plate with no magnetic beads in capillary. B: Sample premixed with magnetic beads for 15 min, injected as a plug, collected in-capillary at the magnet, eluted with 100 mM DTT, and spotted onto the MALDI target plate (see Figure 4.5, steps A/B combined, to E). C: Magnetic beads plug collected in capillary, sample plug injected and mixed for 10 min, eluted with 100 mM DTT, and spotted onto the MALDI plate (see Figure 4.5, steps A to E). Sample plug volume was the same for all three experiments, and spotting conditions diluted the sample plug approximately 3-fold ( $\sim 2.5 \text{ }\mu\text{M}$  **1**). Experimental details are recorded in section 4.2.6. Insets provide a clearer view of the derivatized peptide (**3** and **5**).

## 4.4 Conclusions

The isolation of the derivatized peptides with magnetic beads was optimized in-vial and initial in-capillary experiments were demonstrated. The binding time, washing steps, and eluting conditions of DTT concentration and time were explored in-vial. Procedures tested in-capillary are shown in the dashed enclosure (Figure 4.11). In-vial and in-capillary experiments clearly showed the derivatized peptide while the non-derivatized peptides were removed from the sample. Two sample introduction techniques into the capillary were tested, each with their own application benefits. Premixing the analyte and magnetic beads produced a strong peptide signal, while the results from the in-capillary mixing were poor. The sample recovery and resulting MS signal intensities of the in-capillary experiments must be improved before this method can be applied to real samples.

Thiol-activated magnetic beads were investigated for their phosphopeptide enrichment capabilities. A reversible, covalent binding enrichment procedure that involved replacing the phosphorylated modification with a DTT-tag was optimized for CE applications using the monophosphorylated peptide from a  $\beta$ -casein trypsin digest as a model peptide. The optimization of reaction parameters becomes increasingly important with low abundance samples, where the product yield at each step is crucial in the identification of the analytes of interest. Any analyte loss may compromise the detection of the analytes. Derivatization conditions were optimized for reaction time, DTT concentration, and analyte concentration, as shown in Figure 4.11. The excess DTT and salt were removed from the reaction solution by solid phase extraction with ZipTips<sup>TM</sup>, although future work should employ an on-line solid phase clean-up with C18 magnetic particles. Currently this step is not possible due to the poor retention of peptides on C18 magnetic beads, and the lack of commercial C18 magnetic beads that perform as well as the solid phase in ZipTips<sup>TM</sup>.

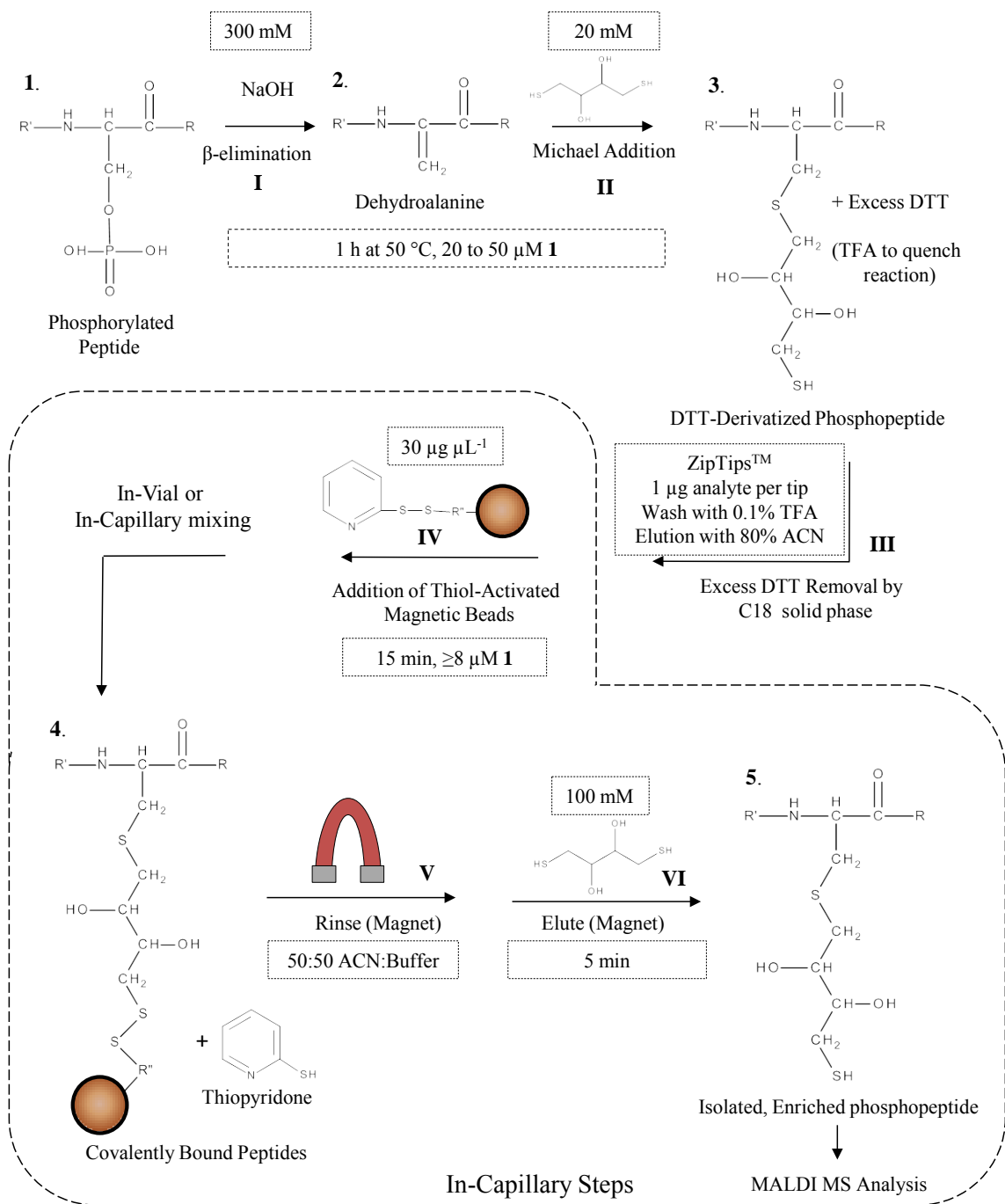


**Figure 4.11.** Concluding schematic of optimized procedures for analyte derivatization and magnetic beads reactions.

Future work must investigate on-line mixing techniques to improve the analyte binding and elution with the magnetic beads. Forward/reverse pressure parameters, mixing time, and even the capillary diameter will contribute to the effectiveness of the mixing. Currently, the sample is eluted in the highly concentrated DTT solution. A subsequent on-line clean-up step, such as one with a second magnetic bead plug of C18, would increase the MS signal. More complex analyte mixtures must also be investigated to determine if and how the optimal conditions may change when other peptides and chemicals are present. A proof-of-principle was demonstrated in this chapter using magnetic beads in capillary.

Miniaturization of analytical techniques can allow samples of low volume to be prepared near the detection limits of mass spectrometry. Low abundance samples require specialized handling and enrichment techniques for successful detection. Capillary electrophoresis uses only nanoliter volumes of sample and is compatible with the low sample volume requirement for MS. Magnetic beads provide a novel platform for selective analyte retention, compatible with CE parameters. The combination of these two methods could provide a powerful solution for the challenges of phosphoproteome analysis.

## 4.5 References

- [1] A.M. Palumbo, S.A. Smith, C.L. Kalcic, M. Dantus, P.M. Stemmer & G.E. Reid. Tandem Mass Spectrometry Strategies for Phosphoproteome Analysis, *Mass Spectrometry Reviews*, **2011**, *30*, 600-625.
- [2] K. Ashman & E.L. Villar. Phosphoproteomics and cancer research, *Clinical & Translational Oncology*, **2009**, *11*, 356-362.
- [3] J.D. Dunn, G.E. Reid & M.L. Bruening. Techniques for Phosphopeptide Enrichment Prior to Analysis by Mass Spectrometry, *Mass Spectrometry Reviews*, **2010**, *29*, 29-54.
- [4] J. Porath, J. Carlsson, I. Olsson & G. Belfrage. Metal Chelate Affinity Chromatography, a New Approach to Protein Fractionation, *Nature*, **1975**, *258*, 598-599.
- [5] L.D. Holmes & M.R. Schiller. Immobilized iron(III) metal affinity chromatography for the separation of phosphorylated macromolecules: Ligands and applications, *Journal of Liquid Chromatography & Related Technologies*, **1997**, *20*, 123-142.
- [6] M.C. Posewitz & P. Tempst. Immobilized gallium(III) affinity chromatography of phosphopeptides, *Analytical Chemistry*, **1999**, *71*, 2883-2892.
- [7] H.J. Zhou, F. Elisma, N.J. Denis, T.G. Wright, R.J. Tian, H. Zhou, W.M. Hou, H.F. Zou & D. Figeys. Analysis of the Subcellular Phosphoproteome Using a Novel Phosphoproteomic Reactor, *Journal of Proteome Research*, **2010**, *9*, 1279-1288.
- [8] M.R. Larsen, T.E. Thingholm, O.N. Jensen, P. Roepstorff & T.J.D. Jorgensen. Highly selective enrichment of phosphorylated peptides from peptide mixtures using titanium dioxide microcolumns, *Molecular & Cellular Proteomics*, **2005**, *4*, 873-886.
- [9] H.C. Hsieh, C. Sheu, F.K. Shi & D.T. Li. Development of a titanium dioxide nanoparticle pipette-tip for the selective enrichment of phosphorylated peptides, *Journal of Chromatography A*, **2007**, *1165*, 128-135.
- [10] H.T. Wu, C.C. Hsu, C.F. Tsai, P.C. Lin, C.C. Lin & Y.J. Chen. Nanoprobe-based immobilized metal affinity chromatography for sensitive and complementary enrichment of multiply phosphorylated peptides, *Proteomics*, **2011**, *11*, 2639-2653.

- [11] L.J. Zhang, H.J. Lu & P.Y. Yang. Recent developments of nanoparticle-based enrichment methods for mass spectrometric analysis in proteomics, *Science China-Chemistry*, **2010**, *53*, 695-703.
- [12] S.B. Ficarro, G. Adelmant, M.N. Tomar, Y. Zhang, V.J. Cheng & J.A. Marto. Magnetic Bead Processor for Rapid Evaluation and Optimization of Parameters for Phosphopeptide Enrichment, *Analytical Chemistry*, **2009**, *81*, 4566-4575.
- [13] Y. Huang, Q.H. Shi, C.K. Tsung, H.P. Gunawardena, L. Xie, Y.B. Yu, H.J. Liang, P.Y. Yang, G.D. Stucky & X.A. Chen. An optimized magnetite microparticle-based phosphopeptide enrichment strategy for identifying multiple phosphorylation sites in an immunoprecipitated protein, *Analytical Biochemistry*, **2011**, *408*, 19-31.
- [14] Y. Oda, T. Nagasu & B.T. Chait. Enrichment analysis of phosphorylated proteins as a tool for probing the phosphoproteome, *Nature Biotechnology*, **2001**, *19*, 379-382.
- [15] F. Thaler, B. Valsasina, R. Baldi, X. Jin, A. Stewart, A. Isacchi, H.M. Kalisz & L. Rusconi. A new approach to phosphoserine and phosphothreonine analysis in peptides and proteins: chemical modification, enrichment via solid-phase reversible binding, and analysis by mass spectrometry, *Analytical and Bioanalytical Chemistry*, **2003**, *376*, 366-373.
- [16] E. Salih, W.L. Siqueira, E.J. Helmerhorst & F.G. Oppenheim. Large-scale phosphoproteome of human whole saliva using disulfide-thiol interchange covalent chromatography and mass spectrometry, *Analytical Biochemistry*, **2010**, *407*, 19-33.
- [17] M.A.M. Gijs, F. Lacharme & U. Lehmann. Microfluidic Applications of Magnetic Particles for Biological Analysis and Catalysis, *Chemical Reviews*, **2010**, *110*, 1518-1563.
- [18] M.R. Condina, M.A. Guthridge, S.R. McColl & P. Hoffmann. A sensitive magnetic bead method for the detection and identification of tyrosine phosphorylation in proteins by MALDI-TOF/TOF MS, *Proteomics*, **2009**, *9*, 3047-3057.
- [19] K. Adachi, M. Yamaguchi, M. Nakashige, T. Kanagawa, M. Torimura, S. Tsuneda, Y. Sekiguchi & N. Noda. Affinity capillary electrophoresis with magnetic beads for multiplex quantitative analysis of bacterial 16S rRNA, *Journal of Bioscience and Bioengineering*, **2009**, *107*, 662-667.
- [20] L. Korecká, J. Ježová, Z. Bílková, M. Beneš, D. Horák, O. Hradcová, M. Slovákova & J.L. Viovy. Magnetic enzyme reactors for isolation and study of heterogeneous glycoproteins, *Journal of Magnetism and Magnetic Materials*, **2005**, *293*, 349-357.



- [21] H. Tsumoto, M. Ra, K. Samejima, R. Taguchi & K. Kohda. Chemical derivatization of peptides containing phosphorylated serine/threonine for efficient ionization and quantification in matrix-assisted laser desorption/ionization time-of-flight mass spectrometry, *Rapid Communications in Mass Spectrometry*, **2008**, *22*, 965-972.
- [22] K. Vosseller, K.C. Hansen, R.J. Chalkley, J.C. Trinidad, L. Wells, G.W. Hart & A.L. Burlingame. Quantitative analysis of both protein expression and serine/threonine post-translational modifications through stable isotope labeling with dithiothreitol, *Proteomics*, **2005**, *5*, 388-398.
- [23] W.L. Siqueira & F.G. Oppenheim. Small molecular weight proteins/peptides present in the *in vivo* formed human acquired enamel pellicle, *Archives of Oral Biology*, **2009**, *54*, 437-444.
- [24] W.L. Siqueira, W. Zhang, E.J. Helmerhorst, S.P. Gygi & F.G. Oppenheim. Identification of Protein Components in *in vivo* Human Acquired Enamel Pellicle Using LC-ESI-MS/MS, *Journal of Proteome Research*, **2007**, *6*, 2152-2160.
- [25] S.J. Ding, W.J. Qian & R.D. Smith. Quantitative proteomic approaches for studying phosphotyrosine signaling, *Expert Rev. Proteomics*, **2007**, *4*, 13-23.
- [26] X. Yan & S.D. Gilman. Improved peak capacity for CE separations of enzyme inhibitors with activity-based detection using magnetic bead microreactors, *Electrophoresis*, **2010**, *31*, 346-354.
- [27] H.-X. Chen, J.-M. Busnel, G. Peltre, X.-X. Zhang & H.H. Girault. Magnetic Beads Based Immunoaffinity Capillary Electrophoresis of Total Serum IgE with Laser-Induced Fluorescence Detection, *Analytical Chemistry*, **2008**, *80*, 9583-9588.
- [28] A.L. Gassner, J. Morandini, J. Josserand & H.H. Girault. Ring magnets for magnetic beads trapping in a capillary, *Analytical Methods*, **2011**, *3*, 614-621.

## Chapter 5: Introduction to Pyrolysis Bio-oils and Potential Application as a Pesticide

---

Reproduced in part with permission from **C.J. Booker**, R. Bedmutha, T. Vogel, A. Gloor, R. Xu, L. Ferrante, K.K.C. Yeung, I.M. Scott, K.L. Conn, F. Berruti & C. Briens. Experimental Investigations into the Insecticidal, Fungicidal, and Bactericidal Properties of Pyrolysis Bio-oil from Tobacco Leaves Using a Fluidized Bed Pilot Plant, *Industrial & Engineering Chemistry Research*, **2010**, *49*, 10074-10079. Copyright (2010) American Chemical Society.

Reproduced in part with permission from **C.J. Booker**, R. Bedmutha, I.M. Scott, K. Conn, F. Berruti, C. Briens & K.K.C. Yeung. Bioenergy II: Characterization of the Pesticide Properties of Tobacco Bio-Oil, *International Journal of Chemical Reactor Engineering*, **2010**, *8*. Copyright (2010) Berkeley Electronic Press.

Reproduced in part with permission from R. Bedmutha, **C.J. Booker**, L. Ferrante, C. Briens, F. Berruti, K.K.-C. Yeung, I.M. Scott & K.L. Conn. Insecticidal and bactericidal characteristics of the bio-oil from the fast pyrolysis of coffee grounds, *Journal of Analytical and Applied Pyrolysis*, **2011**, *90*, 224-231. Copyright (2011) Elsevier.

Biological matrices pose many challenges to sample analysis, and the past four chapters have examined how proteins and peptides can be prepared for mass spectrometry analysis through enrichment and purification using miniaturized techniques. These method developments have successfully isolated, enriched, and purified proteins and peptides using capillary electrophoresis at sub-microliter volumes. A second class of complex samples addressed in this thesis is bio-oil. This chapter provides important background information on the generation, chemical composition, and value of pyrolysis bio-oils as an introduction to Chapter 6, where a series of analytical techniques are employed by the author to investigate the acting pesticide chemicals in bio-oil.

As fossil fuels are depleted and the need for energy increases worldwide, the search for alternative and sustainable energy sources has become a serious, but exciting task. Renewable energy sources that are environmentally compatible are of paramount importance. In light of these considerations, pyrolysis of biomass is currently being investigated around the world for the conversion of bulky, low cost, renewable material to bio-oil, a valuable source of renewable energy and fine chemicals. Bio-oil is a complex mixture of chemicals that is considered a carbon neutral alternative to fossil fuels with low emissions of undesirable components, such as SO<sub>2</sub>, NO<sub>x</sub> and soot [1].

## **5.1 Biomass Sources for Pyrolysis**

Any biological matter, from agricultural plants to animal and food waste, is considered biomass and can be converted into bio-oil via pyrolysis. Not only is biomass a renewable resource, as compared to crude oil, but the actual growth of lignocellulosic materials continually removes increasingly hazardous levels of carbon dioxide from the Earth's atmosphere. In this sense, bio-oil is considered a carbon neutral energy source, as the carbon released in gaseous form is recaptured during the growth of the lignocellulosic materials.

The selection of an appropriate biomass must be considered for bio-oil to be successfully integrated into the energy or fine chemicals markets. Currently, the

conversion of bio-oil into usable fuel cannot compete with crude oils in heat value or production efficiency [2], but the economic value of bio-oil increases if the starting feedstock has a low or even negative worth. Thus, many research groups around the world are working diligently to convert waste or excess agricultural or forestry residues into bio-oil. These residues are abundant, renewable, and available at a low cost. Mill and forestry residues such as bark and sawdust are examples of popular feedstocks for bio-oil as the pulp and paper industry generates great amounts of these excess products [3]. Additional feedstocks of current interest include rice husks, distiller's grain, and straws. Although investigations into bio-oil from edible crops, such as cereals and corn, have been performed, bio-oils from "waste" products are much more valuable and avoid the *food versus fuel* debate.

The selection of the biomass for pyrolysis impacts the cost of the process and value of the product. Most notably, the water content of the original biomass source affects the water content, and hence the heating value, of the bio-oil product. Biomass sources that begin with lower water content, such as hardwood and straw, require less drying before pyrolysis and thus require less energy input prior to pyrolysis to generate high quality bio-oil. Transportation of the biomass to a pyrolysis reactor is also a limiting factor in the economic viability of bio-oil as an energy source. The biomass must be local to the reactor for the transportation costs to balance the energy value of the product. To circumvent the need for a local biomass source, a mobile pyrolyzer has been designed and tested by Agri-Therm to generate bio-oil on-site. Bio-oil has a much higher density than the original biomass, which allows for more efficient transportation of the energy source.

Biomass from agricultural or forestry sources is composed of three building blocks, namely lignin, cellulose, and hemicelluloses. Lignin is a complex, organic polymer that provides structural support and a protective barrier to vascular plants [4]. The chemical structure of the lignin macromolecule changes across plant species and is not completely characterized, although a few complex structures for specific plants have been proposed over the years [5]. The monomeric lignin precursors for lignin are p-coumaryl alcohol, coniferyl alcohol, and sinapyl alcohol. In essence, lignin is a complex arrangement of phenolic and aromatic moieties that can decompose into hundreds of

possible arrangements during pyrolysis. The second component, and most abundant organic compound on Earth, is cellulose. These  $\beta$ -glucose polymers form microfibrils via hydrogen bonding and provide structural support in plant cell walls [6]. The third component of plants is a group of polysaccharides called hemicelluloses. In contrast to cellulose, hemicelluloses are comprised of many different sugar units, such as xylose, glucose, and uronic acids [7].

Although these three building blocks are found in all plants, the proportion of these components changes with the biomass source. In addition to this variable, the chemical arrangement of the lignin, the array of possible hemicelluloses, and the unique extractive chemicals present in each feedstock culminate in a unique composition for each biomass. Thus, the chemical composition of bio-oil from each biomass source is also unique. Not only does the biomass source affect the composition of the bio-oil, but the pyrolysis conditions also have a great effect on the end products.

## 5.2 Pyrolysis Process

Thermal chemical conversion of biomass can be performed in excess air through combustion to give heat, in partial air via gasification to give gases and syngas, or in the absence of air by means of pyrolysis to generate bio-oils. Burning biomass for heat has been exploited for thousands of years. Using wood to heat homes is still a common practice, with over three million homes in Canada using wood as a primary or secondary heating source [8]. The drawbacks to this form of heating include the cost of transporting this bulky energy source and the incomplete burning of the wood that leads to particulate matter, volatile organic carbons, carbon monoxide, polycyclic aromatic hydrocarbons, furans, and nitrogen oxides [8]. Pyrolysis is not the same as simply burning biomass. Pyrolysis occurs in the absence of oxygen under a moderately high temperature (300 – 700 °C) and produces three product states - liquid, solid, and gas (Figure 5.1). The gases can be collected or combusted to heat the reactor [9]. Char is an additional energy source as it has a similar heating value to that of coal, but with significantly lower amounts of

sulphur [10]. Char can also be used as a fertilizer [9,11]. The condensable vapours from the reactor are the dark brown liquid bio-oil product which is currently the product of greatest interest. It has been suggested that pyrolysis is the most efficient process to convert biomass into a potential fuel [10].

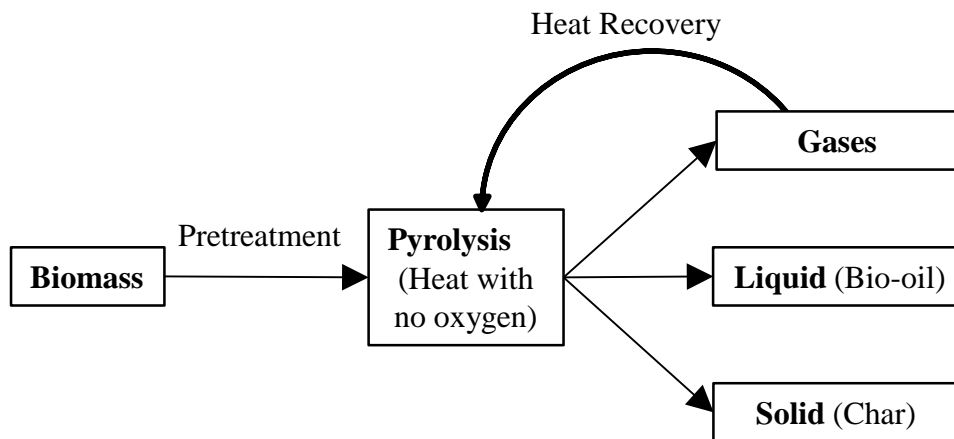


**Figure 5.1.** Simple schematic of the pyrolysis process.

Pyrolysis converts bulky biomass, which is expensive to transport, into an easily transportable liquid bio-oil. Fast pyrolysis, in contrast to slow pyrolysis, can be performed in seconds and generates condensable vapours as the main product with up to 80% yield [12]. Slow pyrolysis occurs over hours and is designed to produce more solid char than liquid products. The residence time of the biomass in the reactor for fast pyrolysis ranges from 0.5 to 10 s [9]. As the residence time increases, the amount of cracking increases, leading to more gasses. The gaseous yield also increases with temperature while the char yield decreases with temperature. The temperature of the reactor can be optimized to produce the greatest proportion of liquid products, with the ideal temperature around 500 °C for most feedstocks [12].

Pretreatment of the biomass improves the quality of the resultant bio-oil. The most common steps are heating, grinding, and chemical treatments. Feedstocks that already have low water content, such as straws, may not need the energy consuming drying step, but for most other feedstocks, such as plant leaves, the biomass is dried to reduce the water content of the final bio-oil. Once the biomass is sufficiently dry, it must be ground

into small particles, on the order of millimetres to hundreds of micrometers. The very short residence time in the reactor requires that the particles are very fine so that the heat can be effectively transferred through the entire biomass in the short reaction time. Chemical pretreatment changes the arrangement of the lignocellulosic material so that the polymers are more accessible for hydrolysis and depolymerisation. For example, the crystalline structure of cellulose can be disrupted in the presence of dilute acid or base (sulphuric acid or sodium hydroxide) yielding greater surface area for reactions. This process can also be used to hydrolyze hemicelluloses into single sugars [13].

A pyrolysis reactor design must allow for fast injection of the biomass into the reactor, effective heat transfer to the biomass, and rapid cooling of the vapours [12]. A common reactor design is that of a fluidized bed reactor. This reactor is full of hot particles (often sand) which allows for effective heat transfer to the biomass. These particles are fluidized by the flow of an inert gas which causes continuous movement in the reactor and removes the char build-up around the biomass particles [9,14]. The vapours are collected through a hot filter and quickly cooled through a series of condensers and collected as gas or bio-oil (Figure 5.2). This reactor design is optimized for bio-oil collection and not char production, as the char is left behind in the reactor with the hot particles. Such a reactor was designed at the University of Western Ontario by the Western Fluidization Group, and it was this pilot plant that was used to generate the bio-oil examined in this thesis (Figure 5.2).

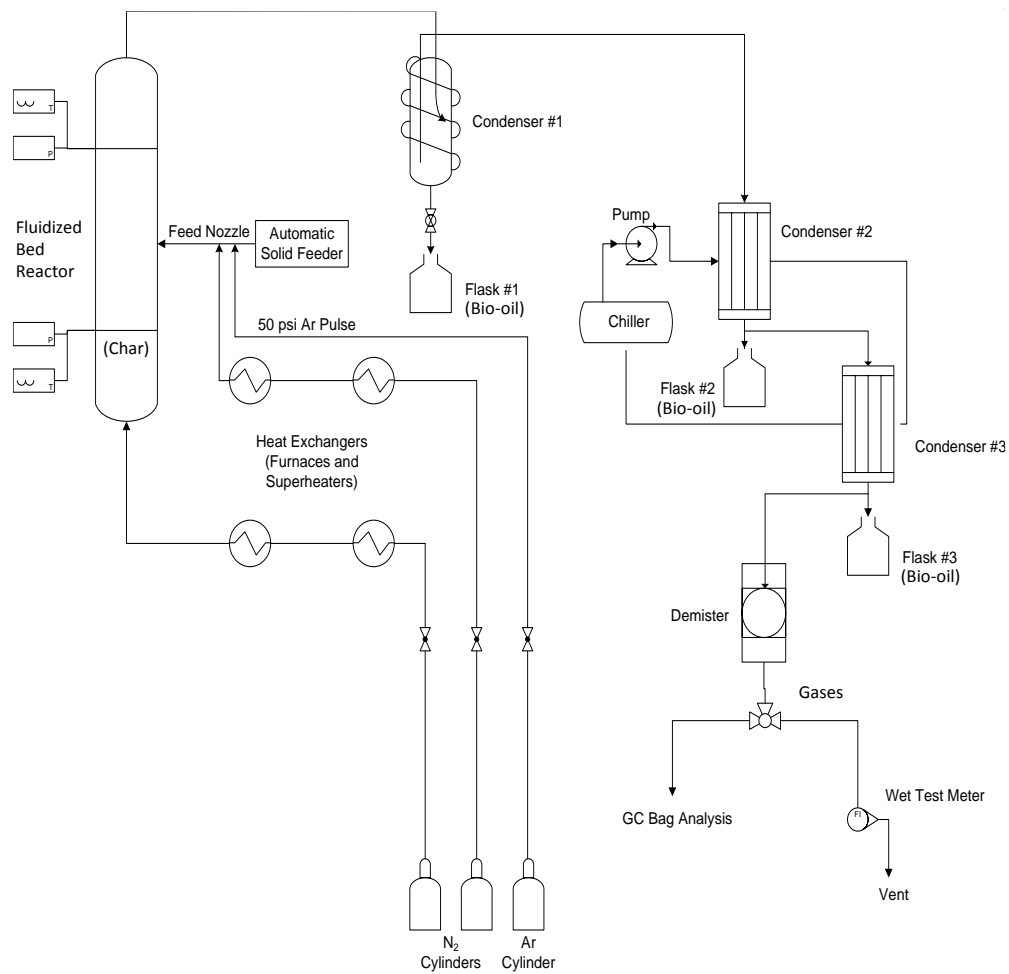


**Figure 5.2.** A schematic of the Western Fluidization Group's fluid bed pyrolysis pilot plant. Figure adapted from [15].



## 5.3 Chemical Composition of Bio-oil

Bio-oil is a complex mixture of the breakdown products of the three main building blocks, cellulose, hemicelluloses and lignin, as well as the decomposition or conservation of any additional chemicals unique to a specific biomass. The exact decomposition scheme and reactions that occur during pyrolysis are highly complex and variable, depending upon the biomass and pyrolysis conditions. The cracking reactions are not fully understood, although scientists are studying these processes now, beginning with cellulose and hemicellulose [16,17].

Analysis of bio-oil has identified a complex mixture on the order of thousands of chemicals [18]. The actual chemical composition of a bio-oil depends on the biomass source [19] and pyrolysis conditions [20], although many common chemicals are found in all bio-oils. Water, sugars, hydroxyaldehydes, hydroxyketones, carboxylic acids, and phenolics are the major groups of chemicals [21]. Lignin is the source for most of the phenolic and aromatic compounds found in bio-oil [22]. The cracking of cellulose and hemicelluloses during heating has been compared using thermogravimetric analysis (TG) and differential thermogravimetric analysis (DTG) [17]. The main depolymerisation reactions for both polymers occurred before 400 °C, although the main xylan chain of hemicelluloses vaporized at a much higher temperature (700 °C). Shen *et al.* determined that the products from the depolymerisation and cracking of cellulose contributed mainly to the bio-oil production, while hemicelluloses contributed more so to the char yield [17]. Although each biomass and resultant bio-oil is unique, the chemical composition between bio-oils is similar due to the common source of these three building blocks.

Although pyrolysis is performed in the absence of oxygen, the pyrolysis oil generally contains a high proportion of oxygenated compounds, which is due to the oxygen content in the original biomass. The elemental composition of bio-oil compared to heavy petroleum oils varies most significantly in the oxygen content, with typical percent weight oxygen values in bio-oil being 35-40 times greater than in petroleum [2]. Petroleum fuels contain greater proportions of carbon and hydrogen, with a minimal amount of water. Water has been recognized as the single most abundant component in

bio-oil, as the moisture content in bio-oil is up to 30% or greater [23]. The water content in bio-oil is attributed to the moisture in the original biomass and is also the product of the dehydration reactions during pyrolysis.

The chemical stability of bio-oils has been studied, and it has been found that the composition changes with time, especially when exposed to higher temperatures [2]. The viscosity of bio-oil increases with time, suggesting polymerization amongst some of the molecules. An increased water content with aging was found by Oasmaa and Kuloppala, but the many polymerization reactions still caused an overall increased viscosity and sludge formation [24]. Ortega and colleagues found that bio-oil with a higher water content that was stored char-free had a slower aging process [25]. This degradation and inconsistency in composition is one of the drawbacks to using bio-oil as a fuel.

The liquid products of pyrolysis have been investigated through a wide variety of techniques, including gas chromatography (GC) [10,25,26] and two-dimensional GC [18] for volatile components, liquid chromatography for nonvolatiles, Karl-Fischer titration to determine water content [25], thermogravimetric analysis to determine the evaporation and cracking mass losses [26], and gel permeation chromatography to determine molecular weight distribution [26]. Detection methods include time of flight mass spectrometry (TOF-MS) [18], electron impact MS [25,27], flame ionization detection [27], nuclear magnetic resonance imaging for functional group analysis, ultraviolet-visible absorbance (UV-vis), and Fourier transform infrared spectroscopy (FTIR) [28]. Prior to analysis, liquid-liquid extraction was often performed to simplify the chemical composition for subsequent analysis. Only about 40% of the liquid products are volatile and can be detected through GC [23]. HPLC is ideal for non volatile compounds, but identification of the compounds is a challenge. UV-vis absorbance is commonly used with HPLC, but cannot identify a compound. Comparing retention times of standard chemicals with the peaks found from HPLC analysis can implicate a compound's identity, but overlapping peaks are possible. HPLC can now be interfaced with mass spectrometry to improve the identification of compounds. Unfortunately, this method is still being developed and libraries of mass spectral fragmentation fingerprints are still in process, which makes the identification of unusual or novel compounds quite challenging.

## 5.4 Potential Value and Applications of Bio-oil

The high moisture level and oxygen content in bio-oil causes a lower heating value for bio-oil compared to crude oil. Bio-oil has additional undesirable properties for a fuel, including its high viscosity, poor volatility, and coking during pyrolysis. Refining bio-oil to a satisfactory level for commercial use has been performed, but currently uses too much energy and occurs at too high a cost to be economically viable [2].

Thus, as research continues into pyrolysis and upgrading of bio-oil to make it a more effective fuel, additional, value-added applications for bio-oil are necessary. If high value, bio-sourced chemical products could be found for even a portion of the bio-oil product, then the energy market may be open to the remainder of this environmentally friendly and renewable energy source. The current drawbacks of bio-oil as an energy source could be off-set by additional high value applications. In a review on value-added products from bio-oil, FitzPatrick has compared the US market for transportation fuel (\$385 billion USD, 2007) which uses 70% of the country's petroleum market to that of the fine chemicals market (\$375 billion) that uses only 3% of the petroleum [29]. Great economic opportunity can be found with the right applications of bio-oil.

A potentially lucrative prospect for bio-oil is as a source for valuable chemicals. These chemicals could be found in the original biomass and preserved during pyrolysis, such as nicotine in tobacco bio-oil, or could be created during the pyrolysis process, such as phenolic chemicals. New chemicals yet to be identified could also be highly valuable. The high abundance of phenol and monomeric phenol species in bio-oil has led to a variety of potential applications of these chemicals. One such application has been investigated by Cheng *et al.* for phenols from woody bio-oil to be a partial substitute for phenol-formaldehyde in plywood adhesives [30]. Bio-oil-phenol-formaldehyde resol resins were found to have comparable or better properties for this application compared to the conventional product obtained from petroleum. Chemicals extracted from bio-oil have also been used as food additives. This "smoky" flavouring agent has been commercialized by Red Arrow Products Company [31].

## 5.5 Bio-oil as a Pesticide

One of the many potential applications of these chemicals is as a pesticide. The search for effective and safe pesticides is a continuing challenge as species quickly adapt to most pesticides that are applied. Many pesticides are also harmful to the environment, to plants, animals, and humans, and are derived from petroleum products – an ever decreasing resource. Pesticides extracted from bio-oil, on the other hand, would be from a renewable resource and available at a low cost. An ideal pesticide would have many components, so that resistance to the pesticide would be more difficult for the species to acquire, and be specific so that only the target species would be negatively affected.

The potential pesticide activity of bio-oil is an exciting research area that has yet to be fully explored. Recently, bio-oil from wood has been investigated for its wood preservative properties against natural biodegradation [32] and specifically for its anti-fungal properties [33,34]. Two species of fungi were tested and found to have inhibited growth patterns in the presence of bio-oil from wood biomass. In contrast, this thesis investigates the pesticide characteristics of bio-oil from tobacco biomass, not only for anti-fungal activity, but also for anti-bacterial activity.

Some of the recurring chemicals found in bio-oil, regardless of the biomass source, are known to be very toxic (50 to 500 mg kg<sup>-1</sup> oral LD<sub>50</sub> values, the median lethal dose). One example is phenol and its derivatives [26,35,36]. Methyl substituted, monomeric phenolic compounds, o-cresol, p-cresol, and m-cresol, have oral LD<sub>50</sub> values of 121 mg kg<sup>-1</sup>, 242 mg kg<sup>-1</sup>, and 207 mg kg<sup>-1</sup>, respectively, for rats [37]. Phenol itself has an oral LD<sub>50</sub> value of 410 - 650 mg kg<sup>-1</sup> for rats. The antifungal and antibacterial properties of cresols have been recognized for many years [38] and cresols have been commonly used as a wood preservative in the form of creosote.

Although the broad, general composition of bio-oil is known (mixture of alcohols, phenols, lignin, etc), no report, to our knowledge, has clearly identified which of these chemicals are responsible for the pesticide characteristics in bio-oil. Phenolic compounds have been assumed responsible for the observed antifungal activity in wood bio-oil, but

this correlation has not been experimentally supported [32,33]. While some of the identified chemicals in bio-oil are known to be active towards pests (ie. o-cresol, m-cresol, and p-cresol) [37], the concentrations at which they are found in bio-oil may not be sufficient to account for the observed activity.

The potential for bio-oil to be a pesticide is investigated in this thesis.

## 5.6 References

- [1] Q. Zhang, J. Chang, T.J. Wang & Y. Xu. Review of biomass pyrolysis oil properties and upgrading research, *Energy Conversion and Management*, **2007**, *48*, 87-92.
- [2] S. Czernik & A.V. Bridgwater. Overview of Applications of Biomass Fast Pyrolysis Oil, *energy & Fuels*, **2004**, *18*, 590-598.
- [3] D. Bradley. Canada- Sustainable Forest Biomass Supply Chains. **2007**, Climate Change Solutions. Climate Change Solutions.
- [4] S. Reale, A.D. Tullio, N. Spreti & F.D. Angelis. Mass Spectrometry in the Biosynthetic and Structural Investigation of Lignins, *Mass Spectrometry Reviews*, **2003**, *23*, 87-124.
- [5] S. Reale, A.D. Tullio, N. Spreti & F.D. Angelis. Mass Spectrometry in the Biosynthetic and Structural Investigation of Lignins, *Mass Spectrometry Reviews*, **2004**, *23*, 87-126.
- [6] N.A. Campbell & J.B. Reece. *Biology* Benjamin Cummings, San Francisco, CA, **2002**.
- [7] F.M. Girio, C. Fonseca, F. Carvalheiro, L.C. Duarte, S. Marques & R. Bogel-Lukasik. Hemicelluloses for fuel ethanol: A review, *Bioresource Technology*, **2010**, *101*, 4775-4800.
- [8] Environment Canada. Residential Wood Heating. Updated **2011-18-01**, <http://www.ec.gc.ca/residentiel-residential/default.asp?lang=En&n=E9FE1750-1> Retrieved 2011-25-08.
- [9] C. Briens. Biomass Valorization for Fuel and Chemicals Production - A Review, *International Journal of Chemical Reactor Engineering*, **2008**, *6*, R2.
- [10] A. Demirbas. Analysis of liquid products from biomass via flash pyrolysis, *Energy Sources*, **2002**, *24*, 337-345.
- [11] M.A. Rondon, J. Lehmann, J. Ramirez & M. Hurtado. Biological nitrogen fixation by common beans (*Phaseolus vulgaris* L.) increases with bio-char additions, *Biology and Fertility of Soils*, **2007**, *43*, 699-708.
- [12] A.V. Bridgwater & G.V.C. Peacocke. Fast pyrolysis processes for biomass, *Renewable & Sustainable Energy Reviews*, **2000**, *4*, 1-73.

- [13] N. Mosier, C. Wyman, B. Dale, R. Elander, Y.Y. Lee, M. Holtzapple & M. Ladisch. Features of promising technologies for pretreatment of lignocellulosic biomass, *Bioresource Technology*, **2005**, *96*, 673-686.
- [14] R. Xu, L. Ferrante, C. Briens & F. Berruti. Flash pyrolysis of grape residues into biofuel in a bubbling fluid bed, *Journal of Analytical and Applied Pyrolysis*, **2009**, *86*, 58-65.
- [15] R. Bedmutha, C.J. Booker, L. Ferrante, C. Briens, F. Berruti, K.K.C. Yeung, I. Scott & K. Conn. Insecticidal and bactericidal characteristics of the bio-oil from the fast pyrolysis of coffee grounds, *Journal of Analytical and Applied Pyrolysis*, **2011**, *90*, 224-231.
- [16] J. Piskorz, D. Radlein & D.S. Scott. On the Mechanism of the Rapid Pyrolysis of Cellulose, *Journal of Analytical and Applied Pyrolysis*, **1986**, *9*, 121-137.
- [17] D.K. Shen, S. Gu & A.V. Bridgwater. The thermal performance of the polysaccharides extracted from hardwood: Cellulose and hemicellulose, *Carbohydrate Polymers*, **2010**, *82*, 39-45.
- [18] J.H. Marsman, J. Wildschut, P. Evers, S. de Koning & H.J. Heeres. Identification and classification of components in flash pyrolysis oil and hydrodeoxygenated oils by two-dimensional gas chromatography and time-of-flight mass spectrometry, *Journal of Chromatography A*, **2008**, *1188*, 17-25.
- [19] J.P. Diebold. in *Fast Pyrolysis of Biomass: A Handbook*. Eds A. Bridgwater, CPL Press, Newbury, U.K., **2002**, pp. 243-292.
- [20] E.J. Soltes & T.S. Elder. in *Organic Chemicals from Biomass*. Eds I.S. Goldstein, CRC Press, Boca Raton, Florida, **1981**, pp. 63.
- [21] J. Piskorz, D.S. Scott & D. Radlein. Composition of oils obtained by fast pyrolysis of different woods, *ACS Symposium Series*, **1988**, *376*, 167-178.
- [22] M. Kleinert & T. Barth. Phenols from lignin, *Chemical Engineering & Technology*, **2008**, *31*, 736-745.
- [23] A.V. Bridgwater, S. Czernik & J. Piskorz. in *Progress in Thermochemical Biomass Conversion*. Eds A.V. Bridgwater, Blackwell Science Ltd, Oxford, **2001**, pp. 977-997.
- [24] A. Oasmaa & E. Kuoppala. Fast pyrolysis of forestry residue. 3. Storage stability of liquid fuel, *energy & Fuels*, **2003**, *17*, 1075-1084.
- [25] J.V. Ortega, A.M. Renehan, M.W. Liberatore & A.M. Herring. Physical and chemical characteristics of aging pyrolysis oils produced from hardwood and

- softwood feedstocks, *Journal of Analytical and Applied Pyrolysis*, **2011**, *91*, 190-198.
- [26] M. Garcia-Perez, A. Chaala, H. Pakdel, D. Kretschmer & C. Roy. Characterization of bio-oils in chemical families, *Biomass & Bioenergy*, **2007**, *31*, 222-242.
- [27] S. Ucar & A.R. Ozkan. Characterization of products from the pyrolysis of rapeseed oil cake, *Bioresource Technology*, **2008**, *99*, 8771-8776.
- [28] A.E. Pütün, E. Önal, B.B. Uzun & N. Özbay. Comparison between the "slow" and "fast" pyrolysis of tobacco residue, *Industrial Crops and Products*, **2007**, *26*, 307-314.
- [29] M. FitzPatrick, P. Champagne, M.F. Cunningham & R.A. Whitney. A biorefinery processing perspective: Treatment of lignocellulosic materials for the production of value-added products, *Bioresource Technology*, **2010**, *101*, 8915-8922.
- [30] C. Cheng, I. D'Cruz, Z. Yuan, M. Wang, M. Anderson, M. Leitch & C. Xu. Use of Biocrude Derived from Woody Biomass to Substitute Phenol at a High-Substitution Level for the Production of Biobased Phenolic Resol Resins, *Journal of Applied Polymer Science*, **2011**, *121*, 2743-2751.
- [31] S. Czernik & A.V. Bridgwater. Overview of applications of biomass fast pyrolysis oil, *energy & Fuels*, **2004**, *18*, 590-598.
- [32] D. Mourant, B. Riedl, D. Rodrigue, D.Q. Yang & C. Roy. Phenol-formaldehyde-pyrolytic oil resins for wood preservation: A rheological study, *Journal of Applied Polymer Science*, **2007**, *106*, 1087-1094.
- [33] D. Mohan, J. Shi, D.D. Nicholas, C.U. Pittman, P.H. Steele & J.E. Cooper. Fungicidal values of bio-oils and their lignin-rich fractions obtained from wood/bark fast pyrolysis, *Chemosphere*, **2008**, *71*, 456-465.
- [34] D. Mourant, D.Q. Yang, X. Lu & C. Roy. Anti-fungal properties of the pyrolygneous liquors from the pyrolysis of softwood bark, *Wood and Fiber Science*, **2005**, *37*, 542-548.
- [35] G.E. Achladas. Analysis of biomass pyrolysis liquids - separation and characterization of phenols *Journal of Chromatography*, **1991**, *542*, 263-275.
- [36] Z.Y. Luo, S. Wang, Y.F. Liao, J.S. Zhou, Y.L. Gu & K.F. Cen. Research on biomass fast pyrolysis for liquid fuel, *Biomass & Bioenergy*, **2004**, *26*, 455-462.
- [37] EI DuPont de Numours & Co. Cresols, ortho-, meta-, and para-. **1983**, NTIS Report. No. OTS0205862.



- [38] Final report on the safety assessment of sodium p-chloro-m-cresol, p-chloro-m-cresol, chlorothymol, mixed cresols, m-cresol, o-cresol, p-cresol, isopropyl cresols, thymol, o-cymen-5-ol, and carvacrol, *International Journal of Toxicology*, **2006**, 25, 29-127.

## Chapter 6: Investigations into the Antimicrobial Activity of Bio-oil: From Biomass Sources to Chemical Composition

---

Reproduced in part with permission from **C.J. Booker**, R. Bedmutha, T. Vogel, A. Gloor, R. Xu, L. Ferrante, K.K.C. Yeung, I.M. Scott, K.L. Conn, F. Berruti & C. Briens. Experimental Investigations into the Insecticidal, Fungicidal, and Bactericidal Properties of Pyrolysis Bio-oil from Tobacco Leaves Using a Fluidized Bed Pilot Plant, *Industrial & Engineering Chemistry Research*, **2010**, *49*, 10074-10079. Copyright (2010) American Chemical Society.

Reproduced in part with permission from **C.J. Booker**, R. Bedmutha, I.M. Scott, K. Conn, F. Berruti, C. Briens & K.K.C. Yeung. Bioenergy II: Characterization of the Pesticide Properties of Tobacco Bio-Oil, *International Journal of Chemical Reactor Engineering*, **2010**, *8*. Copyright (2010) Berkeley Electronic Press.

Reproduced in part with permission from R. Bedmutha, **C.J. Booker**, L. Ferrante, C. Briens, F. Berruti, K.K.-C. Yeung, I.M. Scott & K.L. Conn. Insecticidal and bactericidal characteristics of the bio-oil from the fast pyrolysis of coffee grounds, *Journal of Analytical and Applied Pyrolysis*, **2011**, *90*, 224-231. Copyright (2011) Elsevier.

## 6.1 Introduction

This chapter examines bio-oil from many different excess agricultural and forestry residues for pesticide activity. These feedstocks were selected based upon their abundance and interest in Canada. Roasted coffee beans (*Coffea Arabica* or *Coffea robusta*) are used to make the coffee beverage that is consumed around the world. Considerable coffee grounds waste is generated as the average adult in North America and Europe consumes 500 mL of coffee per day [1], and thus, bio-oil from coffee grounds was examined. Pinewood killed by beetles is becoming an abundant biomass in British Columbia. According to the British Columbia Ministry of Forests, Lands and Natural Resource Operations, an estimated 726 million cubic metres of timber have been killed by the mountain pine beetle as of April 2011. A value added product from this dead wood could be of great benefit to Canada, and thus bio-oil from this biomass was also tested. Agricultural residues of grape seeds and skins (excess product of wine industry) and apple pomace (residue remainder after pressing apples) after pyrolysis were also tested. Finally, three additional bio-oils from straws obtained from Saskatchewan were examined, Canola straw (*Brassica napus*) and mustard straws (*Juncea* and *Carinata*).

The bio-oil of focus was obtained through pyrolysis of tobacco. One of the reasons tobacco biomass was selected for detailed analysis is that tobacco farmers, especially those in Canada, have a decreased demand for their crop [2]. It is well known that smoking tobacco has a significant, negative impact on human health. The transition out of tobacco farming, however, is difficult as it leaves farmers with expensive, specified equipment that can no longer be used. Thus, finding alternative, healthy, high value applications to this highly abundant product is an important research area. During this project, the Canadian government offered a \$300 million buy-out to tobacco farmers in 2008 to cease growing tobacco and transition to another crop or land usage [3]. Already, however, tobacco biomass is being investigated for unique, high value applications, such as for medical or industrial proteins [4-6], and in the case of this research, as a natural pesticide. The nicotine in tobacco leaves has well known pesticide properties, so

converting tobacco leaves into bio-oil to be used as a natural pesticide could increase the value of this crop and aid farmers in their tobacco dilemma.

The products formed from smoking tobacco cigarettes have been analyzed [7-9], but the composition of bio-oil from tobacco has not been fully characterized. Analysis of bio-oil from tobacco stalk was performed with a focus on product yield and small organic chemicals, namely methanol and acetic acid, but investigation into the nicotine content was not included [10]. Another group analyzed pyrolysis on tobacco residues, but focused on the gas and char formation rather than the bio-oil product [11].

Bio-oil from tobacco plants is known to contain the highly toxic chemical nicotine (oral LD<sub>50</sub> of 50 mg kg<sup>-1</sup> for rats) [12]. In addition to its use in pharmaceuticals, nicotine is permitted as a pesticide in Canada, although its use as a pesticide is limited because of its dermal absorption and extreme toxicity to mammals. Thus, it was expected that tobacco bio-oil would have pesticide properties due to the presence of nicotine.

In collaboration with Agriculture and Agri-Food Canada, a variety of problematic pest species to Canada were examined, including microorganisms (bacteria and fungi) and insects (Colorado Potato Beetle, CPB, *Leptinotarsa decemlineata* Say Coleoptera: Chrysomelidae). It was discovered that tobacco bio-oil had a significant negative impact on the CPB and this led to testing tobacco bio-oil on problematic microorganisms as well. In an effort to focus the scope of this chapter, only the investigations into the impact of bio-oil on microorganisms will be discussed. The impact of bio-oil on the CPB and other insects is significant and further research by other investigators continues.

It was found in our research group that nicotine-free fractions of tobacco bio-oil were lethal to the CPB, as well as successful at inhibiting the growth of two bacteria (*Clavibacter michiganensis* subsp. *Michiganensis* and *Streptomyces scabies*) and a fungus (*Pythium ultimum*). The activity of the tobacco bio-oil towards the microorganisms as the chemical complexity of the active bio-oil fractions was reduced is discussed in this chapter. *S. scabies* disfigures potato crops making them unmarketable, *C. michiganensis* seriously disfigures or kills tomato plants, and *P. ultimum* causes

seedling damping off in a variety of vegetable plants. Thus, tobacco bio-oil's pesticide properties are an exciting and potentially economically valuable finding.

## 6.2 Materials and Methods

### 6.2.1 Chemicals and Bio-oil

Chemical standards 2,4-dimethyl phenol (97%), 2,3-dimethyl phenol (99%), 3,4-dimethyl phenol (99%), 4-ethyl phenol (99%), o-cresol (99%), p-cresol (99%), m-cresol (99%), and (R)-limonene were obtained from Aldrich. Phenol and indole (99%) were obtained from Mallinckrodt and Alfa Aesar, respectively. HPLC grade acetone was purchased from Fisher Scientific, while all other solvents (anhydrous ethyl ether, hexanes-200, dichloromethane, and methanol) were purchased from Caledon. Hydrochloric acid and solid sodium hydroxide were obtained from EM Science.

Bio-oil was provided by Rohan Bedmutha and Lorenzo Ferrante through the Faculty of Engineering, University of Western Ontario and the Institute for Chemicals and Fuels from Alternative Resources (ICFAR). Bio-oil samples were generated through flash pyrolysis using an atmospheric fluidized bed pilot plant. Specific design details of this reactor can be found here [13].

Tobacco leaves (dried at 60 °C) were provided by Agriculture and Agri-Food Canada, London, Ontario. The ground leaves used for bio-oil production had a Sauter mean diameter of 60 µm. Tobacco bio-oil samples were collected as the condensable vapours from an atmospheric fluidized bed reactor run at five different temperatures under nitrogen (350, 400, 450, 500, and 550 °C). The vapour residence time was 5 s. Coffee grounds (*Coffea Arabica* or *Coffea robusta*) were obtained from Tim Hortons and Souheil Afara at the University of Western Ontario, London, Ontario, Canada and were dried overnight at 60 °C. The Sauter mean diameter of the dried coffee grounds was 300 µm. Five pyrolysis sample temperatures were collected (400, 450, 500, 550 and 600 °C) with the same vapour residence time of 5 s.

Bio-oil from pinewood killed by beetles (300, 450, 500 °C), mustard straw (*Juncea* and *Carinata* straw, both from Saskatchewan, collected at 300 and 500 °C), canola straw (*Brassica napus* from Saskatchewan and Ontario, collected at 300 and 500 °C), grape seeds and skins (Bioenergy Africa, South Africa, 300 to 600 °C), and apple pomace (400, 450, 500, 550 °C) were also screened for microorganism activity.

## 6.2.2 Bio-oil Sample Preparation

To initially determine which microorganisms were negatively affected in the presence of which bio-oils, a bio-oil mixture of all available production temperatures (300-600 °C) from each biomass was generated. This mixture was prepared in acetone at a concentration of 375 mg mL<sup>-1</sup>. Some bio-oils naturally separated into an organic and aqueous phase, and in these cases, the phases were sometimes tested separately. Bio-oil samples for each pyrolysis temperature from tobacco and coffee were then prepared separately in acetone (375 mg mL<sup>-1</sup>).

### 6.2.2.1 Liquid-Liquid Fractionation

The method used for tobacco bio-oil fractionation is illustrated in Figure 6.1. The tobacco bio-oil (pyrolyzed at 450 °C) was dissolved in ether at a concentration of 375 mg mL<sup>-1</sup> (Fraction Z). This fraction was sterile filtered with a 2.5 cm diameter, 45 µm pore size, nylon membrane syringe (Whatman, NJ, USA). A black residue remained on the walls of the vial and was dissolved in acetone and sterile-filtered (Fraction I). Fraction Z was separated into its aqueous (Fraction A) and organic components (Fraction B), using a water/ether extraction. Fraction B was further extracted by adding water and acidifying the water phase with concentrated HCl to pH 2. It has been suggested that this acidification and neutralization step could alter the chemical composition of the resultant bio-oil fractions. However, this method was extremely successful at removing nicotine from other active chemicals, which was the goal of this step for this work. The ether fraction was collected as Fraction C. The acidified water fraction was then adjusted to pH

9 with NaOH to move the majority of nicotine back into an organic phase. The pH was adjusted only to pH 7 for coffee grounds. Ether was added, creating an ether fraction (Fraction D) and aqueous fraction (Fraction E). The ether in Fraction C was evaporated at room temperature, and a final separation created a methanol fraction (Fraction M) and hexane fraction (Fraction H). Dilution factors were calculated for each fraction and the volume used in the bio-assays was appropriately adjusted to maintain the actual mass of the compounds between experiments. For further fractionations where Fraction M was the only consideration, the first two separations (creating Fraction B and Fraction C), were performed at three times the dilution for better separation. The previous concentration of Fraction M was obtained through the evaporation step of Fraction C.

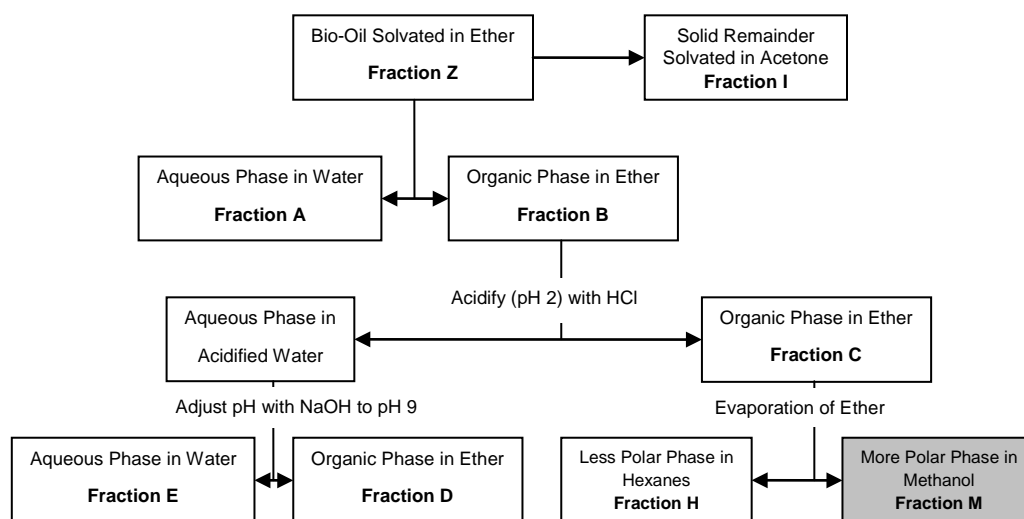


**Figure 6.1.** Fractionation scheme for tobacco bio-oil. Initial concentration for Fraction Z was  $375 \text{ mg mL}^{-1}$ . The shaded box indicates the fraction of interest investigated in this chapter, Fraction M.

### 6.2.2.2 Solid Phase Extraction and Heating

A slurry of C18 (Agela Technologies, 40-60  $\mu\text{m}$ , 925 mg) was prepared in MeOH and added to a 1 mL glass pipette (stopped with glass wool). A 1 mL pipette bulb was used manually as the external pressure to pack the solid phase bed by adding methanol in 500

$\mu\text{L}$  aliquots. This same pressure method was used to elute the sample from the solid phase. Fraction M (100  $\mu\text{L}$ ) was carefully added to the top of the bed and methanol was added in 500  $\mu\text{L}$  increments (to a total volume of 4 mL) to elute the sample. This process caused the C18 beds to change colour from white to brown (Figure 6.9).

The eluent was collected by 500  $\mu\text{L}$  aliquots in 1.7 mL microtubes. These 8 vials were then dried in a speedvac at 65 °C. To examine the heating/evaporation step, water (50 or 200  $\mu\text{L}$ ) was added to each of the microtubes to force a longer drying time, resulting 50 and 90 min drying periods, respectively. A third set of eluent tubes was left to air dry overnight. All samples were resolvated with MeOH to a total of 100  $\mu\text{L}$  to regain the original Fraction M concentration.

### **6.2.2.3 Preparative Scale Liquid Chromatography/Flash Chromatography**

To perform further separation experiments, the concentration of the sample was doubled to ensure detection of microbial activity. Thus, two SPE extraction procedures (100  $\mu\text{L}$  Fraction M through 925 mg of C18 with 4 mL of MeOH) were performed, allowed to air dry, and then resolvated to a total volume of 100  $\mu\text{L}$ . A larger LC preparatory scale column (Falcon polystyrene 5 mL pipet, C18 silica bed of 3.4 g, 11.8 cm tall, 0.6 cm in diameter) was used for this flash chromatography with a large bulb or pressure tubing to apply pressure. The filtered Fraction M was then eluted by a gradient of 9 mL 80:20 MeOH:water followed by 4.5 mL of 95:5 MeOH:water, finishing with 9 mL of 100% MeOH. These fractions were then dried in the speedvac at 65 °C for 90 minutes, or until dryness.

### **6.2.2.4 Derivatization of Active Fraction**

The samples to be derivatized were dried at 65 °C under speedvac conditions. A volume of 150  $\mu\text{L}$  of methoxyamine hydrochloride reagent (MOX, Thermo Scientific, 2% methoxyamine-HCl in pyridine) was added to the sample tube and heated at 50 °C for 90



min. Next, 150  $\mu\text{L}$  of N-methyl-N-TMS-trifluoroacetamide (MSTFA, Thermo Scientific) was added to the solution and the reaction continued at 50  $^{\circ}\text{C}$  for an additional 30 min. The sample was then removed from the heat and analyzed using GC-MS.

### **6.2.3 Gas Chromatography-Mass Spectrometry Sample Analysis**

A HP 6890 Series Gas Chromatography System with a mass selective detector and an autosampler was used to analyze the bio-oil fractions. Experiments were performed on an HP-5MS, 30 m column obtained from Agilent Technologies with an i.d. of 50  $\mu\text{m}$  and a film of 0.25  $\mu\text{m}$ . The injector temperature and auxiliary temperature were maintained at 300  $^{\circ}\text{C}$ . The oven temperature began at 60  $^{\circ}\text{C}$  for 2 min, and then increased at 10  $^{\circ}\text{C min}^{-1}$  to 280  $^{\circ}\text{C}$  and was held for 6 min. Sample injections were 1  $\mu\text{L}$ . A threshold of 150 was used, with a mass to charge scan range of 50 to 300 at a rate of 2.98 scans  $\text{s}^{-1}$ . The obtained spectra were searched through the NIST 2005 library.

Additional GC-MS experiments for the sixteen liquid chromatography fractions before and after silyl derivatization were performed on a new Agilent Technologies 7890A instrument that also had an autosampler and mass selective detector. A new column with the same above parameters was used, namely an Agilent HP-5MS ultra inert, 5% phenylmethyl column 30 m with an inner diameter of 250  $\mu\text{m}$  and film of 0.25  $\mu\text{m}$ . The injector temperature and auxiliary temperature were maintained at 325  $^{\circ}\text{C}$ . The oven temperature began at 70  $^{\circ}\text{C}$  for 5 min, followed by a 5  $^{\circ}\text{C min}^{-1}$  increase to 290  $^{\circ}\text{C}$  where upon the temperature was held for 10 min. A 1  $\mu\text{L}$  sample volume was injected. The mass to charge scan range was 40 – 1050.

### **6.2.4 Bio-assays for Microorganisms**

#### **6.2.4.1 Disk Diffusion Assay**

The disk diffusion assay was used to screen the bio-oil activity on eleven fungi and four bacteria (species listed in Table 6.1). Two additional bacteria were available for testing

against the three straws and apple pomace. Fresh bacterial cultures were maintained by streaking for isolated colonies and for the fungus by transferring an agar plug (5 mm diameter) from the actively growing edge of a culture. All cultures were incubated at 24 °C for up to 1 week before using them in the disk diffusion assay.

The disk diffusion assay was used to test for antimicrobial activity of the bio-oil and standard solutions. Sterile 6 mm diameter filter paper disks were impregnated with 15 µL of the sample or control solution, with the exception of the experiment displayed in Figure 6.2. Here, the volume of sample applied per disk was adjusted to account for the dilution factors during the fractionation steps (ie. Fraction Z was more concentrated than Fraction M, and thus, less volume of Fraction Z was applied to the disk). The disks were allowed to air-dry before being placed onto freshly inoculated plates. For the assay, bacteria from freshly grown plates were streaked onto new agar plates to cover the entire surface obtaining a lawn of growth. The disks were placed onto the inoculated plates and zones of no growth around the disks indicated inhibition (with a minimum measurement of inhibition being 6 mm, the diameter of the disk). Minor inhibition was judged as  $\leq 7$  mm diameter of no growth on some to all of the replicates. Major inhibition was  $> 7$  mm diameter of inhibition on all replicates. For the fungus, an agar plug was transferred from the actively growing edge of a colony to the centre of a new plate, and the disks placed about 1 cm away from the agar plug. Slowed growth of the fungus in the direction of the disk indicated inhibition. The plates were incubated at 24 °C for 3 days whereupon the results were recorded. The data reported is based upon triplicate inhibition measurements. Duplicate measurements were used when one of the triplicate experiments was invalid.

#### **6.2.4.2 Microtiter Plate Bioassay**

A 96 well plate assay was used when sample volumes were limited, such as with the preparative scale liquid chromatography and derivatized samples. Rather than drying the sample fractions on paper disks and measuring the region of inhibited growth, the microwell plate design employed a liquid set-up, where the sample was placed in a solution of broth with the microorganism. The growth was measured as complete (foggy

or fuzzy cell, “100”), partial (minor growth, “50”) or inhibited (no growth, clear cell, “0”). This experimental design allowed for a simple reading of whether or not the sample was active towards the species of interest.

Each sample well was filled to a total volume of 100  $\mu\text{L}$  and each experiment was performed in triplicate wells. Tryptic soy broth (TSB, 30  $\text{g L}^{-1}$  prepared in water) solutions of each bacteria (*S. scabies* and *C. michiganensis*) were made from a scoop of fresh colonies, and 5  $\mu\text{L}$  of the appropriate solution was added to each well, while a small plug of the fungus was added to the fungi experiment wells directly. Each microtitre plate had a series of controls, including a control (only TSB, no microorganism), a positive control (TSB with organism), a negative control (TSB with organism and antibiotic/fungicide), a solvent control (TSB, organism, sample solvent), and a green cell (TSB with sample, no microorganism). The antifungal solution was 2  $\mu\text{L}$  cyclohexamine solution (cyclohexamide prepared in 70% ethanol at 200  $\text{mg mL}^{-1}$ ), 5  $\mu\text{L}$  nystatin solution (2  $\text{mg mL}^{-1}$  in 95% ethanol) to a total volume of 10 mL in TSB. 100  $\mu\text{L}$  of this solution was added to the negative control well for fungi. The antibacterial solution was prepared with 10  $\mu\text{L}$  of 33  $\text{mg mL}^{-1}$  chloroamphenicol and 34  $\text{mg mL}^{-1}$  streptomycin in 33% Tergitol-NPX and 66% mL ethanol, diluted to a total volume of 10 mL in TSB. A sample volume of 1, 2, or 5  $\mu\text{L}$  was applied to each well, depending upon the experiment. The final volume of each well was 100  $\mu\text{L}$ . Results were recorded after four days growth.

In some cases, the growth reading was difficult to make visually in the well due to the colour of the bio-oil samples. In these cases, 5  $\mu\text{L}$  of the well solution was spotted onto an agar plate in a grid formation (20 spots per plate) and the growth was checked within 3 days. For bacterial well experiments, the plug of bacteria was removed and placed on an agar plate and growth was measured within 2 days.

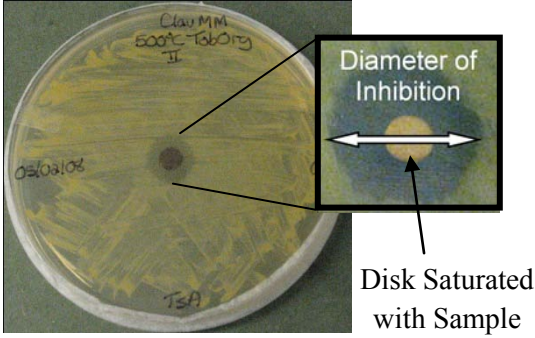
## 6.3 Results and Discussion

### 6.3.1 Antimicrobial Activity from Bio-oil from Multiple Biomass Sources

In the interest of discovering value-added products from bio-oil and based on the discovery that tobacco bio-oil had pesticide activity towards the Colorado Potato Beetle, bio-oil from multiple biomass sources was investigated against an array of problematic microorganisms. The microorganism species were selected for analysis because of their destructive properties towards Canadian agriculture. Pyrolysis bio-oils from the following excess agricultural and forestry residues were tested for antimicrobial activity.

To determine which microorganism species were inhibited by bio-oil, samples from each biomass source were tested against all available microorganisms. Bio-oil from all pyrolysis temperatures were combined for each biomass source for initial screening. The naturally separated organic phases and aqueous phases were examined separately or together, depending on the biomass source, as indicated in Table 1. No inhibition was found from the aqueous phases of coffee grounds, tobacco, or grape seeds and skins. In contrast, the organic phase (or combined phase, including both organic and aqueous phases) of each bio-oil showed clear inhibition for two bacteria, *Streptomyces scabies* (*S. scabies*) and *Clavibacter michiganensis* sub. sp. *michiganensis* (*C. michiganensis*). *Carinata* mustard straw was unique in that it displayed inhibition towards each of the six bacteria. Tobacco bio-oil was the only bio-oil with inhibition towards a fungus, *Pythium ultimum* (*P. ultimum*). This pattern of activity suggests that some of the acting pesticide chemicals are common components found in all of these bio-oils, while some bio-oils either have higher concentrations of some active components or contain unique chemicals that originate from their distinct biomass source.

**Table 6.1.** List of bio-oil biomass sources and microorganism activity. (Inset: photographs of inhibited growth of *C. michiganensis* by a paper disk saturated with tobacco bio-oil.)



	Coffee Grounds* <sup>1</sup>	Pine-wood** <sup>2</sup>	Grape Seed/Skin* <sup>1</sup>	Tobacco Leaves* <sup>1</sup>	Mustard Straw ( <i>Juncea</i> )	Mustard Straw ( <i>Carinata</i> )	Canola Straw	Apple Pomace
<b>Bacteria</b>								
<i>Acidovorax avenae</i>						-	-	
<i>Clavibacter michiganensis</i>	+	+	+	+	+	+	+	+
<i>Erwinia cartotovora</i> pv <i>atroseptica</i> <sup>#</sup>					-	+	-	
<i>Pseudomonas syringae</i> pv. <i>Tomato</i>						+		
<i>Streptomyces scabies</i>	+	+	+	+	+	+	+	+
<i>Xanthomonas gardneri</i> Group D <sup>#</sup>					-	-	-	-
<b>Fungi</b>								
<i>Alternaria panax</i>								
<i>Alternaria solani</i>								
<i>Botrytis cinerea</i>								
<i>Colletotrichum acutatum</i>								
<i>Colletotrichum coccades</i>								
<i>Fusarium oxysporum</i>								
<i>Penicillium expansum</i>								
<i>Pythium ultimum</i>								
<i>Rhizoctonia solani</i>				+				
<i>Sclerotinia sclerotiorum</i>								
<i>Verticillium dahliae</i>								

+ Indicates inhibited growth (a clear region of no growth observed around bio-oil)

- Indicates mildly inhibited growth ( $\leq 1$  mm region of no growth around bio-oil)

<sup>1</sup> Activity in organic fraction only

<sup>2</sup> Activity in both organic and aqueous fractions

\* Naturally separated organic and aqueous phases tested separately.

<sup>#</sup> Species not available for coffee grounds, pinewood, grape seeds/skins, tobacco

*P. ultimum* is a fungus that affects plants as a seedling damping-off disease and was only inhibited by tobacco bio-oil [14]. Plants affected by this fungus include eggplant, pepper, lettuce, tomato, and cucumber. *C. michiganensis*, impacted by a greater number of bio-oils, kills young plants and deforms fruits, primarily tomatoes [15]. *S. scabies* was also sensitive to each bio-oil and is a common potato scab disease that infects potatoes and makes them unmarketable [16]. Finding inhibition for *S. scabies* is particularly exciting because currently, no safe pesticide exists on the market that can control this widespread disease.

The discovery that bio-oil only significantly affected select bacterial species (*C. michiganensis* and *S. Scabies*, Carinata straw bio-oil excluded) and only one fungi (*P. ultimum* by tobacco bio-oil) is particularly interesting. This selective inhibition suggests that the active components in the bio-oil are not destructive to all living things, which is an important quality for a potential pesticide. Based upon this result, as well as the fact that tobacco had by far, the greatest intensity of inhibition towards the microorganisms and is a biomass of great import to Ontario, tobacco bio-oil was selected as the focus species for further chemical analysis. Coffee bio-oil was also investigated as a comparison to tobacco bio-oil, although the parallels could only be investigated for the bacterial activity.

### **6.3.2 Investigation into the Effect of Pyrolysis Temperature on Pesticide Activity for Tobacco and Coffee Bio-oil**

Before further chemical investigations, it was important to determine which pyrolysis temperature provided the best combination of chemicals for pesticide activity. Tobacco bio-oil produced at each available pyrolysis temperature was tested on the affected species (Table 6.1), and the growth of each of the three microorganisms was found to be successfully inhibited by each pyrolysis temperature sample (Figure 6.2).

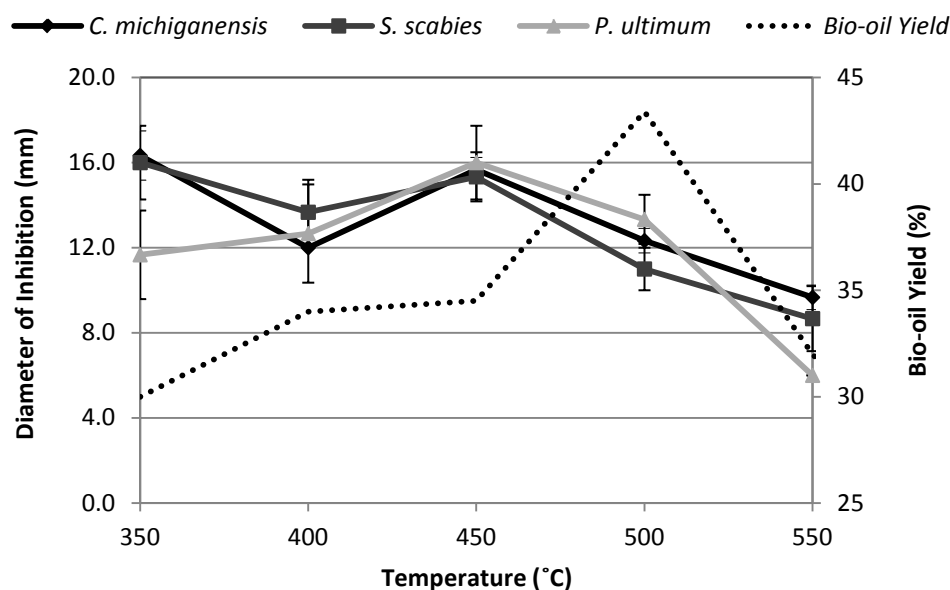


**Figure 6.2.** A graph of the effect of pyrolysis temperature on the diameter of growth inhibition for the three affected microorganism species and bio-oil yield. Error bars indicate  $\pm$  one standard deviation of replicate measurements within an experiment. Data for bio-oil yield was provided by Rohan Bedmutha [17].

As the pyrolysis temperature increased to 550 °C, the activity of the tobacco bio-oil seemed to decrease. This could be due to the active components being cracked into smaller, inactive components at this high temperature. At 450 °C, the greatest inhibition was observed for all three species. For this reason, as well as the fact that this temperature was close to the pyrolysis temperature with the greatest percent yield of bio-oil, (500 °C, [17]), the bio-oil pyrolyzed at 450 °C was selected for continued investigation. It is important to note that although these bio-oil samples were prepared to a specific concentration, the observed variations in the activity with pyrolysis temperature could be affected by the amount of water in each bio-oil sample. The water was not removed from the sample to avoid removing other, potentially important chemicals in the process. Nevertheless, each bio-oil sample was found to successfully inhibit the growth of each species.

Five pyrolysis temperature samples of coffee grounds bio-oil were also tested against the two microorganisms (data not shown). A similar pattern to tobacco bio-oil was

observed, where bio-oil from each temperature displayed activity, with the activity peaking at a mid-range temperature. In the case of coffee grounds, the best activity was observed at 500 °C, which also correlated to its temperature of maximum bio-oil yield [18].

It was possible that the toxicity effect of the bio-oils was caused or greatly impacted by the unique extractive chemicals in these biomass sources, such as the high quantities of nicotine in the tobacco bio-oil or caffeine in the coffee bio-oil. Caffeine is a chemical with known natural pesticide properties and is found in coffee grounds, and thus needed to be investigated. This investigation into coffee grounds was correlated to the tobacco bio-oil results and is discussed in Section 6.3.4.4. Nicotine is a moderately effective insecticide against the CPB with an LD<sub>50</sub> of 61 µg per CPB [19]. Sufficient quantities of nicotine could be present in the bio-oil to account for the observed activity towards the microorganisms, that is, if the microorganisms were affected by nicotine to the same extent as the CPB. Thus, the tobacco bio-oil was separated into nicotine-free and nicotine containing fractions to determine the effect of nicotine in the observed activity.

### **6.3.3 Investigation into the Liquid-Liquid Extraction Fractions of Tobacco Bio-oil**

Bio-oil was fractionated by liquid-liquid extraction according to the scheme shown in Figure 6.1 to separate the nicotine and to simplify the chemical composition. The disk diffusion agar experiment was used to reveal the activity of these generated fractions (Figure 6.3). The inhibition diameter measurements reported herein include the diameter of the 6 mm disks. Measurements were made to the nearest millimetre, so a measurement of 6 mm indicated only a slight region of inhibition around the disk, while measurements greater than this value showed increasing toxicity towards the species. As expected, Fraction Z (the initial fraction) had high activity towards the microorganisms. However, high levels of nicotine were also found in Fraction Z (Figure 6.4), so much so that few other chemicals could be observed in the chromatogram of this fraction.



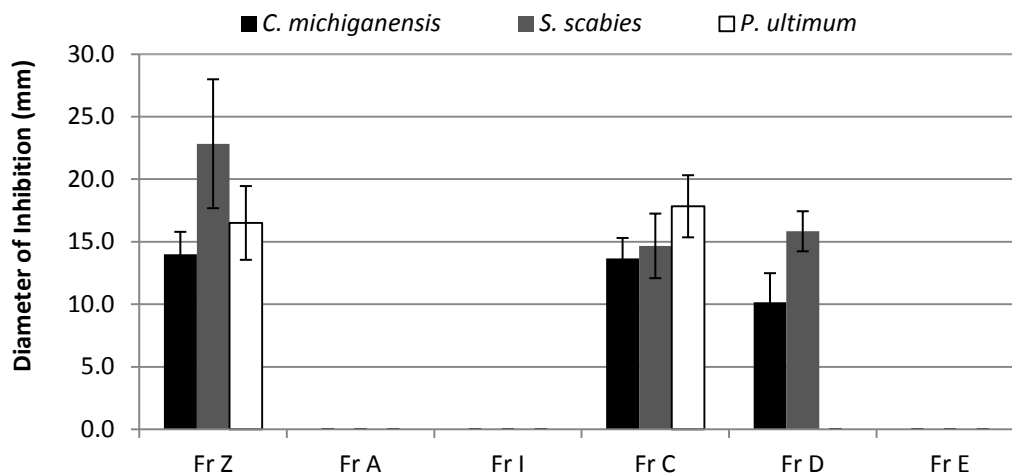


**Figure 6.3.** A graph of the measured diameters of inhibition for three microorganisms by the six tobacco bio-oil fractions (see Figure 6.1 for fractionation scheme) after three days of growth. Fraction C is nicotine-free. Error bars indicate  $\pm$  one standard deviation of replicate measurements within an experiment.

Fraction D, which contained nicotine, was also found to be active. However, when nicotine standards were tested to match and even double the concentration of nicotine found in Fraction D, no inhibition was observed. It is interesting to note that nicotine was the most abundant and almost the only peak detected by GC-MS in this fraction. Therefore, the active components in Fraction D could not be detected by our GC-MS analysis method. These active components either had a boiling point higher than 280 °C (the highest temperature in our GC program) and did not pass through the capillary or could not be detected by an electron impact MS detector.

The fractionation scheme successfully generated a nicotine-free fraction, Fraction C, which was confirmed by the absence of a nicotine peak in the GC-MS data. This fraction was also strongly active (as shown in Figure 6.3). Phenol and a variety of its derivatives were found to be in high concentration in this fraction. Phenolic compounds are known to have pesticide properties [20,21], and the presence of these compounds is examined in the following section.

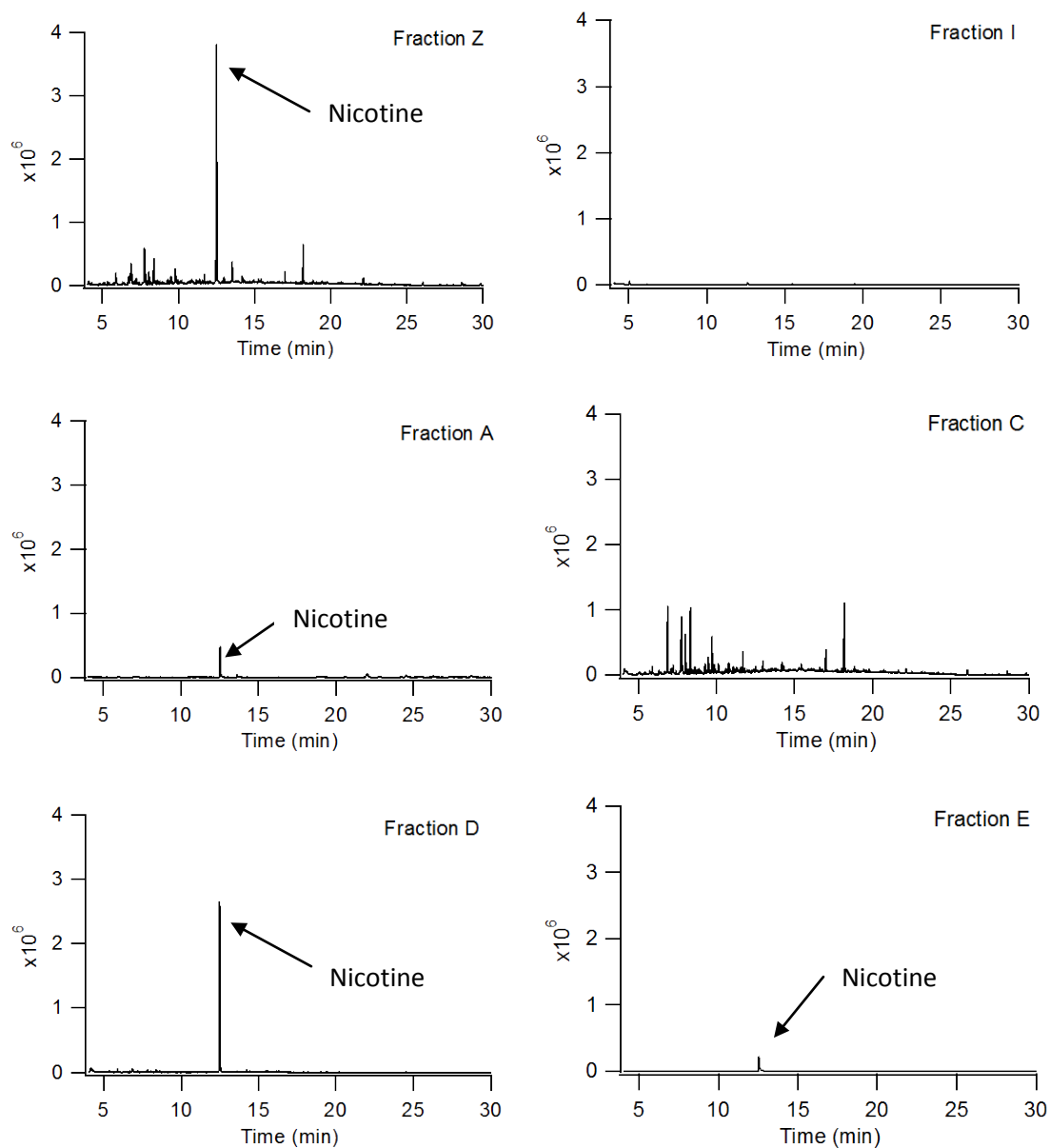


**Figure 6.4.** GC-MS chromatograms for the six tobacco bio-oil fractions (Fractions Z, I, A, C, D, E) tested on the microorganisms. GC-MS conditions are provided in the methods section. Samples were diluted in their appropriate solvent (50  $\mu\text{L}$  bio-oil fraction added to 500  $\mu\text{L}$  of solvent).

### **6.3.4 Composition and Activity Analysis of the Active, Nicotine-Free Tobacco Bio-oil Fraction**

#### **6.3.4.1 Further Liquid-Liquid Extraction**

The active, organic, nicotine-free fraction, Fraction C was further fractionated to separate the more polar, organic compounds, such as phenol (Fraction M) from the less polar, organic compounds, such as large alkanes (Fraction H) as shown in Figure 6.1. The inhibition data for the initial fraction, Fraction Z, and the active, nicotine free, terminal fraction, Fraction M, are included in Figure 6.5. Comparable activity was observed in both fractions. The diameter of inhibition for each experiment can change between experiments. Therefore, positive and negative controls were always performed to properly compare the fraction of interest to a control. In this case, the intensity of activity of Fraction M was compared to the activity of the initial Fraction Z (positive control) and the levels were found to be comparable. Thus, significant, active components were carried through the extraction process to Fraction M.

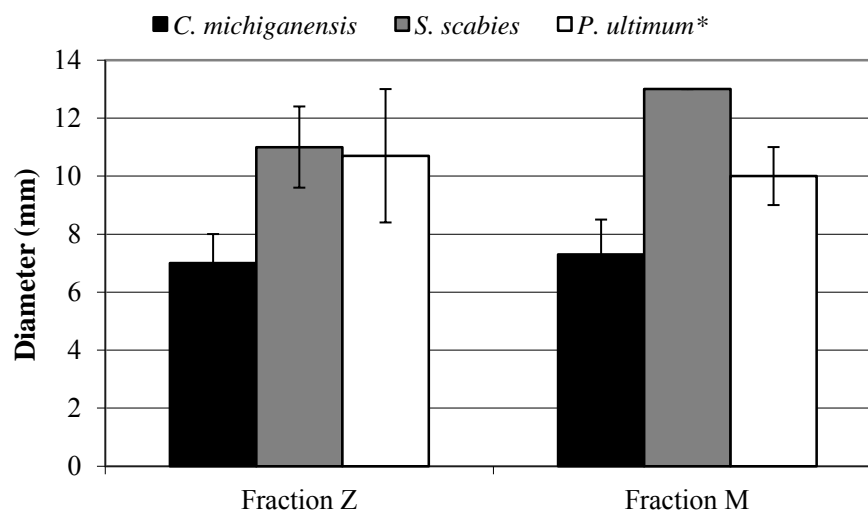


**Figure 6.5.** A graph of the diameters of inhibition for the initial fraction, Fraction Z and the active, terminal fraction, Fraction M. The fractionation scheme is shown in Figure 6.1. \*Measurements for *P. ultimum* indicated regions of substantially less growth, but not complete inhibition. Sample standard deviation values for replicates are shown as error bars ( $\pm$  one standard deviation).

#### 6.3.4.2 Identification of Standards

The 2005 National Institute of Standards and Technology library (NIST 2005) was used to identify the peaks found in the GC-MS chromatogram of Fraction M (Figure 6.6). One hundred and seven peaks were detected and thirty-one chemicals were identified with qualities over 80%. The largest peaks (peak area > 1.0%), reflecting the most abundant chemicals present in Fraction M, were phenolic chemicals (Table 6.2). Six standards were obtained for the largest five peaks (one peak included both 3-methyl phenol and 4-methyl phenol). Being available in our inventory, four additional standards with relatively high peak areas were examined (peak area % >1.2%). Thus, a total of ten standards were examined and their chemical structures are provided in Figure 6.6.

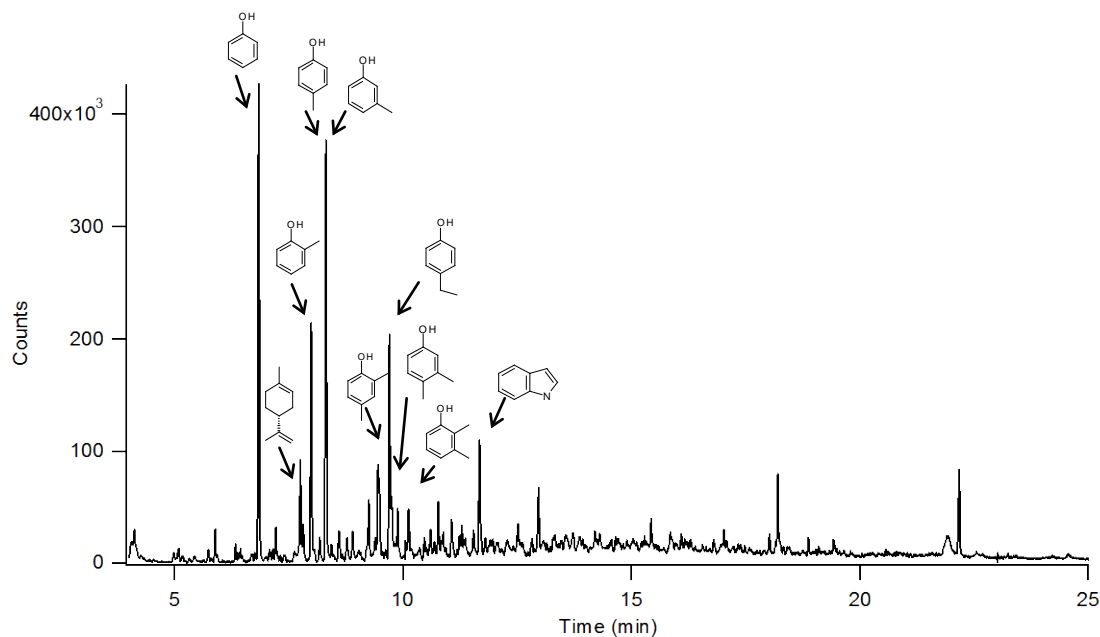


**Figure 6.6.** GC-MS chromatogram of Fraction M (50  $\mu\text{L}$  of Fraction M diluted to 1 mL in MeOH). The peaks identified by chemical structures indicate the standard chemicals tested. For experimental conditions, see Methods section.

The concentrations of these standards in Fraction M were calculated using calibration curves (Table 6.2). Initially, to confirm the NIST 2005 identification, the standards were run individually and their retention times were compared to the peaks in Figure 6.6. After successful confirmation, these ten standards were run at three concentrations, ranging from  $6.25 \mu\text{g mL}^{-1}$  to  $100 \mu\text{g mL}^{-1}$  such that the diluted sample peak fell between three standard calibration points. The integrated peak areas from these runs generated calibration curves with  $R^2$  values greater than 0.991. The slopes of the calibration curves for each standard were not the same, however. The slopes ranged from  $1.00 \times 10^8$  area counts per concentration unit for 2,3-dimethyl phenol to  $1.39 \times 10^8$  area counts per concentration unit for 4-ethyl phenol. Thus, it was necessary that a calibration curve was generated for each standard as the peak area to concentration ratio was not constant between standards. These ten standards accounted for 54% of the GC-MS chromatogram peak area of Fraction M, leaving the remaining 97 peaks to account for 46% of the peak area. Based upon the calculated concentration values, a mixture of these ten standards was tested on the three microorganisms.

**Table 6.2.** List of the largest peaks (peak area > 1.0%) identified from the GC-MS chromatogram of Fraction M. The remaining 89 peaks (<1.0% area each) are not included in this list. The NIST 2005 library was used to identify the peaks, and standards were used to confirm the identity of the indicated peaks. Chemicals confirmed by standards were used in the standard mixture at the indicated concentration. Concentration values were calculated using calibration curves.

Percent Area (%)	Retention Time (min)	Chemical Name (Identified by NIST 2005)	Quality (%)	Chemical Name (Confirmed by Standard)	Concentration* (mg mL <sup>-1</sup> )
14.203	6.880	Phenol	91	Phenol	1.378
14.064	8.344	3-methyl phenol	96	3-methyl phenol and 4-methyl phenol	1.340
7.757	9.734	4-ethyl phenol	95	4-ethyl phenol	0.726
6.631	8.025	2-methyl phenol	98	2-methyl phenol	0.646
3.836	11.699	indole	95	indole	0.514
2.790	22.173	cis-3-methyl-exo-tricyclo[5.2.1.0(2.6)]decane	58		
2.658	7.786	d-limonene	96	d-limonene	0.288
2.480	9.483	2,4-dimethyl phenol	96	2,4-dimethyl phenol	0.273
2.210	9.284	2-ethyl phenol	95		
2.159	12.992	5-methyl-1H-phenol	95		
2.083	9.785	3,5-dimethyl phenol	96		
1.960	9.506	2,5-dimethyl phenol	96		
1.787	18.215	1-methoxy-3-(2-hydroxyethyl)nonane	58		
1.534	11.095	2-ethyl-6-methyl phenol	60		
1.465	10.805	2-ethyl-5-methyl phenol	93		
1.302	10.155	2,5-dimethyl phenol	76	3,4-dimethyl phenol	0.248
1.243	9.916	2,3-dimethyl phenol	96	2,3-dimethyl phenol	0.120
1.056	8.634	1H-indene, octahydro-, cis-	58		

### 6.3.4.3 Bio-assays of the Standard Compounds in the Active, Nicotine-Free Fraction

Surprisingly, this standard mixture was unsuccessful at inhibiting the growth of the three microorganisms. In contrast to the large region of inhibition observed for Fraction M, no region of inhibition was observed for the standard mixture. This result demonstrated that the cumulative action of the 10 chemicals accounting for 54% of the peak area was not responsible for the activity observed in Fraction M.

Past research shows that some of these standards are indeed active towards certain bacteria and fungi [21]. Thus, before presuming that these ten standards had absolutely no impact on the activity of Fraction M, it was of interest to test these standards at a higher concentration. These standards were therefore tested individually at  $100 \text{ mg mL}^{-1}$ , well over the calculated concentration of the standards in Fraction M (shown in Table 6.2). Nine of the ten standards were quite potent towards the three microorganisms (Figure 6.7). Only d-limonene was not active at this high concentration. The di-alkylated phenols (2,4-dimethyl phenol, 2,3-dimethyl phenol, 3,4-dimethyl phenol) were found to be more potent than the mono-alkylated phenols (2-methyl phenol, 3-methyl phenol, 4-methyl phenol). This was reflected by the larger regions of inhibition for the former compounds and the smaller regions of inhibition for the latter. However, the concentrations of the di-alkylated phenols ( $0.120$  to  $0.273 \text{ mg mL}^{-1}$ ) in Fraction M were much lower than those of the mono-alkylated phenols ( $0.646$  to  $0.670 \text{ mg mL}^{-1}$ ). Based on the results in Figure 6.7, a cumulative toxic effect from the standards would be expected in the tobacco bio-oil.

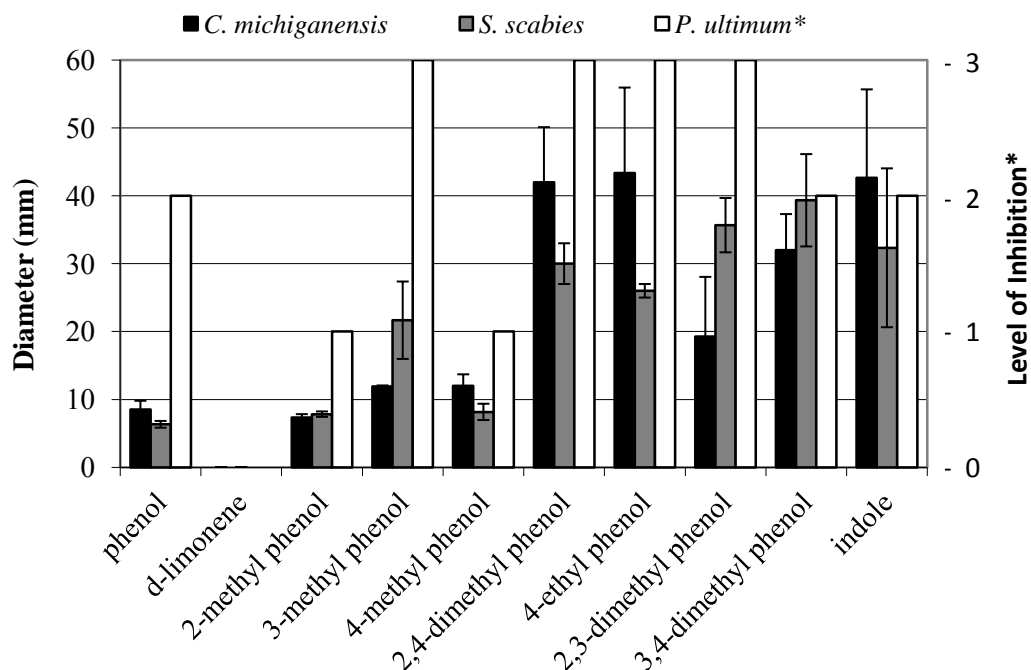


**Figure 6.7.** A graph showing the diameters of inhibition for the bacteria *C. michiganensis* and *S. scabies*, and the level of inhibition for the fungus, *P. ultimum*\*. Sample standard deviation values for replicates are shown as error bars ( $\pm$  one standard deviation) for *C. michiganensis* and *S. Scabies*. \*Diameter of inhibition measurements were not possible for this experiment with *P. ultimum* due to the extreme toxicity of the standards towards the fungus. Instead, a level system was used. The standard compounds were tested at  $100 \text{ mg mL}^{-1}$  in methanol. \*Level 0: complete growth; Level 1: thinner growth over part of plate; Level 2: thinner growth over entire plate; Level 3: no growth.

Although nine of the ten standards were toxic to the microorganisms at high concentration, the low concentration at which these standards were found in the bio-oil was not sufficient to account for the activity in Fraction M. However, it must be noted that not all of the phenolic and indole compounds in Fraction M were tested in this standard mixture. An additional ten other simple, alkyl-substituted phenolic compounds and one simple, alkyl-substituted indole compound were identified by the NIST 2005 library (quality  $>80\%$ ). These eleven compounds accounted for an additional 20% of the peak area. Therefore, to determine the extent to which the additional, related chemicals



and the current, active standards contributed to the activity in Fraction M, the concentration of the standard mixture was increased.

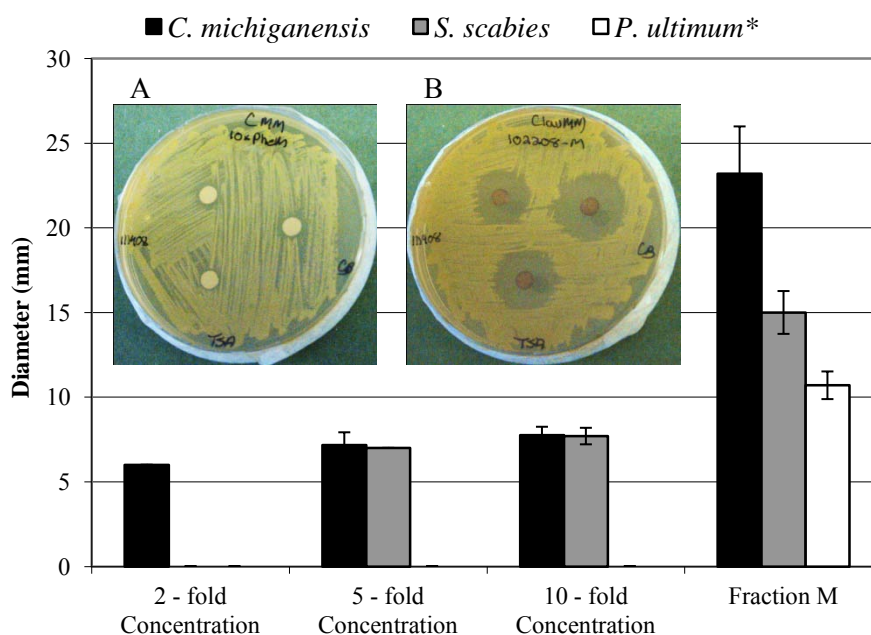


**Figure 6.8.** A graph showing the diameters of inhibition for *C. michiganensis*, *S. scabies*, and *P. ultimum*. Disks were impregnated with the stated concentration of the standard mixture in methanol or with Fraction M. \*Measurements for *P. ultimum* indicated regions of substantially less growth, but not complete inhibition. Sample standard deviation values for replicates are shown as error bars ( $\pm$  one standard deviation). Inset A: Photo of *S. scabies* growth around disks with 10-fold concentration of standard mixture. Inset B: Photo of *S. scabies* growth with disks with Fraction M.

Figure 6.8 displays the inhibition results of increasing the standard mixture concentration towards *C. michiganensis*, *S. scabies*, and *P. ultimum*. If the remaining eleven identified alkyl-substituted phenol and indole chemicals (20% peak area) had similar potency to the ten obtained standards (54% peak area), a two fold increase in concentration of the standard mixture would more than account for these missing compounds. This, however, was not the case. At two-fold concentration, only the smallest detectable activity was observed (6 mm diameter of inhibition). Again, theoretically, if all the remaining chemicals (46% peak area) had similar potency to the ten standards,

increasing the standard mixture concentration two-fold would more than account for the activity in Fraction M. However, this was not found. Only the most minor inhibition was observed at 2-fold concentration.

An increase to five-fold concentration of the standard mixture showed minimal increase in activity (ie. inhibition could be detected for *S. scabies*). Even at ten-fold concentration the standard mixture was still not comparable to the larger regions of no growth around the disks impregnated with Fraction M. Therefore, the activity observed in Fraction M was not due to the tested standards, and was unlikely due to the remaining, eleven, simple phenol or indole compounds. Potential synergistic effects between the phenolic compounds and other, unidentified compounds in the bio-oil were not explored.

#### **6.3.4.4 Chemical Composition Comparison between Tobacco and Coffee Grounds Bio-oils**

Tobacco and coffee grounds bio-oils had a similar chemical composition in terms of phenol-related compounds. The fractionation scheme (Figure 6.1) performed on tobacco bio-oil was also executed with coffee bio-oil, yielding similar activity results. Coffee Fraction C and Coffee Fraction M were active, while Coffee Fraction I was not. (Fractions D and E were not tested). Upon comparison of the active Fraction M's of both coffee grounds and tobacco bio-oil, it was found that phenol had a peak area of approximately 15% in both bio-oils. As well, the total cresol peak area for both bio-oils (2-methyl, 3-methyl, and 4-methyl phenols) was approximately 22%. Although the relative amounts of these phenol-related compounds were similar in tobacco and coffee bio-oil, the total concentration of the identified phenolic compounds was greater in tobacco bio-oil. Thus, the conclusions drawn from the phenolic content analysis of tobacco bio-oil could be correlated to coffee grounds bio-oil. Coffee grounds bio-oil demonstrated antimicrobial activity in the presence of even lower phenolic concentrations, so it can be concluded that the most abundant, phenol-related compounds are not individually or collectively responsible for the observed bactericide activity in coffee grounds bio-oil.

Just as phenol is a pesticide chemical of interest found in bio-oil, caffeine is a chemical with natural pesticide properties found in coffee grounds. The coffee grounds used for this experiment, however, were waste coffee grounds (obtained for pyrolysis after percolation for the coffee beverage). Thus, most of the caffeine from the dried coffee grounds was removed by hot water prior to pyrolysis and no caffeine was detected by GC-MS in Fraction M. A small amount of caffeine was detected by GC-MS in a separate, dichloromethane extraction of the whole bio-oil, so any residual caffeine in the bio-oil would likely be present in Fraction A. Thus, the activity found in Fraction M coffee was not due to caffeine nor phenol.

#### **6.3.4.5 Activity from Other Chemicals**

At ten-fold concentration, the standard mixture still did not match the inhibition levels of tobacco bio-oil Fraction M. Thus, the ten standards accounted for less than 10% of the activity in the bio-oil. The origin of the majority of the activity has yet to be identified.

One option is that collectively, the chemicals comprising the remaining 46% peak area were responsible for the activity. In this case, the remaining chemicals would need to account for over 90% of the activity. This would mean, on average, each remaining chemical would need to be nine times more potent than the tested standards. Therefore, it is most probable that a few, extremely active chemicals have yet to be identified in Fraction M. These chemicals would need to be particularly potent, since the peak area for each remaining compound not tested in this paper was less than 2.8%. Additionally, these potent chemicals would most likely not be simple, alkyl-substituted phenolic or indole compounds.

A second option is that synergistic effects could explain the observed activity. It could be possible that other, unidentified compounds must be present with the high abundance phenolic species for pesticide activity to be observed.

It is also possible that the potent chemicals are simply not detected by GC-MS, as only 40% of chemicals in bio-oil are GC-MS detectable [22]. However, the fractionation

scheme to create Fraction M seems to provide optimal conditions for selecting chemicals that would be detected by GC-MS. Chemicals in Fraction M are small (filtered through 0.45  $\mu\text{m}$  filter), polar enough to select the solvent methanol over the non-polar solvent hexane, but not polar enough to remain in water when an organic solvent is available (ether). The components in Fraction M are more likely to be detected by GC-MS over the other terminal fractions (Figure 6.1). However, if a new, potent chemical was generated during pyrolysis of the tobacco bio-oil, its mass spectra would not be available in a library of chemicals. Very potent chemicals remain to be identified in Fraction M.

### **6.3.5. Reduction of the Chemical Complexity of the Active, Nicotine-Free Tobacco Bio-oil Fraction**

#### **6.3.5.1 Solid Phase Extraction**

After determining that the most abundant phenol components were not responsible for the activity observed towards the microorganisms, it was important to reduce the chemical complexity in the active, organic, Fraction M. The first step was to develop a solid phase separation technique that could fractionate the bio-oil into active and inactive fractions. Silica (C18) was packed into a 1 mL glass pipette to make a small column by which to separate Fraction M and isolate the active components. Initial experiments were executed to generate active and inactive elution fractions, but when this small scale elution was performed, the silica column turned from white to dark brown. This colour change dramatically demonstrated that the collected eluent did not contain all of the original components from Fraction M. Figure 6.9 shows a photo of the C18 column with 100  $\mu\text{L}$  of fraction added to the top of the column, and a second photo of the same column after methanol was used to elute the Fraction M components.

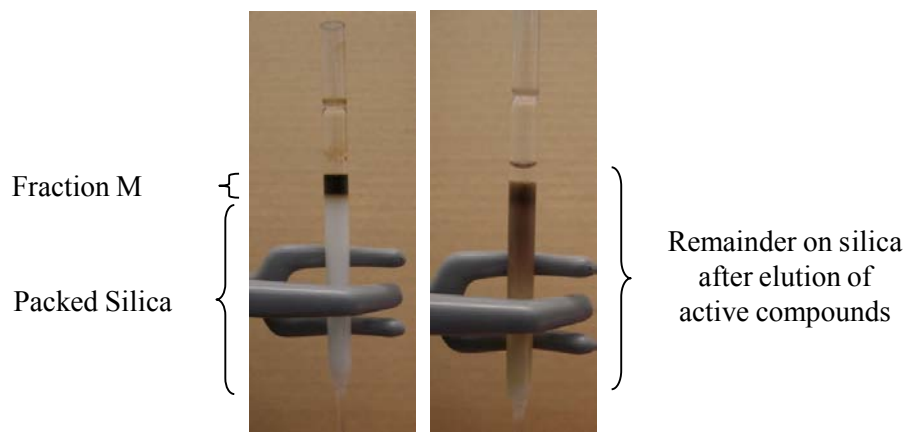


**Figure 6.9.** Photographs of a packed C18 column for a solid phase extraction technique on tobacco Fraction M. The C18 (925 mg) was packed with methanol in a 1 mL glass pipette before (left) and after (right) elution with 4 mL of methanol. The dark colour (right) demonstrates the removal of inactive components.

This result was especially unexpected as the tobacco bio-oil had been sterile filtered through a 45  $\mu\text{m}$  pore filter before the liquid-liquid extraction technique so that large particles would have already been removed from the sample. Even so, the eluent, after air evaporation to obtain the original concentration, was assayed against the microorganisms. Surprisingly, the activity of this eluent matched the activity of the original Fraction M. After testing a range of elution solutions and volumes, it was determined that enough active components eluted off the column with 4 mL of methanol to match the activity of the original Fraction M. Therefore, this separation step became an excellent solid phase extraction technique to remove large, inactive components from Fraction M.

The GC-MS of this eluent from the solid phase extraction of Fraction M closely matched that of the initial Fraction M trace. No components detected through GC-MS had been removed. A slight reduction in the signal intensity of the phenolic chemicals was noted. The components removed by adsorption onto the C18 were not detected by GC-MS due to their large, bulky size or low volatility. These darkly coloured components

were clearly not the active chemicals of interest, so this step became a solid phase extraction procedure resulting in an active fraction with reduced complexity.

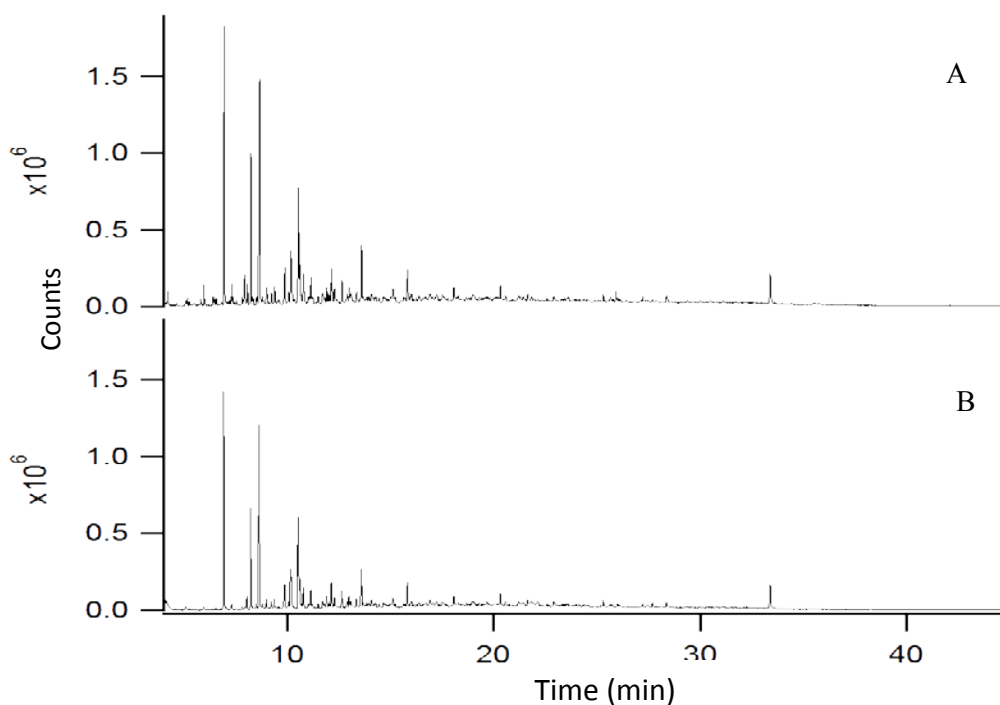


**Figure 6.10.** Chromatograms of Fraction M before (A) and after (B) solid phase extraction with methanol. The SPE sample was air evaporated and resolvated with methanol to recreate the original concentration.

### 6.3.5.2 Low Temperature Heating

A simple procedure to remove volatile compounds from a mixture is through heating, and the eluent from the SPE of Fraction M was heated to examine the resultant activity. The solid phase extract of Fraction M was heated in a speedvac at 65 °C for 30 to 300 min to examine the effect of heating on reducing the chemical complexity and of the remaining activity. To allow for evaporation to occur over the entire heating time, small amounts of water were added to the sample vials so that complete evaporation occurred by the specified time. Lower boiling point components were removed from Fraction M as the heating time increased. Although the boiling point of phenol is 182 °C, and the speedvac

was only set to 65 °C, phenol and many other chemicals with higher boiling points were removed during heating. Bioassays run at each heating time demonstrated that the antimicrobial activity, and thus the chemicals responsible for this activity, were retained during heating. Experiments performed for 0, 50 and 90 min heating are shown in Figure 6.11 demonstrating the reduced concentration of GC-MS detectable compounds with the comparable, corresponding antimicrobial activity. Activity was retained after 90 min of heating, although additional experiments investigating heating times up to 300 min demonstrated reduced activity for *P. ultimum* (data not shown).

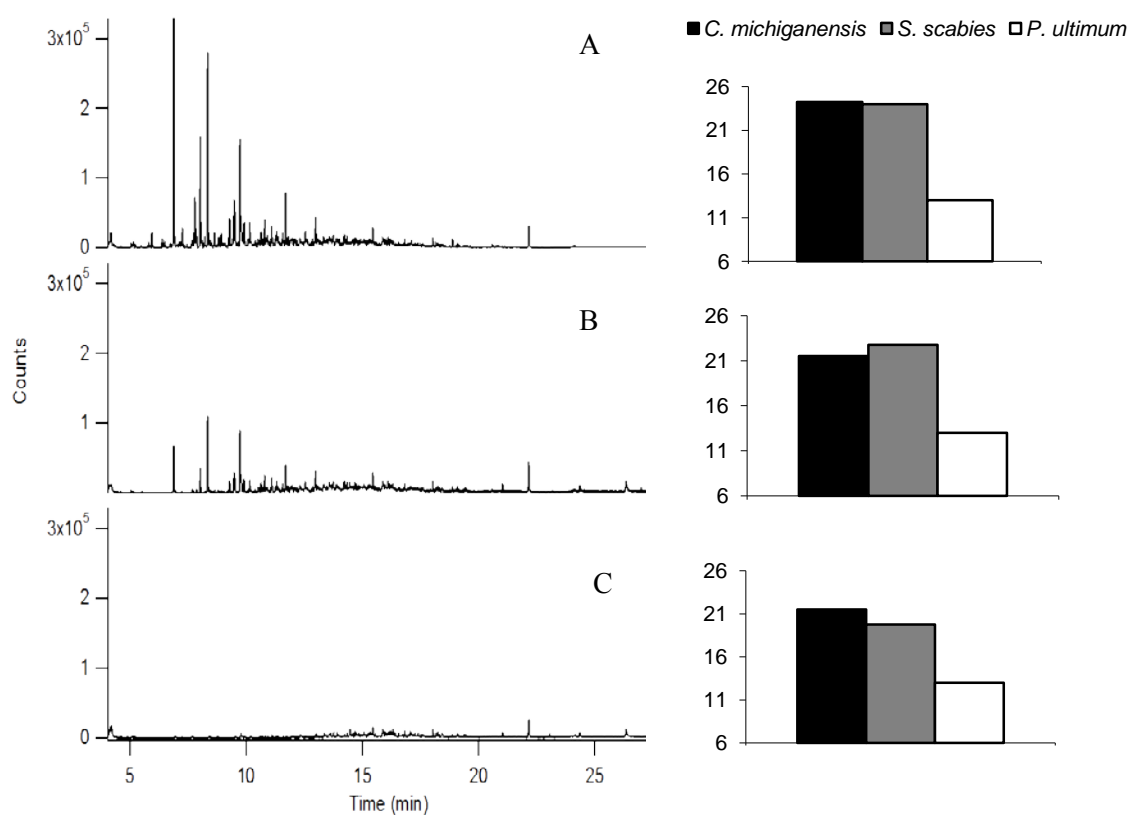


**Figure 6.11.** GC-MS chromatograms and corresponding microorganism growth on Fraction M after solid phase extraction and heating at 65 °C for 0 min (A), 50 min (B), and 90 min (C).

### 6.3.5.3 Preparative Scale Liquid Chromatography/ Separation by Flash Chromatography for GC-MS Analysis

Further separations of Fraction M were performed on the preparatory scale C18 column (Figure 6.9) with methanol/water gradients in combination with speed-vac drying and air evaporation. Multiple samples were generated under different elution gradients and the GC-MS traces of these samples were compared manually (based on retention times) to determine common peaks between the active samples. This analysis method was very basic, and a more advanced technique, using a computer program that could compare the mass spectra of peaks between samples was used in the following section. Even so, this crude analysis technique led to the identification of a peak of interest.

These samples were analyzed through an adjusted GC-MS method. Most notably the sample injection volume was increased (1  $\mu\text{L}$  to 2  $\mu\text{L}$ ) and the rate of temperature change from 100°C to 280°C was decreased from 10 °C  $\text{min}^{-1}$  to 5°C  $\text{min}^{-1}$  in order to detect the low abundance compounds. The peak with a retention time of 33.4 minutes (new GC-MS scheme) was the only compound found to be present in every active fraction and not present in any inactive fractions. This peak can be observed in Figure 6.11 as the last peak eluted in A, and still present in C (22 min). No match was found using NIST 2005 based upon the obtained mass spectra.

Separation by flash chromatography was then explored on the solid phase extract and heated Fraction M. A method was developed to collect this peak of interest that was present in the active fractions and absent in the inactive fractions. Sixteen fractions were collected from the eluent of a methanol/water elution gradient using a larger, slurry packed C18 column. Two of these fractions (vial 10 and 11) contained the peak of interest. These two fractions were combined to make one sample, while the remaining 14 vials were combined to make a second sample. The GC-MS chromatograms of the two collective fractions are shown in Figure 6.12. A third sample was generated as a control for the preparation process that contained all sixteen fractions.



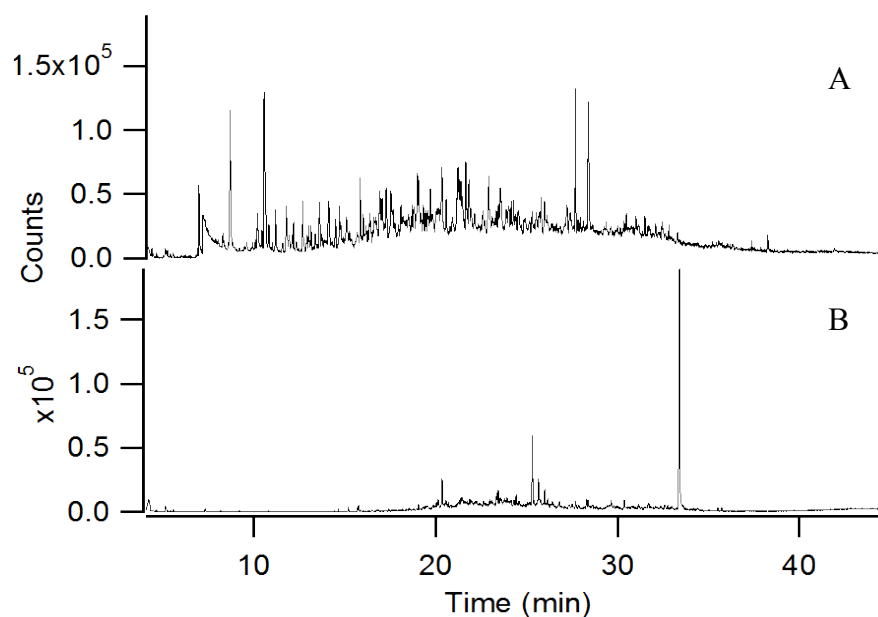


**Figure 6.12.** GC-MS chromatograms of flash chromatography samples generated from Fraction M. Combined sample of the fourteen remaining fractions (A) and combined sample of two fractions containing a peak of interest (B).

Since the identification of this peak was not easily obtained, the activity of the sample containing the peak of interest was examined using a bioassay. It was determined that the sample with the peak of interest did have activity, but that the sample containing the remaining fractions also had comparable activity (Figure 6.13). The sample containing all sixteen fractions generated antimicrobial activity comparable to Fraction M. Thus, if this peak of interest was an active compound, it was not the only acting compound. As well, the sample containing the peak of interest also contained other components that were not identified. This experiment did not confirm the exclusive activity of this peak.

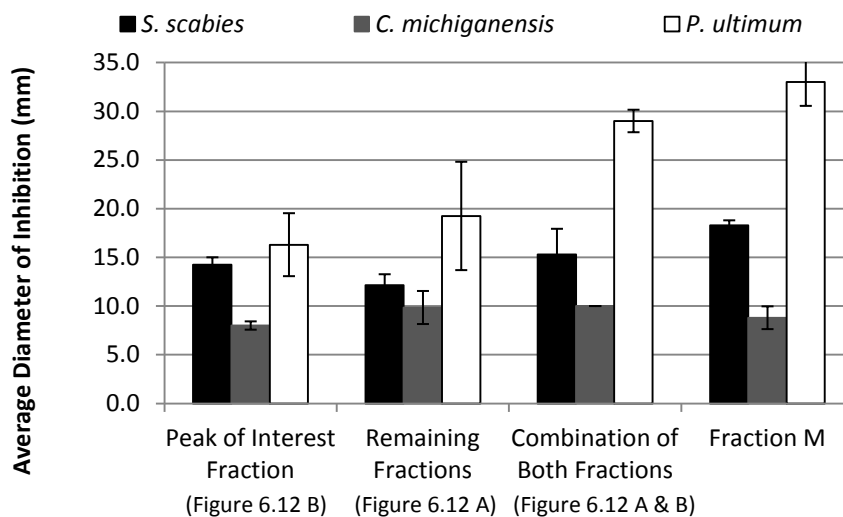


**Figure 6.13.** A graph showing the activity of four related samples, a sample containing the peak of interest (total ion chromatogram of sample in Figure 6.12 B), a sample of the remaining fractions (Figure 6.12 A), a sample combining all of the fractions (Figure 6.12 A & B), and Fraction M before separation.

Once it was determined that activity was also found in the sample that did not contain the peak of interest, and that this peak of interest could not easily be identified, these sixteen fractions were tested individually. This step increased the number of samples to be tested, while the volume and concentration of the samples decreased. It was important to test the activity of each sample, but the disk diffusion assay was labour intensive, required a significant sample volume and concentration ( $\geq 15 \mu\text{L}$  for triplicate experiments), and required many disposable materials. To miniaturize and streamline the assays required for activity detection, a microwell plate procedure was put into operation. Using this experimental design, only 1  $\mu\text{L}$  of sample was required per trial, and each experiment was performed in triplicate. The sixteen fractions obtained through flash chromatography of tobacco bio-oil Fraction M were analyzed individually in this microwell plate design. The activity pattern results shown in Figure 6.14 were observed over multiple experiments, each with triplicate replicates confirming the observed trends.

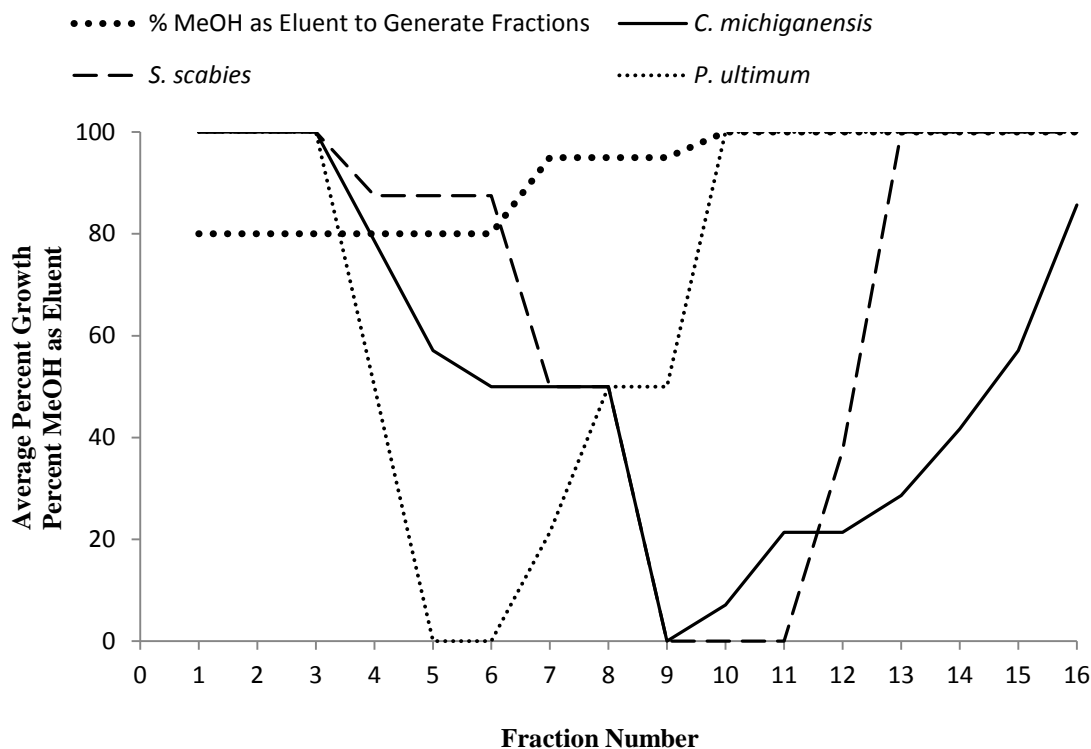


**Figure 6.14.** A graph showing the average percent growth over multiple microwell assays of Fraction M fractions after SPE, separation by flash chromatography, and heating at 65 °C.

Both bacteria followed a similar activity pattern, with limited inhibition observed at either end of the fraction collections, and with fractions 8-12 containing the chemicals that led to the greatest inhibition. This similar inhibition pattern between the two bacteria could reflect that the same chemicals inhibited both bacteria, or that at least the same classes of chemicals inhibited the bacteria. The negative effects towards *C. michiganensis* were observed as early as fraction 4 and as late as fraction 16, while *S. scabies* had a narrower range of inhibition. This suggested that *C. michiganensis* was either more sensitive to lower concentrations of the same chemicals or to a greater range of chemicals than *S. scabies*.

Limited inhibition was also observed for the fungus at both ends of the fractionation, but the most active components for *P. ultimum* were found in the earlier fractions, fractions 4-8. This result correlated to the pattern observed between the biomass source and the microorganisms species inhibited (Table 6.1). Tobacco was the only

biomass source that generated bio-oil that was active towards a fungus, and the results in Figure 6.15 clearly showed that different groups of chemicals were responsible for the activity towards the fungus and bacteria. It is likely that the components active towards the tobacco bio-oil were exclusive to this biomass source, although it is possible that the other biomass sources also contained this same group of chemicals but at a lower concentration.

Although these fractions were clearly active towards the microorganisms, the ability to detect the chemicals present in these fractions by gas chromatography with electron impact mass spectrometry was questionable. Figure 6.11 demonstrated that the heating step removed many volatile components that could be successfully detected by GC-MS, leaving many low abundance compounds that were difficult to resolve. Even so, GC-MS was performed on each of these fractions using a new GC-MS instrument and column, and it was possible to observe peaks just above the baseline.

AMDIS (Automated Mass Spectral Deconvolution and Identification System) was used to analyze the chromatograms to determine the number of detectable compounds and to analyze the GC-MS spectra for common peaks among the active fractions. AMDIS is an excellent program for isolating pure mass spectral peaks from a complex sample. The unique MS fragmentation pattern for each compound allows AMDIS to separate peaks that co-elute within one scan of each other. This deconvolution removes the 'background' ions from the spectra and presents a cleaner spectrum for comparison to the NIST library. The purity value is the percentage of the deconvoluted spectra from the entire peak in the total ion chromatogram. AMDIS used a scaled dot product (default comparison of mass spectrum of unknown with compound in library database) to determine the quality match in the NIST 2005 library.

Fractions 5 and 6 were found to contain the greatest number of peaks that could be detected by GC-MS (Figure 6.15, Original Fraction). Through AMDIS, it was possible to detect a greater number of unique compounds compared to analysis by simple peak shape and retention time. Very few peaks were detected in the first or last fractions, which correlates to the lack of activity in these fractions. However, due to the low concentration of most peaks, the number of peaks with an 85% match or greater by NIST 5.0 was poor.

This disjoint between the number of peaks and peaks identified with an 85% match or greater is reflected by the overlaid, dashed line in Figure 6.15.

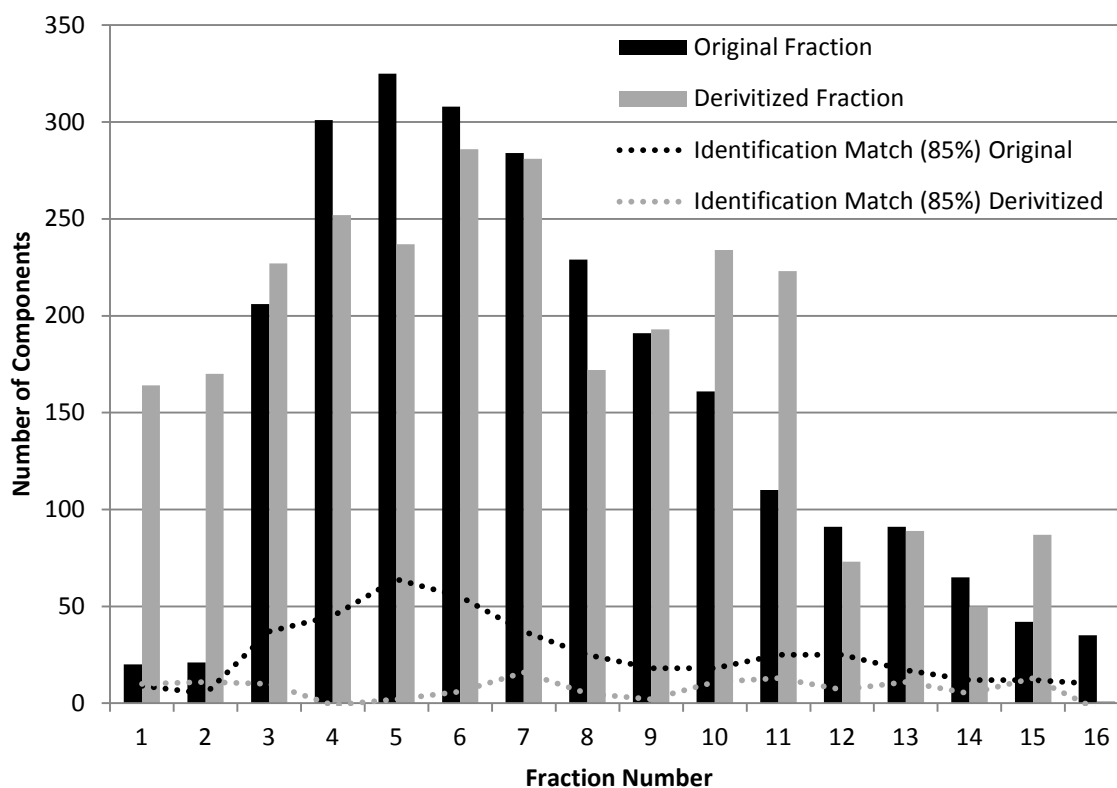


**Figure 6.15.** Histogram showing the number of compounds identified by AMDIS from various fractions with and without sample derivatization. Corresponding activity for each fraction is shown in Figure 6.14.

In order to determine which compounds were present in the active fractions and absent from the inactive fractions, a library was generated through AMDIS containing the common peaks (based on the mass spectra) found in Fractions 9, 10 and 11, the active fractions towards the bacteria. Only twenty four common peaks were identified. Data from the inactive fractions 1, 2, and 3 was compared to this library and the common compounds were removed from the list of common peaks between the active fractions, reducing the peak count to thirteen. The remaining peaks that were found in all three active fractions and absent in the inactive fractions were then compared to the NIST 2005 database. Those peaks with a quality match of  $\geq 80\%$  are listed in Table 6.3. 4-methyl phenol was identified at a low concentration, significantly less than the peak size

observed in the original Fraction M sample (Figure 6.6). This compound was previously tested as a standard (Table 6.2), and it was determined that this compound was not responsible for the observed pesticide activity.

**Table 6.3.** List of compounds found in Fraction 9, 10, and 11 (the most active fractions towards the bacteria) and absent in Fraction 1, 2, and 3 (no activity towards the bacteria). GC-MS results were analyzed using AMDIS with the NIST 2005 library with a quality value of  $\geq 80\%$  listed below.

Retention time (min)	Name of Compound Matched using AMDIS and NIST 2005	Purity (%)	Amount	Quality
9.76	Phenol, 4-methyl-	99%	0.10%	86
14.62	Methenamine	91%	0.05%	80
38.64	4,8,13-Cyclotetradecatriene-1,3-diol, 1,5,9-trimethyl-12-(1-methylethyl)-	75%	0.65%	84

The largest peak found in the active fractions and absent from the inactive fractions, was the peak that eluted at 38.64 min with an amount value of 0.65%. This peak was identified in the NIST library as 4,8,13-duvatriene-1,3-diol (synonym to the name in Table 6.3) with an 84% quality match (Figure 6.16). The mass spectrum of this peak is similar to that of the peak of interest identified manually based upon retention time that was present in the active fractions discussed above. This peak was identified by NIST 2005 from this experiment for a few reasons, including the deconvolution data analysis step with AMDIS, and a new GC-MS instrument and column that provided a more complete mass spectrum. Most notably, the mass spectrum collected from this instrument captured the molecular ion peak, 288 Da, while the spectrum collected earlier did not include this peak. This compound is a diterpene ( $C_{20}$ ) that was identified and isolated from tobacco leaves in 1962 as the first identified fourteen-membered ring [23]. Research has suggested that this compound exhibits antifungal activity, as was discussed by Reuveni *et al.* when they dipped tobacco leaves in acetone for 1 s and observed increased susceptibility of the leaf to blue mold growth [24]. The acetone extract contained 95% of the leaf's the  $\alpha$ - and  $\beta$ - Duvatrienediol, and when this extract was added to the leaf's

surface again, the antifungal activity was restored. Our findings demonstrated that fractions containing this compound exhibit anti-bacterial activity, rather than anti-fungal activity. This compound likely contributed to the pesticide activity observed in fractions 9 to 11, but cannot be the sole active compound in bio-oil as this compound was not observed in the GC-MS chromatograms of other active bio-oil, namely coffee grounds bio-oil.

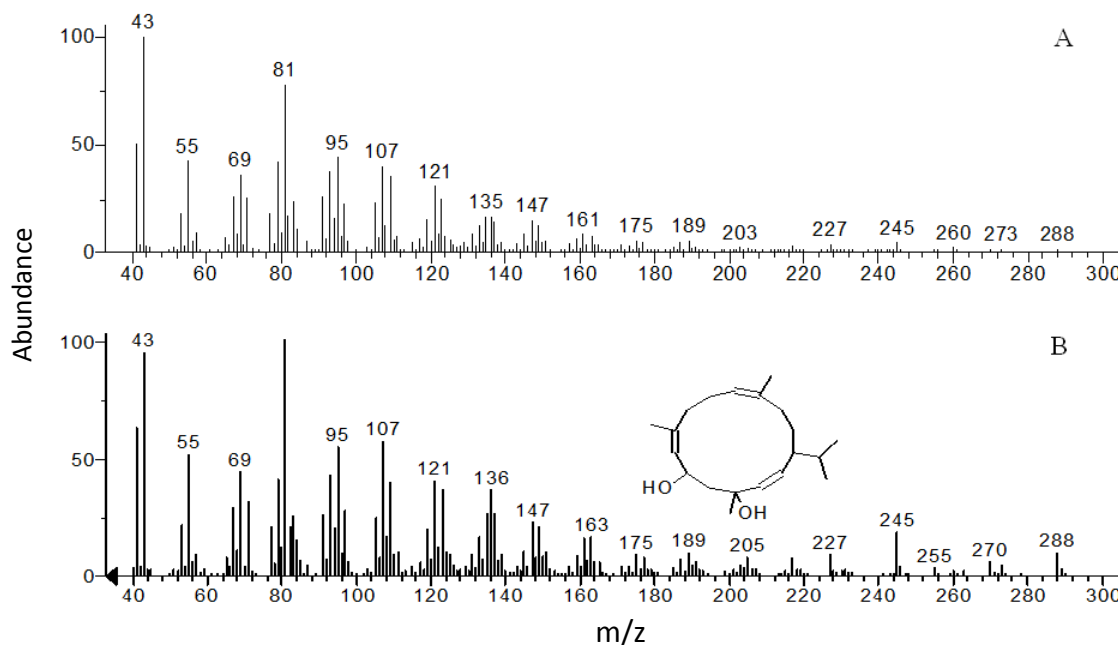


**Figure 6.16.** Mass spectrum isolated from Fraction 10 at 38.68 min (A) and the mass spectrum of Duvatriene from the NIST 2005 library (B).

Methenamine was also identified in the active fractions towards bacteria (Figure 6.17), but present in a very small amount (0.05% of the total ion chromatogram, Table 6.3). This compound is a known and commonly used antibiotic to prevent or control urinary tract infections [25,26]. Methenamine could potentially contribute to the observed antimicrobial activity of the tobacco bio-oil. This compound was not identified in other bio-oils, but could potentially be present in other bio-oils at a very small concentration, as was observed in the tobacco bio-oil. Further investigation into this compound will continue.

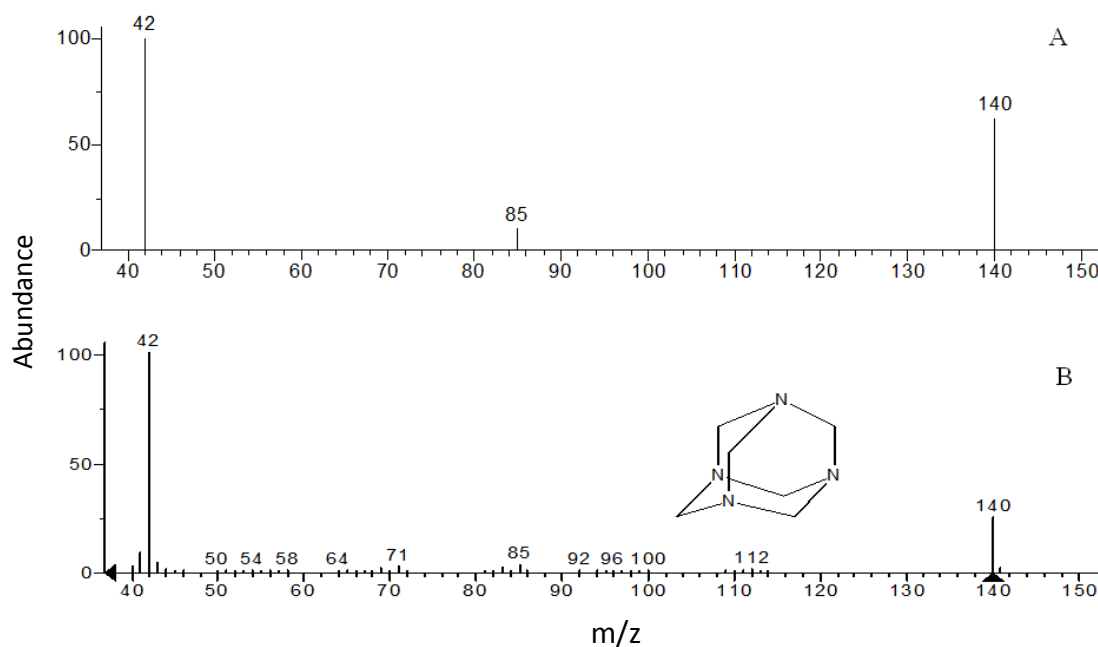


**Figure 6.17.** Mass spectrum isolated from Fraction 10 at 14.62 min (A) and the mass spectrum of methenamine from the NIST 2005 library (B).

In a similar manner to the active bacterial fractions, the common peaks between the three active fractions towards the fungus (Fraction 5, 6 and 7) were identified in a library. Forty five common compounds were found, and from this list, thirteen were removed due to the fact that they were also found in the inactive fractions collected before and after the active ones, fractions 1, 2, 3, 10, 11, and 12. NIST 2005 identified nineteen of these common compounds with an 80% quality match, and these compounds are listed in Table 6.5. This list demonstrates that although the heating step removed a great amount of the phenolic compounds, residual amounts remained and were detected by AMDIS. The fact that the largest phenolic peaks (identified in Table 6.2) were not responsible for the activity, and that the heating step removed many phenolic compounds but did not remove the activity of the fractions suggests that the simple substituted phenolic compounds are not responsible for the activity. Each of these identified components was present at a very low abundance. As was discussed in section 6.3.4.5, the tested standards accounted for over 50% of the peak area and less than 10% of the observed activity, requiring the remaining chemicals to each have a factor of nine times greater potency than the tested standards. The fractions analyzed in Table 6.4 have



reduced phenolic composition due to the heating step, suggesting that the combined effect of this list of chemicals does not fully account for the observed activity. Some of these chemicals may have high antifungal potency, but this information remains to be determined.

**Table 6.4.** List of compounds found in Fraction 5, 6 and 7 (the most active fractions towards the fungus) and absent in Fraction 1, 2, 3, 10, 11, and 12 (no activity towards the fungus). GC-MS results were analyzed using AMDIS with the NIST 2005 library with a quality value of  $\geq 80\%$  listed below.

Retention Time (min)	Name of Compound Matched using AMDIS and NIST 2005	Purity	Amount	Quality
10.08	Pyrazine, tetramethyl-	71%	0.01%	80
13.17	Phenol, 2-ethyl-	64%	0.02%	88
13.99	Phenol, 2,3,5-trimethyl-	66%	0.03%	88
14.77	Phenol, 2-ethyl-4-methyl-	70%	0.11%	92
15.56	Phenol, 2-(1-methylethyl)-, methylcarbamate	33%	0.03%	88
15.76	Phenol, 3-ethyl-5-methyl-	71%	0.34%	88
16.31	Phenol, 3,4,5-trimethyl-	64%	0.10%	81
17.36	Phenol, 2-methyl-5-(1-methylethyl)-	65%	0.22%	87
17.80	2-Methyl-6-propylphenol	56%	0.07%	87
18.36	Phenol, 3,5-diethyl-	65%	0.28%	83
19.43	Pentandioic acid, (p-t-butylphenyl) ester	29%	0.08%	80
20.77	6-Methyl-4-indanol	40%	0.21%	81
22.14	Benzonitrile, 2,4,6-trimethyl-	75%	0.89%	83
23.91	1-Phthalanol, 1,3,3-trimethyl-	78%	0.78%	81
25.45	1-Naphthalenol, 2-methyl-	69%	0.50%	91
27.07	2,2'-Isopropylidenebis(5-methylfuran)	56%	0.19%	80
29.07	1-Naphthol, 6,7-dimethyl-	59%	0.15%	86
30.34	$\alpha$ -Guaiene	74%	0.24%	80
32.46	2-Hydroxyfluorene	39%	0.05%	89

### 6.3.6 Sample Derivatization for GC-MS Analysis

No large peaks were found by GC-MS in the active fractions. If the lack of detection of abundant chemicals by GC-MS was due to their low volatility, then it would be possible to make some of these chemicals visible by chemically derivatizing them, which is discussed in the next section.

Labile hydrogen atoms were replaced with a trimethylsilyl group in this silylation derivatization which reduced the polarity of the affected molecules. Each of the sixteen fractions was derivatized in this manner and GC-MS was performed on the product solution. The number of peaks detected increased significantly, although the control experiment with methanol also produced an additional 83 peaks. This number was subtracted from the total number of peaks detected in each derivatized fraction, and these adjusted values are plotted in Figure 6.16, along with the number of peaks detected in each fraction before derivatization. Unfortunately, the identities of these peaks were even more difficult to confirm with the NIST 2005 library.

Fraction 10 and 11 had the greatest increase in the amount of peaks detected after derivatization. These vials also had the greatest activity towards the bacteria. The earlier fractions 5 and 6, did not show as large an increase in the number of peaks detected. Derivatization of these fractions generated many trimethylsilyl- compounds, but the abundance of these new peaks was low. No new large peaks were observed that were present in the active fractions (Fraction 5 to 7, or Fractions 9 to 11) and absent in the inactive fractions. Thirty five common peaks were found for the bacterial activity, but only four of these peaks had a quality match greater than eighty. Twenty four of these common peaks had a peak area of less than 0.05% of the total ion chromatogram. Twenty of the common peaks had trimethylsilyl functionalities, while the other compounds were derivatives of benzene and alkanes. Since these latter compounds were not found in the underivatized fractions, only the silyl derivatized compounds were examined. The four silyl compounds with a quality match over 75% are listed in Table 6.5.

**Table 6.5.** List of common silyl derivatized compounds and their original analog found in derivatized Fractions 9, 10, and 11 (and not in Fractions 1, 2, and 3) with a NIST 2005 quality match greater than 75%.

Retention Time (min)	Name of Compound Matched using AMDIS and NIST 2005	Purity	Amount (Fr 11)	Quality	Nonderivatized Analog
7.189	Silanamine, N,N'-methanetetraylbis[1,1,1-trimethyl-	9.40%	0.11%	84	cyanamide
9.678	Silane, trimethylphenoxy-	33%	0.03%	92	phenol
11.614	Tris(trimethylsilyl)hydroxylamine	65%	0.08%	92	hydroxylamine
16.119	Octanoic acid, trimethylsilyl ester	50%	0.01%	78	octanoic acid

The highest quality match was for derivatized phenol. Surprisingly, this compound was not removed from the common list upon comparison with inactive Fractions 1, 2, and 3, as phenol was found in the original fraction 2. This compound has a very low amount and was just pulled out of the baseline from both fractions. Therefore, phenol is listed, but its potential activity can be ruled out as this compound was tested under standard analysis. Hydroxylamine (b.p. 58 °C) should have been completely removed during the heating step (65 °C), and so this compound is also unlikely to be an active compound as the activity remained constant after heating and the majority of this compound would have been removed. Cyanamide (calcium or hydrogen cyanamide) also has a high quality match, but is a known fertilizer, not a pesticide [27,28]. Octanoic acid, also known as caprylic acid, is generally recognized as a safe antimicrobial compound. This fatty acid has been investigated against *Salmonella* Enteritidis in chickens (44 and 63 mM) [29], *Cronobacter* spp. (*E. sakazakii*) in reconstituted infant formula (5-30 mM) [30], and shrimp pathogens (1-100 mM) [31], to name a few. Thus one of these compounds may have potential antimicrobial activity towards the bacteria tested in this thesis, although the concentration of this compound in the tobacco bio-oil would need to be investigated further.

Although hundreds of peaks were found in Fractions 5, 6, and 7, only 131 common peaks (based upon the common mass spectra, using AMDIS libraries) were found. Out of these 131 common peaks, 114 peaks were removed from the list as they were also found in the inactive fungal Fractions 1, 2, 3, 10, 11, or 12. This remaining list of 17 compounds

only contained 8 hits from the NIST 2005 library which contained silyl derivatization, and none of the 17 compounds had a match quality of over 80%. Therefore, although hundreds of peaks were found in the fractions active towards the fungus, none of these common derivatized peaks could be identified using NIST 2005. The largest common peak between the derivatized fractions (and absent from the inactive fractions) was only 0.50% of the total ion chromatogram, and this peak was not silyl derivatized and was not identified in the non-derivatized fractions. Since this peak could not be identified in the non-derivatized fractions, this suggests that this compound may have not been deconvoluted from the first chromatogram, or was somehow added to the sample from one of the reagents, but in such a low quantity as to not be detected from the other inactive fractions.

The trimethylsilyl derivatization was not successful at identifying any new components for the fungal activity, but may have uncovered a compound of interest, caprylic acid, in the active bacterial fractions.

## 6.4 Conclusions

Biomass from agricultural and forestry residues was converted into bio-oil through pyrolysis. These bio-oils were found to have valuable pesticide characteristics towards select microorganisms, demonstrating that the active chemicals may be selective in their toxicity, which is a desirable quality in a potential pesticide. Bio-oil from each biomass source displayed antibacterial activity while only tobacco bio-oil demonstrated anti-fungal activity. Bio-oil from tobacco leaves and coffee grounds produced at all pyrolysis temperatures was effective at inhibiting the growth of select microorganisms. A moderate increase in antimicrobial activity was observed at 450 °C for tobacco and 500 °C for coffee grounds bio-oils.

Tobacco bio-oil contains nicotine, but nicotine is not responsible for the pesticide activity observed towards *C. michiganensis*, *S. scabies*, or *P. ultimum*. Liquid-liquid extraction was used to generate unique bio-oil fractions. Activity assays identified an

organic, nicotine-free fraction that was active towards the above species. According to the GC-MS data, this fraction was found to be rich in phenolic compounds, and standards were obtained for the largest peaks. A mixture was generated, accounting for 54% of the GC-MS peak area, but these chemicals did not account for the inhibition observed from Fraction M. These ten standard chemicals were responsible for less than 10% of the activity toward the microorganisms. Therefore the active chemicals in Fraction M were not the alkyl substituted phenolic or indole chemicals tested in this thesis.

To simplify the chemical composition of the active bio-oil fraction, solid phase extraction and heating was applied to the nicotine-free, active sample, reducing the number and concentration of components while retaining the activity of the fraction. Flash chromatography with C18 silica generated active and inactive fractions of bio-oil, further isolating the active components. GC-MS was valuable in identifying many components in the fractions, although this method could not detect nor identify all the components in the active fractions.

A few interesting compounds were found in the active fractions and absent from the inactive fractions. Notably, a diterpene compound that can be extracted from a tobacco leaf surface was detected in the active bacterial fractions. 4,8,13-divatriene-1,3-diol has been identified as a compound that has antifungal properties, although this compound was found by our research in the active fractions towards the bacteria. Methenamine was also found in the active bacterial fractions and has known antibiotic properties. From the silyl derivatization of these same fractions, caprylic acid was identified, which is a commonly used agent against microorganisms. The common fungal activity fractions contained many simple phenol derivative peaks, but simple phenolic peaks were already investigated and found to be present at concentrations too low to be active. The fungal fractions contained many peaks, but no common peaks with high quality match values could be identified from the silyl derivatization. These correlations do not confirm that the activity from the bio-oil is due to these compounds, but future investigation into the concentration and activity of these compounds are necessary to draw further conclusions.

Bio-oil activity towards the microorganisms is not due to only one chemical, as was confirmed through liquid-liquid extraction and liquid chromatography. Standard analysis confirmed that nicotine, phenol, and the most abundant cresols were not responsible for the activity. Low boiling point compounds were removed by heating and the activity of the fraction remained. Solid phase extraction removed the large, bulky compounds and this also did not affect the activity towards the microorganisms.

Three potential active compounds were identified towards the bacteria, namely methenamine, caprylic acid, and 4,8,13-duvatriene-1-3-diol. The list of compounds in the active fractions towards the fungi is extensive, although the simple phenolic compounds were ruled out as the active compounds by standard analysis. The identity of the active chemicals will reveal the potential for the use of tobacco bio-oil as a pesticide.

A natural pesticide that targets problematic species would be a very valuable find. However, it is quite possible that a single, highly active compound may not exist in the bio-oil. No abundant, active chemicals could be identified in the bio-oil, and due to the complexity of the bio-oil composition, it may be very challenging to find such a chemical using currently available technology. The search continues for valuable products from bio-oil, especially bio-oils made from low cost biomass.

## 6.5 References

- [1] C.M. Villanueva, K.P. Cantor, W.D. King, J.J.K. Jaakkola, S. Cordier, C.F. Lynch, S. Porru & M. Kogevinas. Total and specific fluid consumption as determinants of bladder cancer risk, *International Journal of Cancer*, **2006**, *118*, 2040-2047.
- [2] The Canadian Tobacco Market Place. Recent trends in tobacco agriculture in Canada. **2008**, Physicians for a Smoke-Free Canada.
- [3] Agriculture and Agri-Food Canada. Tobacco Transition Program Fact Sheet. Updated **2009-02-18**, [http://www.agr.gc.ca/cb/index\\_e.php?s1=n&s2=2009&page=n90105](http://www.agr.gc.ca/cb/index_e.php?s1=n&s2=2009&page=n90105) Retrieved 2011-11-09.
- [4] J.J. Joensuu, K.D. Brown, A.J. Conley, A. Clavijo, R. Menassa & J.E. Brandle. Expression and purification of an anti-Foot-and-mouth disease virus single chain variable antibody fragment in tobacco plants, *Transgenic Research*, **2009**, *18*, 685-696.
- [5] R. Menassa, C.G. Du, Z.Q. Yin, S.W. Ma, P. Poussier, J. Brandle & A.M. Jevnikar. Therapeutic effectiveness of orally administered transgenic low-alkaloid tobacco expressing human interleukin-10 in a mouse model of colitis, *Plant Biotechnology Journal*, **2007**, *5*, 50-59.
- [6] S.W. Ma, Y. Huang, A. Davis, Z.Q. Yin, Q.S. Mi, R. Menassa, J.E. Brandle & A.M. Jevnikar. Production of biologically active human interleukin-4 in transgenic tobacco and potato, *Plant Biotechnology Journal*, **2005**, *3*, 309-318.
- [7] N. Kaur, M. Lacasse, A. Furtos, K.C. Waldron & A. Morin. Sequential fractionation with concurrent chemical and toxicological characterization of the combustion products of chlorogenic acid, *Journal of Chromatography A*, **2009**, *1216*, 4703-4712.
- [8] D. Prefontaine, A. Morin, C. Jumarie & A. Porter. In vitro bioactivity of combustion products from 12 tobacco constituents, *Food and Chemical Toxicology*, **2006**, *44*, 724-738.
- [9] R.L. Stedman. Chemical composition of tobacco and tobacco smoke, *Chemical Reviews*, **1968**, *68*, 153-&.
- [10] A. Demirbas. Analysis of liquid products from biomass via flash pyrolysis, *Energy Sources*, **2002**, *24*, 337-345.

- [11] J.M. Encinar, F.J. Beltran, J.F. Gonzalez & M.J. Moreno. Pyrolysis of maize, sunflower, grape and tobacco residues, *Journal of Chemical Technology and Biotechnology*, **1997**, 70, 400-410.
- [12] D.S. Scott, R.L. Legge, J. Piskorz, P. Majerski & D. Radlein. in Developments in thermochemical biomass conversion. Eds A.V. Bridgewater & D.G.B. Boocock, Blackie Academic & Professional, London, **1997**.
- [13] R. Xu, L. Ferrante, C. Briens & F. Berruti. Flash pyrolysis of grape residues into biofuel in a bubbling fluid bed, *Journal of Analytical and Applied Pyrolysis*, **2009**, 86, 58-65.
- [14] P.A. Abbasi & G. Lazarovits. Effects of AG3 phosphonate formulations on incidence and severity of Pythium damping-off of cucumber seedlings under growth room, microplot, and field conditions, *Canadian Journal of Plant Pathology-Revue Canadienne De Phytopathologie*, **2005**, 27, 420-429.
- [15] M.L. Gleason, E.J. Braun, W.M. Carlton & R.H. Peterson. Survival and dissemination of *Clavibacter michiganensis* sub. sp. *michiganensis* in tomatoes, *Phytopathology*, **1991**, 81, 1519-1523.
- [16] A.X. Wang & G. Lazarovits. Role of seed tubers in the spread of plant pathogenic *Streptomyces* and initiating potato common scab disease, *American Journal of Potato Research*, **2005**, 82, 221-230.
- [17] C.J. Booker, R. Bedmutha, T. Vogel, A. Gloor, R. Xu, L. Ferrante, K.K.C. Yeung, I.M. Scott, K.L. Conn, F. Berruti & C. Briens. Experimental Investigations into the Insecticidal, Fungicidal, and Bactericidal Properties of Pyrolysis Bio-oil from Tobacco Leaves Using a Fluidized Bed Pilot Plant, *Industrial & Engineering Chemistry Research*, **2010**, 49, 10074-10079.
- [18] R. Bedmutha, C.J. Booker, L. Ferrante, C. Briens, F. Berruti, K.K.C. Yeung, I. Scott & K. Conn. Insecticidal and bactericidal characteristics of the bio-oil from the fast pyrolysis of coffee grounds, *Journal of Analytical and Applied Pyrolysis*, **2011**, 90, 224-231.
- [19] D. Mota-Sanchez, R.M. Hollingworth, E.J. Grafius & D.D. Moyer. Resistance and cross-resistance to neonicotinoid insecticides and spinosad in the Colorado potato beetle, *Leptinotarsa decemlineata* (Say) (Coleoptera : Chrysomelidae), *Pest Management Science*, **2006**, 62, 30-37.
- [20] EI DuPont de Numours & Co. Cresols, ortho-, meta-, and para-. **1983**, NTIS Report. No. OTS0205862.
- [21] Anonymous. Final report on the safety assessment of sodium p-chloro-m-cresol, p-chloro-m-cresol, chlorothymol, mixed cresols, m-cresol, o-cresol, p-cresol,



- isopropyl cresols, thymol, o-cymen-5-ol, and carvacrol, *International Journal of Toxicology*, **2006**, *25*, 29-127.
- [22] D. Meir. in Fast pyrolysis of biomass: a handbook. Eds A. Bridgwater & al, CPL Press, Newbury, UK, **1999**, pp. 92-101.
- [23] D.L. Roberts & R.L. Rowland. Macrocyclic diterpenes - alpha and beta-4,8,13-duvatriene-1,3-diols from tobacco, *Journal of Organic Chemistry*, **1962**, *27*, 3989.
- [24] M. Reuveni, S. Tuzun, J.S. Cole, M.R. Siegel, W.C. Nesmith & J. Kuc. Removal of duvatrienediols from the surface of tobacco-leaves increase their susceptibility to blue mold, *Physiological and Molecular Plant Pathology*, **1987**, *30*, 441-451.
- [25] K. Everaert, N. Lumen, W. Kerckhaert, P. Willaert & M. van Driel. Urinary tract infections in spinal cord injury: Prevention and treatment guidelines, *Acta Clinica Belgica*, **2009**, *64*, 335-340.
- [26] B.B. Lee, J.M. Simpson, J.C. Craig & T. Bhuta. Methenamine hippurate for preventing urinary tract infections, *Cochrane Database of Systematic Reviews*, **2007**, 33.
- [27] Y. Nagumo, K. Tanaka, K. Tewari, K. Thiraporn, T. Tsuchida, T. Honma, N. Ohtake, K. Sueyoshi, Y. Takahashi & T. Ohyama. Rapid quantification of cyanamide by ultra-high-pressure liquid chromatography in fertilizer, soil or plant samples, *Journal of Chromatography A*, **2009**, *1216*, 5614-5618.
- [28] C. Foti, D. Bonamonte, A. Conserva, M.L. Pepe, L. Soleo & G. Angelini. Allergic contact dermatitis with a fertilizer containing hydrogen cyanamide (DORMEX (R)), *Cutaneous and Ocular Toxicology*, **2008**, *27*, 1-3.
- [29] A.K. Johny, S.A. Baskaran, A.S. Charles, M.A.R. Amalaradjou, M.J. Darre, M.I. Khan, T.A. Hoagland, D.T. Schreiber, A.M. Donoghue, D.J. Donoghue & K. Venkitanarayanan. Prophylactic Supplementation of Caprylic Acid in Feed Reduces Salmonella Enteritidis Colonization in Commercial Broiler Chicks, *Journal of Food Protection*, **2009**, *72*, 722-727.
- [30] H.I. Jang & M.S. Rhee. Inhibitory effect of caprylic acid and mild heat on Cronobacter spp. (*Enterobacter sakazakii*) in reconstituted infant formula and determination of injury by flow cytometry, *International Journal of Food Microbiology*, **2009**, *133*, 113-120.
- [31] G. Immanuel, M. Sivagnanavelmurugan & A. Palavesam. Antibacterial effect of medium-chain fatty acid: caprylic acid on gnotobiotic *Artemia franciscana* nauplii against shrimp pathogens *Vibrio harveyi* and *V. parahaemolyticus*, *Aquaculture International*, **2011**, *19*, 91-101.

## **Chapter 7: Conclusions and Future Work**

## 7.1 Discussion of Conclusions and Future Work

The past six chapters have focused on the isolation of analytes of interest. The first four chapters examined large biological molecules at small volumes, and demonstrated how capillary electrophoresis could be transformed into a sample preparation tool for enrichment and purification of low abundance analytes for subsequent mass spectrometry. The second type of sample was bio-oil, where the pesticide properties were explored using various analytical techniques to narrow the search for the acting antimicrobial chemicals. Both classes of compounds presented their own challenges, and required different analytical approaches.

Capillary electrophoresis offers automation and fast separations, with only sub-microliter sample volume requirements. Discontinuous buffers can enrich an entire capillary of low abundance analytes with isoelectric points that falls between the pH values of the two buffers. The application of discontinuous buffers to biological samples requires that the method can tolerate contaminating salt and/or buffering ions. Through experimentation and computer simulations, the pH junction was shown to withstand the contamination and even remove the original background of ions. Removal of sodium chloride was demonstrated up to 50 mM, and the removal of the unwanted ions was visualized using bromide and benzyltrimethylammonium. The stacking of the discontinuous buffering ions in place of the contaminating ions in the sample was discovered through computer simulation and confirmed by monitoring the absorbance of UV-absorbing buffering ions benzylamine and benzoate. The discontinuous buffers were selected to be MS compatible, and even with this collection of ions at the pH junction, the MS spectra of the original sample was enhanced after enrichment and removal of the sodium chloride. Subsequent separation of a protein mixture was performed on an enriched protein band. Contaminating buffering ions of TRIS, MES, and phosphate were also removed from the analyte by preparing the sample in an appropriate buffer solution which demonstrated the flexibility of the discontinuous buffers method.

One solution to this accumulation of discontinuous buffer ions at the junction is to take advantage of the moving reaction boundary. The direction and velocity of the pH

junction migration can be manipulated by adjusting the type of buffering ions and the pH of the discontinuous buffers. Previous work has demonstrated the potential to have a moving reaction boundary in a capillary between two unique buffers [1]. Work is continuing in our lab with simulations and experiments that suggest it is possible to titrate the pH junction out of the zone of stacked buffering ions (from the removal of sample salt ions) and thus truly remove the enriched protein band from all contaminating ions. Further work into this process will add to the value of discontinuous buffers as a sample preparation technique.

The current method by which we perform subsequent MS on the capillary content is to spot the content in discrete spots on the MALDI MS sample target plate. A continuous flow of the capillary content onto the MALDI plate (rather than in discrete spots) could provide a more efficient deposition method as well as better resolution of the separation of the contents. MS imaging is a developing field which allows spatial resolution of the analytes of interest [2]. This technique is currently being performed on tissues but could easily be applied to linear sample zones from a capillary. Complicating factors include the concurrent deposition of matrix with the analyte, which could be performed by a second capillary filled with matrix solution that could flow at the same rate as the sample capillary. This would require some innovation in hardware design, but could be as simple as an external syringe set to a constant flow rate.

On-line plugs of magnetic beads enhance the sample preparations options in CE. It is possible to selectively retain a type of analyte while the contaminants are removed and even change the buffer/sample solution that the sample is eluted in. Preliminary in-capillary experiments with thiol-activated magnetic beads were used to isolate DTT-derivatized phosphopeptides. Derivatization conditions as well as binding, washing, and eluting conditions with the magnetic beads were optimized in-vial for further applications in-capillary. In-vial experiments required greater amounts of sample, as one is limited by the volume that can be manipulated by pipettes and recovered from even the smallest vials. In-vial procedures also required many labour intensive steps to add and remove solutions from the magnetic beads. In contrast, the CE experiments were automated and only required one to prepare the solutions in separate vials and begin the program. CE is

an excellent choice for samples that are of limited volume, and especially for those samples that have low abundance analytes. Magnetic beads in the capillary is a very new field and a great deal of method development must be performed to fully capitalize on the possibilities. Our enrichment of phosphorylated peptides with thiol-activated beads must be examined with more complex samples, such as a digest of  $\alpha$ -casein, and then also be tested with cell lysates, to compare its performance with other novel, miniaturized developing methods [3]. This magnetic beads technique must also be integrated with other on-line techniques, such as discontinuous buffers, trypsin digest [4], and sample derivitization, to demonstrate its real advantages.

Additional on-line procedures must be optimized, including the on-line mixing of the magnetic beads and analyte, and the solid phase clean-up steps. The in-capillary mixing for chemical reactions must be improved to obtain enhanced retention and elution of the analyte. Preliminary mixing techniques have involved the moderate  $\pm 50$  mbar pressure to move the sample back and forth across the magnetic beads plug. It is expected that this movement would temporarily disrupt the plug, but that it would collect again with forward pressure. This process could be analyzed under a microscope. The optimal amplitude of the pressure during mixing should also be determined. Currently, an off-line solid phase extraction with ZipTips<sup>TM</sup> is used to remove the excess DTT before the reaction with the magnetic beads and the final elution from the magnetic beads is analyzed in the second addition of DTT. C18 magnetic beads, or C18 resin retained by magnetic bead frits, must be examined for on-line analyte retention. Currently, the iron oxide core of the C18 magnetic particles seems to result in selective binding of peptides, which limits the application of this process. ZipTips<sup>TM</sup> (C18 resin) are capable of retaining peptides from a wide range of isoelectric points, and it is probable that with time, the synthesis of the commercial C18 magnetic beads will be improved through better coating of the beads. In the interim, magnetic particles could be used as a "frit" to collect non-magnetized silica in the capillary to allow for flexible on-line clean-up. This work is currently being explored in our lab which will open many new opportunities for collecting non-magnetized particles to improve sample clean-up. On-line sample clean-up would allow for less sample handling, translating to lower labour costs of time and money, and higher analyte recovery.

Further technology developments will also allow for more comprehensive analysis of bio-oil. No abundant chemical was found with pesticide properties, suggesting that no single, highly active compound is formed through pyrolysis. It is more likely that many, low abundance components are working synergistically to provide the observed pesticide activity. The most abundant phenolic compounds were examined through quantitative standard analysis and it was demonstrated that these components were not solely responsible for the observed antimicrobial activity. Although these compounds were not found to be independently active at the concentrations found in the bio-oil, potential synergistic effects of these phenolic compounds with other, unidentified compounds in the bio-oil could be investigated by spiking the bio-oil with these chemical standards. Many analytical techniques were employed to reduce the chemical complexity of the bio-oil, but no single component could be identified as the one active compound. A few specific chemicals were identified through GC-MS of the most refined chromatography fractions, and standards of these compounds could be obtained in the future and analyzed against the microorganisms at the observed concentrations to determine if these chemicals contributed to the over-all antimicrobial activity. Due to the fact that bio-oil from several biomass sources contains antimicrobial activity, a common chemical source seems to be responsible for the active compounds. Thus, bio-oils generated from lignin and cellulose are currently being generated and analyzed for pesticide activity. Detailed comparisons between pyrolysis bio-oils from different feedstocks may also provide additional insight into the observed pesticide activity.

Each component in a pesticide must be identified and quantified before it can be used in Canada [5]. Indeed, Health Canada has reported that it often takes years to rigorously test the health and environmental risks of a new pesticide before it can be used and sold in Canada [5]. The identification of each component in our tobacco bio-oil is likely not possible at this time with current technologies. The research in this thesis was limited to GC-MS, as the database libraries for LC-MS are only in their infancy stages. A comprehensive LC-MS technique may lead to the identification of more chemicals that add to the pesticide activity. If the bio-oil had revealed only a few, new and abundant acting chemicals, it would have been possible to isolate, or even perhaps synthesize, these chemicals for pesticide application, but this result was not found. Mildly acting

compounds and selections of natural products, such as mineral oils, can circumvent the traditional years of testing to reach the Canadian pesticide market faster [5]. However, it is also unlikely that bio-oil would be allowed in the faster accreditation route for licensing in Canada as this pesticide as it is known to contain many toxic chemicals, like phenols.

Analytical chemistry is an exciting field with new technologies and new methods to apply these technologies. Many specialized samples require methods that can accommodate their low available sample volumes and enhance their low abundance components. Two unique classes of compounds have been explored in this thesis, and new methods have been developed, built upon the current progress in analytical chemistry. Further work in on-line sample preparation for capillary electrophoresis and method development for bio-oil analysis will enhance the MS identification of the analytes of interest.

## 7.2 References

- [1] C.X. Cao, L.Y. Fan & W. Zhang. Review on the theory of moving reaction boundary, electromigration reaction methods and applications in isoelectric focusing and sample pre-concentration, *Analyst*, **2008**, *133*, 1139-1157.
- [2] J.D. Watrous & P.C. Dorrestein. Imaging mass spectrometry in microbiology, *Nat. Rev. Microbiol.*, **2011**, *9*, 683-694.
- [3] H.J. Zhou, F. Elisma, N.J. Denis, T.G. Wright, R.J. Tian, H. Zhou, W.M. Hou, H.F. Zou & D. Figeys. Analysis of the Subcellular Phosphoproteome Using a Novel Phosphoproteomic Reactor, *J. Proteome Res.*, **2010**, *9*, 1279-1288.
- [4] C.A. Nesbitt & K.K.C. Yeung. In-capillary enrichment, proteolysis and separation using capillary electrophoresis with discontinuous buffers: application on proteins with moderately acidic and basic isoelectric points, *Analyst*, **2009**, *134*, 65-71.
- [5] Health Canada. Pesticides and Pest Management. Updated **2011-04-13**, <http://www.hc-sc.gc.ca/cps-spc/pest/faq-eng.php#isi> Retrieved 2011-11-01.



## **Appendix 1: Copyright Permissions**



RightsLink®

[Home](#)[Account Info](#)[Help](#)ACS Publications  
High quality. High impact.**Title:** In-Capillary Protein Enrichment and Removal of Nonbuffering Salts Using Capillary Electrophoresis with Discontinuous Buffers**Author:** Christina J. Booker et al.**Publication:** Analytical Chemistry**Publisher:** American Chemical Society**Date:** Nov 1, 2008

Copyright © 2008, American Chemical Society

Logged in as:  
Christina Booker[LOGOUT](#)**PERMISSION/LICENSE IS GRANTED FOR YOUR ORDER AT NO CHARGE**

This type of permission/license, instead of the standard Terms & Conditions, is sent to you because no fee is being charged for your order. Please note the following:

- Permission is granted for your request in both print and electronic formats.
- If figures and/or tables were requested, they may be adapted or used in part.
- Please print this page for your records and send a copy of it to your publisher/graduate school.
- Appropriate credit for the requested material should be given as follows: "Reprinted (adapted) with permission from (COMPLETE REFERENCE CITATION). Copyright (YEAR) American Chemical Society." Insert appropriate information in place of the capitalized words.
- One-time permission is granted only for the use specified in your request. No additional uses are granted (such as derivative works or other editions). For any other uses, please submit a new request.

[BACK](#)[CLOSE WINDOW](#)

Copyright © 2011 [Copyright Clearance Center, Inc.](#) All Rights Reserved. [Privacy statement.](#)  
Comments? We would like to hear from you. E-mail us at [customercare@copyright.com](mailto:customercare@copyright.com)

**ELSEVIER LICENSE  
TERMS AND CONDITIONS**

Oct 20, 2011

This is a License Agreement between Christina J. Booker ("You") and Elsevier ("Elsevier") provided by Copyright Clearance Center ("CCC"). The license consists of your order details, the terms and conditions provided by Elsevier, and the payment terms and conditions.

**All payments must be made in full to CCC. For payment instructions, please see information listed at the bottom of this form.**

Supplier	Elsevier Limited
Registered Company Number	1982084
Customer name	Christina J. Booker
Customer address	
License number	2773370689479
License date	Oct 20, 2011
Licensed content publisher	Elsevier
Licensed content publication	Journal of Chromatography A
Licensed content title	Removal of sample background buffering ions and myoglobin enrichment via a pH junction created by discontinuous buffers in capillary electrophoresis
Licensed content author	Christina J. Booker, Samuel Sun, Sarah Woolsey, Jose S. Mejia, Ken K.-C. Yeung
Licensed content date	19 August 2011
Licensed content volume number	1218
Licensed content issue number	33
Number of pages	7
Start Page	5705
End Page	5711
Type of Use	reuse in a thesis/dissertation
Portion	full article
Format	both print and electronic
Are you the author of this Elsevier article?	Yes
Will you be translating?	No
Order reference number	
Title of your thesis/dissertation	Miniaturized Fractionation and Purification of Analytes of Interest in Complex Mixtures: Protein Enrichment and Purification with Capillary Electrophoresis and Identification of Pesticide Chemicals in Bio-oils

Expected completion date	Nov 2011
Estimated size (number of pages)	200
Elsevier VAT number	GB 494 6272 12
Permissions price	0.00 USD
VAT/Local Sales Tax	0.0 USD / 0.0 GBP
Total	0.00 USD
<a href="#">Terms and Conditions</a>	

### INTRODUCTION

1. The publisher for this copyrighted material is Elsevier. By clicking "accept" in connection with completing this licensing transaction, you agree that the following terms and conditions apply to this transaction (along with the Billing and Payment terms and conditions established by Copyright Clearance Center, Inc. ("CCC"), at the time that you opened your Rightslink account and that are available at any time at <http://myaccount.copyright.com>).

### GENERAL TERMS

2. Elsevier hereby grants you permission to reproduce the aforementioned material subject to the terms and conditions indicated.

3. Acknowledgement: If any part of the material to be used (for example, figures) has appeared in our publication with credit or acknowledgement to another source, permission must also be sought from that source. If such permission is not obtained then that material may not be included in your publication/copies. Suitable acknowledgement to the source must be made, either as a footnote or in a reference list at the end of your publication, as follows:

“Reprinted from Publication title, Vol /edition number, Author(s), Title of article / title of chapter, Pages No., Copyright (Year), with permission from Elsevier [OR APPLICABLE SOCIETY COPYRIGHT OWNER].” Also Lancet special credit - “Reprinted from The Lancet, Vol. number, Author(s), Title of article, Pages No., Copyright (Year), with permission from Elsevier.”

4. Reproduction of this material is confined to the purpose and/or media for which permission is hereby given.

5. Altering/Modifying Material: Not Permitted. However figures and illustrations may be altered/adapted minimally to serve your work. Any other abbreviations, additions, deletions and/or any other alterations shall be made only with prior written authorization of Elsevier Ltd. (Please contact Elsevier at [permissions@elsevier.com](mailto:permissions@elsevier.com))

6. If the permission fee for the requested use of our material is waived in this instance, please be advised that your future requests for Elsevier materials may attract a fee.

7. Reservation of Rights: Publisher reserves all rights not specifically granted in the combination of (i) the license details provided by you and accepted in the course of this licensing transaction, (ii) these terms and conditions and (iii) CCC's Billing and Payment terms and conditions.

8. License Contingent Upon Payment: While you may exercise the rights licensed immediately upon issuance of the license at the end of the licensing process for the transaction, provided that you have disclosed complete and accurate details of your proposed use, no license is finally effective unless and until full payment is received from you (either by publisher or by CCC) as provided in CCC's Billing and Payment terms and conditions. If full payment is not received on a timely basis, then any license preliminarily granted shall be deemed automatically revoked and shall be void as if never granted. Further, in the event that you breach any of these terms and conditions or any of CCC's Billing and Payment terms and conditions, the license is automatically revoked and shall be void as if never granted. Use of materials as described in a revoked license, as well as any use of the materials beyond the scope of an unrevoked license, may constitute copyright infringement and publisher reserves the right to take any and all action to protect its copyright in the materials.

9. Warranties: Publisher makes no representations or warranties with respect to the licensed material.

10. Indemnity: You hereby indemnify and agree to hold harmless publisher and CCC, and their respective officers, directors, employees and agents, from and against any and all claims arising out of your use of the licensed material other than as specifically authorized pursuant to this license.

11. No Transfer of License: This license is personal to you and may not be sublicensed, assigned, or transferred by you to any other person without publisher's written permission.

12. No Amendment Except in Writing: This license may not be amended except in a writing signed by both parties (or, in the case of publisher, by CCC on publisher's behalf).

13. Objection to Contrary Terms: Publisher hereby objects to any terms contained in any purchase order, acknowledgment, check endorsement or other writing prepared by you, which terms are inconsistent with these terms and conditions or CCC's Billing and Payment terms and conditions. These terms and conditions, together with CCC's Billing and Payment terms and conditions (which are incorporated herein), comprise the entire agreement between you and publisher (and CCC) concerning this licensing transaction. In the event of any conflict between your obligations established by these terms and conditions and those established by CCC's Billing and Payment terms and conditions, these terms and conditions shall control.

14. Revocation: Elsevier or Copyright Clearance Center may deny the permissions described in this License at their sole discretion, for any reason or no reason, with a full refund payable to you. Notice of such denial will be made using the contact information provided by you. Failure to receive such notice will not alter or invalidate the denial. In no event will Elsevier or Copyright Clearance Center be responsible or liable for any costs, expenses or damage incurred by you as a result of a denial of your permission request, other than a refund of the amount(s) paid by you to Elsevier and/or Copyright Clearance Center for denied permissions.

#### LIMITED LICENSE

The following terms and conditions apply only to specific license types:

15. **Translation:** This permission is granted for non-exclusive world **English** rights only unless your license was granted for translation rights. If you licensed translation rights you may only translate this content into the languages you requested. A professional translator must perform all translations and reproduce the content word for word preserving the integrity of the article. If this license is to re-use 1 or 2 figures then permission is granted for non-exclusive world rights in all languages.

16. **Website:** The following terms and conditions apply to electronic reserve and author websites:

**Electronic reserve:** If licensed material is to be posted to website, the web site is to be password-protected and made available only to bona fide students registered on a relevant course if:

This license was made in connection with a course,

This permission is granted for 1 year only. You may obtain a license for future website posting,

All content posted to the web site must maintain the copyright information line on the bottom of each image,

A hyper-text must be included to the Homepage of the journal from which you are licensing at <http://www.sciencedirect.com/science/journal/xxxxx> or the Elsevier homepage for books at <http://www.elsevier.com> , and

Central Storage: This license does not include permission for a scanned version of the material to be stored in a central repository such as that provided by Heron/XanEdu.

17. **Author website** for journals with the following additional clauses:

All content posted to the web site must maintain the copyright information line on the bottom of each image, and

the permission granted is limited to the personal version of your paper. You are not allowed to download and post the published electronic version of your article (whether PDF or HTML, proof or final version), nor may you scan the printed edition to create an electronic version,

A hyper-text must be included to the Homepage of the journal from which you are licensing at <http://www.sciencedirect.com/science/journal/xxxxx> , As part of our normal production process, you will receive an e-mail notice when your article appears on Elsevier's online service ScienceDirect ([www.sciencedirect.com](http://www.sciencedirect.com)). That e-mail will include the article's Digital Object Identifier (DOI). This number provides the electronic link to the published article and should be included in the posting of your personal version. We ask that you wait until you receive this e-mail and have the DOI to do any posting.

Central Storage: This license does not include permission for a scanned version of the material to be stored in a central repository such as that provided by Heron/XanEdu.

18. **Author website** for books with the following additional clauses:

Authors are permitted to place a brief summary of their work online only.

A hyper-text must be included to the Elsevier homepage at <http://www.elsevier.com>

All content posted to the web site must maintain the copyright information line on the bottom of each image

You are not allowed to download and post the published electronic version of your chapter, nor may you scan the printed edition to create an electronic version.

Central Storage: This license does not include permission for a scanned version of the

material to be stored in a central repository such as that provided by Heron/XanEdu.

19. **Website** (regular and for author): A hyper-text must be included to the Homepage of the journal from which you are licensing at <http://www.sciencedirect.com/science/journal/xxxxx>. or for books to the Elsevier homepage at <http://www.elsevier.com>

20. **Thesis/Dissertation**: If your license is for use in a thesis/dissertation your thesis may be submitted to your institution in either print or electronic form. Should your thesis be published commercially, please reapply for permission. These requirements include permission for the Library and Archives of Canada to supply single copies, on demand, of the complete thesis and include permission for UMI to supply single copies, on demand, of the complete thesis. Should your thesis be published commercially, please reapply for permission.

21. **Other Conditions:**

v1.6

**If you would like to pay for this license now, please remit this license along with your payment made payable to "COPYRIGHT CLEARANCE CENTER" otherwise you will be invoiced within 48 hours of the license date. Payment should be in the form of a check or money order referencing your account number and this invoice number RLNK500649768.**

**Once you receive your invoice for this order, you may pay your invoice by credit card. Please follow instructions provided at that time.**

**Make Payment To:  
Copyright Clearance Center  
Dept 001  
P.O. Box 843006  
Boston, MA 02284-3006**

**For suggestions or comments regarding this order, contact RightsLink Customer Support:**

**Gratis licenses (referencing \$0 in the Total field) are free. Please retain this printable license for your reference. No payment is required.**

---

---

**Berkeley Electronic Press**

From: Bepress Support Team

Date: Fri, Oct 21, 2011 at 12:42 PM

Dear Ms. Booker,

Thank you for your inquiry and for providing this information. Our fair-use policy allows authors to utilize their work in the manner you've requested, assuming the article is cited appropriately and that proper credit is given to Berkeley Electronic Press as copyright holder (e.g. Berkeley Electronic Press © 2010). For your convenience, I've included a link to our Attribution and Usage Policies below:

<http://www.bepress.com/ijcre/policies.html#rights>

If you have any questions or concerns about this, please don't hesitate to contact us.

Thank you.

All the best,

Jessica Robles

Berkeley Electronic Press

[www.bepress.com](http://www.bepress.com)

----- Forwarded message -----

From: Christina Joanne Booker

Date: Thu, Oct 20, 2011 at 7:01 PM

Subject: thesis copyright

Hello,

I am writing to obtain formal permission to reproduce my article in my own thesis. This letter of permission is required for publication of my thesis. The article is:

C.J. Booker, R. Bedmutha, I.M. Scott, K. Conn, F. Berruti, C. Briens & K.K.C. Yeung.  
Bioenergy II: Characterization of the Pesticide Properties of Tobacco Bio-Oil,  
International Journal of Chemical Reactor Engineering, 2010, 8.

Thank-you.

Sincerely,

Christina Booker





RightsLink®

Home

Account  
Info

Help



ACS Publications  
High quality. High impact.

**Title:**

Experimental Investigations into the Insecticidal, Fungicidal, and Bactericidal Properties of Pyrolysis Bio-oil from Tobacco Leaves Using a Fluidized Bed Pilot Plant

Logged in as:

Christina Booker

LOGOUT

**Author:** Christina J. Booker et al.

**Publication:** Industrial & Engineering Chemistry Research

**Publisher:** American Chemical Society

**Date:** Oct 1, 2010

Copyright © 2010, American Chemical Society

#### PERMISSION/LICENSE IS GRANTED FOR YOUR ORDER AT NO CHARGE

This type of permission/license, instead of the standard Terms & Conditions, is sent to you because no fee is being charged for your order. Please note the following:

- Permission is granted for your request in both print and electronic formats.
- If figures and/or tables were requested, they may be adapted or used in part.
- Please print this page for your records and send a copy of it to your publisher/graduate school.
- Appropriate credit for the requested material should be given as follows: "Reprinted (adapted) with permission from (COMPLETE REFERENCE CITATION). Copyright (YEAR) American Chemical Society." Insert appropriate information in place of the capitalized words.
- One-time permission is granted only for the use specified in your request. No additional uses are granted (such as derivative works or other editions). For any other uses, please submit a new request.

BACK

CLOSE WINDOW

Copyright © 2011 Copyright Clearance Center, Inc. All Rights Reserved. [Privacy statement](#).  
Comments? We would like to hear from you. E-mail us at [customercare@copyright.com](mailto:customercare@copyright.com)

**ELSEVIER LICENSE  
TERMS AND CONDITIONS**

Oct 20, 2011

This is a License Agreement between Christina J. Booker ("You") and Elsevier ("Elsevier") provided by Copyright Clearance Center ("CCC"). The license consists of your order details, the terms and conditions provided by Elsevier, and the payment terms and conditions.

**All payments must be made in full to CCC. For payment instructions, please see information listed at the bottom of this form.**

Supplier	Elsevier Limited
Registered Company Number	1982084
Customer name	Christina J. Booker
Customer address	
License number	2773371319291
License date	Oct 20, 2011
Licensed content publisher	Elsevier
Licensed content publication	Journal of Analytical and Applied Pyrolysis
Licensed content title	Insecticidal and bactericidal characteristics of the bio-oil from the fast pyrolysis of coffee grounds
Licensed content author	Rohan Bedmutha, Christina J. Booker, Lorenzo Ferrante, Cedric Briens, Franco Berruti, Ken K.-C. Yeung, Ian Scott, Kenneth Conn
Licensed content date	March 2011
Licensed content volume number	90
Licensed content issue number	2
Number of pages	8
Start Page	224
End Page	231
Type of Use	reuse in a thesis/dissertation
Intended publisher of new work	other
Portion	full article
Format	both print and electronic
Are you the author of this Elsevier article?	Yes
Will you be translating?	No
Order reference number	

Title of your thesis/dissertation	Miniaturized Fractionation and Purification of Analytes of Interest in Complex Mixtures: Protein Enrichment and Purification with Capillary Electrophoresis and Identification of Pesticide Chemicals in Bio-oils
Expected completion date	Nov 2011
Estimated size (number of pages)	200
Elsevier VAT number	GB 494 6272 12
Permissions price	0.00 USD
VAT/Local Sales Tax	0.0 USD / 0.0 GBP
Total	0.00 USD
Terms and Conditions	

### INTRODUCTION

1. The publisher for this copyrighted material is Elsevier. By clicking "accept" in connection with completing this licensing transaction, you agree that the following terms and conditions apply to this transaction (along with the Billing and Payment terms and conditions established by Copyright Clearance Center, Inc. ("CCC"), at the time that you opened your Rightslink account and that are available at any time at <http://myaccount.copyright.com>).

### GENERAL TERMS

2. Elsevier hereby grants you permission to reproduce the aforementioned material subject to the terms and conditions indicated.

3. Acknowledgement: If any part of the material to be used (for example, figures) has appeared in our publication with credit or acknowledgement to another source, permission must also be sought from that source. If such permission is not obtained then that material may not be included in your publication/copies. Suitable acknowledgement to the source must be made, either as a footnote or in a reference list at the end of your publication, as follows:

“Reprinted from Publication title, Vol /edition number, Author(s), Title of article / title of chapter, Pages No., Copyright (Year), with permission from Elsevier [OR APPLICABLE SOCIETY COPYRIGHT OWNER].” Also Lancet special credit - “Reprinted from The Lancet, Vol. number, Author(s), Title of article, Pages No., Copyright (Year), with permission from Elsevier.”

4. Reproduction of this material is confined to the purpose and/or media for which permission is hereby given.

5. Altering/Modifying Material: Not Permitted. However figures and illustrations may be altered/adapted minimally to serve your work. Any other abbreviations, additions, deletions and/or any other alterations shall be made only with prior written authorization of Elsevier Ltd. (Please contact Elsevier at [permissions@elsevier.com](mailto:permissions@elsevier.com))

6. If the permission fee for the requested use of our material is waived in this instance, please be advised that your future requests for Elsevier materials may attract a fee.

7. Reservation of Rights: Publisher reserves all rights not specifically granted in the

combination of (i) the license details provided by you and accepted in the course of this licensing transaction, (ii) these terms and conditions and (iii) CCC's Billing and Payment terms and conditions.

8. License Contingent Upon Payment: While you may exercise the rights licensed immediately upon issuance of the license at the end of the licensing process for the transaction, provided that you have disclosed complete and accurate details of your proposed use, no license is finally effective unless and until full payment is received from you (either by publisher or by CCC) as provided in CCC's Billing and Payment terms and conditions. If full payment is not received on a timely basis, then any license preliminarily granted shall be deemed automatically revoked and shall be void as if never granted. Further, in the event that you breach any of these terms and conditions or any of CCC's Billing and Payment terms and conditions, the license is automatically revoked and shall be void as if never granted. Use of materials as described in a revoked license, as well as any use of the materials beyond the scope of an unrevoked license, may constitute copyright infringement and publisher reserves the right to take any and all action to protect its copyright in the materials.

9. Warranties: Publisher makes no representations or warranties with respect to the licensed material.

10. Indemnity: You hereby indemnify and agree to hold harmless publisher and CCC, and their respective officers, directors, employees and agents, from and against any and all claims arising out of your use of the licensed material other than as specifically authorized pursuant to this license.

11. No Transfer of License: This license is personal to you and may not be sublicensed, assigned, or transferred by you to any other person without publisher's written permission.

12. No Amendment Except in Writing: This license may not be amended except in a writing signed by both parties (or, in the case of publisher, by CCC on publisher's behalf).

13. Objection to Contrary Terms: Publisher hereby objects to any terms contained in any purchase order, acknowledgment, check endorsement or other writing prepared by you, which terms are inconsistent with these terms and conditions or CCC's Billing and Payment terms and conditions. These terms and conditions, together with CCC's Billing and Payment terms and conditions (which are incorporated herein), comprise the entire agreement between you and publisher (and CCC) concerning this licensing transaction. In the event of any conflict between your obligations established by these terms and conditions and those established by CCC's Billing and Payment terms and conditions, these terms and conditions shall control.

14. Revocation: Elsevier or Copyright Clearance Center may deny the permissions described in this License at their sole discretion, for any reason or no reason, with a full refund payable to you. Notice of such denial will be made using the contact information provided by you. Failure to receive such notice will not alter or invalidate the denial. In no event will Elsevier or Copyright Clearance Center be responsible or liable for any costs, expenses or damage incurred by you as a result of a denial of your permission request, other than a refund of the amount(s) paid by you to Elsevier and/or Copyright Clearance Center for denied permissions.

#### **LIMITED LICENSE**

The following terms and conditions apply only to specific license types:

15. **Translation:** This permission is granted for non-exclusive world **English** rights only unless your license was granted for translation rights. If you licensed translation rights you may only translate this content into the languages you requested. A professional translator must perform all translations and reproduce the content word for word preserving the integrity of the article. If this license is to re-use 1 or 2 figures then permission is granted for non-exclusive world rights in all languages.

16. **Website:** The following terms and conditions apply to electronic reserve and author websites:

**Electronic reserve:** If licensed material is to be posted to website, the web site is to be password-protected and made available only to bona fide students registered on a relevant course if:

This license was made in connection with a course,

This permission is granted for 1 year only. You may obtain a license for future website posting,

All content posted to the web site must maintain the copyright information line on the bottom of each image,

A hyper-text must be included to the Homepage of the journal from which you are licensing at <http://www.sciencedirect.com/science/journal/xxxxx> or the Elsevier homepage for books at <http://www.elsevier.com> , and

Central Storage: This license does not include permission for a scanned version of the material to be stored in a central repository such as that provided by Heron/XanEdu.

17. **Author website** for journals with the following additional clauses:

All content posted to the web site must maintain the copyright information line on the bottom of each image, and

the permission granted is limited to the personal version of your paper. You are not allowed to download and post the published electronic version of your article (whether PDF or HTML, proof or final version), nor may you scan the printed edition to create an electronic version,

A hyper-text must be included to the Homepage of the journal from which you are licensing at <http://www.sciencedirect.com/science/journal/xxxxx> , As part of our normal production process, you will receive an e-mail notice when your article appears on Elsevier's online service ScienceDirect ([www.sciencedirect.com](http://www.sciencedirect.com)). That e-mail will include the article's Digital Object Identifier (DOI). This number provides the electronic link to the published article and should be included in the posting of your personal version. We ask that you wait until you receive this e-mail and have the DOI to do any posting.

Central Storage: This license does not include permission for a scanned version of the material to be stored in a central repository such as that provided by Heron/XanEdu.

18. **Author website** for books with the following additional clauses:

Authors are permitted to place a brief summary of their work online only.

A hyper-text must be included to the Elsevier homepage at <http://www.elsevier.com>

All content posted to the web site must maintain the copyright information line on the bottom of each image

You are not allowed to download and post the published electronic version of your chapter,

nor may you scan the printed edition to create an electronic version.

Central Storage: This license does not include permission for a scanned version of the material to be stored in a central repository such as that provided by Heron/XanEdu.

19. **Website** (regular and for author): A hyper-text must be included to the Homepage of the journal from which you are licensing at <http://www.sciencedirect.com/science/journal/xxxxx>. or for books to the Elsevier homepage at <http://www.elsevier.com>

20. **Thesis/Dissertation**: If your license is for use in a thesis/dissertation your thesis may be submitted to your institution in either print or electronic form. Should your thesis be published commercially, please reapply for permission. These requirements include permission for the Library and Archives of Canada to supply single copies, on demand, of the complete thesis and include permission for UMI to supply single copies, on demand, of the complete thesis. Should your thesis be published commercially, please reapply for permission.

#### 21. **Other Conditions:**

v1.6

**If you would like to pay for this license now, please remit this license along with your payment made payable to "COPYRIGHT CLEARANCE CENTER" otherwise you will be invoiced within 48 hours of the license date. Payment should be in the form of a check or money order referencing your account number and this invoice number RLNK500649771.**

**Once you receive your invoice for this order, you may pay your invoice by credit card. Please follow instructions provided at that time.**

**Make Payment To:  
Copyright Clearance Center**

**For suggestions or comments regarding this order, contact RightsLink Customer Support:**

**Gratis licenses (referencing \$0 in the Total field) are free. Please retain this printable license for your reference. No payment is required.**

---

---

# Curriculum Vitae

*of Christina J. Booker*

---

## EDUCATION

**PhD Candidate**, University of Western Ontario

Sept. 2007- Jan. 2012

- Analytical Chemistry

**Honours Bachelor of Science**, University of Western Ontario

Sept. 2003- Apr. 2007

- Specialization in Chemistry, Minor in Psychology
- 

## HONOURS AND AWARDS

**NSERC Canadian Graduate Scholarship (CGS D2)**

Sept. 2009- Dec. 2011

**Analytical Chemistry Division Graduate Student Award in Honour of Walter E. Harris**

June 2011

**NSERC Alexander Graham Bell Canadian Graduate Scholarship (CGS M)**

Jan. 2008- Aug. 2009

**NSERC Post Graduate Scholarship (PGS M)**

Sept. 2007- Dec. 2007

**NSERC Undergraduate Student Research Award (USRA)**

May 2007- Aug. 2007, May 2006- Aug. 2006

**Hypercube Scholar Award**

April 2007

**Dean's Honour Roll**

Sept. 2003- Apr. 2007

**Group Health Centre Endowment Fund Scholarship**

Sept. 2003- Apr. 2007

**The Western Continuing Admission Scholarship of Excellence**

Sept. 2003- Apr. 2007

**Governor General's Award**

June 2003

**Ontario Scholar**

June 2003

**Korah Teachers' Gold Medal Scholarship**

June 2003

Declined Awards: OGS 2009, OGS 2007

**LABORATORY WORK EXPERIENCE****Interim MALDI Mass Spectrometry Facility Manager**, London Regional

Proteomics Facility

May 2011- Jan. 2012

**Graduate Research Assistant**, University of Western Ontario

Sept. 2007- Dec. 2011

**NSERC Undergraduate Student Research Award**, University of Western Ontario

May 2007- Aug. 2007, May 2006-Aug. 2006

**Undergraduate Honours Thesis Research**, University of Western Ontario

Sept. 2006- Apr. 2007

**TEACHING EXPERIENCE****Teaching Support Centre Instructor**, University of Western Ontario

Aug. 2009- Jan. 2012

**Teaching Assistant**, University of Western Ontario

Sept. 2007- Apr. 2009

**PUBLICATIONS**

8. **C.J. Booker**, S. Sun, S. Woolsey, J.S. Mejia & K.K.-C. Yeung. Removal of sample background buffering ions and myoglobin enrichment via a pH junction created by discontinuous buffer in capillary electrophoresis, *Journal of Chromatography A*, **2011**, 1218, 5705-5711.
7. R. Bedmutha, **C.J. Booker**, L. Ferrante, C. Briens, F. Berruti, K.K.-C. Yeung, I.M. Scott & K.L. Conn. Insecticidal and bactericidal characteristics of the bio-oil from the fast pyrolysis of coffee grounds, *Journal of Analytical and Applied Pyrolysis*, **2011**, 90, 224-231.
6. **C.J. Booker**, R. Bedmutha, I.M. Scott, K. Conn, F. Berruti, C. Briens & K.K.C. Yeung. Bioenergy II: Characterization of the Pesticide Properties of Tobacco Bio-Oil, *International Journal of Chemical Reactor Engineering*, **2010**, 8.



5. **C.J. Booker**, R. Bedmutha, T. Vogel, A. Gloor, R. Xu, L. Ferrante, K.K.C. Yeung, I.M. Scott, K.L. Conn, F. Berruti & C. Briens. Experimental Investigations into the Insecticidal, Fungicidal, and Bactericidal Properties of Pyrolysis Bio-oil from Tobacco Leaves Using a Fluidized Bed Pilot Plant, *Industrial & Engineering Chemistry Research*, **2010**, *49*, 10074-10079.
4. J.G. Zhou, **C. Booker**, R.Y. Li, X.L. Sun, T.K. Sham & Z.F. Ding. Electrochemistry and electrochemiluminescence study of blue luminescent carbon nanocrystals, *Chemical Physics Letters*, **2010**, *493*, 296-298.
3. **C.J. Booker** & K.K.C. Yeung. In-Capillary Protein Enrichment and Removal of Nonbuffering Salts Using Capillary Electrophoresis with Discontinuous Buffers, *Analytical Chemistry*, **2008**, *80*, 8598-8604.
2. **C. Booker**, X. Wang, S. Haroun, J.G. Zhou, M. Jennings, B.L. Pagenkopf & Z.F. Ding. Tuning of electrogenerated silole chemiluminescence, *Angewandte Chemie-International Edition*, **2008**, *47*, 7731-7735.
1. J.G. Zhou, **C. Booker**, R.Y. Li, X.T. Zhou, T.K. Sham, X.L. Sun & Z.F. Ding. An electrochemical avenue to blue luminescent nanocrystals from multiwalled carbon nanotubes (MWCNTs), *Journal of the American Chemical Society*, **2007**, *129*, 744-745.

---

## SELECTED PRESENTATIONS

7. **C.J. Booker** & K.K.C. Yeung. Selective Purification of Proteins and Peptides at Small Volumes using CE. *94<sup>th</sup> Canadian Chemistry Conference and Exhibition* (Montreal, June **2011**). Award Lecture.
6. **C.J. Booker**, L. Ferrante, C. Briens, F. Berruti, K.L. Conn, I.M. Scott, B. McGarvey & K.K.C. Yeung. Analytical Separation of Tobacco Bio-oils and Characterization of Pesticide Activity.” *Conference of the Agricultural Biorefinery Innovation Network* (London, March **2010**). Lecture.
5. **C.J. Booker**, J. Mejia & K.K.C. Yeung. Desalting and Concentration of Proteins with Capillary Isoelectric Trapping. *Canadian Chemistry Conference and Exhibition* (Hamilton, June **2009**). Lecture.
4. **C.J. Booker**, R. Bedmutha, T. Vogel, I.M. Scott, K.L. Conn, F. Berruti, C. Briens & K.K.C. Yeung. Characterization of the Pesticide Properties of Tobacco Bio-oil. *Bioenergy-II: Fuels and Chemicals from Renewable Resources* (Rio De Janeiro, Brazil, March **2009**). Poster and Lecture.
3. **C.J. Booker**, T. Vogel, A. Gloor, R. Bedmutha, R. Xu, L. Ferrante, F. Berruti, C. Briens & K.K.C. Yeung. Characterization of Bio-Oils from Agricultural and Forestry Waste as Pesticides. *91<sup>st</sup> Canadian Chemistry Conference and Exhibition* (Edmonton, May **2008**). Lecture.

2. **C.J. Booker** & K.K.C. Yeung. Sub-Microliter Volume Desalting for Intact Proteins by Capillary Electrophoresis (CE). *91<sup>st</sup> Canadian Chemistry Conference and Exhibition* (Edmonton, May **2008**). Poster.
1. **C.J. Booker**, X. Wang, J. Zhou, B. L. Pagenkopf & Z. Ding. Electrogenerated Chemiluminescence of Silole Compounds. *34<sup>th</sup> Southern Ontario Undergraduate Student Chemistry Conference* (Oshawa, March **2007**). Lecture.